Pulse Sequence Analysis and Pulse Shape Analysis: Methods to Analyze Partial Discharge Processes

Vom Fachbereich Elektrotechnik und Informatik der Universität Siegen

zur Erlangung des akademischen Grades

Doktor der Ingenieurwissenschaften
(Dr.-Ing.)

genehmigte Dissertation

von
Dipl.-Phys. Djamal Benzerouk

1. Gutachter: Prof. Dr. rer. nat. Rainer Patsch
2. Gutachter: Prof. Dr.-Ing. Dirk Peier

Tag der mündlichen Prüfung: 6. Juni 2008

A la mémoire de mon père
et ma grand mère

Acknowledgement

Kurzfassung

Puls Sequenz- und Impulsform-Analyse:
Diagnoseverfahren zur Untersuchung von Teilentladungsprozessen

Das Isoliersystem von hochspannungstechnischen Geräten, Anlagen und elektrischen Maschinen wird während des Betriebes zahlreichen Kombination von Belastungsfaktoren wie z.B. thermischen, mechanischen und insbesondere elektrischen Belastungen ausgesetzt, die zum Teil durch Umweltfaktoren beeinflusst werden und langfristig ebenfalls einen Beitrag zur allmählichen, meist irreversiblen Alterung des Isoliersystems und damit zur Verminderung der Isolationsfähigkeit leisten. Der Zustand der elektrischen Isoliersysteme von hochspannungstechnischen Anlagen beeinflusst stark deren ökonomische und technische Lebensdauer sowie die Zuverlässigkeit der elektrischen Energieversorgung.

Da sich die elektrische Belastung an den energietechnischen Betriebsmitteln in den letzten Jahren signifikant erhöht hat, ist einerseits eine werksseitige Qualitätskontrolle und anderseits einer Überwachung des aktuellen Isolationszustands während des Betriebes erforderlich. Zur Beurteilung des aktuellen Zustandes von Isolationssystemen werden unterschiedliche Diagnoseverfahren angewendet. Messungen und die **Analyse von Teilentladungen** sind eine weit verbreitete und heutzutage im industriellen Bereich etablierte zerstörungsfreie Methode zur Untersuchung des Zustandes des Isoliersystems elektrotechnischer und speziell energietechnischer Betriebsmittel.

In der vorliegenden Arbeit wurde die Puls Sequenz-Analyse (**Pulse Sequence Analysis**) und die Impulsform-Analyse (**Pulse Shape Analysis**) als Verfahren der Teilentladungsdiagnostik zur Untersuchung der Schädigungsprozesse in Isoliersystemen von energietechnischen Betriebsmitteln eingesetzt.

Mit Hilfe der im Rahmen dieser Arbeit entwickelten **PSA** Software erfolgt die Auswertung und Analyse der gemessen TE-Daten auf Basis unterschiedlicher Parameter. Der Vergleich der unterschiedlichen verwendeten **PSA**-Parameter zeigt, dass die **Analyse der Sequenzen von Teilentladungen** eine bessere Charakterisierung der Fehlstellen ermöglicht als die herkömmlichen Auswertung von lediglich phasenbezogen akkumulierten Daten.

Die Impulsform-Analyse erweist sich als sehr aussagefähiges Verfahren zur Charakterisierung und Lokalisierung von Fehlstellen in Isoliersystemen. Bei räumlich ausgedehnten Objekten entstehen in Abhängigkeit vom Ort der Fehlstelle unterschiedliche Kurvenformen des TE-Signals, die benutzt werden können, um TE-Impulse unterschiedlicher Herkunft zu selektieren. Hierdurch ergeben sich gute Möglichkeiten einer gezielten Analyse zur Erkennung des Fehlerortes und des Fehlertyps. Damit können unterschiedliche Schädigungsprozesse erkannt wer-

den. Die **Analyse der Kurvenform von Teilentladungssignalen** kann auch verwendet werden, um Störsignale von realen Teilentladungssignalen zu trennen.

Teilentladungsmessungen an Laborproben sowie an unterschiedlichen hochspannungstechnischen Geräten deckten auf, inwieweit eine Teilentladung durch den Aufbau lokaler Oberflächen- und Raumladungen die Zündung nachfolgender Entladungen beeinflusst. Dieser Einfluss wird anhand eines **erweiterten elektrischen Ersatzschaltbildes** diskutiert. Ergebnisse von Messungen an electrical trees in Polyethylen und an einem Hochspannungstransformator werden hinsichtlich spezieller Zusammenhänge zwischen einzelnen TE-Parametern interpretiert.

Impulsfolgen-Analyse und **Impulsform-Analyse** können erfolgreich zur Analyse von Teilentladungsuntersuchungen an Isolationssystemen elektrischer Geräte eingesetzt werden. Unterschiedliche Typen von Fehlstellen in Statorwicklungen von Kleinmotoren und Statorstäben von Hochspannungsmaschinen wurden lokalisiert und charakterisiert. Der Einfluss thermischer Belastung sowie der Einfluss der Messtemperatur auf das Teilentladungsverhalten wurden untersucht und diskutiert.

Contents

Introduction

The insulation system of high voltage equipment, especially electric machines, is subjected to combined electrical, mechanical, thermal and environmental stresses during operation which may alter the dielectric properties. The condition of the electrical insulation systems of high voltage equipment will strongly influence the economical and technical lifetime as well as the reliability of the supply of the generated or distributed electrical power.

Since the electric stress imposed on HV insulating materials has been increased significantly over the past few years and equipment becomes older, there is a greater need for monitoring the actual stage of insulation ageing or deterioration. Various diagnostic methods are applied for investigating the conditions of the insulating materials and the systems. Partial discharges (PD) are the main source of ageing and the most prominent indicator of the degradation of the insulation of electric equipments. **Partial discharge measurements** and analyses have been widely used as a non-destructive diagnostic tool to monitor and to examine the long term degradation of electrical equipment. Over the years an immense effort has been put into the development of sophisticated statistic software tools, to extract meaningful analyses out of the empirical data, unfortunately without taking care of relevant correlations between consecutive discharge pulses. In contrast to these classical methods of partial discharge analyses the application of the Pulse Sequence Analysis allows a far better insight into the PD processes at local defects.

The work reported in this thesis is focused on the use of the **Pulse Sequence Analysis** and the **Pulse Shape Analysis** as diagnostic tools to investigate the degradation phenomena in electric power apparatus, by means of the evaluation of **partial discharge measurements**.

The Pulse Sequence Analysis has been introduced more than a decade ago and has grown in importance continuously. The method is especially meaningful for partial discharges at comparatively low electric fields when there are only a few discharges per cycle of the applied AC voltage. In this case it is e.g. possible to determine whether there are different PD active points that produce the discharges or there is only one active spot. If two identical defects are active, the phase resolved analysis cannot separate this from the activity of one spot only. If the Pulse Sequence Analysis is used, the patterns that can be constructed are characteristically different for two separate discharge processes at different places or discharges in one point.

At high electric fields where typically several discharge processes may occur simultaneously in different spots of the apparatus, the **Pulse Shape Analysis**, i.e. the analysis of the shape of the PD signals after the band pass filter has proven to be very helpful to separate partial discharge

signals from different defects and hence the method can be used to improve the effectiveness of the **Pulse Sequence Analysis**.

The basic structure of this thesis is initially the presentation of the partial discharge theory, measurements and evaluation software, followed by the analysis and the characterization of the PD signals, the discussion of the influence of local surface or space charges and finally examples for PD diagnostics in the insulating system of electric machines.

In chapter 1, some basic physical properties of PD that are important for understanding the main ideas behind the concepts of PD analysis are presented. Chapter 2 describes the PD detection setup and the different test objects used in this work. Chapter 3 is devoted to the presentation of the developed PSA software and its use as a tool to analyze the partial discharge data. Chapter 4 is dedicated to the description of the pulse shape of a partial discharge signal and its use as a diagnostic tool to improve the Pulse Sequence Analysis method.

A special emphasis on different shapes of the oscillating PD signals is taken care of, thus different parameters are extracted from the shapes of the PD signals and used as a characteristic of the type of the PD-active defects. According to different classifications of these parameters different sources of the PD-active defects are identified and separated and even different stages of the degradation process are characterized. Noise signals are also removed on the basis of these parameters.

It will be shown in chapter 5 in how far the partial discharge phenomena are influenced by charges accumulated as the consequence of prior discharges. This influence of space charges will then be discussed on the basis of an **improved PD equivalent circuit**.

Chapter 6 reports on the investigation of partial discharge measurements and analyses on the insulation system of rotating machines using the **Pulse Sequence Analysis** and the **Pulse Shape Analysis**.

1   Partial Discharges, Theory and Models

In this chapter, some basic physical properties of PD that are important for the understanding of the main ideas behind the concepts of PD analysis are presented.

1.1   Basics of partial discharges

A partial discharge is a locally confined breakdown in an insulating system restricted to a certain region of the dielectric material and thus does not lead to a failure of the whole system. Partial discharges (PD) occur in a region of an insulating system where the local electric field exceeds the electric strength of the insulating material. The insulation may consist of solid, liquid or gaseous materials, or of any combination. The name partial discharge includes a wide group of discharges [Dan93, Bog90]:

 - **Corona discharges** occur in strongly inhomogeneous electric fields in gaseous dielectrics.
 - **Surface discharges** appear at the boundaries between different insulation materials.
 - **Internal discharges** may occur in voids or cavities within solid or liquid dielectrics.
 - **Electrical trees** occur usually in polymer materials in non-homogeneous field due to the continuous impact of discharges, which lead to the formation of hollow gas filled channels.

These different types of partial discharges represented schematically in **Fig. 1.1** will be described in details.

| Corona discharges | Surface discharges | Internal discharges | Electrical trees |
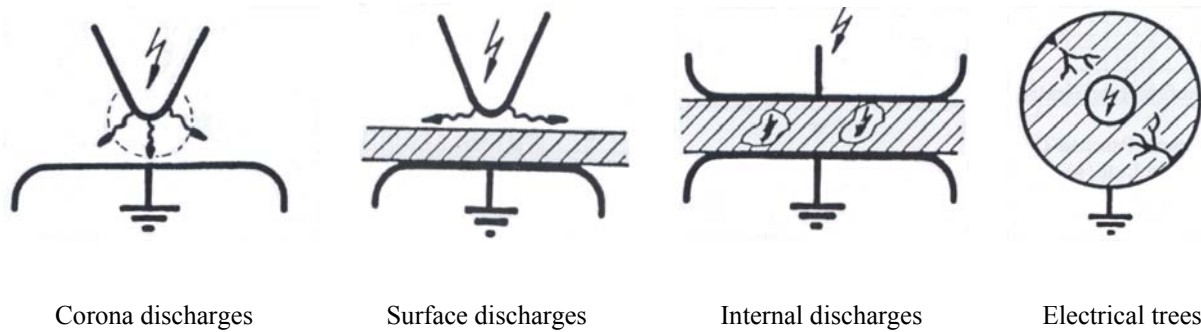
Fig. 1.1: Types of partial discharges

1.1.1   Corona discharges

Corona is defined as a type of localized discharge that results from transient gaseous ionization in non-uniform electric fields in an insulation system when the voltage stress locally exceeds a critical value. This external discharge occurs mainly in gases at sharp metallic electrodes of

electrical apparatus or devices. Usually these discharges are not dangerous unless decomposition products of the gas (e.g. SF_6) are formed that may be harmful for other materials in the vicinity of the discharge gap. This phenomenon is of particular importance in power engineering where non-uniform fields are unavoidable. It is responsible for considerable power losses in HV transmission lines and often leads to deterioration by the combined action of the discharge ions bombarding the surface and the action of chemical compounds that are formed by the discharges. On the other hand, the phenomenon is used in various industrial applications (high-speed printing devices, electrostatic precipitators, etc.).

The corona process under alternating voltage for a sharp electrode in air has been extensively investigated [Cha02]. When the applied voltage amplitude is increased, a point-plane arrangement with the needle on high potential will cause discharges first at negative polarity. These discharges called **Trichel-pulses** are of a relatively small magnitude but of a high repetition rate. At higher voltage amplitudes, **streamer discharges** will start to appear around the positive peak of the voltage. These streamers are much larger in magnitude than the Trichel-pulses under negative polarity but have a much lower repetition rate and are more fluctuating.

1.1.2 Surface discharges

Surface discharges occur along dielectric interfaces (e.g. solid/liquid or solid/gaseous interfaces) if there is a strong field component in parallel to the interface. These discharges occur phase to phase or phase to ground propagating via cracks or contaminated paths on the insulation or between components with inadequate electrical clearance. Contamination may be in the form of condensate, dirt, cleaning product residues, oils and greases. Even not switching on the sub station heating can cause water to condense on the surface of insulators leading to eventual electrical breakdown.
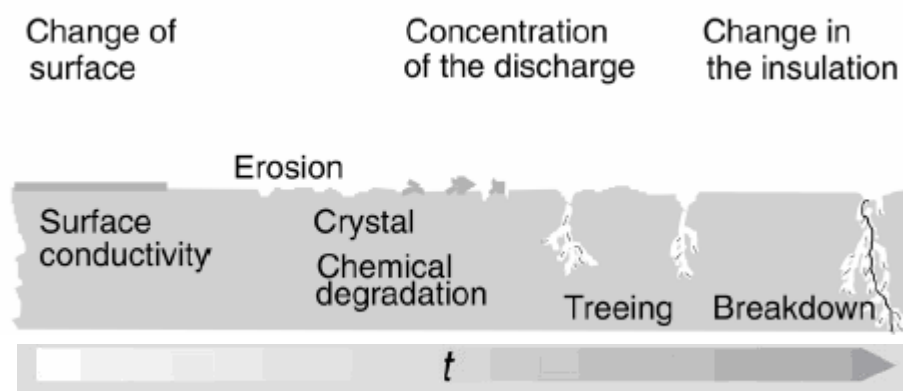
Fig. 1.2: Stages of PD induced damage at the insulator surface, after [Tem00].

In high voltage equipment, usually the surface discharges result in a deterioration of the dielectric due to depolymerization and other chemical processes that lead to an erosion of the surface. Common places of surface discharges in the electric apparatus are terminations of cables or the end-windings of stators. **Fig. 1.2** illustrates the different stages of PD induced damage at the insulator surface, after [Tem00].

1.1.3   Internal discharges

Electrical insulations may contain cavities or voids within the dielectric material or at boundaries between the dielectric and the electrodes. These cavities are usually filled with a medium (gas or liquid) of lower electric strength than the solid and thus may initiate a breakdown in the void under high electrical field.

In literature, different physical mechanisms to explain the evolution of the discharges in voids bounded to the dielectric are described. A classification with different nomenclatures for the discharges is proposed according to the duration of the discharge activity (**Tab. 1.1**). According to [Mor93] they may be characterized in three groups only:

- **Streamer-like discharges**: Occur in the initial stage of discharge activity (in virgin samples), characterized by a short discharge current pulse and ignite in rapid succession with a time interval between discharges of several ten nanoseconds.
- **Townsend-like discharges**: Start after some minutes of discharge activity, characterized by a broad discharge current pulse proportional to the dimension of the void.

Tab.1.1: Overview of the nomenclature of discharges mechanisms [Mor93]

Discharge stage	Discharge nomenclature	Origin	Morshuis classification
I	Spark type Streamer-like type Fast developing type	Classic breakdown theory [Dev84] [Luc79]	Streamer-like type
II	Townsend-like type Pseudo-glow type Slowly developing type	[Dev84] [Bar68] [Luc79]	Townsend-like type
II*	Glow type Pulse-less type Swarming micro PD	Classic breakdown theory [Kön69] [Tan83]	
III	Corona-like type Pitting type	[Mor91] [Mor93]	Pitting type

- Pitting discharges: Start after some ten hours of discharge activity, characterized by a high repetition rate of several tens per millisecond and a very small pulse height.

In the insulation of high voltage apparatus, internal discharges may occur in gas-filled voids, delaminations, cracks, etc. Voids may have their origin from cast insulation like epoxy spacers in SF_6 bus bars, from dried out regions in oil-impregnated paper cables, from gas bubbles in plastic insulation, etc. Delaminations occur in laminated insulation like the stator bars of large electrical machines that are often composed of mica-based tapes with binding enamel like epoxy. Cracks could for example occur in mechanically stressed insulation, e.g. in loose stator bars that are vibrating.

Fig. 1.3 shows an example of partial discharges within an insulation system of a motor. These discharges might occur in any void between the copper conductor and the grounded motor frame. Voids may be located between the copper conductor and the insulation surface, or in the insulation itself, between the outer insulation surface and the grounded frame, or along the surface of the insulation.
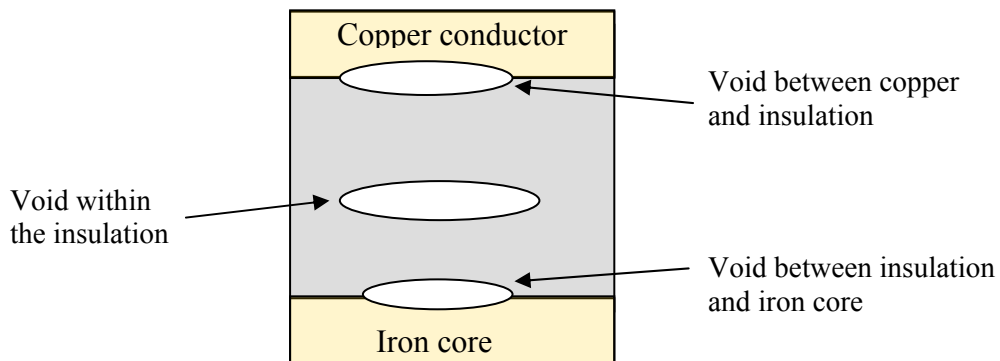
Fig1.3: Partial discharges within an insulation system

1.1.4   Electrical trees

Electrical treeing is an **internal discharge** that occurs in **polymeric insulating materials**. Treeing in a solid dielectric is a phenomenon, which results in the growth of a pattern of tiny channels (network of hollow branches with diameters of some μm) which eventually traverse the gap between the electrodes and cause a failure of the insulating system. The processes start with tree initiation in which an initial void is formed at a region of high electrical stress within the insulation, followed by the growth of branch structures consisting of **gas-filled tubules**. Electrical discharges within the tree structure drive the growth process until the tree structure reaches the opposite electrode. Electrical trees can initiate from voids within the dielectric as a result of a void discharge and also from metallic particles that lead to local field stress en-

hancements (at foreign inclusions). The growth of trees is related to the pressure inside the gaseous channels [Löf76, Lau81], to the number of detected partial discharge [McM64] and to the radius of the void tip [ElM82]. Electrical treeing in polymers is the most dangerous type of discharges because it inevitably leads to a complete breakdown of the insulation material.

Electrical treeing in polymers is a phenomenon that has been examined since more than three decades. Polymers and especially polyethylene are widely used as insulation for high voltage cables and many attempts have been made to improve the susceptibility of polyethylene against degradation via electrical treeing. The mechanism is explained as a result of **high energetic electrons** (accelerated in the electric field and often called **'hot electrons'** because their kinetic energy is much higher than that of electrons in thermal equilibrium with the surrounding material) **cleave bonds** and thus degrade the polymer by forming tiny hollow channels [Pat92], but there are still some open questions, especially with regard to the **influence of space charges** in this process.

If the electric field is sufficiently high – which means significantly **more than 100 kV/mm** – electrons gain sufficient energy in the electric field to interact with molecules, lead to an excitation and **break chemical bonds**. As a consequence the chains of the polymer are broken and **low molecular weight fragments** are formed that diffuse off and leave permanent hollow channels in which gas discharges may be ignited [Pat75]. In dependence on the actual conditions, different phenomena will prevail with the consequence of a different appearance of the electrical trees generated. In liquids small, non permanent gas filled voids may be generated [Pat07].

Fig. 1.4 shows an example of tree growth after PD measurements in a point-plane arrangement (gap of 2 mm) with low-density polyethylene (LDPE) filled with nano-particles. The specimen was aged with a stress voltage of 5 kV from several minutes (first photo) to some hours (last photo).
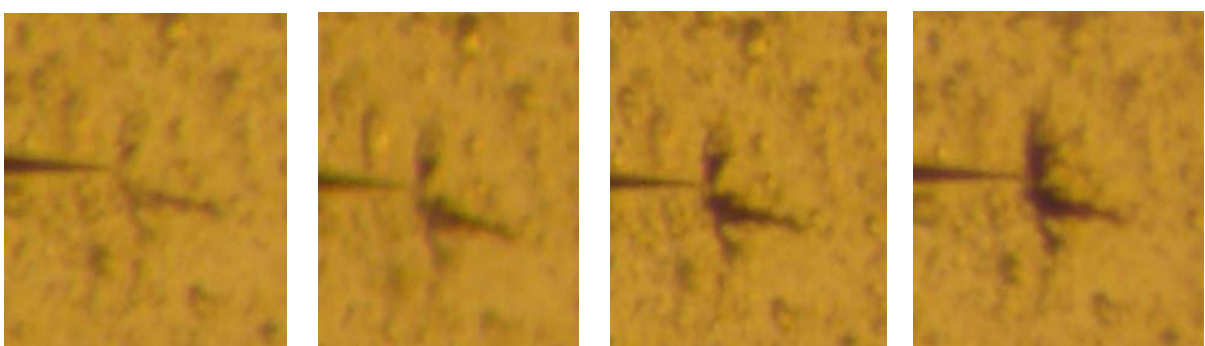
Fig. 1.4: Tree growth in low-density polyethylene LDPE

In electrical machine insulations the electrical treeing process causes fine erosion channels which propagate through the material. This phenomenon is often referred to as the most important degradation mechanism in solid polymeric insulation [Dis92, Dis97, Kan00, Suw96]. In this case the electrical treeing can start at rough structures of the inner conductor, locations of abraded outer varnish, metallic particles or other conducting contaminants, gas-filled voids or delaminations in the insulation.

1.2   Physics of partial discharges

A partial discharge is **locally confined breakdown** within a region of the insulating system where the local electrical field exceeds the **breakdown strength** of the dielectric material. Several theories were proposed by a number of researchers in an attempt to explain the electrical breakdown phenomenon. Some theories were based on the avalanche mechanism of breakdown [Hip37, Fro47, Sei49, Kle78], others on the pressure effects [Sta55], yet others on electromagnetic theory [Cro59] and fractals [Nie84].

The mechanism of the **electron avalanche**, described first by [Tow01] afterwards visualized by [Rae64], was introduced to explain the phenomenon of the discharges in gas. Since the most partial discharges occur in gas-filled volumes, the avalanche model describes well the physical process of partial discharges [Hoo97, Lau03]. According to this, there are two essential conditions that must be prerequisite for the occurrence of partial discharges. The first condition is the existence of **starting electron** (free electron) within the cathodic part of the critically stressed volume. The generation rate of these starting electrons, which are provided by thermal and field supported emission out of the surface [Nie95, Bru91], depends on the material and the characteristics of the surface [Tem00]. The second condition is the existence of a high voltage drop necessary to accelerate the electron to a **kinetic energy** which is sufficient to ionize gas molecules via particle collision.
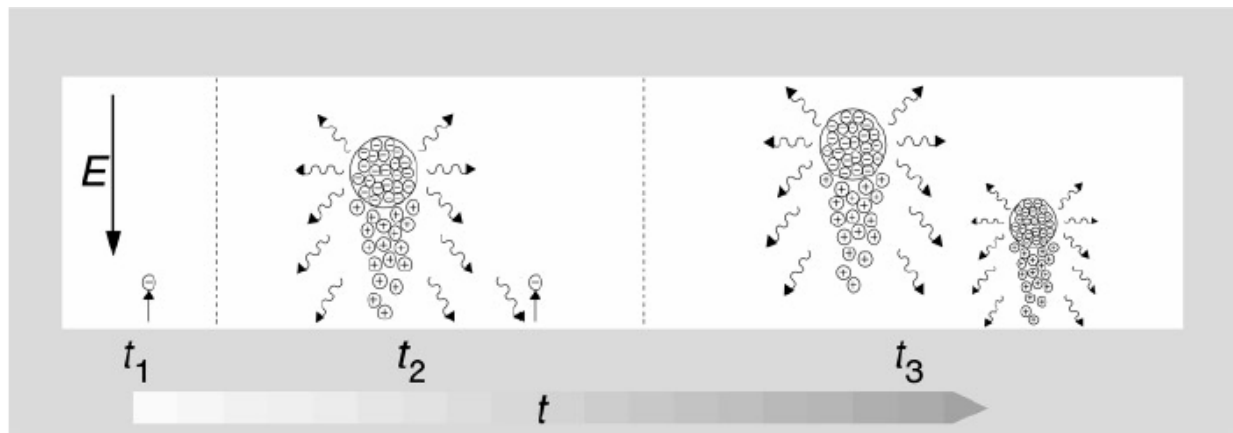
Fig. 1.5: Generation of starting electrons in flat cavities, after [Tem00]

If these two necessary conditions are fulfilled i.e. if a starting electron is available after having reached the inception field strength, a first electron avalanche will initially start (**Fig. 1.5**). A PD will develop out of this first electron avalanche, if enough secondary electrons are provided by the dielectric through photo-emission. Once the ionisation process has started, an exponential multiplication of charge carriers occurs within the critical region, resulting in a very fast current pulse that is restricted to a limited region in which the discharge conditions are fulfilled.

The development of the electron avalanche, and thus the discharge mechanism is influenced by several physical parameters of the discharge region and their complex interactions. Thus during this local breakdown charges are moved under the influence of the force of the electric field, they gain energy from the electric field and generate additional free charges by their impact on molecules. If the movement of these charges is not hindered, and the local electric field along the path of the moving charges is high enough the avalanche is accentuated and there will be a **complete breakdown** of the insulation.

In case the movement of the charges is hindered by parts of the insulation – mainly solid regions – or the local electric field is decreased due to geometric reasons, the moving charges immobilize and **local space charges** are generated that reduce the local electric field below the electric field necessary to sustain the avalanche. The discharge stops and only a **local breakdown**, the so-called **partial discharge**, occurs.

$$E(t_n) = \hat{E}\sin(\omega t_n) + \left(\Delta E_q + \Delta E^{\pm}\right)\,\exp\left(-\frac{\Delta t_{n-1}}{\tau_q^{\pm}}\right) \qquad (1.1)$$
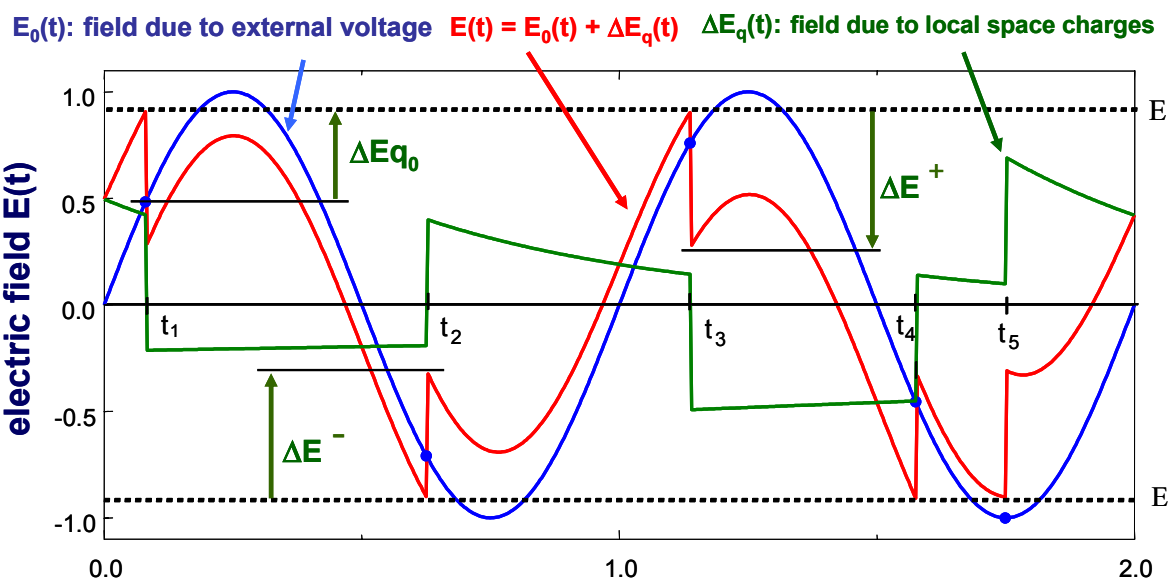
Fig. 1.6: Influence of the space charges on the local electric field

According to the **Poisson equation** space charges influence the local electric field by superimposing an internal DC field onto the externally applied AC field. Thus the actual value of the local electrical field within the specimen is determined by the external voltage, the geometric dimensions of the electrodes and local space charges within the electrode gap. As a consequence of these space charges, the highest local electrical stress in general will not occur at the peak value of the externally applied AC voltage. The unipolar space charge will reduce the local electrical field for one polarity of the applied voltage and increase it for the other polarity as shown in **Fig. 1.16**. As can be seen from the graph the field modifying space charge may change continuously with time or in discrete steps due to PD events. Numerical simulations of the processes discussed in this chapter lead to a correct description of PD processes in different specimens [Hoo97, Pat98, Pat02].

It has long been recognized that polymeric solid dielectrics are particularly susceptible to partial discharges, which may cause **irreversible material degradation** and finally may lead to a complete breakdown of the insulating system [Mas51]. The main deleterious influence is usually due to the de-polymerization of the dielectric, i.e. the production of **low molecular weight components** resulting from the bombardment of **high energetic electrons**.

1.3   Phenomenology of partial discharges

Not depending on the actual situation, i.e. degradation or not, the partial discharge generates a local short circuit and thus modifies the **local field distribution** within the specimen. This leads to a tiny drop of the voltage at the external connections of the object under test. The monitoring of the partial discharge is done by the measurement of the external current that is needed to restore the voltage across the specimen that had been present before the partial
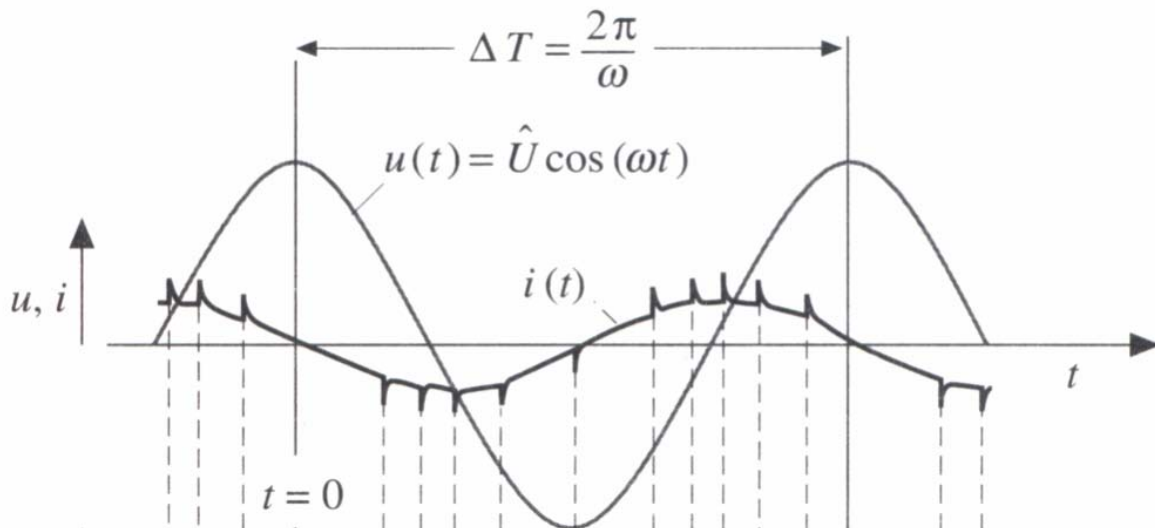
Fig. 1.7: Schematic representation of the PD current

discharge. A schematic representation of the current over time at the voltage terminals of a capacitive PD specimen during PD is shown in **Fig. 1.7**.

If an AC voltage is applied to the specimen and increased beyond the PD inception voltage, in addition to the capacitive component of the current pulse-like components occur.

The reason for the spikes in the current (pulse-like current components) is a 'short circuit' of a part of the insulating system that leads to a quick decrease of the voltage between the contacting electrodes. This leads to an external current that charges the specimen to the voltage level before the PD. The phenomenon can be described by an equivalent circuit.

1.4   Partial discharges equivalent circuit

Equivalent circuits consisting of a network of the basic elements capacitor, resistor and/or inductance are widely used in electrical engineering to explain the electrical phenomena. The commonly used equivalent circuit to describe internal partial discharge phenomena has been introduced in 1932 by Gemant & Philippoff [Gem32].
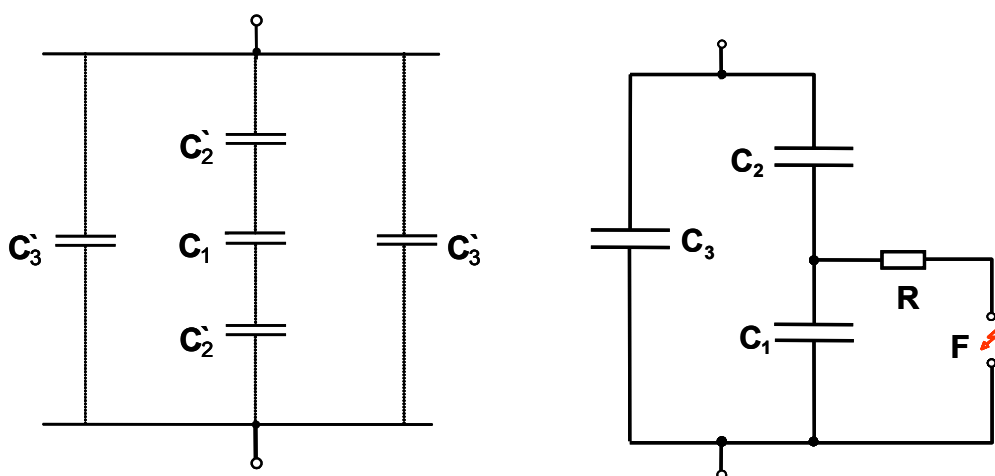
Fig. 1.8: Model for a simple insulating arrangement and classical equivalent circuit of a PD active specimen after [Gem32]

Fig. 1.8 shows the model for a simple insulating arrangement and the equivalent circuit. This model assumes the presence of a defect (void or cavity) in a solid or liquid insulating material. The defect can be represented with a capacitance C_1 connected in series with the capacitance C_2 of the sound insulation. The defect free insulation represented by a capacitance C_3 is connected in parallel to the series combination of C_1 and C_2. The spark gap F parallel to the capacitance C_1 characterizes the ignition of a partial discharge. The resistor R shown in series with the spark gap F limits the discharge current. The capacitors C_2' take into account the field

lines that emanate from the electrodes and end in the cavity. Their series connection leads to the capacitance C_2. The elements C_3' connected in parallel represent C_3.

The **real charge** ΔQ_1 moved on the site of the defect is given by the product of the capacitance C_1 of the void and the voltage diminution ΔU_1 at the void during the ignition of the spark gap.

$$\Delta Q_1 = C_1 \cdot \Delta U_1 \tag{1.2}$$

Since it is not possible to measure the charge at the site of occurrence, the classical approach to measure partial discharges is to determine the fluctuation charge at the specimen's terminals (**apparent charge** of the PD). The measured voltage change on the terminals of the equivalent circuit corresponds to:

$$\Delta U_3 = \frac{C_2}{\left(C_2 + C_3\right)C_1} \cdot \Delta Q_1 \tag{1.3}$$

The so-called **apparent charge q** at the terminals of the specimen can be related to the **real charge** at the site of the defect with:

$$q = C_3 \cdot \Delta U_3 = \frac{C_2 C_3}{\left(C_2 + C_3\right)C_1} \cdot \Delta Q_1 \tag{1.4}$$

Based on the empirical estimates $C_3 \gg C_2 \gg C_1$, the measured external voltage change ΔU_3 is in the range of **mV** to **Volt**, while the magnitude of ΔU_1 is much higher.

$$q \approx \frac{C_2}{C_1} \cdot \Delta Q_1 \tag{1.5}$$

If the terminals of the specimen are connected to a coupling capacitor, charges will flow from this capacitance to the specimen to compensate the voltage reduction. These charges can be detected as current impulses $i_t(t)$ or $i_c(t)$ in the circuit formed by specimen and coupling capacitor. The basic electric circuits for PD measurements are shown in **Fig. 1.9**. C_t is the capacitance of the specimen, C_c is the capacitance of the coupling capacitor and Z_m is the measurement impedance.
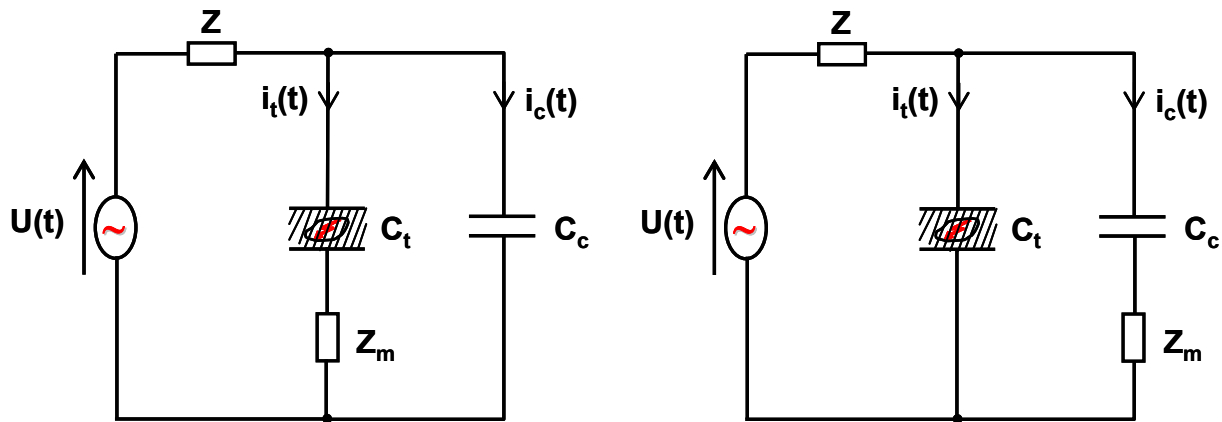
Fig. 1.9: Basic electric circuit for the PD measurements

The voltage drop ΔU_3 is more or less compensated by a measurable current $i_t(t)$ or $i_c(t)$. As shown in Fig. 1.7 the short duration circular current is not the only one that flows in the event of discharge in the specimen. The total current $i(t)$ is the superimposition of these mains frequency current and the PD current $i_t(t)$ or $i_c(t)$. The PD current is illustrated with strong magnification in the form of small peaks.

The relation between the real charge and the measurable charge is given by:

$$q_m = C_c \cdot \frac{C_2 / C_1}{C_2 + C_3 + C_C} \cdot \Delta Q_1 \tag{1.6}$$

With $C_3 \gg C_2 \gg C_1$, the measurable charge can be related to the apparent charge:

$$q_m = \frac{C_c}{C_C + C_t} \cdot q \tag{1.7}$$

The **measurable charge** i.e. the magnitude of the measurable PD circular current $i(t)$ depends on the ratio C_c / C_t. The value C_c / C_t is an essential quantity for the measuring sensitivity in PD testing. For sensitive measurements, a sufficiently large coupling capacitor should be installed, depending on the capacitance C_t of the test object. **Fig. 1.10** illustrates the influence of the coupling capacitor C_c on the measuring sensitivity q_m / q.
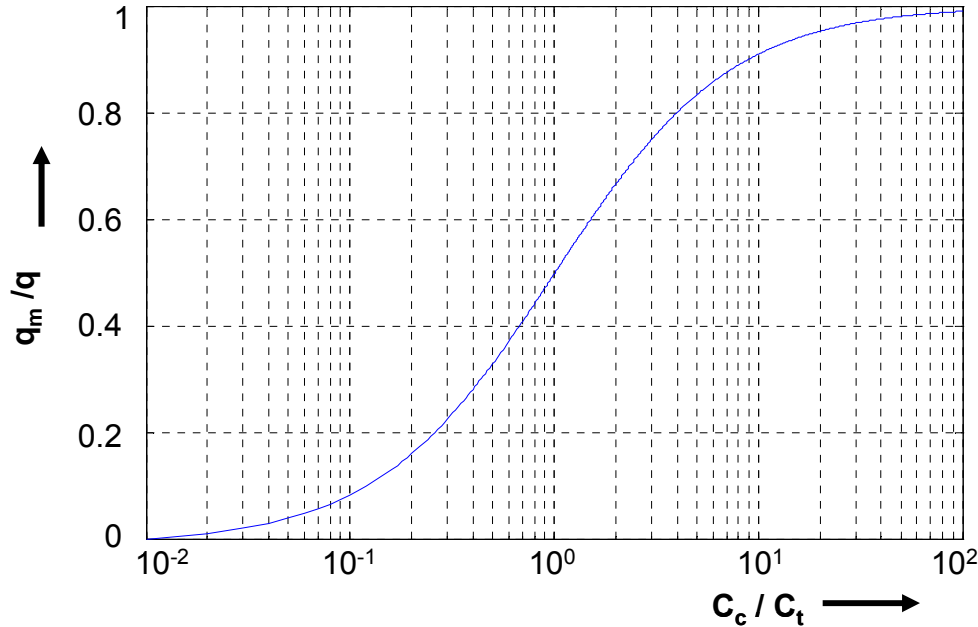
Fig. 1.10: Influence of the coupling capacitor C_c on the measuring sensitivity q_m/q

1.5 PD analysis and representation

PD measurements generate enormous amounts of data. Over the years different analysis methods and techniques have been developed in the aim to organize and to characterize these empirical data for the understanding of the PD phenomenon [Eng98, Kum02].

1.5.1 Stochastic analysis of partial discharges

Usually frequency distributions of accumulated data are considered and displayed as purely descriptive ϕ-q-n-patterns to extract information about the characteristics of defects as well as PD induced ageing of the insulating materials [Fru90, Kri97]. The usually comparatively broad distributions of the phase angles of occurrence are supposed to be a result of a statistical scatter in the discharge process.

The basic idea of all standard analysis methods is to accumulate discharge data collected during a certain recording time with numerous voltage cycles and to transform it into one reference cycle of the applied voltage, as shown in **Fig. 1.11**. Thus only phase angles between **0** and **360** degrees occur. This interval is divided into a certain number of phase windows. All discharge pulses are superimposed within this reference cycle, synchronized to the beginning of this cycle (phase angle ϕ = **0)**. Since no correlation between pulses in the same or different cycles of the applied voltage is taken into consideration **partial discharges are treated like independent events**.

The statistical distributions are usually analyzed by applying more or less meaningful parameters that quantitatively describe these distributions, and thus are assumed to be a characteristic **fingerprint** of the process. The parameters of interest are the pulse height q_i , the voltage U_i or the phase angle ϕ_i of each discharge pulse. The subsequent interpretation of the discharge activity consists in analyzing so-called **ϕ-q**, **ϕ-n** or the three dimensional **ϕ-q-n** patterns with some more or less meaningful statistical parameters (skewness, kurtosis etc.)[Gul95, Kre93]. In addition to this purely descriptive kind of analysis by means of a few parameters, computer-aided systems have been developed in which discretised **phase resolved distributions** are directly used as input for e.g. neutral network analysis [Pei95, Kra93, Kra06].
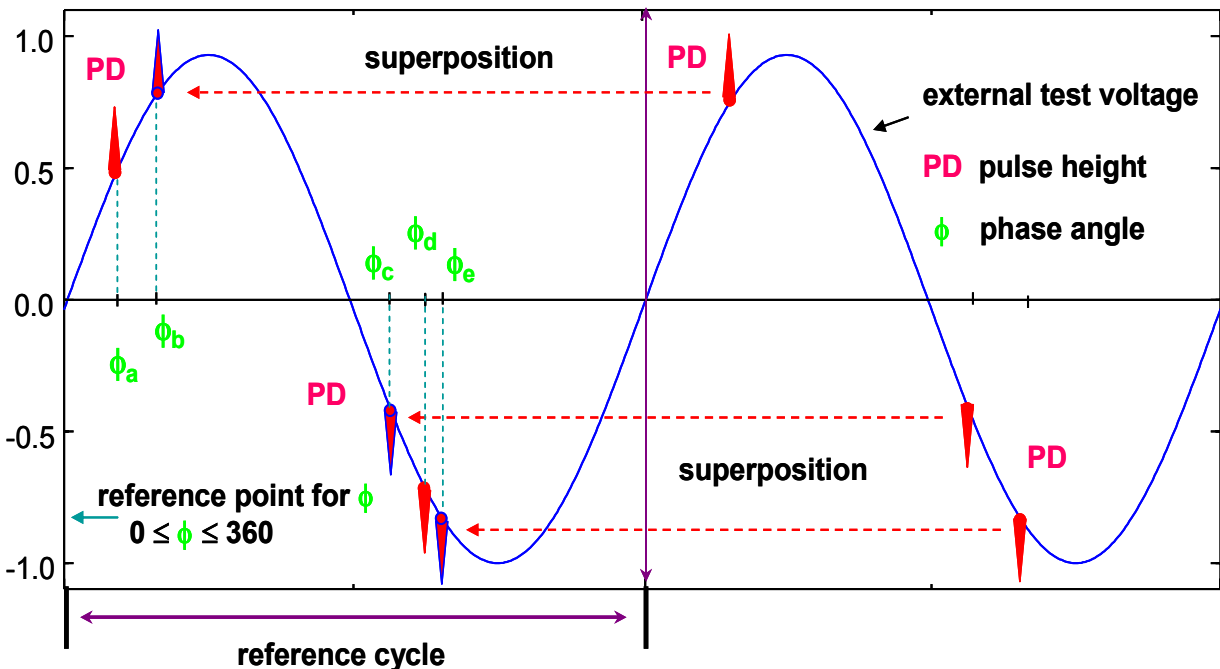
Fig. 1.11: Basic principles of the standard PD analysis methods

1.5.2   Pulse Sequence Analysis

The analysis of the sequences of partial discharges, first published in 1993 [Pat93a, Pat93b], revealed that there is much less scatter in partial discharge processes than anticipated. **Consecutive discharges** in a discharge site do usually **not occur at random** but in a **specific sequence that is characteristic for the local conditions at the defect site** and the voltage applied. Over the years several papers have been published, in which specific details of pulse-pulse-correlations were shown [Hoo94, Hoo95a, Hoo97a].

In contrast to the stochastic analysis, the characteristic parameters for the **Pulse Sequence Analysis** are not the phase angles with regard to the corresponding voltage cycle, or the absolute values of the applied voltage, but the **voltage changes** or the **time intervals** between consecutive discharge events and the corresponding **changes of the local electric fields**.

At first glance partial discharge processes seem to occur to a large extent at random. But this appearance is often due to the fact, that in many cases partial discharge processes are influenced by **local charge accumulations** in the region of the defect that are generated by the discharges themselves. Especially in solids these charges prevent the ignition of the next consecutive discharge until the field reset generated by the preceding discharge is overcome, either by a change of the external voltage or by a decrease of the local accumulation of charges.
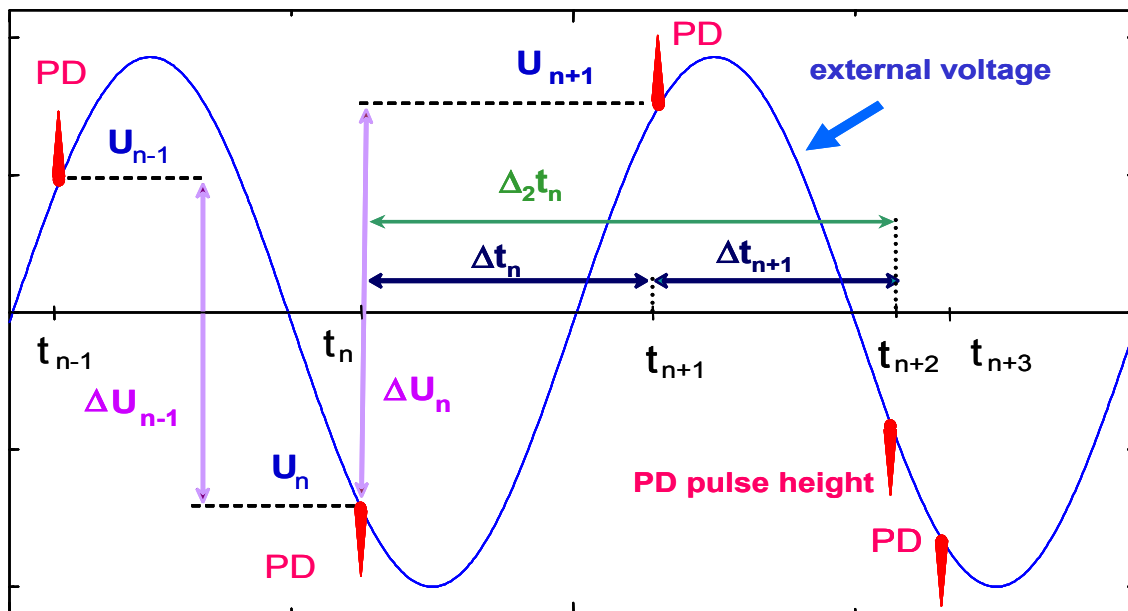
Fig. 1.12: Basic principles of the PSA method

Since space charges from the previous pulses that remain near the discharge site affect the ignition condition of the following pulse, strong **correlations between consecutive partial discharges** must be expected. Thus, taking external parameters, the most significant parameter is the **voltage change** which occurs before the next discharge because the corresponding change of the local electric field at the discharge site determines the ignition of the next discharge. Analyzing the sequence of discharge pulses and its change with continuing insulation degradation provides a better understanding of the physical processes in partial discharge phenomena. It reveals basic information on space charge build-up and decrease, the corresponding time

constants and the field modifying influence of positive and negative space charges as well [Pat94, Ben07].

The parameter used most frequently in the early times of the application of the **Pulse Sequence Analysis** is the change $\Delta\mathbf{U}$ of the external voltage between consecutive discharges [Hoo94, Asc00]. Since then many other parameters were introduced, such as the time difference $\Delta\mathbf{t}$ between consecutive discharge events and/or the combination of parameters e.g. $\Delta\mathbf{U}/\Delta\mathbf{t}$. More details of the **Pulse Sequence Analysis** and their applications to the analysis of partial discharges are described in chapter 3. **Fig. 1.12** shows the basic principles of the PSA method.

2   Partial Discharges, Measurements and Materials

This chapter describes the partial discharge detection setup and the different test objects used in this work.

2.0   Introduction

Partial discharges can be measured electrically, acoustically and optically. Electrical methods are widely used and complete test systems are available [Kön93]. Capacitive, inductive and capacitive-inductive sensor techniques are applied on-site both off-line and on-line. In electrical PD measurements the apparent charge due to a PD pulse is measured. A PD measuring system comprises of coupling device (sensor), transmission system (connecting cables or optical link) and measuring instrument (fast digitizer, computer, etc.). Instruments for apparent charge measurement can be characterized as narrow-band, wide-band and ultra-wide-band instruments [IEC00].

2.1   Partial discharge detection

Partial discharges are sparks (fast current pulses) with a rise time of a few ns and a half-value time of some tens of ns. The classical approach to measure partial discharges is to determine the apparent charge of the PD (fluctuation at terminals of the specimen) because usually it is not possible to measure the charge at the site of occurrence. This charge is transferred to the test circuit giving rise to current pulses through the measurement impedance. This impedance, in combination with the test object, the coupling capacitor and the PD detector, determines the duration and the shape of the measured voltage pulse [Bar02].

Measurement of the apparent charge is possible in many different ways, all of which are predominantly dependent upon the bandwidth of the PD measuring system used [Kön93]. There are thus basically two different principles available: PD measuring equipments measuring in time domain and those measuring in frequency domain.

2.1.1   Integration in the time domain

The PD current pulse shape can be theoretically described by a superposition of two exponential functions as follows:

$$i(t) = i_0 \left(e^{-\frac{t}{\tau_2}} - e^{-\frac{t}{\tau_1}} \right) \quad \text{with } \tau_1 < \tau_2 \tag{2.1}$$

Fig. 2.1 shows a representation of a waveform of a partial discharge pulse $i(t)/i_{max}$ and the corresponding charge q. T_1 is the time to reach the maximum value i_{max} and T_2 is the time to decay to the half-value $i_{max}/2$. The charge q is obtained in the time domain by integrating the waveform of the pulses (area below the current over time curve) as:

$$q = \int_0^\infty i(t)\,dt = i_0 \cdot (\tau_2 - \tau_1) \tag{2.2}$$

According to eqn.(2.2) the apparent charge is determined by the use of measuring instruments with very large bandwidth amplifiers. Due to the small number of commercially available instruments working on this principle (the bandwidth lies mostly above 1 MHz) their application to PD tests is not very common. The PD analysis is based on the possible relation between the ageing of the insulating material and the individual PD parameters by studying the waveform of the PD pulses [Mor92].

for: τ_1 = 5 ns and τ_2 = 15 ns

↓

T_1 = 8.2 ns and T_2 = 24.1 ns
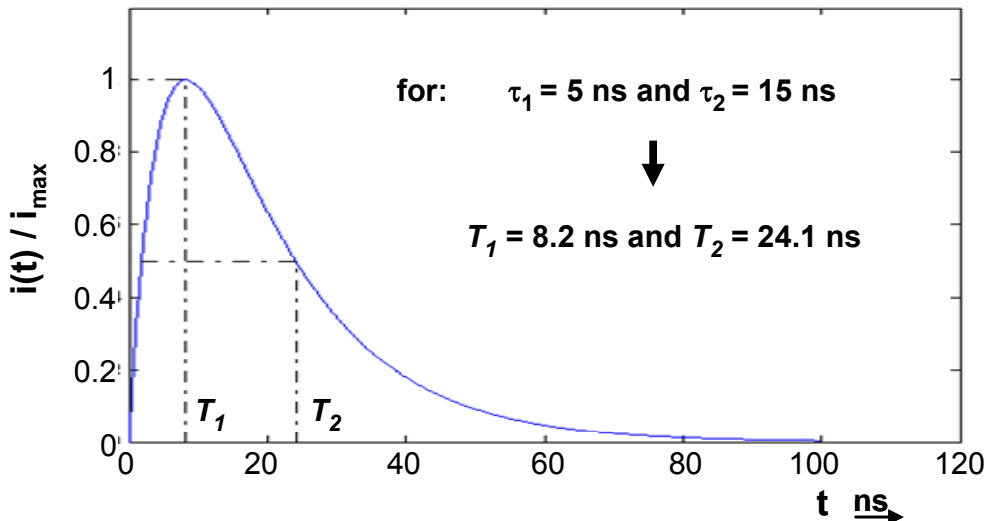
Fig. 2.1: Idealized PD current pulse

2.1.2   Integration in the frequency domain

According to this principle the determination of the apparent charge is based on the knowledge of the spectrum of the PD waveform. The complex frequency spectrum for a given non-periodic current pulse of PD can be obtained by the Fourier integral as:

$$\underline{F}(j\omega) = F\{i(t)\} = \int_{-\infty}^{+\infty} i(t)\,e^{-j\omega t}\,dt \tag{2.3}$$

$$\underline{F}(j\omega) = \frac{i_0 \cdot (\tau_2 - \tau_1)}{\sqrt{(1 + 4\pi^2 f^2 \tau_1^2) \cdot (1 + 4\pi^2 f^2 \tau_2^2)}} \tag{2.4}$$
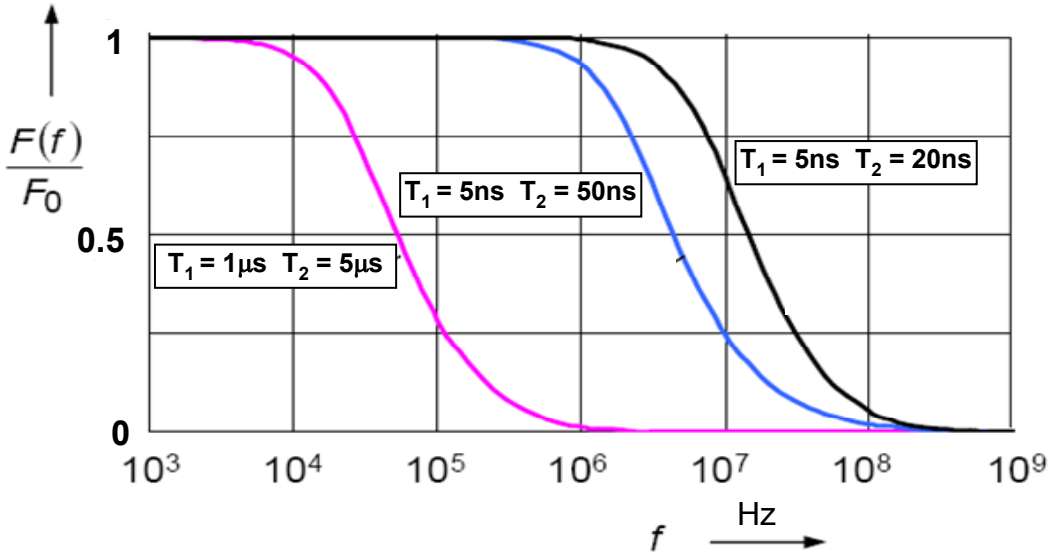
Fig. 2.2: Normalized spectral amplitude density $F(f)/F_0$

Fig. 2.2 shows the normalized spectral amplitude density $F(f)/F(0)$ plotted against the frequency for different values of T_1 and T_2. It may be seen that the amplitude frequency spectrum of a pulse is approximately constant up to a certain frequency and equal to the DC component $\underline{F}(0)$ at the frequency $f = 0$ Hz. It clearly shows that the DC content in the spectrum corresponds to the pulse charge q according to eqn. (2.2), eqn. (2.3) and eqn. (2.4) at $\omega = 2\pi f = 0$.

$$\underline{F}(0) = i_0 \cdot (\tau_2 - \tau_1) = q \tag{2.5}$$

Equipments widely used in PD measurement are according to eqn.(2.4). The integration takes place in frequency domain, which is also referred to as quasi-integration. The bandwidth of charge measuring instruments built on this principle is smaller than the frequency range of a PD pulse. Integration of the PD pulse is performed in most cases with so-called "wide-band" or "narrow-band" measuring systems (measuring impedance and measuring instrument). These are basically band-pass filter systems with electronic amplification [Kön93]. The choice of the measuring impedance (usually simplified as a resistance in the range of **100 Ω**) and the measuring instrument (amplifier) determine the order of the measuring system.

As example, the response signals for impulse excitation of the two idealized measuring systems (selectively wideband system and narrow-band system) are represented in **Fig. 2.3**. To determine the impulse response of the Dirac pulse of each system, the lower and the upper cut-off frequencies f_1, f_2 and the transfer factor A are considered. The amplitude A_0 of the transfer factor and the spectral amplitude of the Dirac pulse F are taken constant.
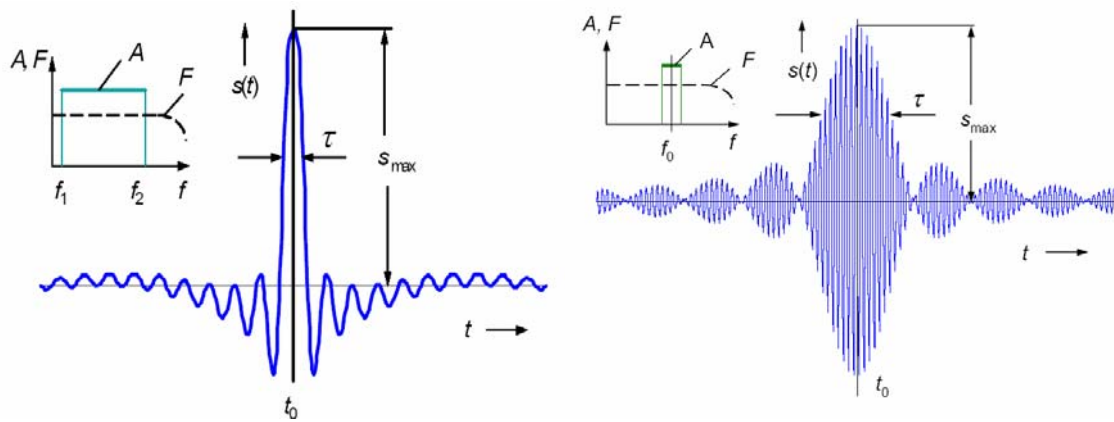
Fig. 2.3: Impulse response of an idealised selectively wideband system and narrow-band system (f_1 =10 kHz and f_2 =100 kHz , f_0 = 100 kHz and Δf = 9 kHz)

For demonstration calibration signals were registered with a commercially available PD detector Haefely type 561. The PD detector is equipped with an active wideband and two selected active narrowband band-pass filters. **Fig. 2.4** shows typical responses of calibration signals formed by the coupling device for a wideband band-pass filter with the frequency band **40 kHz** to **400 kHz** and for the two narrow-band band-pass filters with the frequency bands **130** to **170 kHz** and **70** to **80 kHz**.

The two active narrow-band band-pass filters are implemented to avoid interferences appearing frequently within certain limited frequency ranges or to find the resonance sites in the PD measuring circuit. With the use of the narrow-band band-pass filter it is possible to avoid frequent noise sources and select a centre frequency where the interference signals have minimal effect. A disadvantage of the narrow-band band-pass filter is that PD pulses cannot be distinguished according to their polarity.
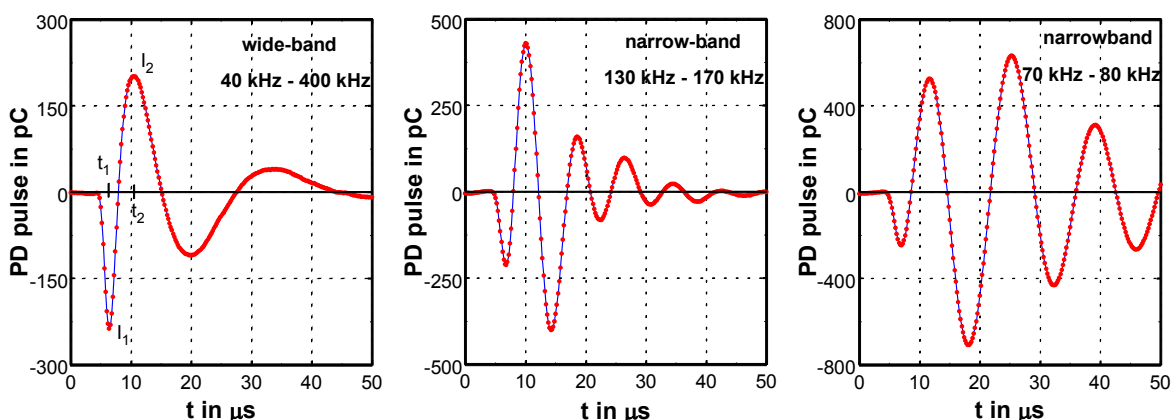
Fig. 2.4: Typical PD pulse responses of calibration signals for the different frequency bands

The active wide-band band-pass filter is implemented with a second order high- and low-pass filter with the cut-off frequencies **40 kHz** and **400 kHz**. Sufficient integration of the wideband band-pass filter is achieved with the upper cut-off frequency of the PD measuring device that is much lower than that of the spectrum of the PD pulses to be measured. The advantage here is that the PD pulses can be distinguished according to their polarity. The scaling of the peaks l_1 and l_2 is usually given in **pC** in accordance to the calibration process (see 2.4).

For all PD measurements reported in this work, the PD signals were registered with the active wideband band-pass filter with the cut-off frequencies **40 kHz** and **400 kHz**.

2.2   PD pulse shape registration

Conventional PD data acquisition and processing systems register the PD data continuously or register only the peak value of PD pulses [Hoo94] and the phase angles of the applied voltage at which PD events occur. The first system needs a large memory for the registration of the data and the second does not allow the registration of the PD pulse shape, which is very important for PD analysis [Pat02].

The PD measuring device used in this work records the actual voltage at which the discharges occur and the total shape of the PD pulse. It consists of an analog PD measurement device [Hae86], two separate simultaneous Analog-to-Digital (A/D) converters with a sampling frequency of **5 MHz** and **12** bits resolution, a logical event trigger circuit and a digital signal processor. The analog PD detector with integration in frequency domain and with selectable input ranges from **1mV** to **100 V** can be controlled either manually or via IEEE bus. The detector contains three selectable band-pass filters with frequency bands **40** to **400 kHz**, **130** to **170 kHz** and **70** to **80 kHz**. The digital signal processor controlled PD measuring system is a stand-alone data acquisition and processing system, which allows long-term measurements of the physically relevant parameters for PD analysis. The PD data acquisition and processing system contains a logic **event trigger circuit** that starts the measurement window. Each partial discharge pulse will be sampled **256** times with the sample frequency of **5 MHz** and stored together with a time stamp. A second channel stores the corresponding external voltage. After this the system waits for the next trigger signal. The time intervals between discharges can be calculated from the corresponding time stamps. After the registration of **4096** sample points, the data are transferred to the memory of the PC for the off-line PD analysis.

The output voltage $U_{PD}(t)$ of the analogue PD measuring device as shown in **Fig. 2.4** is a damped oscillation. The PD shape is registered with a sampling frequency of **5 MHz** i.e. with a time resolution between two sampling points of **200 ns**. This system allows the PD analysis in dependence on the shape of the PD pulses. The first and the second peak l_1 and l_2 of the PD pulse, the corresponding times of occurrence t_1 and t_2 (measured from the beginning of a seg-

ment) and the zero crossings t_3, t_4 and t_5 (see chapter 4) give information about the type and site of the PD.

2.3   PD measurement system

The experimental setup used in this investigation consists of the PD standard test circuit according to IEC 60270 [IEC00]. The complete measurement system and its components are schematically represented in **Fig. 2.5**. The measurement system is composed of the high voltage system and the PD detection system. The high voltage was supplied by a **100 kV** test transformer (MWB TEO 100/10). A second test transformer can be connected in cascade if more than **100 kV** is necessary. A laboratory built voltage ramp mechanism allows the linear increase in time of the sinusoidal **50 Hz** voltages with a pre-selected ramp rate.

To detect the apparent charge of the PD the setup is equipped with a commercially available PD detector (Haefely type **561**) [Hae86] and a two channel A/D converter **T3012** (resolution of **12 bits** and a sampling frequency of **5 MHz**) with acquisition hardware. When a partial discharge occurs in the test object (represented simply as a capacitor C_t) the charge is drawn from the coupling capacitor C_c (two **500 pF** HV capacitors in series) and generates a voltage impulse across the measuring coupling device (Haefely type **565**). Due to its comparatively high impedance and negligible stray capacitance the high voltage source cannot supply a compensation current for the voltage drop across the specimen caused by the PD. In order to avoid any external noise source (interferences), measurements are taken in an electromagnetically shielded test laboratory (PD cabin). The whole experiment is automated and controlled by a PC.
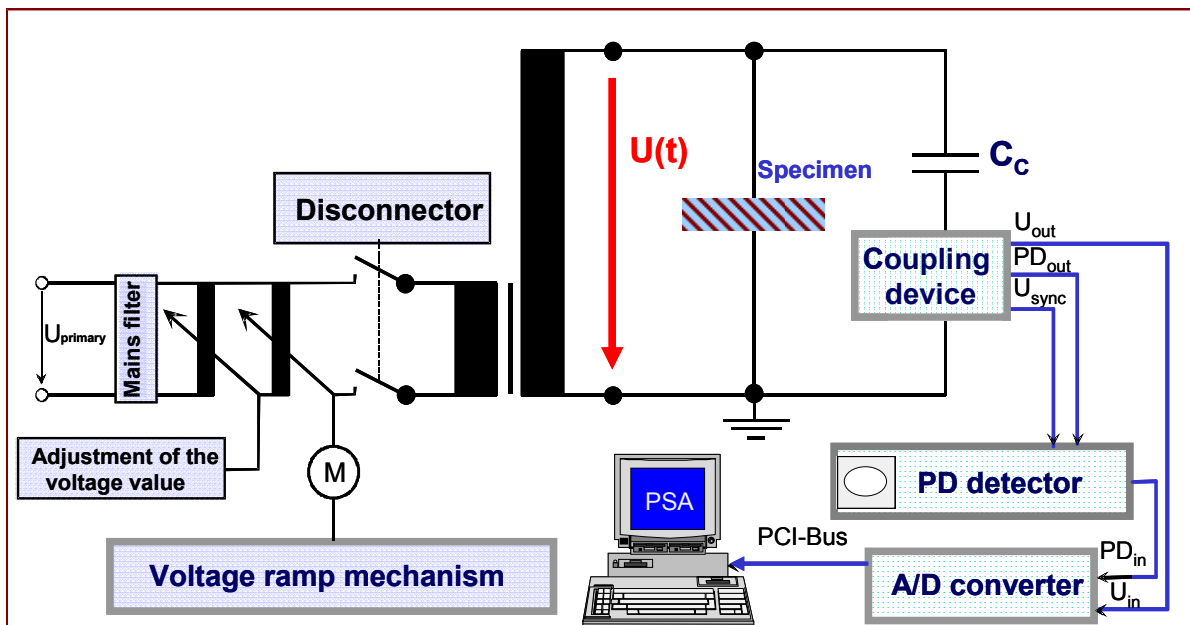
Fig. 2.5: Schematic representation of the PD experimental setup

The measuring coupling device may be placed either directly in series with the test object or in series with the coupling capacitance C_c. In the first case the measuring sensitivity is higher because the stray capacitances are parallel to the coupling capacitor C_c and thus add to its capacitance, but the disadvantage of this connection is that the equipment can be damaged by a puncture in the test object C_t. The coupling capacitor should be as large as possible to ensure a low impedance path for the PD impulses and also keep the voltage drop across the test object as small as possible. However, a large coupling capacitor loads the supply and should in this aspect be not too large (see chapter 1.4). The measurement charge is equally measured in series with C_c as in series with the test object if the stray capacitance can be neglected and if the impedance of the high voltage supply circuit is high compared to the capacitors [Pra73]. However, the sign of the voltage impulse is opposite in the two measurement circuits.

The output signals i.e. the complete sequence of discharge pulses (in general 4096 PD pulse shapes) with the corresponding actual voltage levels at which the PD pulses occur and the times of the PD events (time stamp) are automatically recorded. The measured values are stored on the hard disk of the PC in binary format, and then converted into a nine columns and 4096 lines ASCII matrix. In this nine columns matrix $[I_1, I_2, U, t, t_1, t_2, t_3, t_4, t_5]$, I_1 and I_2 represent the magnitudes of the first and the second peak of the PD pulse, U symbolises the actual voltage at which the discharge occurs (voltage level) and t the corresponding time of the PD event. The times t_1 and t_2 correspond to the first and the second peak of the PD pulse. The times t_3 and t_4 correspond to the zero crossings after the first and the second peak and the time t_5 marks the first data point of the signal that deviates from zero. These basic PD data are transferred to the PSA software for further analysis.

2.4 Calibration of the PD magnitude

The calibration process involves injecting a known amount of charge into the high voltage circuit and determining the voltage or current magnitude that is produced by the PD measurement system in response to the injected charge [IEC00]. The quantity of injected charge comes from a fast rise time pulse generator, which generates a voltage step V_{cal}, which is connected to the test object via a capacitor C_{cal}. The injected charge is $Q_{cal} = C_{cal}V_{cal}$. This calibration pulse is an important part of a partial discharge setup and is very decisive as far as the accuracy of the measurement is concerned. Thus, it is necessary to calibrate the system at the start of every experiment to get the exact corresponding charge value from the displayed voltage. The electronic calibrator used in the experimental is a Haefely PD calibrator type 451, with calibration charge magnitudes in the range between **2** and **2000 pC**. The peak height I_1 of the oscillating signal produced by the injected charge divided by this charge amount gives the sensitivity in **mV / pC**

The relation between the actual measured charge $\mathbf{Q_{meas}}$ and the calibration charge $\mathbf{Q_{cal}}$ in the circuit with the coupling capacitor is given by the capacitances in the circuit (specimen capacitance $\mathbf{C_t}$, calibrator capacitance $\mathbf{C_{cal}}$ and the coupling capacitor $\mathbf{C_c}$).

$$Q_{meas} = \cfrac{1}{1 + \cfrac{C_t + C_{cal}}{C_c}} \; Q_{cal} \tag{2.6}$$

Usually $\mathbf{C_c} \gg \mathbf{C_t} \gg \mathbf{C_{cal}}$ holds, so the condition $\mathbf{Q_{meas} = Q_{cal}}$ is fulfilled.

2.5   Test objects

To study partial discharge phenomena, different PD experiments were performed with small laboratory specimens (e.g. a needle in polyethylene and needle in epoxy resin) as well as with commercial apparatuses (stators bars of high voltage machines, stator coils of small motors, AlN cooling devices and HV transformers).

2.5.1   Laboratory specimens

Polymeric insulating materials are widely used in power apparatuses due to their advantages in electrical and mechanical properties. Partial discharge investigations in polymeric insulation materials have been performed since decades because the application of polymeric materials in electrical apparatus increased. However, the PD characteristic during electrical treeing, the relevant degradation process in dry polyethylene, is still of interest, because the analysis of partial discharge processes is helpful to understand the degradation phenomena and thus can be used for improvement of materials.

To study electrical treeing in polymeric materials, a needle plane arrangement with an electrode gap of **2 mm** was used. Needle tests are generally applied to imitate conductive or semiconductive protrusions in cable or accessory insulations or at interfaces. The insulating materials examined were the low density polyethylene (**PE**) and/or the epoxy resin (**EP**) in which a needle of about **5 μm** tip-radius was moulded. Polyethylene is the polymeric insulating material that is widely used as solid insulating materials in power cables and epoxy resin is widely used as an insulating material for rotating machines.

The laboratory samples were produced according to the following procedure:

The polyethylene granules and/or epoxy powder were poured into a hollow support (mould) with parallelepipedic shape from stainless steel (**23 x 7 x 2 cm³**). Five needles were fixed per-

pendicularly to the upper surface of the support. The distance between the tips of the needles and the lower surface of the support was **2 mm** (**Fig. 2.6**).

The arrangement is introduced into a vacuum chamber to undergo a degasification under a pressure of about 200 mbar for two hours. This degasification makes it possible to minimize any impurity due to the atmospheric environment (oxygen, moisture...). The system (always under vacuum) is then heated up to a constant temperature of about **160°C** for **24 hours**.
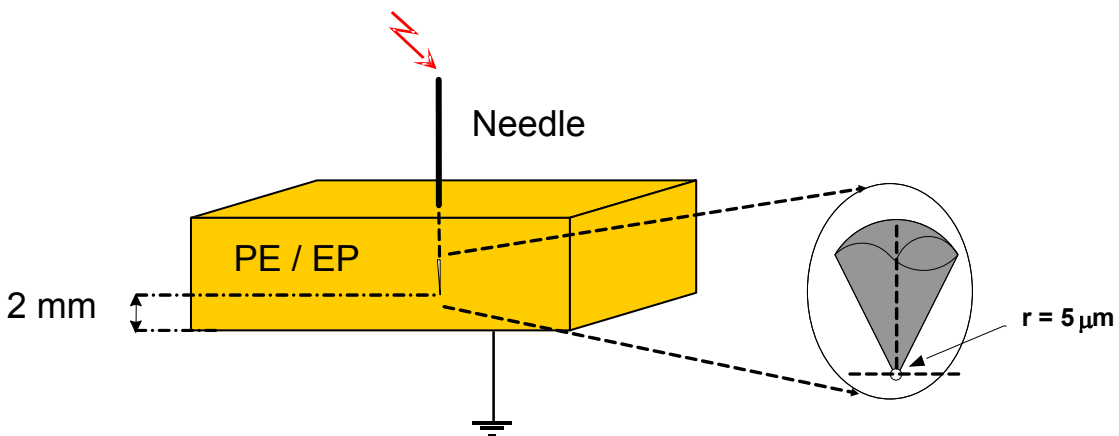
Fig. 2.6: Needle with **5 μm** tip radius embedded in polymeric insulating materials
(**PE** polyethylene / **EP** epoxy resin)

During this stage of heating, the polyethylene grains and/or the epoxy powder undergo a transition phase and form a homogeneous rod. In the case of epoxy powder, the specimens must be hardened for about **5** to **6 h** at **180 °C**. After cooling and solidification, the rod of **20 cm** can be cut into five samples of dimensions **40** x **40** x **10 mm^3**. In order to get a good electric contact, a circular electrode was fixed opposite to the needle.
To measure partial discharges a high voltage is applied to the needle and the circular electrode is connected to ground.

2.5.2   Stator windings

One of the main causes of generating unit shutdown in an electric machine is a stator winding failure. The principal function of a stator winding coil or bar is to provide a conductive path for the currents (to create the rotating magnetic field in the case of motors or the induced in it by the rotating magnetic field in the case of generators). Winding designers have gone to great lengths to make sure they put in as much copper and as little insulation as possible in each coil or bar. The construction chosen depends on the size of the machine and economics. Medium to

high voltage machines are usually made with form-wound coils or bars, while lower voltage machines tend to contain random-wound coils [Cha88].

In order to diagnose stator winding conditions, PD experiments were performed in two test objects: stator windings of small motors and stator bars of large rotating machines.

2.5.2.1   Stator windings of small AC motors

Small AC motors (less than **1 kW**) are usually single-phase motors. They are generally confined to applications with low or very low ratings, mainly in small machines, domestic applications and office machines. In industrial drives they are used as servo-motors, primarily for driving electric tools.

The stators in the low voltage AC motors consist of wire coils usually randomly wound; their task is to produce a rotating magnetic field [Mue03]. The three main components in a stator are the copper conductors (although aluminium is sometimes used), the stator core (thin sheets of magnetic steel) and the insulation (usually varnish or various mixtures between epoxy resins and mica paper). Electric insulation is one of the most vulnerable components in stator windings. The expected life of a stator winding depends on the ability of the electrical insulation to prevent winding faults. The need to examine the stator windings during the production of motors as early as possible is therefore necessary in order to recognize failures before further manufacturing steps will go through. Off-line partial discharge measurements are widely recognized as a testing method for identification of those types of failures [Sto02].

Fig. 2.7: Stator windings of a small motor and a schematic representation
of the electrical connection

Fig. 2.7 shows a photo of the examined test object and a schematic representation of the electrical connection during the PD measurements. The specimens are **125 W** stators of commercial single-phase AC motors. The corresponding rated voltage is **230 V**, the rated current is **0.47 A** and the insulation class is **H** (**180 °C**). **Tab. 2.1** contains more characteristic values.

The stator of this motor consists of two windings, a main winding usually connected to ground potential and an auxiliary winding usually connected to high voltage during the PD measurements. This electrical connection allowed to get less deformed PD signals due to the small capacitance of the auxiliary winding. The iron core is always connected to the ground potential.

Tab. 2.1: Characteristic values of the stator [Dan00]

Parameters	Auxiliary winding	Main winding
steel thickness	0.6 mm	
package height	40 mm	
conductor material	copper	
insulation material	+++	
insulation thickness	> 0.0019 mm	> 0.0245 mm
number of windings	172	403
wire diameter	0.335 mm	0.580 mm
wire with insulation diameter	0.397 – 0.411 mm	0.635 – 0.653 mm
resistance	16.57 Ohm	16.28 Ohm
tolerance	5 %	5 %

2.5.2.2   Stator bars of high voltage machines

The stator bars of high voltage machines consist of copper conductors which are (under a vacuum impregnation process) wound with a composite insulation material, i.e. fine mica glass fabric and epoxy resin (epoxy-bonded mica tapes) [Sto02]. **Fig. 2.8** illustrates an example of the internal structure of the winding insulation with half-lap tape wrapping and conductive coating [Vog06].
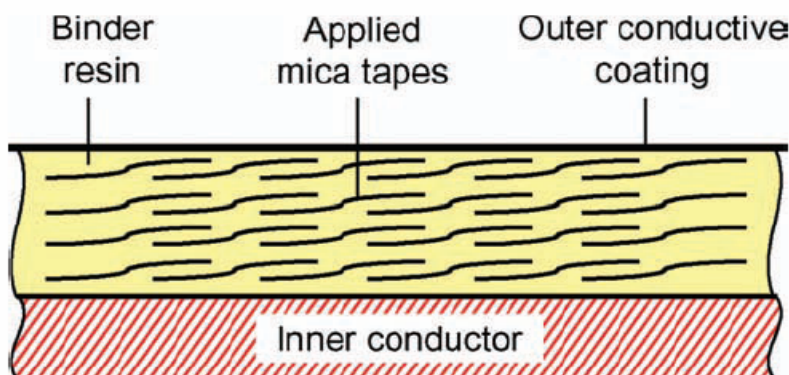
Fig. 2.8: Structure of winding insulation, after [Vog06]

The main wall insulation consists of three basic components, a barrier that is resistant to partial discharges and tree growth, a support material that gives mechanical strength, and a binder resin that fills any voids between the mica and the support material.

The model stator bars used in this investigation belong to an insulation system with a rated voltage of **13.8 kV** (phase to phase). The bar insulation is based on the epoxy VPI technology (Vacuum Pressure Impregnation) in which the winding is impregnated with the epoxy to seal the winding against moisture [Wei06, War00], according to manufacturer's standard.

The schematic representation of the examined stator bars is given in **Fig. 2.9.** The specimens were **1400 mm** in length and have the dimension of **40 x 17 mm^2** in lateral size. The length of the main insulation is **850 mm** and the thickness is **2.1 mm**. The ends of the stator bars (**180 mm**) were wound with semi-conductive anti-corona insulating tape to prevent surface discharges. The surface of the main insulation area was coated with conductive anti-corona varnish. A guard ring was established at both ends to avoid edge effects. The capacitance of the model stator bars was about **1.4 nF** at **50 Hz**. Their insulation class is **F (155 °C)**. To measure partial discharges, the high voltage was applied to the inner conductor and the outer corona protection varnish was connected to ground potential.
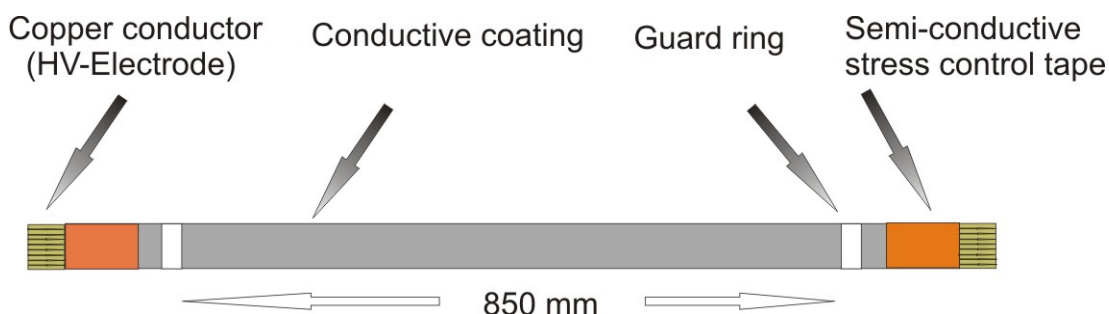
Fig. 2.9: Schematic representation of stator bar

2.5.3   AlN cooling devices

Aluminium nitride (**AlN**) is a newer material in the technical ceramics family. While its discovery occurred over 100 years ago, it has been developed into a commercially viable product with controlled and reproducible properties within the last 20 years [Jon95]. It has a high thermal conductivity (**200 W/mK**) combined with a high electrical resistivity (about **1 kΩcm**) and outstanding corrosion resistance in most chemical environments [Rue99]. The outstanding and unique combination of electrical, thermal and chemical properties of Aluminium nitride makes it an ideal material for a number of industrial applications. Successful applications encompass

diverse industrial and varied operating conditions such as: heat sinks, microwave packages, DBC substrates, liquid-cooled cooling devices for semiconductors and other applications.

The examined specimens are octagonal slabs (**100** x **115** x **15 mm³**) with a particular shape as shown the **Fig. 2.10**. The system is filled with a solution of water with 50% antifreeze. In order to have a good electric contact, the AlN cooling device was contacted on both sides with polished brass disks of a thickness about **5 mm** and a diameter of **70 mm**. To measure partial discharges the high voltage is applied between the water solution inside the cooling device and the grounded brass disks at the outside. A high voltage gradient exists then between the water-filled inside of the cooling device and the disk electrodes.
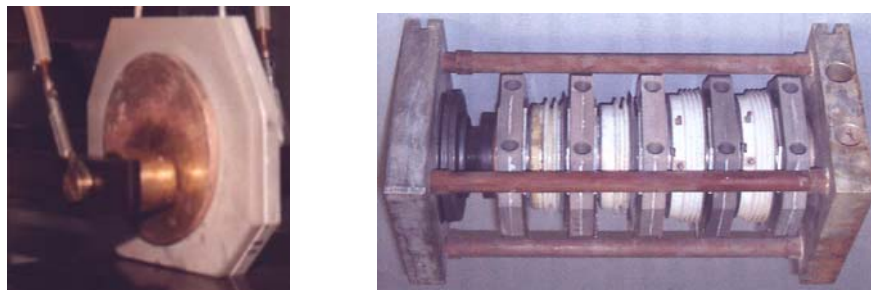
Fig. 2.10: Photograph of a single AlN cooling device during measurement and a complete press-pack

2.5.4 High voltage transformers

High voltage transformers convert power-level voltages from one level or phase configuration to another. They can include features for electrical isolation, power distribution, and control and instrumentation applications. The electric insulation in transformers is one of the vulnerable components which are subject during the service to different ageing mechanisms (thermal, mechanical, environmental and in particular electrical stresses) that eventually may result in local degradation phenomena. The insulation system in oil-impregnated transformer consists primarily of organic dielectric materials, including mineral oil and cellulose-based materials such as pressboard, paper and wood, used for creating supports and cooling ducts for the windings [Kuf84]. An appropriate description of the dielectric situation in a HV transformer with paper-oil insulation is given by the **XY-model** that describes the different geometries of the different dielectric materials contained in the insulation [Gae05]. These organic materials will deteriorate over the operating lifetime of the transformer and their insulating properties deteriorate as a result. Paper in particular may deteriorate rapidly if the operating temperature is high in oil-impregnated insulation [Jam97, Sah99].

Partial discharges in HV transformer are generated due to fault conditions related to moisture or surface contamination at the terminals, cavities (voids or cracks) in the solid insulation, metallic particles or gas bubbles within liquids and delaminations at interfaces [Lun00, Fuh05].

PD measurements were performed on two commercial **100 kV** high voltage test transformers used in cascade (MWB TEO 100/10) used as well as high voltage source and as a test object.
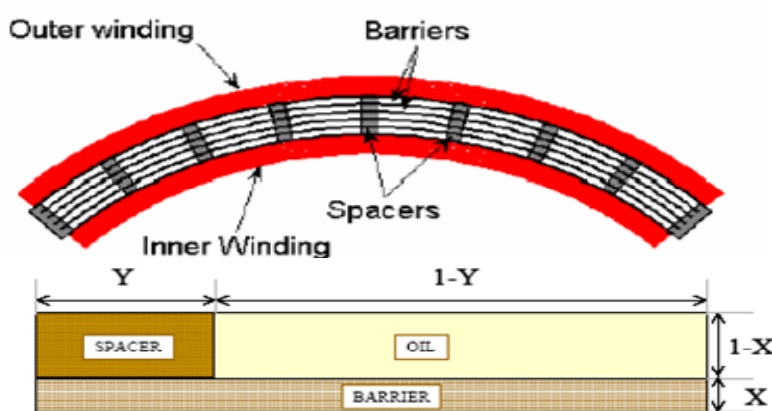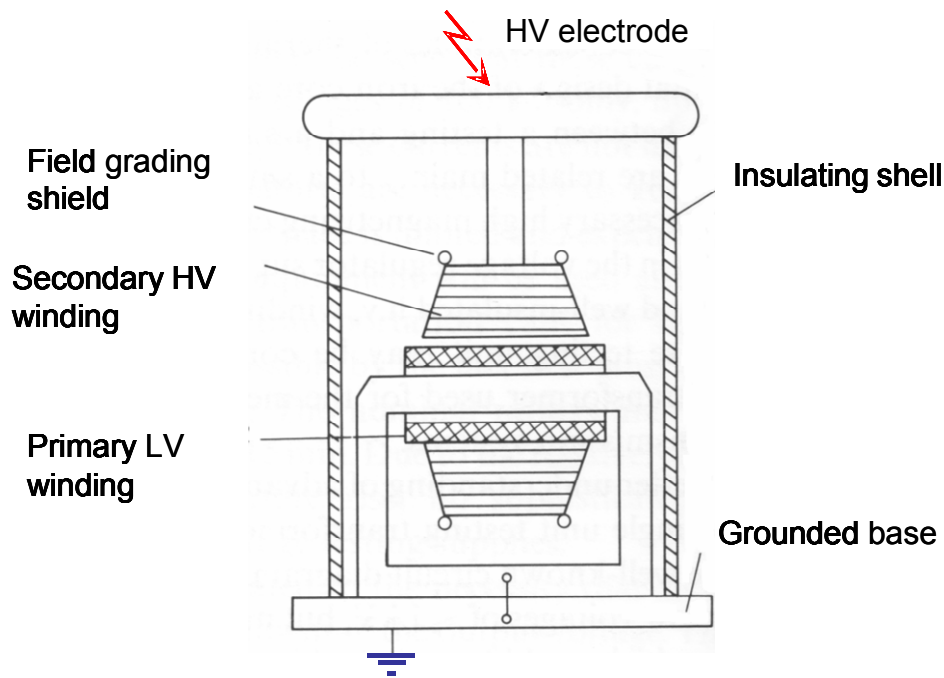
Fig. 2.11: 100 kV test transformer TEO 100/1[MWB85] and a segment of transformer insulation and **XY**-model of the transformer insulation (after [Gae05])

The main characteristic values of the transformers are contained in **Tab. 2.2.** A schematic representation of the **100 kV** test transformer with a segment of transformer insulation and the **XY**-model of the transformer insulation (with paper-oil-dielectric) are illustrated in **Fig. 2.11**.

Tab. 2.2: Characteristic values of the transformer

parameters	characteristics
Type	LT
Frequency	50 Hz
Ind. appl. test voltage	120/3 kV
Rated voltage	2x0.22/100/0.22 kV
Rated current	2x11.4/0.05/15,1 A
Rated output	5 kVA
Impedance voltage	3.5 %

3 Pulse Sequence Analysis

This chapter is devoted to the presentation of the PSA software and its use as a tool to analyze the partial discharge data.

3.0 Introduction

Basically partial discharges are processes that occur under well-defined conditions (only in few cases starting electrons that may occur at random are of importance). The problem with the analysis of measurement data is that in most cases not all relevant data are collected and evaluated. Hence the **Pulse Sequence Analysis** has been developed to analyze the enormous amounts of data and to separate different defects. The ideal way to display and analyze these complex data is the use of an adequate software. In this context and in order to facilitate the data processing and analysis a software program based on JAVA has been developed [Hij06]. The main interest of this software is not just a presentation and visualization of the sequence correlated parameters, but also to have a suitable tool to select the individual sequences from the data sets which give a better insight into the physics of the local degradation processes in order to characterize partial discharge phenomena.

In the following a general description of the PSA software will be explained. Then a more detailed description of the correlated parameters of the Pulse Sequence Analysis using the PSA software will be given. The analysis starts first with 'simple' frequency distributions of different parameters like the externally applied voltage load and pulse height derived from the data set as a whole. Then the sequence correlated data such as voltage differences or time differences between consecutive discharges and combined parameters will be discussed.

3.1 Software description

The PSA software is written in the object-oriented JAVA language [Kru00]. It is essentially a graphic program built on a structured treatment of data. Its function is the presentation of the PD data for the analysis in visual form. This informative software has an intuitive and versatile interface and is rapid and easy to use. The PD data are first loaded from virtually any program or database, then different parameters will be adjusted and with only a single click on the scatter plot button or on the histogram button the corresponding graph will be created.

In order to display sequences of PD data and to represent the different possibilities of the correlations between pulses, the software is programmed to be able to extract the derived parameters from the main parameters (raw data), to filter the PD data and to make mathematical op-

erations between different parameters. The scatter plots and the histograms are regarded as a better graphical representation for the analysis of the pulse sequences.

The main parameters are: $[I_1, I_2, U, t, t_1, t_2, t_3, t_4, t_5]$

The derived parameters are: $[t_2 - t_1, |I_2| / I_1, \Delta U, \Delta t, \Delta U/\Delta t, U_{rms}, t_{mod20}, \phi]$

with $\Delta U_{(n)} = U_{(n+1)} - U_{(n)}$ and $\Delta t_{(n)} = t_{(n+1)} - t_{(n)}$

The schematic block diagram of the PSA software is shown in **Fig. 3.1**. The current program contains four subsystems: the data processing, the filter operations, the mathematic operations and the graph plotting. After the main data processing, the result can be sent directly to the graph plotting for printing the selected graph or for an additional processing in the filtering management or in the mathematic operations management.
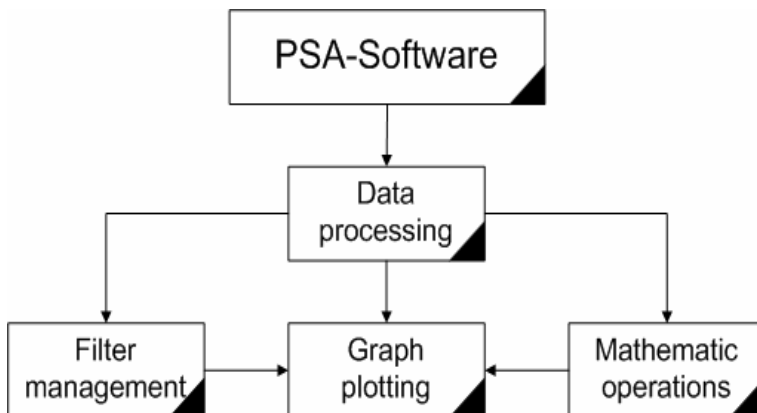
Fig. 3.1: Block diagram of PSA software

3.1.1   Data processing

Fig. 3.2 shows the flow chart of the main data processing. The PD data are imported from the database as a nine columns ASCII matrix. The elements of the matrix are $[I_1, I_2, U, t, t_1, t_2, t_3, t_4, t_5]$. The elements I_1 and I_2 are respectively the magnitude of the first and the second peak of the PD signal; U is the voltage level at which the discharges occur; t is the time at which the discharges occur (beginning of the voltage ramp as reference); t_1 and t_2 are the times corresponding to the first and the second maximum of the PD impulse respectively and t_3 and t_4 to the zero crossings of the PD pulse after the first and the second peak; t_5 is the time of the first data point of the signal that deviates from zero. The software is also able to read the old PD data with a six columns ASCII matrix (without the times of the zero crossings).
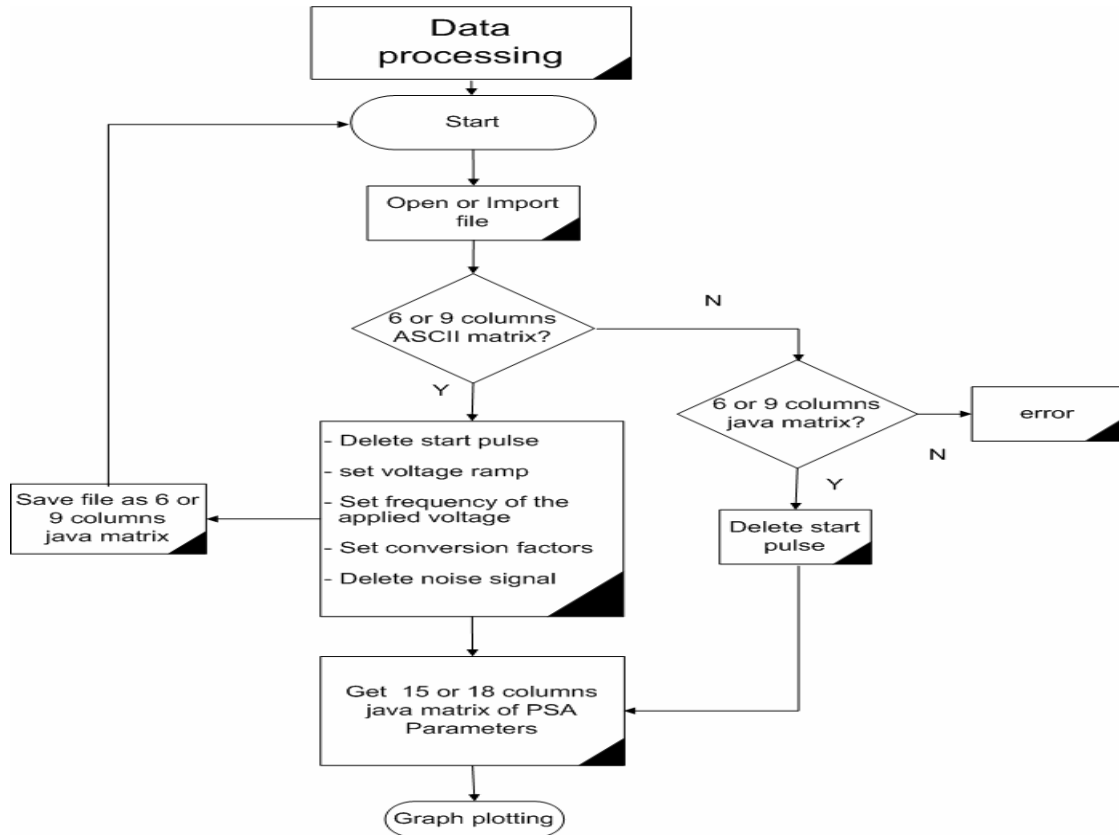
Fig. 3.2: Flow chart of the data processing

After loading the PD data and before printing any graph, some operations must be done to adjust the different parameters:

1. **Delete the start impulses**: In order to register the reference time of the beginning of the voltage ramp and the reference time-stamps of the PD events, artificial start impulses were created. The first step in the data processing is to remove these artificial impulses from the data sets.

2. **Set the applied voltage ramp:** Partial discharges measurements with the ramped applied voltage are a practical and effective method to characterize the PD-defects in technical objects. Here, the change of partial discharges in dependence on the magnitude of the applied voltage is particularly interesting. The second step in the data processing is the setting of the slope of the applied voltage ramp.

3. **Set the frequency of the applied voltage:** Usually the frequency of the applied voltage is **50 Hz** but partial discharge measurements can be done at different frequencies.

4. **Set the conversion factors:** Since one can not directly measure the pulse height in **pC** and the voltage level in **kV**, the readings of the pulse height must be converted from

mV to **pC** and the units of the applied voltage from **mV** to **kV** according to the calibration factors.

5. **Delete the noise signals:** Partial discharge measurements are usually performed with a high sensitivity to enable the registration of small partial discharge signals. In dependence on the trigger level more or less noise will be contained in the data sets. One method to remove these non-desirable impulses is to delete the pulses corresponding to $t_1 < 0$ (for more details see chapter 4).

Then, the calculations of the derived parameters ($\Delta U, \Delta t, \phi$ etc.) can be started. At the end, a list with 18 parameters (called PSA parameters) is obtained. This list can be sent to the plot management (graph plotting) or to an additional processing (filtering management or mathematic operations management.

3.1.2   Filter management

The use of the pulse shape of the PD signal to separate noise from real PD signals or to separate PD signals from different sources can often be done via Pulse Sequence Analysis [Pat03]. Also in many cases the evaluation of the sequences of a small number of consecutive dis-
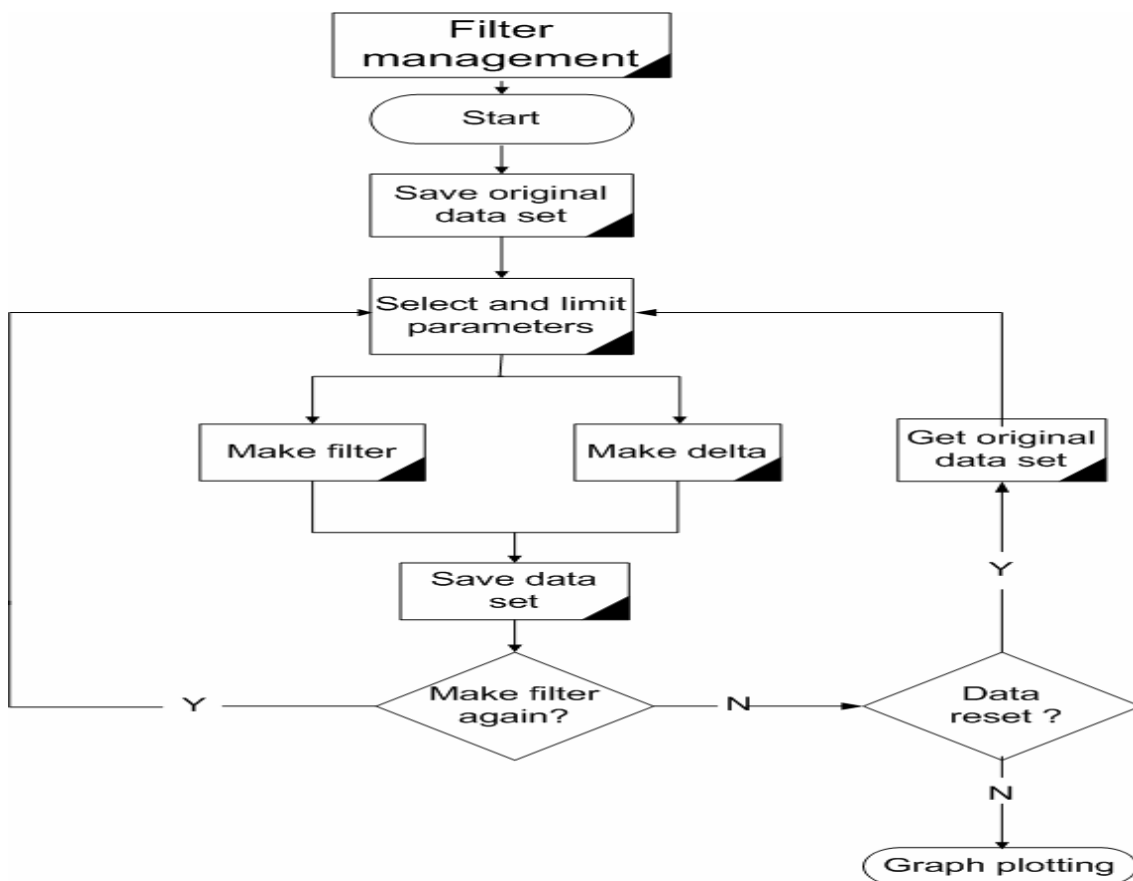
Fig. 3.3: Flow chart of the filter management

charges is more meaningful instead of the evaluation of a huge number of discharge pulses accumulated without taking care of the sequence [Ber01]. In this context the PSA software is equipped with a mathematical tool which makes the selection of any range of each PSA parameter possible in order to be analysed separately.

Fig. 3.3 shows the flow chart of the filter management. After choosing the PSA parameter from the list and the selection of the desired range domain, the filter function can be done with or without a new calculation of the voltage difference and/or the time difference between consecutive discharges. Sometimes the recalculation of the delta parameters is not necessary (i.e. **ΔU** and/or **Δt**) if only the behaviour of the discharge packets is taken into consideration and not the correlation between consecutive discharges. The results are saved in the offset memory and the operation can be done many times to filter again or can be reset to get the original value. The final result can be sent to the graph plotting for the selected printing.

3.1.3 Mathematic operations

In many cases, the use of more than one basic parameter is advisable for PD analysis. The use of combinations of sequential parameters is more or less useful to get additional information in
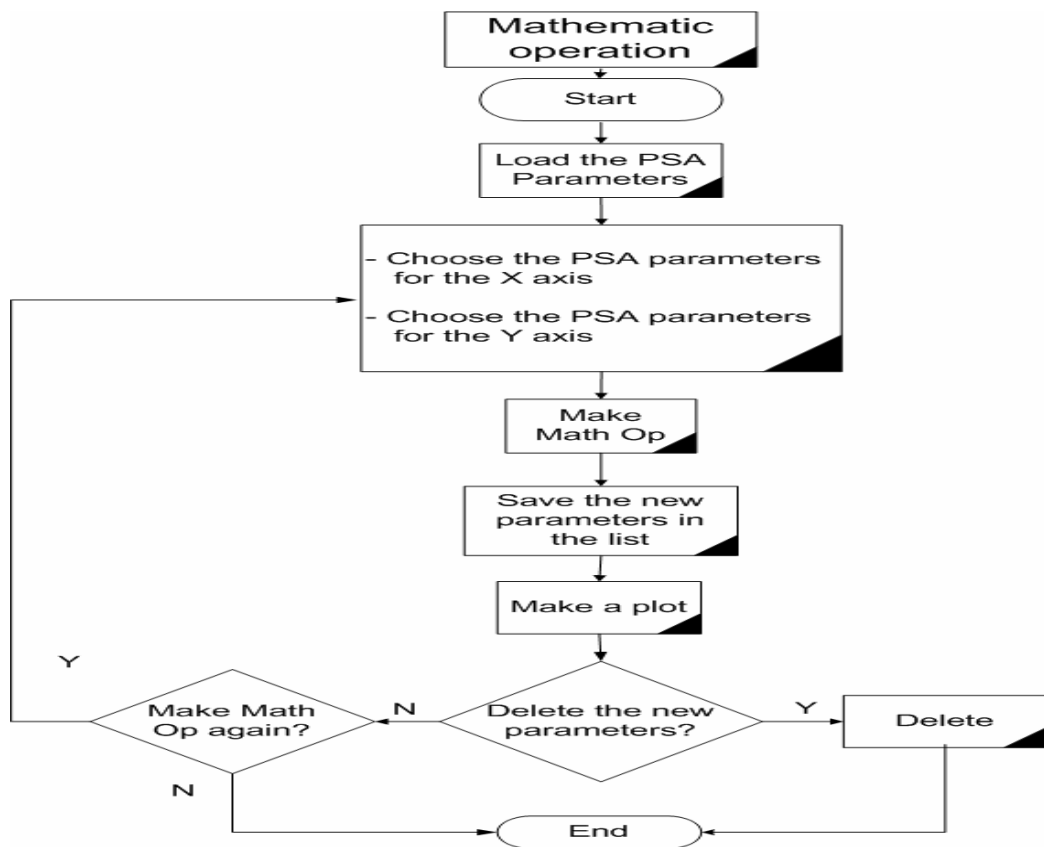
Fig. 3.4: Flow chart of the mathematic operations

order to recognize the different PD sources [Ber02a]. The PSA software with its tool of mathematic operations makes it possible to combine different basic PSA parameters in order to get more parameters for evaluation. The flow chart of the mathematic operations is shown in **Fig. 3.4.** After choosing the basic parameters from a list, the mathematic operations can be done (multiplication, addition, subtraction or division) between the parameters or between parameters and numbers. The new parameters are then saved in the offset memory and the operation can be redone or the saved parameters can be sent to plotting. At the end of the operation the new parameters can be saved or deleted from the PSA parameters list.

3.1.4   Graph plotting

Fig. 3.5 shows the flow chart of the function of graph plotting. Two kinds of graphics format are available, scatter plot and histogram plot. After choosing the plotting format and the setting of the PSA parameters in the corresponding X axis and Y axis, the diagram can be plotted just with a single keystroke. Graphs of high resolution can be printed or saved in a list of graphs.
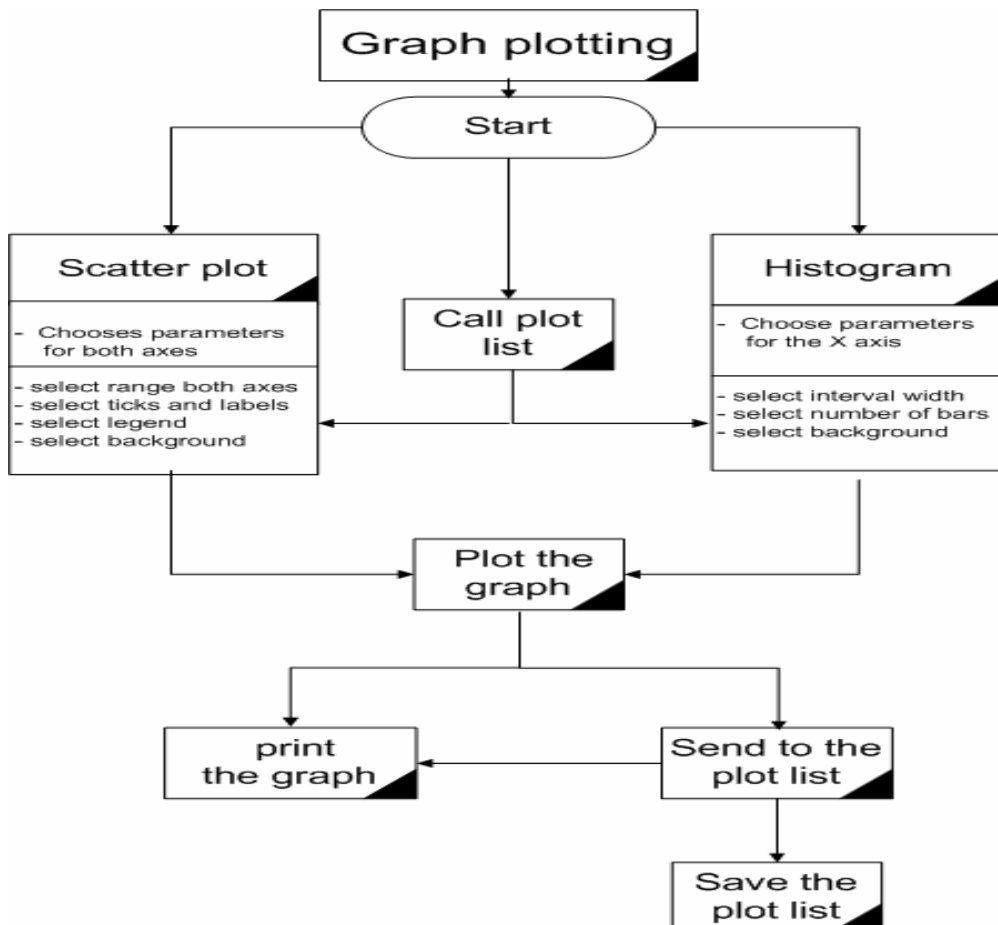
Fig. 3.5: Flow chart of the data plotting

3.2 Graphical user interface

The PSA software is based on the implementation of a graphical user interface design (GUI). The visible graphical interface features of the PSA software contain graphical elements: menus, windows, buttons, dialog boxes and scroll bars. These widgets (graphical elements) are functionally independent from and indirectly linked to program functionality, so that the GUI can be easily extended for more applications.

The start interface shown in **Fig. 3.6** contains a PD data table and a PD data processing window. After the loading of the data from the menu file or from the menu border box, the user can adjust the different scaling parameters by using the dialog box. Then the processing of the data can be started and the desired graph will be plotted.
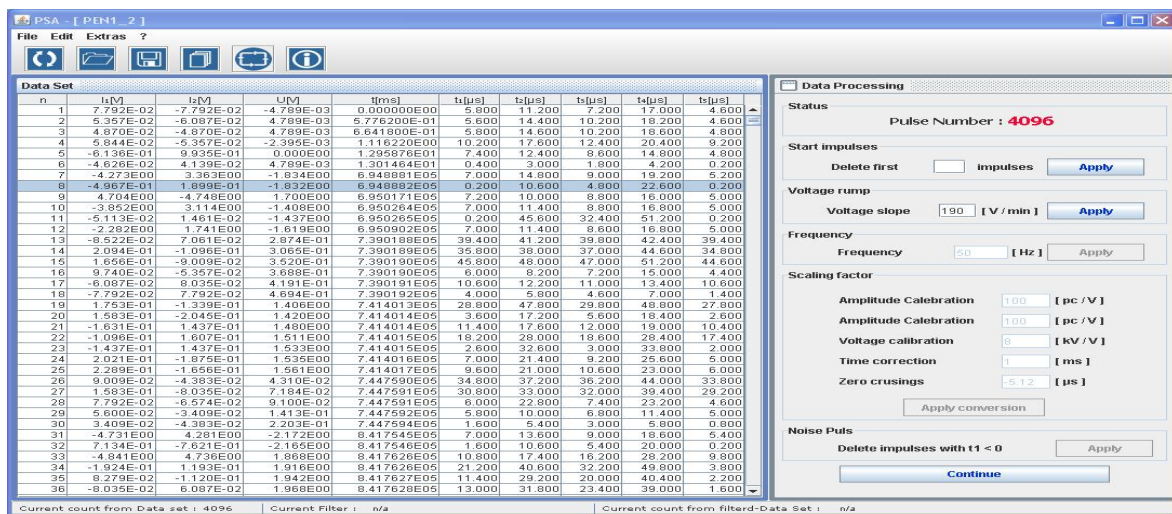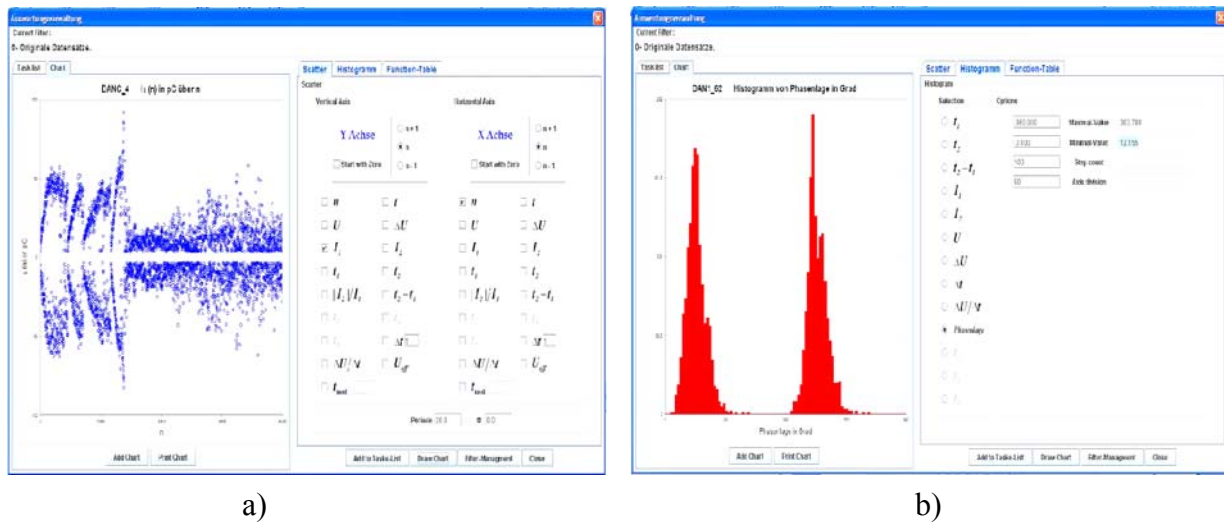
Fig. 3.6: Graphical interface of the data processing in PSA software

Fig. 3.7.a) shows the graphical interface corresponding to the scatter plot. The user select the PSA parameter corresponding to the X axis and that corresponding to the Y axis, and with a simple click on the plot button, the corresponding diagram appears instantaneously at the left window. The range, the ticks and the labels of both axes are set automatically to optimized values but can be also manually selected.

The software gives not only the possibility to correlate parameters of each pulse, but also to correlate parameters of a pulse to parameters of previous or following pulses.

The software gives also the possibility to correct the effect of frequency fluctuations by adjusting the time indicated by the system clock of the PC. This is necessary to get the actual shape of the frequency distribution of the phase angles at which the discharge occurs.

Fig. 3.7.b) shows the graphical interface corresponding to the histogram plot. The user can select one of the PSA parameters by using the dialog box and the histogram will be created. The number of bars and the interval width are selected automatically and can be manually changed.
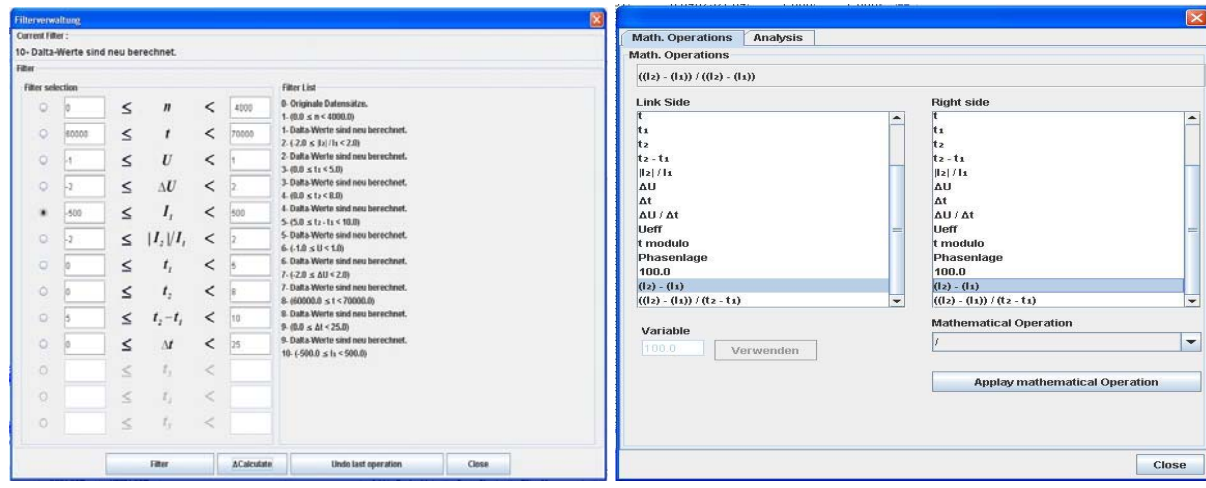
a)	b)

Fig. 3.7: Graphical interface of the PSA software
a) scatter plot and **b)** histogram plot

Fig. 3.8.a) shows the graphical interface related to the filtering management. The user can choose the PSA parameter from the list, which will be filtered and select the desired values range domain, then the data set will be filtered. According to the wish the delta function (for **ΔU** and **Δt**) can be recalculated. Each operation will be listed and can be removed by using the button "undo".

a)	b)

Fig. 3.8: Graphical interface of the PSA software
a) for filtering management and **b)** for mathematic operations

Fig. 3.8.b) shows the graphical interface related to the mathematic operations. The user can select the mathematic operation (**+**, **-**, **x** or **/**) that shall be done from the dialog box and the desired parameters from the lists. The results are stored internally and can be used for further operations. It is also possible to perform operations between parameters and numbers, which are necessary for example if the plot of more than one curve in the same graph (normalization) is necessary.

The user has the possibility to create an analysis list (**Fig. 3.9a**). This list can be stored for a later use or sent to plotting as shows in **Fig. 3.9.b**.

a)   b)
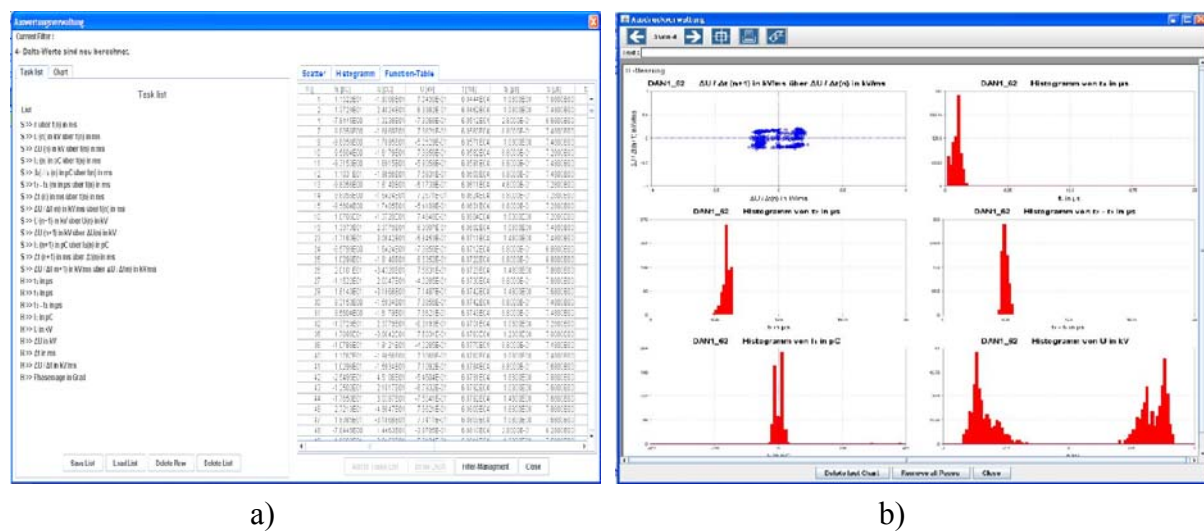
Fig. 3.9: Graphical interface of the PSA software
a) for analysis list and **b)** for the selected graph

3.3   Characteristic parameters for Pulse Sequence Analysis

To characterize partial discharge phenomena different analysis parameters can be used. In the standard method the distribution of the phase angles at which the discharges occur is frequently used as main parameter [Kre93]. This analysis usually examines only the whole data sets accumulated in dependence of the actual phase angles of the applied voltage and does not take into account any correlations between consecutive discharges. However, each partial discharge generates space or surface charges and/or modifies the distribution of these space or surface charges and hence changes the local electric field and consequently modifies the condition for the ignition of the next discharge [Pat94]. The analysis of the sequence correlated parameters and the combination of sequential parameters introduced by the **Pulse Sequence Analysis** give a better insight into the physical degradation phenomena [Pat04]. The physical

significance of these different PSA parameters as well as their use for diagnostics (with different graphical representations) will be described in detail.

The analysis of each parameter will be done on an **example of a PD measurement of a stator winding of a small motor** (see Fig. 2.7). The experiment was performed with a ramped AC voltage. The test voltage was ramped with a rate of **190 V_{rms}/min** until **4096** partial discharges had occurred. The high voltage was applied to both ends of the auxiliary winding while the main winding and the iron core were grounded. The sensitivity was adjusted to about **2.5 pC**.

3.3.1 Phase of occurrence of the applied voltage

The historically first and until now most frequently used parameter is the phase angle of the external voltage. Usually as a first step the frequency distributions of the phase angles at which discharges occur are taken and discussed with regard to their actual shape [Gul91, Bru91]. If in addition the pulse heights are also taken, three dimensional **ϕqn** patterns can be drawn and used for comparison with the results of other measurements. On the basis of these data a classification system has been developed [Gul95a]. These visualisations just describe a specific data set but do not tell too much about the local physical processes. The problem of an evaluation of the underlying physical phenomena and the characterization of the relevance of the processes for electrical ageing of the specimen remains unresolved.
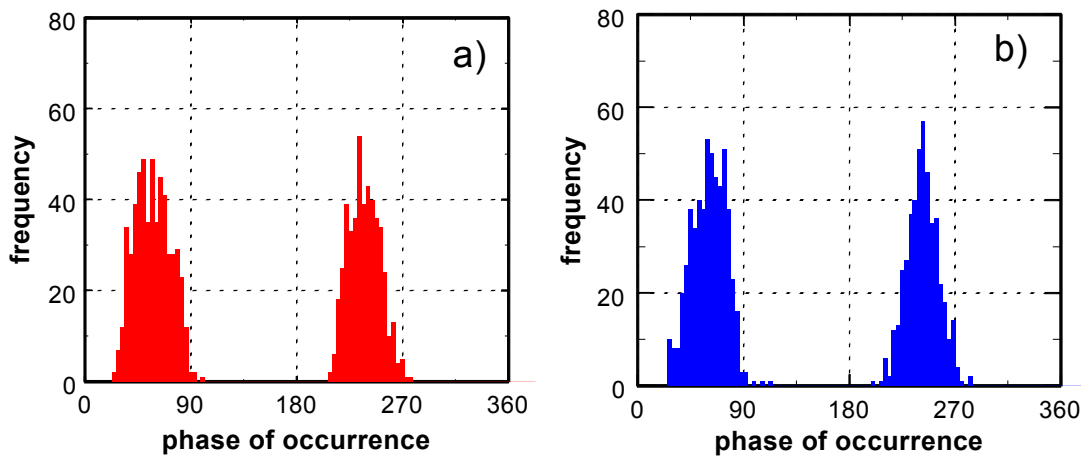
Fig. 3.10: Frequency distributions of the phase angles ϕ at which discharges occurred
a) for the first 1000 discharges and **b)** for the following 1000 discharges

Fig. 3.10 shows the frequency distributions of the phase angles for the first 1000 and the following 1000 discharge events. Due to the voltage ramp, the first 1000 discharges occurred at voltages between **734** and **748 V_{rms},** the following 1000 discharges occurred at voltages between **748** and **756 V_{rms}.** Obviously there is no basic difference between these two subsets of

the data set of 2000 consecutive discharges except a small statistic scatter due to the systematic periodic shift of the external voltages at which the discharges occur.

3.3.2 Cumulative number of the discharge events

As a first step in the evaluation of PD measurement data, the number of discharges over time is analyzed. The graphic representation of the pulse number as a function of the time **t** or of the applied voltage **U_rms** (in the case with a ramped voltage load) delivers us information about the partial discharge activity. These representations show the behaviour of the partial discharge process over time or with the increasing applied voltage. The slope of the curve over time **t** corresponds to a mean pulse rate that can be taken as a characteristic for the discharge activity. The extrapolation of the curve of the pulse number over externally voltage **U_rms** gives the PD inception voltage that can also be taken as characteristic parameter to analyze the partial discharges.

Fig. 3.11a) shows the cumulative number of the discharge events over time. Two distinct regions with different partial discharge rates were found during the voltage ramp. After about **1000** discharges the discharge rate changes from about **4.6** to **8.3** events per cycle. **Fig. 3.11b)** shows the cumulative number of the discharge events over the applied voltage for the underlying experiment. The PD inception voltage is about **734 V**. Obviously in dependence on the magnitude of the applied voltage different partial discharge processes prevail. The explanation for this behaviour lies in the fact that at about **748 V** a second defect starts to produce partial discharges. This change in the discharge rate was not visible in the phase angle distributions (Fig. 3.10).
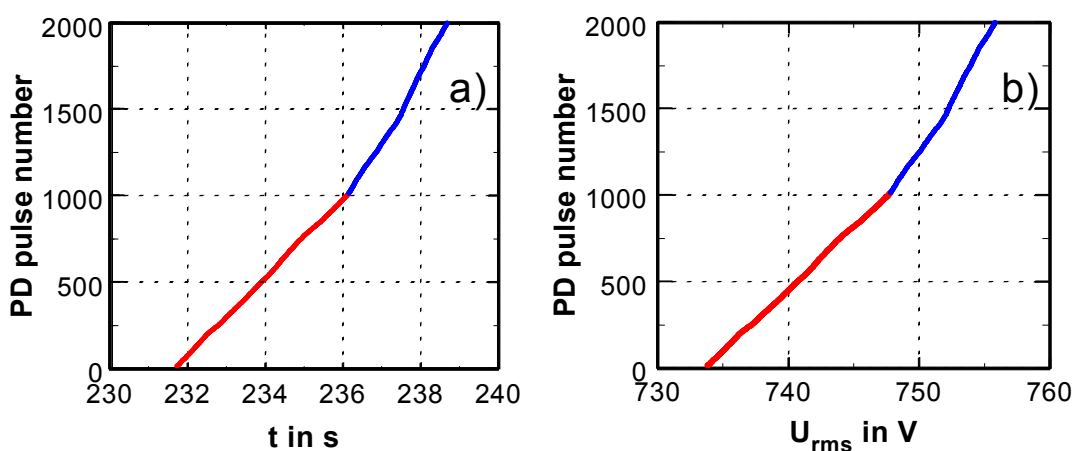
Fig. 3.11: Pulse numbers **a)** over time and **b)** over the externally applied voltage
U_rms for the first 2000 discharges

3.3.3   Actual voltages at which the discharges occur

A further parameter that can be analyzed is the actual voltages U at which the discharges occur. The corresponding frequency distributions of the actual voltages U at which discharges occur for the two subsets of 1000 discharges each are illustrated in **Fig. 3.12**. The behaviour is the same as the one showed in Fig. 3.10. Also these histograms show no significant differences compared to the representation of the phase angle. **Fig. 3.13** illustrates the actual voltage U at which the discharges occurred over the externally applied voltage for the two subsets of 1000 discharges. As can also be seen in Fig 3.12 the partial discharges did not always occur at the peak of the AC voltage, but in some cases also at lower voltages. Consequently the curve of the actual voltage level U at which the discharges occurred over applied voltage U_{rms} shows some scatter as shown in Fig. 3.10.
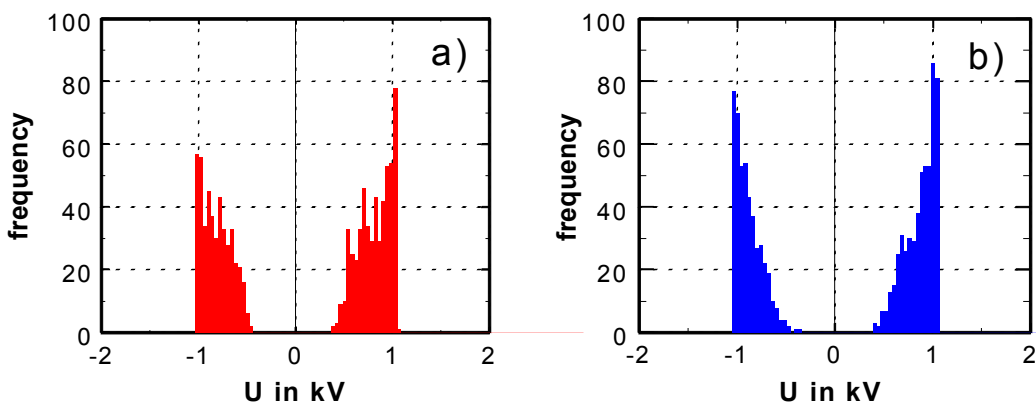

Fig. 3.12: Frequency distributions of the actual voltages U at which discharges occur **a)** for the first and **b)** for the following 1000 discharges
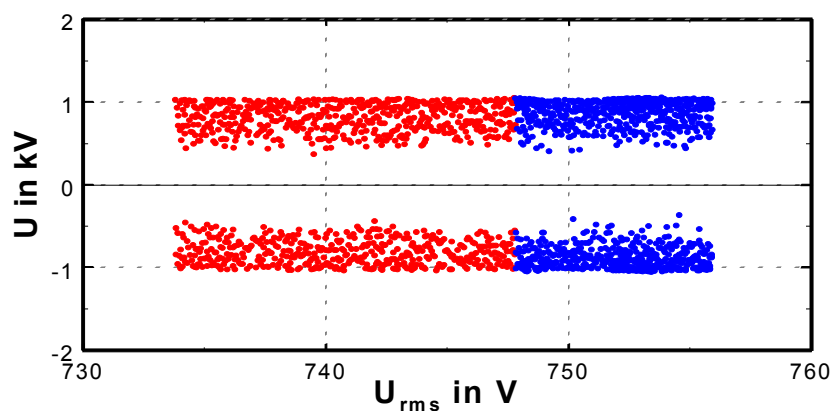
Fig. 3.13: Actual voltages U over the applied voltage U_{rms} for the first 2000 discharges

3.3.4   Voltage differences between consecutive discharges

In contrast to the aforementioned parameters phase angle and voltage, the voltage differences $\Delta U_n = U_{n+1} - U_n$ between consecutive discharges are much more sensitive to changes in the discharge process. In many cases this parameter allows the separation between correlated and non-correlated discharges [Hoo94], an important information for the decision whether there is one or more defects in the test object.

The first analyses took the **sequence of the external voltages** at which discharges occurred**,** and plotted the **voltage differences** in a scatter plot. The results revealed that there are distinct voltage differences after which discharges occur. The voltage differences do not occur at random but in specific sequences characterizing the discharge processes in the defect. The reason for these definite voltage differences between consecutive discharges are **space charges** built-up by the discharge process [Ben07]. This leads to a **reset of the local electric field** and the next discharge starts only after the local electric field again exceeds the initiation field strength, either by variation of the electric field produced by the applied voltage or a decrease of the field reducing influence of the local space charges. If local space charges can be built-up and play an important role – and this is usually the case in **solid dielectrics** – this phenomenon prevails.

Fig. 3.14 shows the frequency distributions of the voltage changes between consecutive discharges. The frequency distributions of voltage differences between consecutive discharges show much less scatter than those of the voltages at which discharges occur. A characteristic change is shown between the first and the next 1000 discharges. During the first 1000 discharges four different groupings of voltage differences occur in both polarities around **1.6 kV** and **0.2 kV**. In the following 1000 discharges for small voltage changes only one large group with a maximum probability around zero occurs.
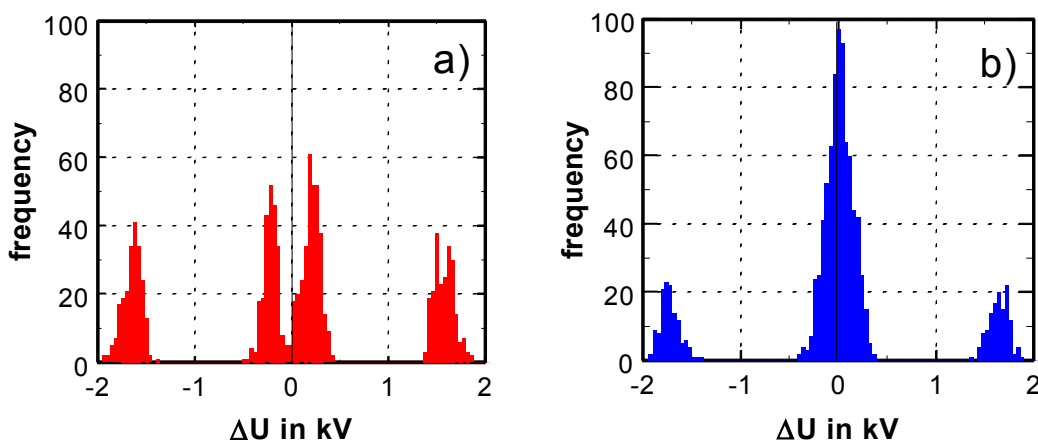
Fig. 3.14: Frequency distributions of the voltage changes ΔU between consecutive discharges **a)** for the first and **b)** for the following 1000 discharges
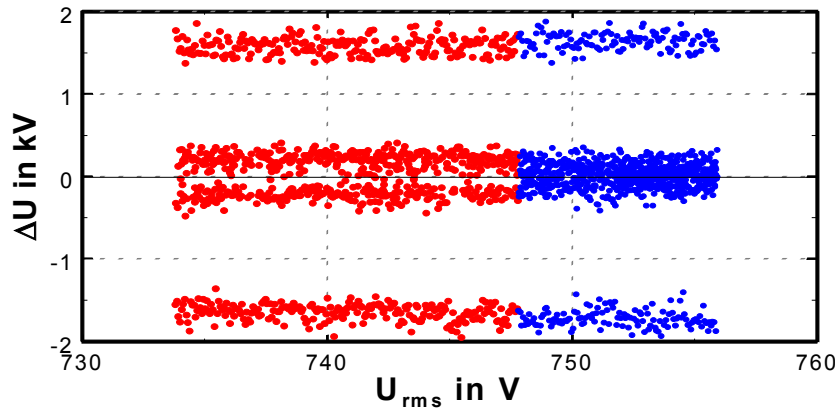
Fig. 3.15: Voltage changes ΔU between consecutive discharges over the externally applied voltage U_{rms} for the first 2000 discharges

Fig. 3.15 shows the voltage changes between consecutive discharges over the externally applied voltage U_{rms} for the first 2000 discharges. Also in this representation the characteristic change within the 2000 consecutive discharges is shown. After 1000 discharges i.e. at about **748 V** a characteristic change in the ΔU diagram occurs that corresponds to the change that appears in the discharge rate (see Fig 3.11).

3.3.5   Discharge magnitudes

A very helpful parameter in addition to the sequence of the voltage changes used in most analyses so far is the **discharge magnitude I_1**. In general, if in a partial discharge measurement the voltage is ramped up with time, the first discharges are small in intensity and they increase with increasing applied voltage. The discharge magnitude does not really depend on the magnitude of the applied voltage (except in the case where the space charges play no role see chapter 5.3) but on the **preceding voltage change** and on the type of defect too.
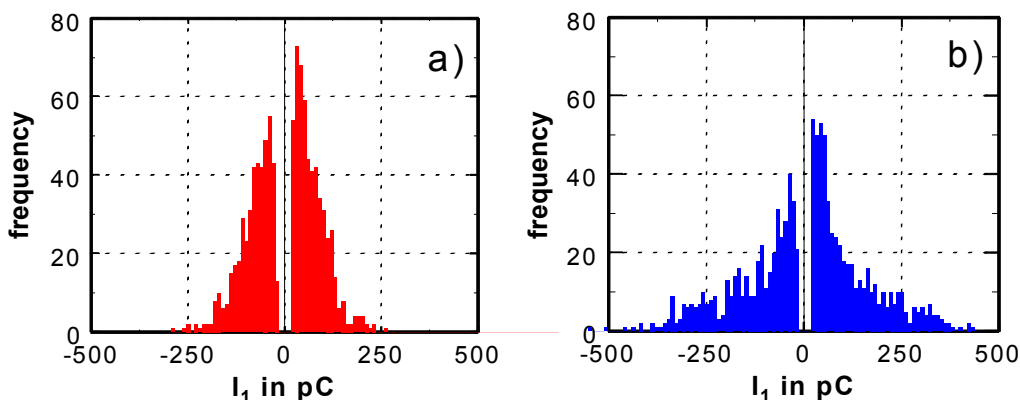
Fig. 3.16: Frequency distributions of the discharge magnitudes I_1
a) for the first and **b)** for the following 1000 discharges
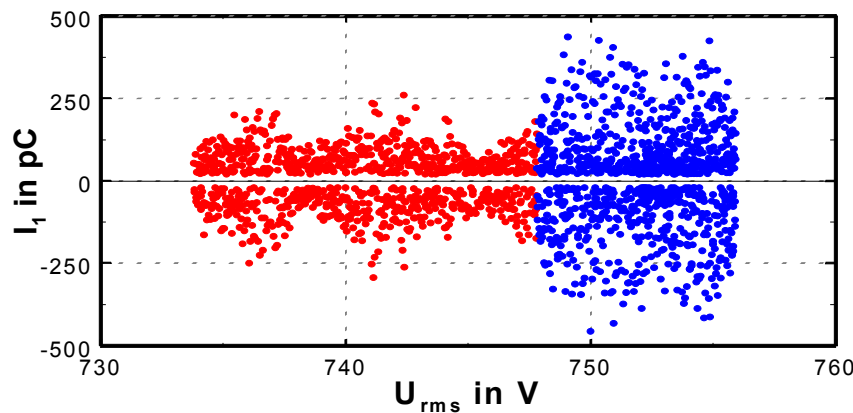
Fig. 3.17: Discharge magnitudes I_1 over the externally applied voltage U_{rms} for the first 2000 discharges

Fig. 3.16 shows the corresponding frequency distributions of the pulse heights I_1 of the discharges. It shows clearly that the frequency distributions of the discharge magnitudes in both diagrams are not the same. **Fig. 3.17** illustrates the discharge magnitudes I_1 over the externally applied voltage U_{rms}. The result shows that there is some scatter without any apparent correlation between the pulses, but there is an indication that for voltages above **748 V** more discharge pulses with higher magnitudes occurs.

3.3.6   Time differences between consecutive discharges

Due to the phenomena of correlated or non-correlated discharge sequences the evaluation of the time differences $\Delta t_n = t_{n+1} - t_n$ between consecutive discharges may be a very helpful analysis tool [Pat03, Cav05]. While with one discharge site in a solid dielectric, discharges occur only after distinct voltage changes ΔU, and hence after distinct time differences Δt, discharge events from the second discharge site often occur 'at random' with regard to the first mentioned discharge site.

In some cases, initially only one discharge per cycle occurs (mostly at the peak value in one of the half waves of the applied voltage). In this case the voltage change ΔU between successive discharges is about zero. If the voltage is increased, either more discharges occur in the same half waves (in the inclining part before the crest voltage) or discharges occur in the opposite half waves also. In the first mentioned case the voltage differences do not change significantly, but in the distribution of the time differences Δt between consecutive discharges in addition to the value of **20 ms** (or multiples of this) values less than a few **ms** occur. In the other case voltage differences ΔU of twice the peak value of the applied voltage and time differences Δt

around **10 ms** occur. With higher applied voltages also in this case additional smaller time differences occur.
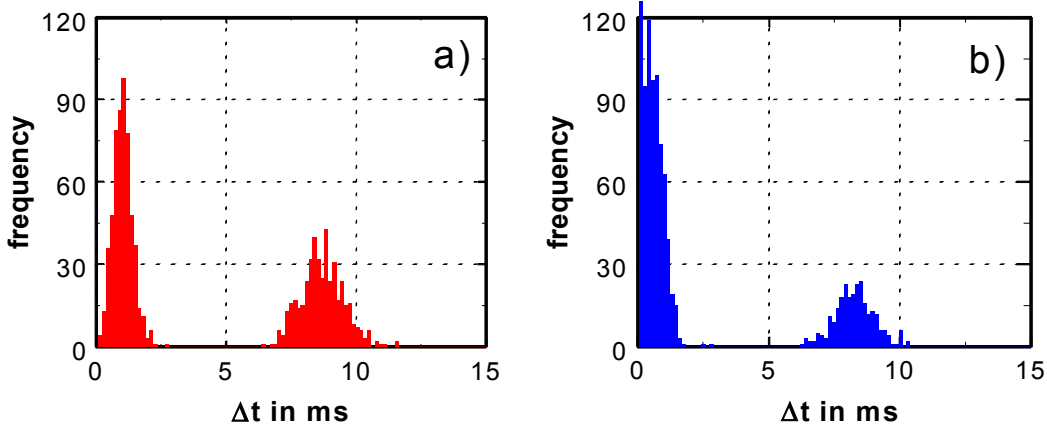
Fig. 3.18: Frequency distributions of the time differences Δt between consecutive discharges **a)** for the first 1000 and **b)** for the following 1000 discharges
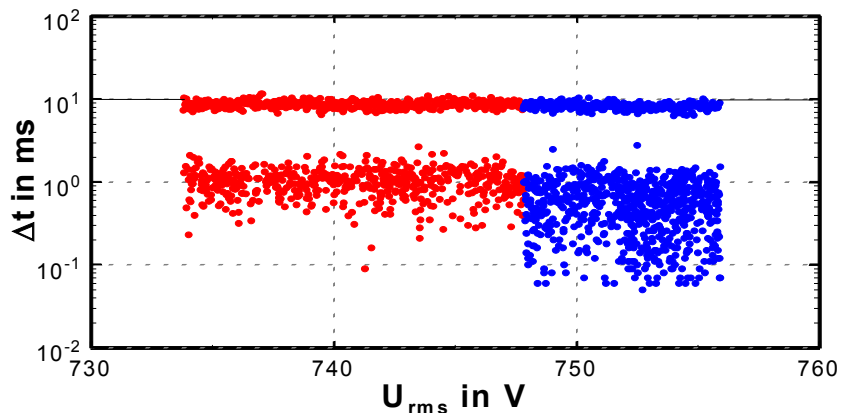
Fig. 3.19: Time differences Δt between consecutive discharges over the externally applied voltage U_{rms} for the first 2000 discharges

The corresponding frequency distributions of the time differences are shown in **Fig. 3.18**. While for the first 1000 discharges the time differences are around **9 ms** and around **1 ms**, for the following 1000 discharges much smaller time differences down to less than **0.1 ms** occur. Those small time differences indicate the existence of at least two non correlated discharge processes. Looking at the time differences between consecutive discharges over the externally applied voltage U_{rms} (**Fig. 3.19**), at about **748 V** a characteristic change occurs that corresponds to the change that appears in the pulse heights (see Fig. 3.12). After 1000 discharges many small time differences below **1 ms** occur. Also the voltage differences show a very pronounced change (Fig. 3.13).

3.3.7 Time differences between next but one discharges

Additional information about the discharge process can also be gained if not only the time differences Δt between consecutive discharges, but also the time differences $\Delta_2 t_n = t_{n+2} - t_n$ between next but one discharges are included in the evaluation process. **Fig. 3.20** displays the frequency distributions of next but one time differences between consecutive discharges for the two sets of the PD data. For the test object (small stator) the interesting effect occurs that – particularly for small time differences Δt – the frequency distribution for the first 1000 discharges shows nearly the same shape as the time differences $\Delta_2 t$ for the second 1000 discharges (see Fig. 3.18 a) and Fig. 3.20 b)).

The explanation for this astonishing similarity lies in the fact that at about **748 V** a second defect starts to produce partial discharges (see Fig. 3.15 or Fig. 3.19). The phase angles at which these discharges occur are not correlated to the discharges of the first discharge active defect and hence many small time differences will occur (see Fig. 3.18 b). The discharges of the second defect will occur at random between two consecutive discharges of the first defect. Hence the time differences $\Delta_2 t$ between next but one discharges of the second subset of the data will show the same frequency distribution as the time differences Δt between discharges of the first subset of the data, in which only one defect was active.
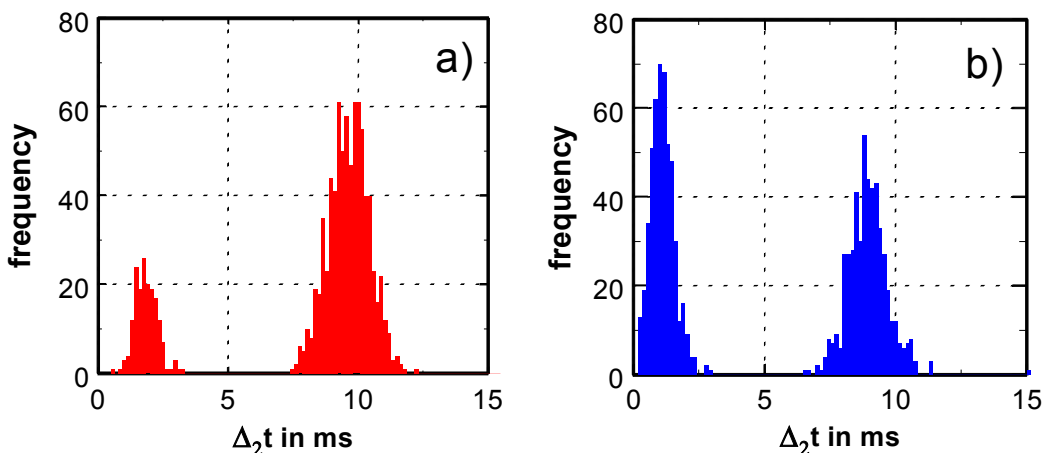
Fig. 3.20: Frequency distributions of the time differences next but one discharges $\Delta_2 t$
a) for the first 1000 pulses and **b)** for the following 1000 pulses

3.3.8 Combinations of sequential parameters

In many cases the use of more than one 'discharge parameter' is advisable for PD analyses. If instead of ΔU the differential ratio $\Delta U / \Delta t$ is used, pulse sequences with short time intervals between are emphasized in contrast to those with longer discharge free intervals.

As shown in [Pat99] this may give a different impression of the scatter plot, especially as discharges adjacent to long discharge free time intervals are 'suppressed'. If solids are involved, most discharges occur around the zero crossings of the applied voltage i.e. in the nearly linear part of the voltage curve.
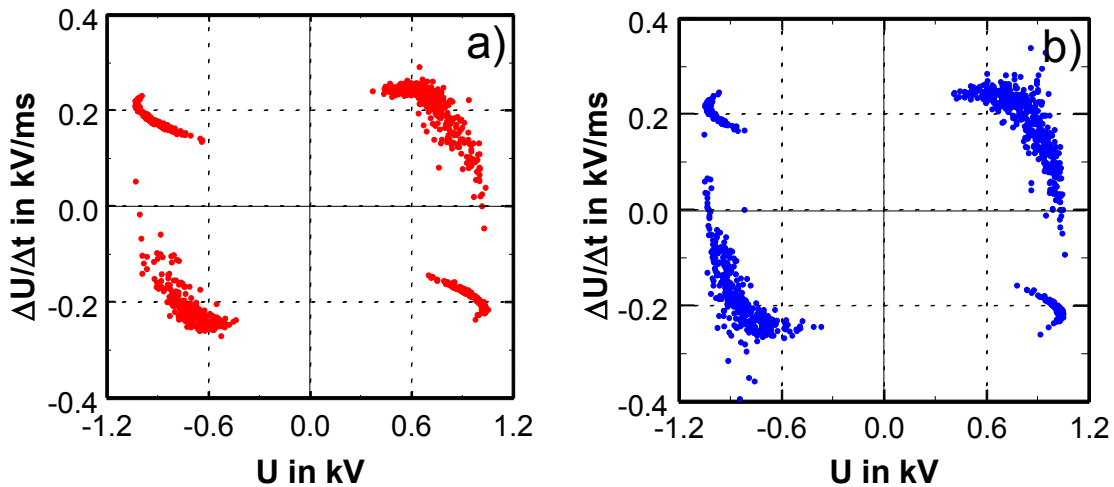
Fig. 3.21: Mean differential ratios **ΔU/Δt** between discharges over the actual voltages **U**,
a) for the first 1000 discharges and **b)** for the following 1000 pulses

The length of the time intervals **Δt** between discharges is in the region of a few milliseconds and the scatter resembles a corresponding scatter in the voltage differences **ΔU**. If for these discharge pulses the differential ratio **ΔU/Δt** is taken instead of **ΔU** or **Δt**, this scatter disappears because **ΔU/Δt** represents the nearly constant incline of the voltage curve in this region.

Fig. 3.21 shows the plots of the mean differential ratios **ΔU/Δt** between discharges over the instantaneous voltages **U** at which the discharges occur. In this diagram sequences with short time intervals between discharges are emphasized in contrast to those with longer discharge free intervals. PD pulses in the inclining part of the external voltage curve with short time differences in between generate an accumulation of data points in the first and third quadrant in the **ΔU/Δt** over **U** diagrams. Those regions are typical for corona or surface discharges [Ber02].

3.3.9   Correlation diagrams

Another very powerful tool is the analysis of correlations between consecutive values of a parameter. In this context different defects may behave quite differently and thus give a good chance for characterization.

Often a pronounced polarity dependence shows up, that indicates the existence of surface or space charges that influence the discharge process [Pat96]. Different correlation diagrams can be represented e.g. U_{n+1}-U_n-correlation, ΔU_{n+1}-ΔU_n-correlation, ΔU_n-U_n-correlation, I_n-U_n-correlation, I_n-ΔU_n-correlation, etc.

Fig. 3.22 and **Fig. 3.23** show an example of correlation diagrams between consecutive voltages (U_{n+1}-U_n-correlation) and between consecutive voltage differences (ΔU_{n+1}-ΔU_n-correlation) for the aforementioned measurement. A clear difference between the first and next 1000 discharges can be seen in the second and fourth quadrants of the diagrams.
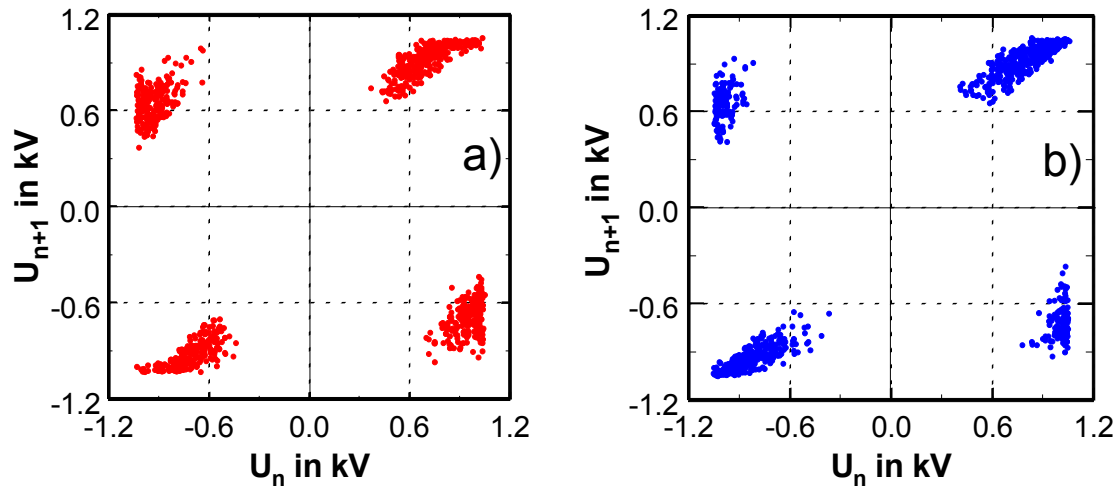
Fig. 3.22: U_{n+1}-U_n-correlation between voltages of consecutive discharges
b) for the first 1000 discharges and **b)** for the following 1000 pulses
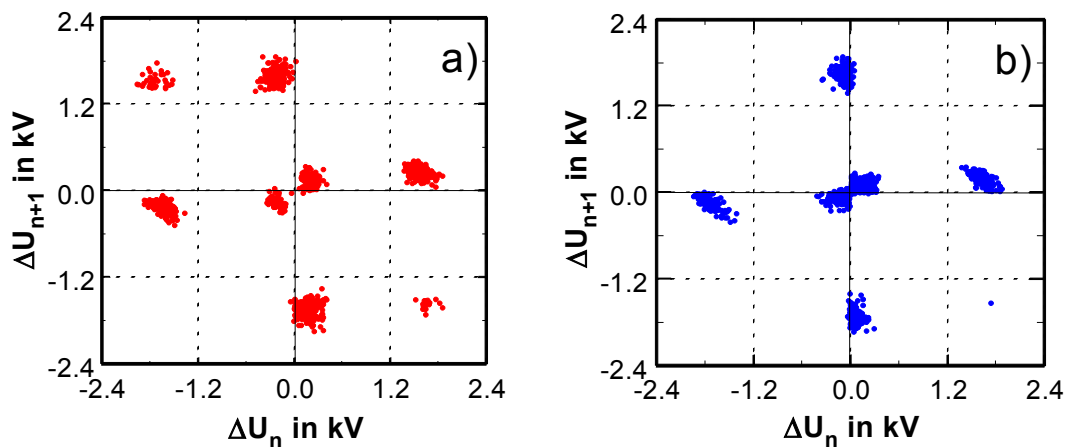
Fig. 3.23: ΔU_{n+1}-ΔU_n-correlation between voltage differences of consecutive discharges
a) for the first 1000 discharges and **b)** for the following 1000 pulses

3.3.10 PD pulse shape parameters

In addition to the parameters discussed up to now, the analysis of the pulse shape of the signal after the coupling device and the band-pass filter may be a very effective tool, either to separate discharge signals from noise [Pat02] or to separate signals from different spots within the specimen [Pat03]. The most frequently used parameters are t_1, t_2, t_3 and t_4 and their combinations as well as $|I_2|/I_1$ (more details in chapter 4).

For this measurement with the small stator the ratios of the heights of the first two peaks of the PD signal can be taken as parameter for analysis. A characteristic difference between the first
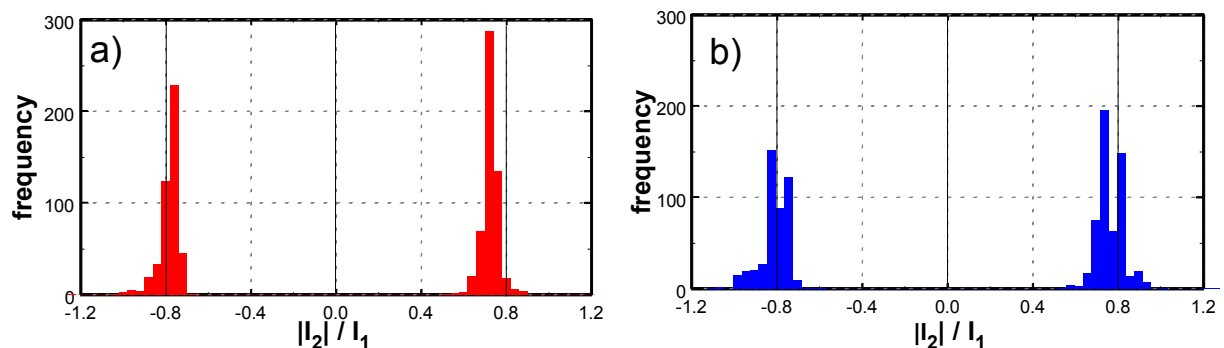
Fig. 3.24: Frequency distributions $|I_2|/I_1$ of the ratios of the magnitudes of the second and the first peak of the discharge signals
a) for the first 1000 pulses and **b)** for the following 1000 pulses
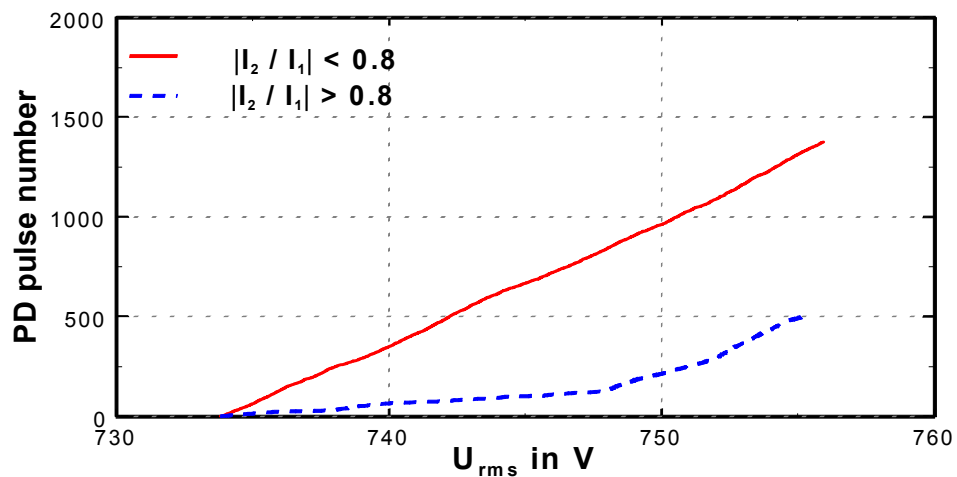
Fig. 3.25: Pulse numbers over voltage for discharge signals split-up in accordance to the ratios of the heights of the second and the first peak of the discharge signals I_2/I_1

1000 and the following 1000 discharge pulses appears. **Fig. 3.24 a)** shows single-peaked distributions for negative and positive pulses, while **Fig. 3.24 b)** shows distributions with two peaks for both polarities. The additional peak represents discharge pulses in which the second peak l_2 is higher than 80 % of the magnitude of the first peak l_1. The suppression of these discharge pulses reveals that the first discharge type, representative for the first 1000 discharge pulses, continues to occur with the same discharge rate also in the following 1000 discharge pulses. In addition a second type with different pulse shape occurs.

Fig. 3.25 shows the pulse numbers over voltage for the 2000 discharges split up in accordance to the ratio l_2 to l_1. While for pulses with $|l_2 / l_1| < 0.8$ the pulse rate is constant, for $|l_2 / l_1| > 0.8$ the rate is initially much lower and increases at about **748 V**.

3.4   Summary

The analysis of the enormous amounts and complex data generated by PD measurements required the development of an adequate software. The developed PSA software for the PD analysis significantly facilitated the analysis of acquired data and it is an essential tool in the analysis of sequence correlated data. Different possibilities to analyze partial discharge data sets using PSA software were proposed. The use of several parameters was discussed with a special emphasis on sequence correlated data such as the change of the external voltage or the time difference between consecutive discharges or next but one discharges.

The occurrence of partial discharges is mostly determined by the local electric field at the site of the defect. Space and/or surface charges generated in the discharge process affect the local electric field. Thus it becomes obvious that rather the change of the external voltage or the time interval since the preceding discharge than the actual voltage level itself or the corresponding phase angle are the decisive parameters. This has been shown and discussed in detail with data obtained by the analysis of an example of two consecutive subsets of a PD measurement of a stator winding of a small motor.

- The evaluation of the phase angles of occurrence or the instantaneous voltages at which discharges occur have shown no basic difference between the two sub-sets of the PD data.
- Evaluations with different parameters used in the PSA for the interpretation of partial discharge measurements shows that **sequence-correlated parameters** contain much more relevant information.
- The analysis of the cumulative number of the discharges events has shown that a change in the discharge rate of the two subsets has occurred. This is related to the fact that a second defect starts to produce partial discharges.

- A characteristic change in the ΔU diagram corresponding to the change in the cumulative number was shown between the two subsets.
- The discharge magnitudes in the two subsets also appear different.
- A characteristic change also occurs in the Δt diagram which corresponds to the change that appears in the pulse heights.
- In the diagrams that show combinations of sequential parameters and in the correlation plots the difference between the two subsets of data is noticeable.
- In many cases even more details can be seen in ΔU_{n+1}-ΔU_n and Δt_{n+1}-Δt_n patterns which show physically relevant correlations between consecutive discharges. Those patterns can be very characteristic for some types of defects.
- With the use of the pulse shape parameters (e.g. the ratio $|I_2|/I_1$ of the magnitudes of the first two peaks of the PD signal) the two defects could be separated.

4   Pulse Shape Analysis

The analysis of partial discharges is a common tool for the diagnosis of electric equipment, whereby in most cases only the phase angles at which the discharges occur and the pulse heights of PD are registered. The actual shape of the signal is usually not taken into account. This chapter is dedicated to the description of the pulse shapes of the partial discharge signal and its use as diagnostic tool to improve the Pulse Sequence Analysis method.

4.0   Introduction

In contrast to the situation with geometrically small specimens, for geometrically extended test objects the pulse shape of a partial discharge signal may be modified on its way from the location of the defect to the measuring points. Due to the local inductance, the discharge induced quick change of the local voltage distribution may lead to a high frequency **travelling wave** which may be distorted or reflected at any spots where the impedance changes [Lem06, Vee05, Pem00]. This leads to the superposition of additional oscillations on the initial pulse shape of the discharge. Hence the **analysis of the registered pulse shape** will give some additional information on the location of the defect producing the partial discharge within the test object or apparatus.

In commercial power equipment in many cases discharges occur simultaneously at different spots in the apparatus. The Pulse Sequence Analysis works best if there is only one or only a few defects that are active in parallel. Hence the analysis of the actual PD pulse shape may be helpful to separate partial discharge signals from different defects and hence can be used to improve the effectiveness of the Pulse Sequence Analysis. In addition the pulse shape of a discharge may change with increasing degradation of the site of the defect. After separation of discharge pulses on the basis of this approach, in some cases the PSA method may still be more efficient. In addition the analysis of the actual pulse shape can be used to separate noise-signals from discharge pulses [Pat02].

For discharges at different spots in geometrically extended test objects different pulse shapes may occur even without the aforementioned effect of the travelling wave [Ber01a]. On the other hand in some cases even for the small test object a modification of the partial discharge shape may occur due to solid state phenomena [Ari07]. In addition partial discharges in insulating liquids in extremely non-homogeneous electrode arrangements (needle-plane geometry) may show different pulse shapes in dependence on the degree of ageing of the liquid [Pat07].

4.1   Partial discharge pulse shape

The earlier evaluations of partial discharge data on the basis of the Pulse Sequence Analysis took only the polarity and the pulse magnitude of the highest peak of a discharge signal as characteristic parameter of a discharge pulse [Hoo97]. The initially used three parameters, the pulse height I_1, the actual externally applied voltage **U** and the time **t** at which the discharge occurred are very useful, but do not allow taking into account the actual shape of the oscillating PD signal [Pat02].

For better insight into the partial discharge process not only the behaviour of the PD magnitude (pulse height) and its polarity should be observed but also other characteristic parameters of the pulse shape. More additional information can be drawn from the actual shape of the single discharge pulse [Pat02a]. These parameters depend on the type of the defect and its localization within a geometrically large specimen and the parameters of the partial discharge detector. Hence for further analysis the program that handles the raw data was extended to take not only the highest amplitude of the PD signal, but the first two peaks I_1 and I_2 of the oscillating PD signal, the corresponding times t_1 and t_2 at which they occur and the times of the first zero crossings t_3, t_4 and the time t_5 of the PD signal that corresponds to the time of the first data point of the PD signal that deviates from zero [Pat03, Ari07]. **Fig. 4.1** shows an example of a typical PD oscillating signal and the corresponding parameters used in the Pulse Shape Analysis. The amplitude of the second peak of the oscillating signal is typically about **80%** of the amplitude of the first peak. Commonly the calibration is done on the basis of the magnitude of the first peak I_1 for a given calibration signal of some **pC** fed into the measurement system.
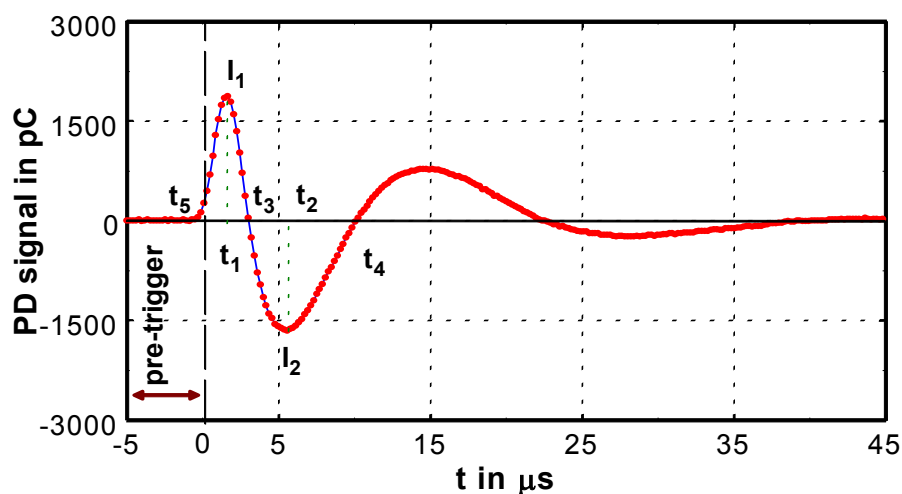
Fig. 4.1: Example of a typical PD oscillating signal and the corresponding parameters used in the Pulse Shape Analysis

It is important that on one hand the preparation of the initial data with regard to the Pulse Sequence Analysis does not depend on these phenomena but on the other hand these differences can be used in addition to get more information about the defects. Hence the program used should be able to differentiate between different pulse shapes.

The data acquisition hardware usually takes **256** data points in a time window of about **51 μs** (sampling frequency of **5 MHz**). **10%** of the window time (**5.1 μs**) was set as a pre-trigger. The last data point before the steep rise of the signal is taken by the evaluation software as the zero reference of the times t_1 and t_2 of the two highest peaks, of the times t_3 and t_4 of the zero crossings and of the time t_5. The newly introduced parameters allow a better characterization of the PD signals.

4.2   Anomalous discharge signals

Numerous analyses of the discharge signals from different specimens revealed that, depending on the type and location of a PD-active defect, the shape of the PD signal may be different. **Fig. 4.2** shows a sequence of five consecutive PD pulses generated in the winding of the stator of a small motor and the actual voltage levels at which the PD pulses occur. The figure shows only the **50 μs** time windows of an actual discharge. The discharge free times in-between are quenched. The signals look characteristically different. In many cases not the first but the second relative maximum was counted as l_1 or the third or fourth relative maximum as l_2. It is worth mentioning that for some of those signals standard analyses would even indicate a wrong polarity of the pulses. In these cases the indicated polarity of l_1 may be opposite to the polarity of the external voltage.
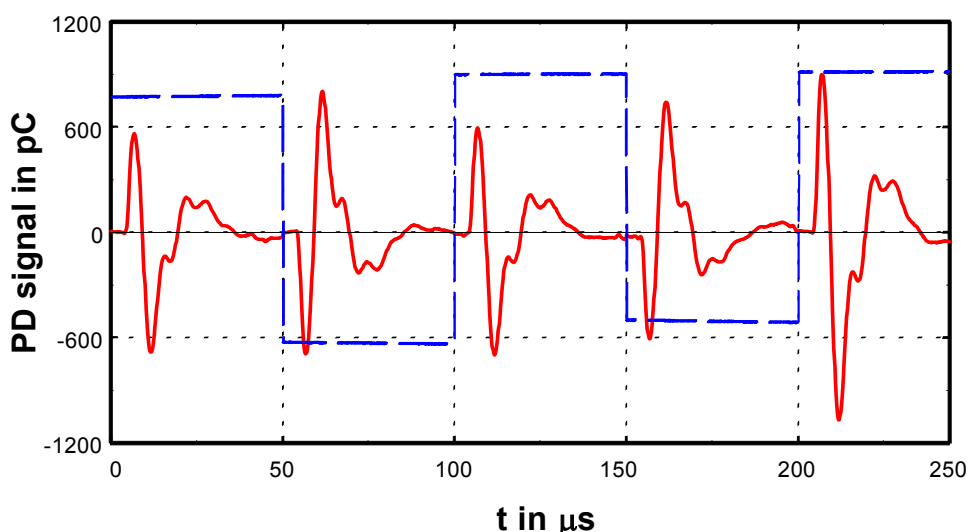
Fig. 4.2: Sequence of five PD signal (−) generated in a stator winding of a motor and the corresponding voltages (---)

Even without the 'electro-technical phenomenon' of the travelling wave, a modification of the PD signal may occur due to **solid state phenomena**. Quick alterations of the local space charge distribution may trigger an **anomalous discharge** that modifies the PD signal and generates a signal with the second peak higher than the first peak. This phenomenon may occur as well with commercial apparatuses (stator windings of motors) as well as with small laboratory specimens (e.g. a needle-plane arrangement in polyethylene or in oil) [Ber01, Pat02a]. More detailed analysis of this phenomenon is shown in measurements with needles moulded into polyethylene [Ber02a].

For demonstration **Fig. 4.3** shows such a type of discharge signal and a standard PD signal (typical for electrical treeing) generated by a sharp needle embedded in polyethylene (a good model for partial discharge processes at local defects in solid insulations). Interestingly the anomalous discharges occur before the initiation of a tree channel in which a gas discharge may burn [Ber01] .
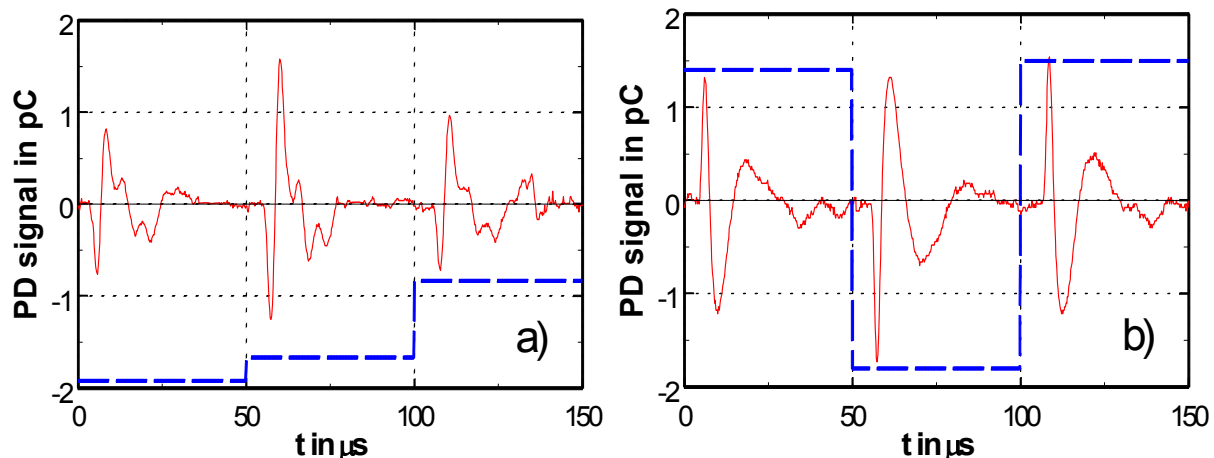
Fig. 4.3: Typical PD signals (−) and the corresponding voltages (- - -) with needles embedded in polyethylene **a)** for anomalous discharges and **b)** for standard discharges

Fig. 4.4 shows the cumulative discharge numbers in an experiment done for four successive test runs with linearly ramped voltage. The voltage was ramped up with **0.525 kV$_{rms}$/min** and the sensitivity of the partial discharge detector was set to **0.75 pC**. In the first region only anomalous discharges occur, in the second region the typical discharges for electrical treeing occur. After a pause without voltage load a second ramp was applied. The discharges started again as anomalous discharges but at a lower voltage. The change to typical tree discharges also took place earlier. In the third run the start was still earlier, an indication that the tree had grown.
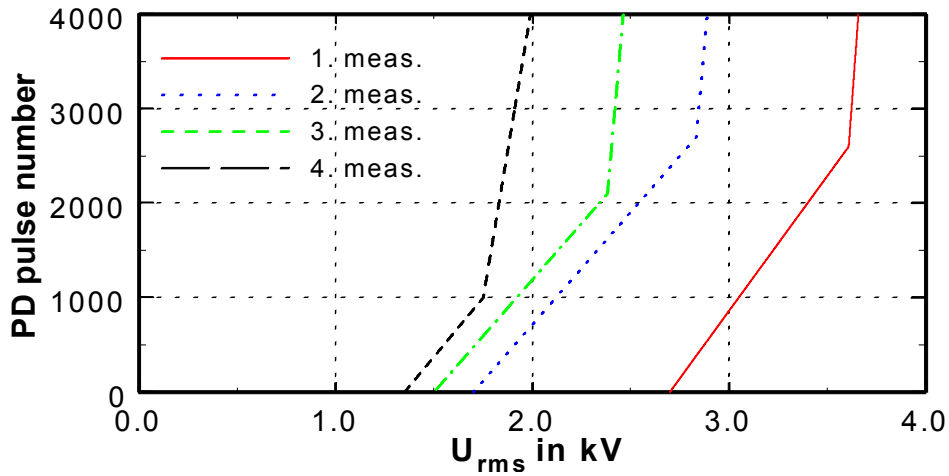
Fig. 4.4: Cumulative number of PD events in dependence on the applied test voltage
for four successive tests runs (voltage ramp, **0.525 kV/min**)

4.3   Double and multiple discharge pulses

In general for electrical treeing in polyethylene discharges occur in both polarities of the applied AC voltage [Ari07]. For discharges occurring in the positive half waves the magnitudes of the discharges are higher, show the 'standard shape', and in most cases only one discharge per half cycle occurs.

Usually discharges in the **negative half waves** have small amplitudes. The first peak is usually 'standard', while in some cases the shape of the second peak may be changed. In some cases discharges occur with time differences in the range of some ten **µs**, and hence more than one discharge is found in the measuring window of about **50 µs** length. **Fig. 4.5** shows some exam-
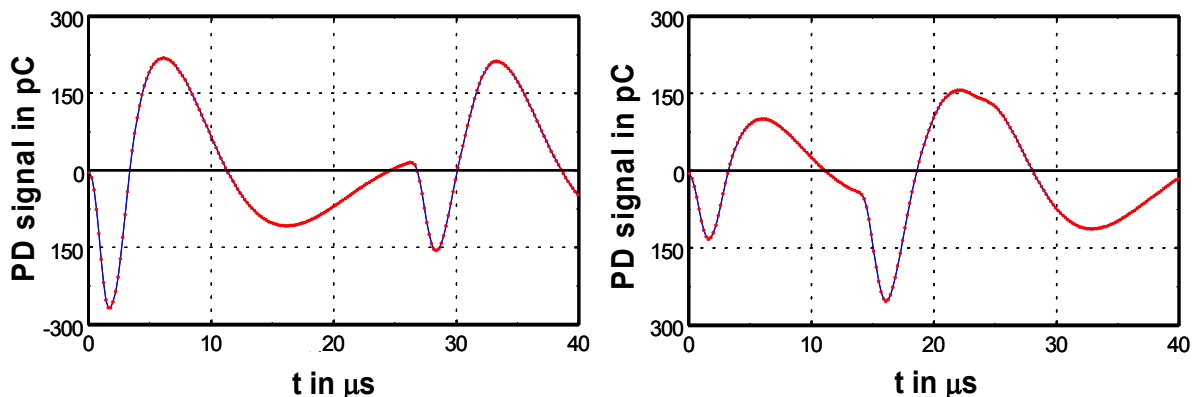
Fig. 4.5: Oscillating signals from the PD detecting device for partial discharges during
electrical treeing in polyethylene with more than one partial discharge in the
measurement time window

ples of the oscillating signals from the PD detecting device for partial discharges during elec-
trical treeing in polyethylene with more than one partial discharge in the measurement time
window. As mentioned already, discharges at **positive polarity** of the needle tip are usually
higher in intensity, but there are **no consecutive discharges** with time differences in the re-
gion of a few **10 μs**.

For experiments with an already existing electrical tree in polyethylene in about **6%** of all
measurement windows triggered by the system in negative half waves, more than one dis-
charge event per window occurred. The question was if these discharges occurred in the same
branch of the tree or at random in another one. The decision whether the one or the other pos-
sibility is correct, can be done by the analysis of the **time differences** between these dis-
charges. For independent discharges of the same type an exponential distribution of the time
differences is found [Pat03]. In the experiments discussed here, a distribution of the time dif-
ferences centred on a mean time interval of about **27 μs** was found. **Fig. 4.6** shows this distri-
bution. Interestingly the same distribution was found for the first 1000 pulses and for the last
1000 pulses of a set of 4000 partial discharge events. These seem to be a correlation that indi-
cates an influence of the first discharge in the time window on the ignition of the next dis-
charge. This indicates **negative "repetitive" discharges in the same tree branch**.
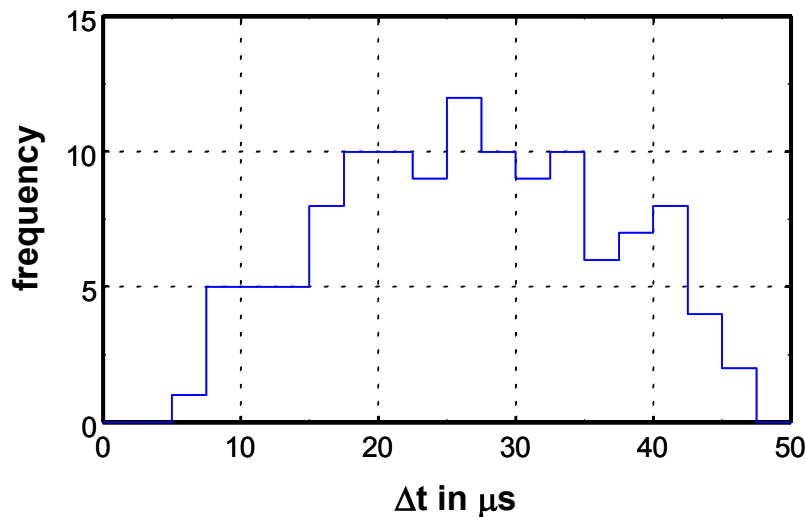
Fig. 4.6: Frequency distribution of the time intervals **Δt** between 'multiple discharges'
at negative voltages at the needle tip during electrical treeing

4.4   Separation of the noise signals from discharge pulses

Partial discharge measurements are usually performed with a high sensitivity to enable the reg-
istration of small partial discharge signals. This leads to the side effect that also noise signals
may be registered, whereby in dependence on the trigger level more or less noise will be con-

tained in the data sets. The use of different parameters of the pulse shape such as t_1, t_2, t_3, t_4 and their combinations and also $|l_2|/l_1$ can be helpful to separate noise from PD signals [Pat02].

4.4.1 Classification according to t_1

For demonstration **Fig. 4.7** shows a distorted pulse shape formed by the response of the band-pass filter of the PD measuring device for a PD signal generated in the stator windings of a small motor. In this case the system generates an oscillating signal that decreases in time, but that after **45 µs** is still high enough to trigger the following time window of the measuring system about **6 µs** after the end of the first signal window. To eliminate a double registration of these pulses, only signals with $t_1 > 0$ (time corresponding to the first maximum of the PD signal) are used for evaluations.
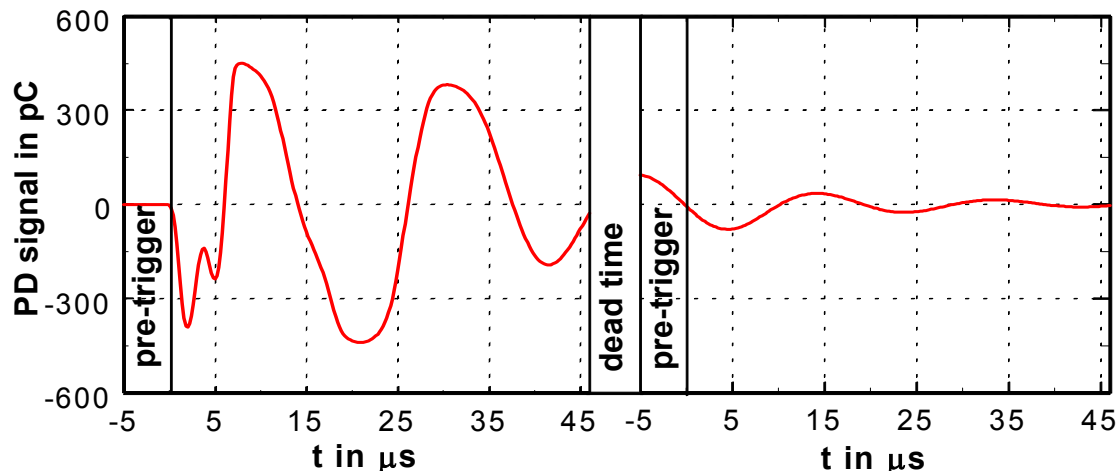
Fig. 4.7: Pulse shapes of the output signals of the PD measuring device for a PD signal measured at the winding of a stator; the time difference between the two windows (dead time of the monitoring system) is about **6 µs**

4.4.2 Classification according to t_2 - t_1

To check the efficiency of a PD signal characterization on the basis of the difference between the times t_2 and t_1 of the second and the first peak of the PD signal, the following experiment was done. A model of a stator bar was connected to the measuring system and –- without applying an external voltage to the specimen – the sensitivity of the measuring system was increased until noise signals were registered. After the registration of about **700** impulses a calibration signal of about **10 pC** is applied to the system. After another **1500** impulses the calibration system is switched off and after another **1000** impulses the calibration signal is applied again.
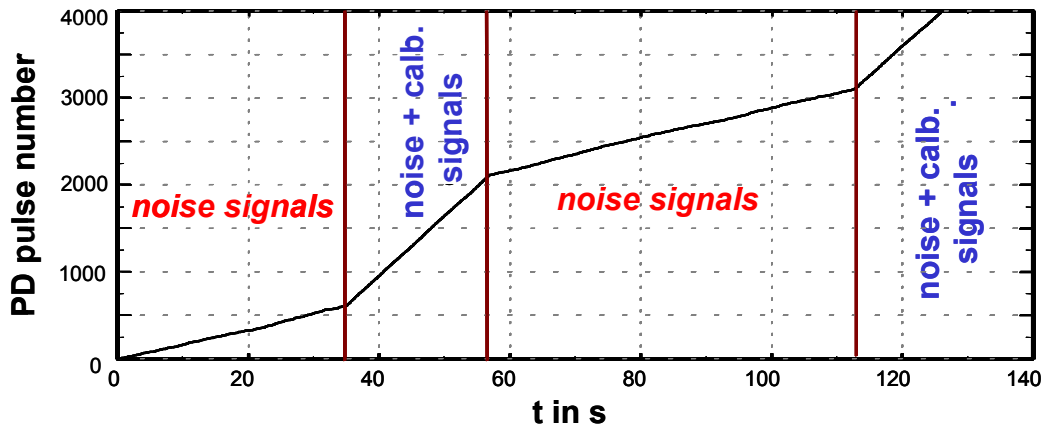
Fig. 4.8: Pulse numbers over time for 'noise' and 'noise' together with calibration pulses

Fig. 4.8 shows the corresponding pulse numbers over time diagram. Four different regions are clearly marked by the different pulse rates. In the first and the third region the pulse rate was about **0.36 pulses/cycle** while in the second and the fourth region the pulse rate was about **3 pulses/cycle**.

The more detailed analysis of the pulse shapes revealed that there are significant differences. These differences in the shapes of signals can be used to separate discharge signals from the noise. **Fig. 4.9** shows the frequency distributions of the time differences t_2 - t_1 between the first two peaks for 500 consecutive pulses taken from regions with 'noise' only and 'noise' and calibration pulses respectively. The two distributions are different; for 'noise' the time differences are predominantly above **5 µs**, for calibration pulses predominantly below **5 µs**.
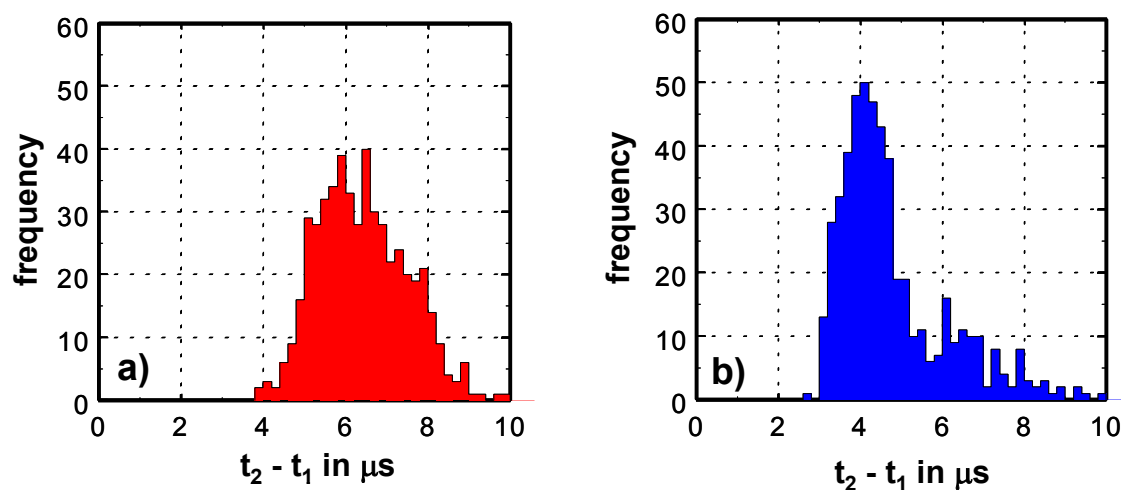
Fig. 4.9: Frequency distributions of t_2 - t_1 for pulses from different regions
a) noise, pulses **1** to **500** and **b)** noise and calibration signals, pulses **1001** to **1500**

On the basis of the difference shown in the frequency distributions of the time differences t_2 - t_1, a separation of the pulses can be performed. **Fig. 4.10** shows the pulse numbers over time diagrams for the two classes of signals. The curve from Fig. 4.8 is included in the graph for comparison. The 'noise' signals (with constant frequency of occurrence) and the calibration pulses (between **38** and **58 s** and **112** and **126 s** respectively) are fairly well separated.
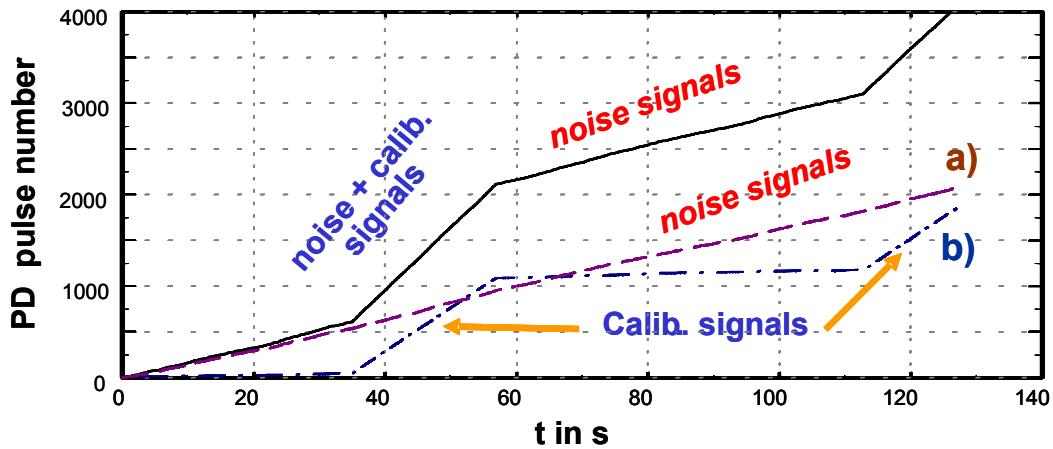
Fig. 4.10: Pulse numbers over time for pulses selected by
a) 5 μs < t_2 - t_1 (noise only) and **b) t_2 - t_1 < 5 μs** (calibration pulses only)

4.4.3   Classification according to I_2 / I_1

Another differentiation can be found if the ratio of the magnitudes I_2 / I_1 of the two first peaks of the signal is taken. As shown in **Fig. 4.11**, for the noise signals the ratio I_2 divided by I_1 is
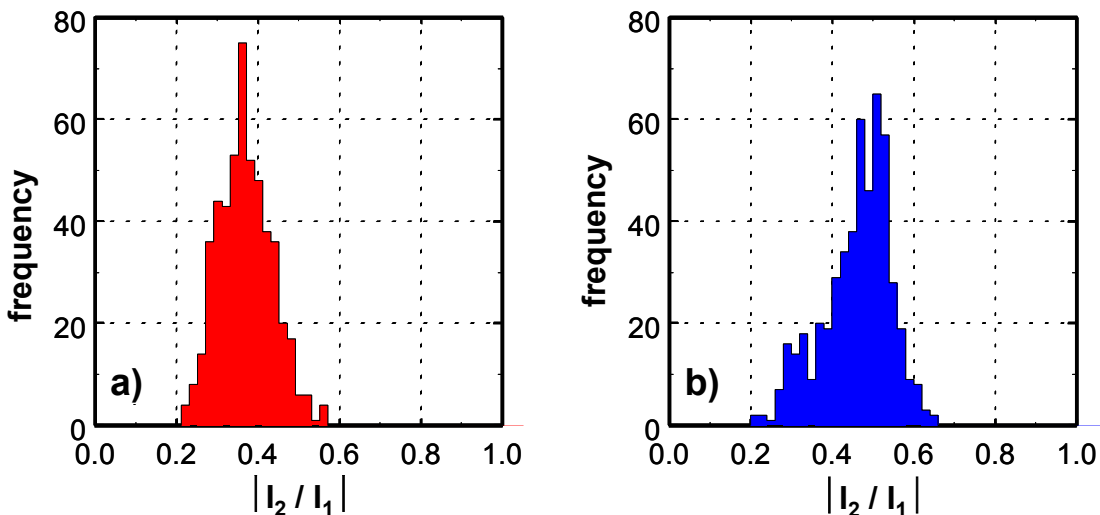
Fig. 4.11: Frequency distributions of $|I_2$ / $I_1|$ for pulses from different regions of Fig. 4.7
a) noise, pulses **1** to **500** and **b)** noise and calibration signals, **1001** to **1500**

below **0.5**, while for the calibration pulses together with noise the ratio is above **0.5**. Hence there is a quicker decline for the noise pulses. **Fig. 4.12** shows the separation of the pulses on the basis of this classification. The result is comparable to that found with t_2 - t_1.

The same classification is valid not only for the data set of calibration signals but also for the measured data-set independently of the test objects. Large test objects as well as laboratory specimens (a sharp needle embedded in polyethylene) have been used; more details see [Pat02a].
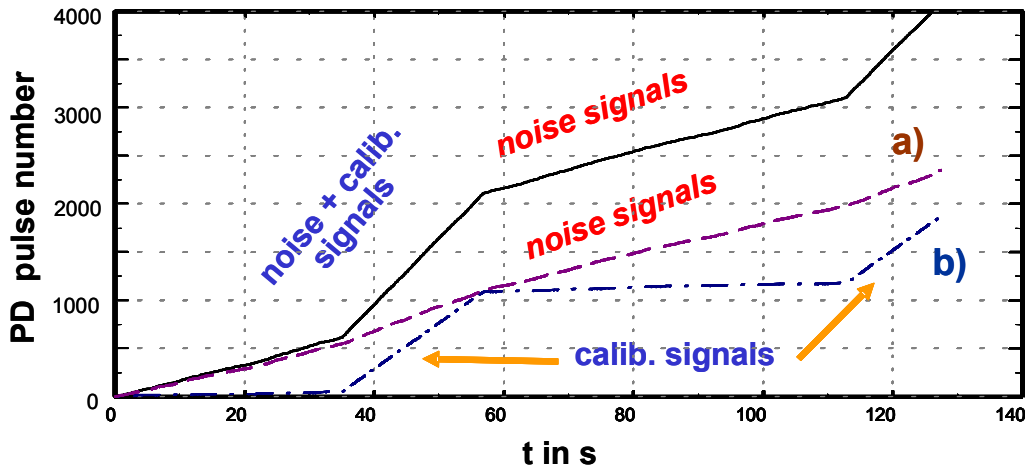
Fig. 4.12: Pulse numbers over time for pulses selected by
a) $|I_2 / I_1| < 0.5$ (noise only) and **b)** $0.5 < |I_2 / I_1|$ (calibration pulses only)

4.5   Identification and separation of PD sources in stator windings

In commercial power equipment in many cases discharges occur simultaneously at different spots in the apparatus. In this case, the Pulse Sequence Analysis (PSA) correlates partial discharges from different sources and this may lead to an erroneous interpretation. The more detailed analysis of the pulse shapes of the PD signals revealed that there are differences in accordance to the type of the PD-active defect [Pat03a]. These differences can be used to separate discharge signals from different sources and to split up the measured data sets into different sets that are characteristic for one specific defect and that can be analysed separately. With this procedure different sources or even different stages of the degradation process can be identified. In the following a more detailed analysis of the pulse shapes of PD signals from a stator of a small motor will be performed and it will be shown that characteristic differences may be used to obtain more information out of the registered data.

4.5.1 Experimental procedure

For the analysis of the stator windings of a motor, the voltage is usually applied to both ends of one of the phase windings while the others and the iron core are grounded. In our experiments stators of small 125 W AC motors were loaded with a ramped voltage with a rate of rise of **0.525 kV$_{rms}$/min** until 4096 partial discharges had occurred. The sensitivity was set to about **2.5 pC.** In the course of the research work presented here a series of measurements was performed with various ways of application of the voltage load. In the two first measurements (**meas. A** and **meas. B**) the voltage was applied at one end of the winding, while the other end was on free potential. In the last measurement run both ends of the winding were connected to the voltage (**meas. C**) (**Fig. 4.13**). With regard to the voltage distribution and the local AC field the three different measurements were identical; hence a similar discharge behaviour could be expected.
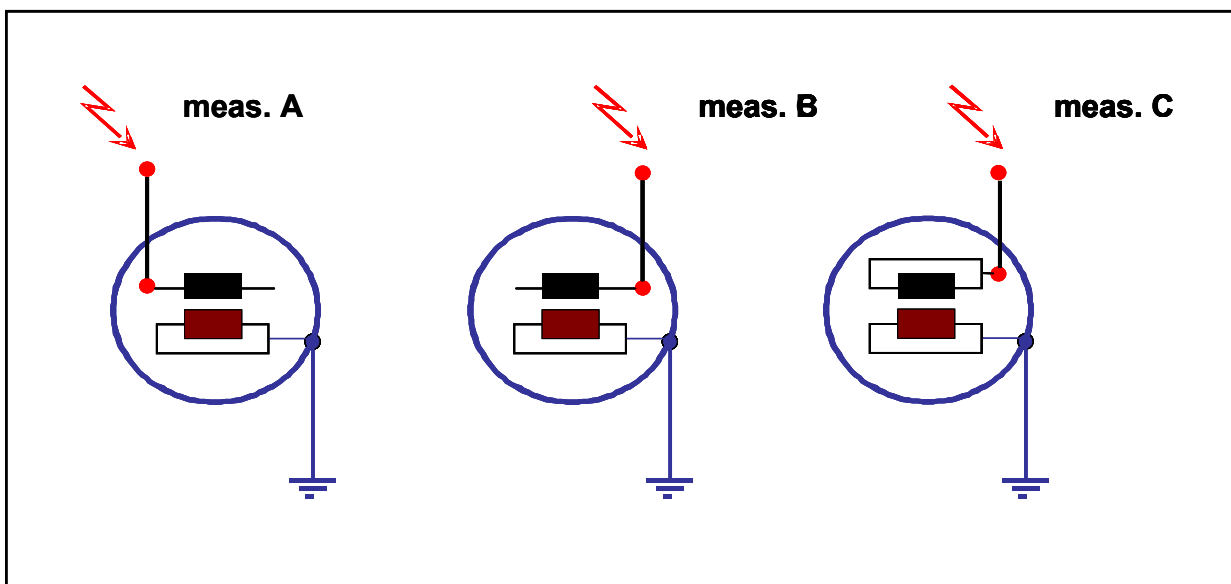
Fig. 4.13: Different ways of application of the voltage load to the stator windings of a small motor

4.5.2 Standard analysis (phase resolved evaluations)

In the standard evaluations of partial discharge data the frequency distributions of the phase angles at which the discharges occur are commonly used. **Fig. 4.14** shows corresponding plots for the three measurements. Nearly all discharges had occurred in the inclining part of the voltage curve and there are no characteristic differences between the measurements. This is not surprising, because the **50 Hz** voltage load was identical in all three measurements and – ex-

cept of a possible ageing effect due to the repetition of the measurements – the partial discharge process should have been basically the same.
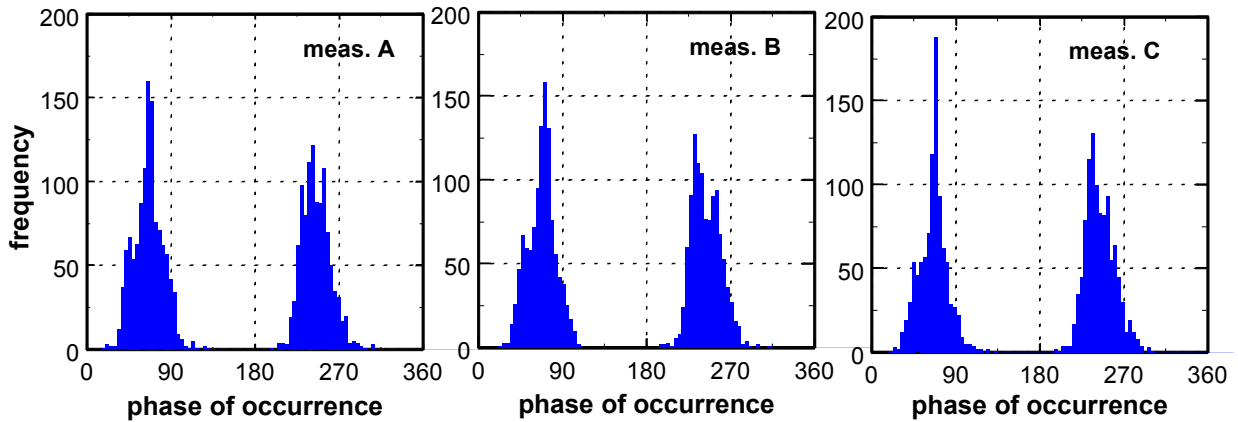
Fig. 4.14: Frequency distributions of the phase angles ϕ at which the discharges occurred in the three measurements with different experimental setups

Fig. 4.15 shows the pulse numbers over time for the three measurements. Apart from a little shift to lower voltages, the discharges started at nearly the same voltage in all three cases. The initial incline of the pulse number count over time equals a pulse rate of two per cycle, i.e. the discharge processes started with one discharge per half wave of the applied voltage. For the measurement **meas. A** after about three seconds a marked increase of the discharge rate occurred, while for the measurements **meas. B** and **meas. C** the corresponding change occurred already within one second after discharge inception.
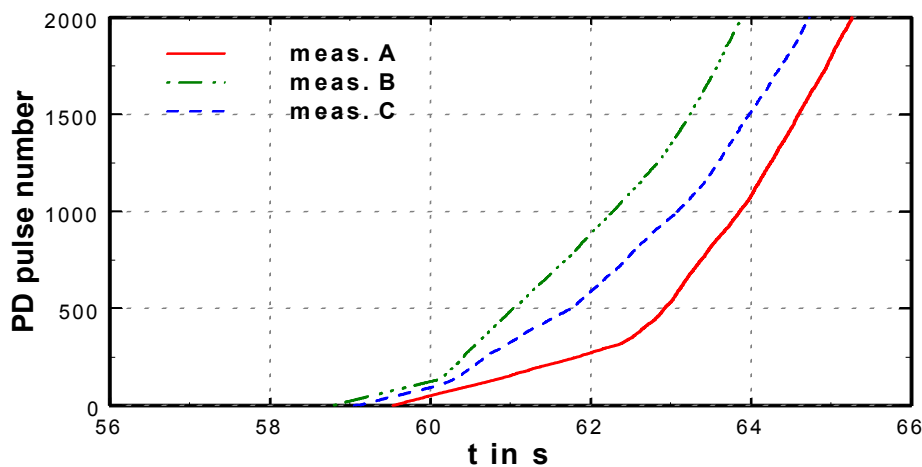
Fig. 4.15: Pulse numbers over time for the three measurements of the stator windings of a small motor with different experimental setups

4.5.3 Identification of PD signals from different spots

It is known that in large test objects the shape of a PD pulse may be modified on the path from its origin to the coupling device [Gro03]. Hence, although the PD activity is similar in all three cases, with the same defects producing the discharges, the PD pulses arriving at the coupling impedance may be different in dependence of their place of origin, and different oscillating signals may be formed by the band pass filter. The basic influence of the test object geometry on the pulse shape can easily be demonstrated if a calibration signal is fed into the winding of a stator in different ways.
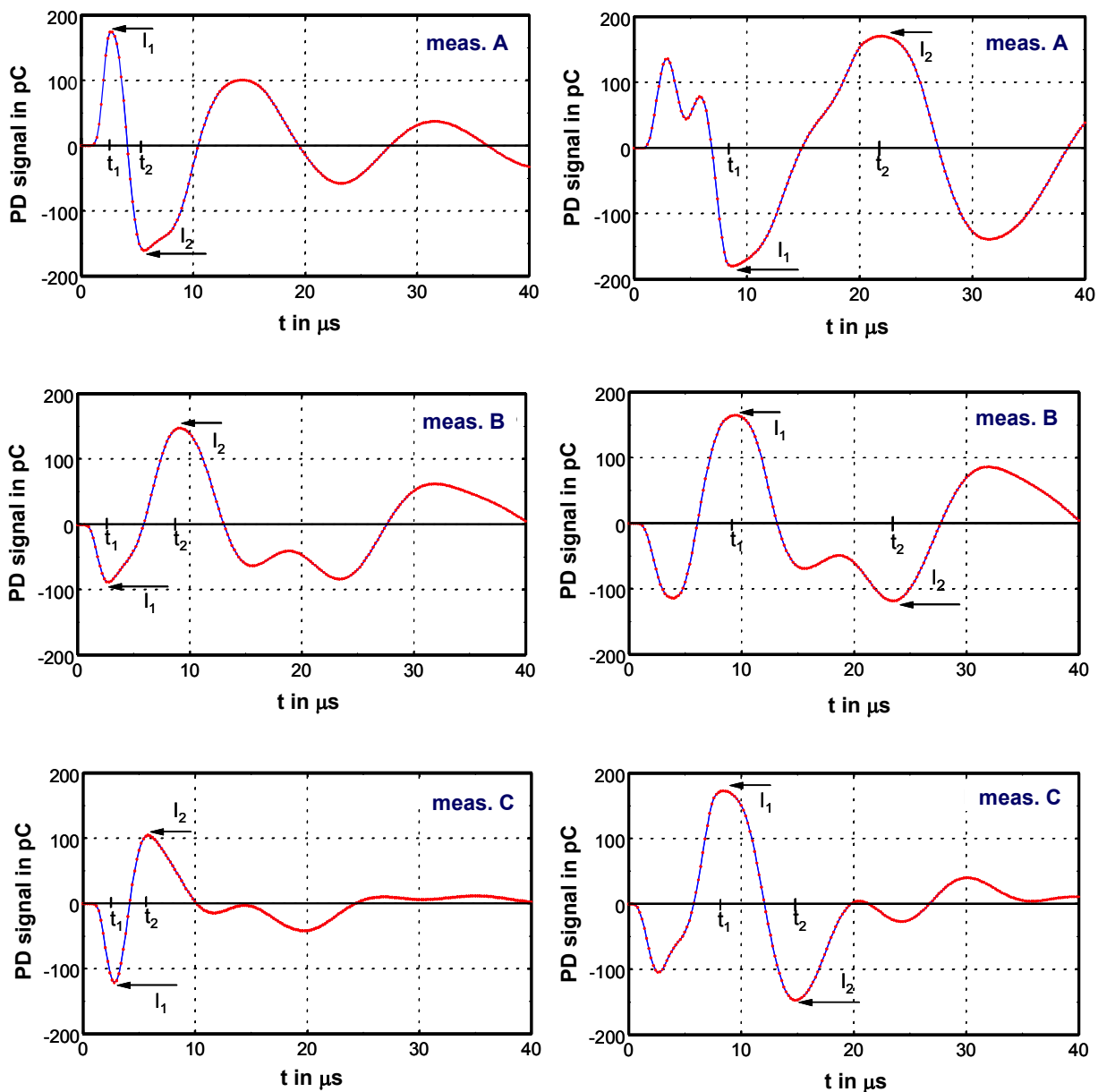
Fig. 4.16: Examples of typical discharge signals found in the three measurements and the corresponding parameters l_1, l_2 and t_1, t_2

Fig. 4.16 shows typical output signals of the PD measuring device found in the three measurements of a small stator under different measurement conditions. If only the highest peak of the oscillating signal is taken to characterize the discharge intensity a misinterpretation may occur. It is worth mentioning that for some of those signals standard analyses would even indicate a wrong polarity of the pulse.

Fig. 4.17 shows the frequency distributions of t_1, t_2 and $t_2 - t_1$ for the three measurements of a stator. The patterns are significantly different, except for the time interval below **5 µs**, in which
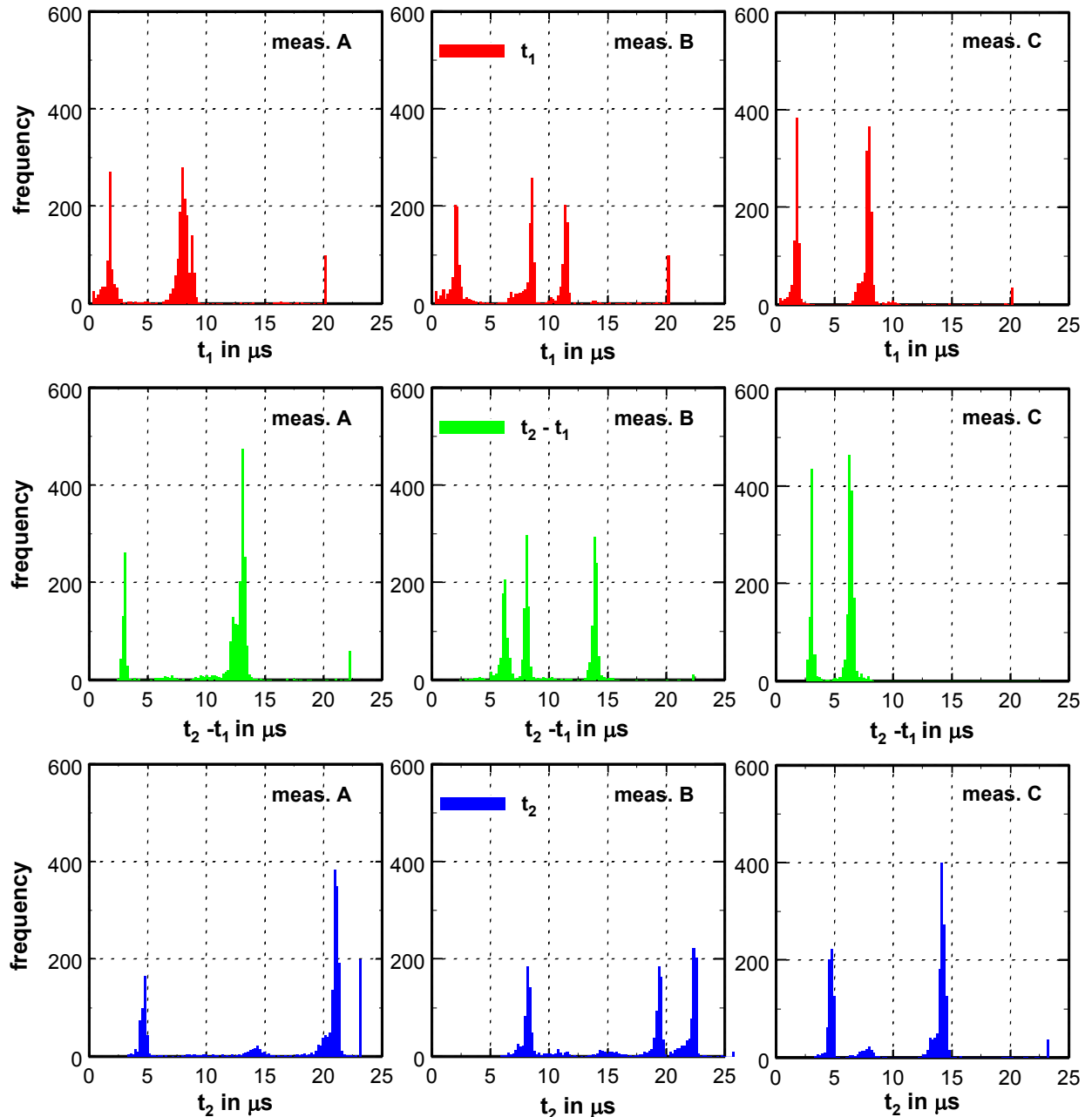
Fig. 4.17: Frequency distributions of the times t_1, t_2 and $t_2 - t_1$ for the three measurements of a stator windings of small motor

for **meas. A** and **meas**. **C** all three parameters appear similarly. For **meas. B** only t_1 values appear in this time interval.

As shown in Fig. 4.14 the phase angle distributions of the discharges are identical in all three cases, but the shapes of the oscillating signals are different. The reason for this is different paths that the signals had to travel within the winding of the stator in the different experimental setups. In addition, Fig. 4.17 indicates that there exist at least two different spots within the winding at which partial discharges occur.

4.5.4   Separation of PD signals from different spots

The different shapes of the signals can thus be used to separate signals with different origins. **Fig. 4.18** shows the pulse numbers over time with $t_2 < 5\ \mu s$ for **meas. A** and **meas. C** and with **18 μs < t_2 < 20 μ**s for **meas**. **B**. In all three measurements the partial discharges occur with a constant discharge rate of about three discharges per cycle. Except of the earlier start of the discharges in **meas. B** and **meas. C** the discharge behaviour is the same as in **meas**. **A**.

Fig. 4.19 shows the pulse numbers over time for $t_2 > 5\ \mu s$ for the **meas. A** and **meas**. **C** and $t_2 > 20\ \mu s$ for the **meas. B**. The curves are nearly identical up to **62 s** and not too different above. The initial discharge rate is two discharges per cycle and at about **63 s** in all three measurements a marked increase of the discharge rate up to about ten discharges per cycle occurs. In dependence of the actual setup, the defect produced different output signals of the band pass filter.
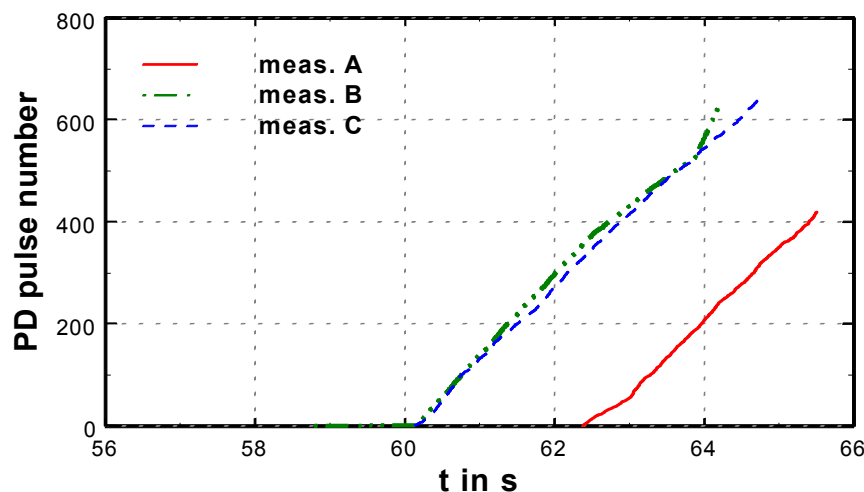
Fig. 4.18: Pulse numbers over time for $t_2 < 5\ \mu s$ for **meas. A** and **meas. C**
and **18 μs < t_2 < 20 μs** for **meas. B**
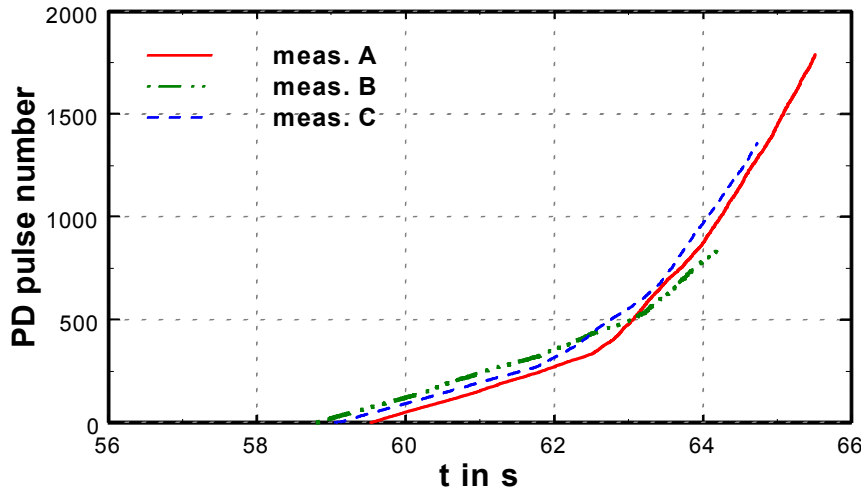
Fig. 4.19: Pulse numbers over time for $t_2 > 5\ \mu s$ for **meas. A** and **meas. C**

and for $t_2 > 20\ \mu s$ for **meas. B**

Fig. 4.18 and Fig. 4.19 show clearly the different behaviour of the two defects. While Fig. 4.18 shows no change of the activity in time (and applied voltage), in Fig. 4.19 the increase of the applied voltage with time led to a significant increase of the discharge rate.

Another interesting result is shown in **Fig. 4.20**. For the first partial discharges (from the most critical defect with regard to its PD inception voltage) we find similar values for t_1 for all three measurements but different values for t_2 and $t_2 - t_1$. The data for the very first signals of the measurements **meas. A** and **meas. B ($t < 60$ s)** are nearly identical. **Fig. 4.21** shows the corresponding graphs for the time interval between **62** and **64 s**, in which at least two defects are active.
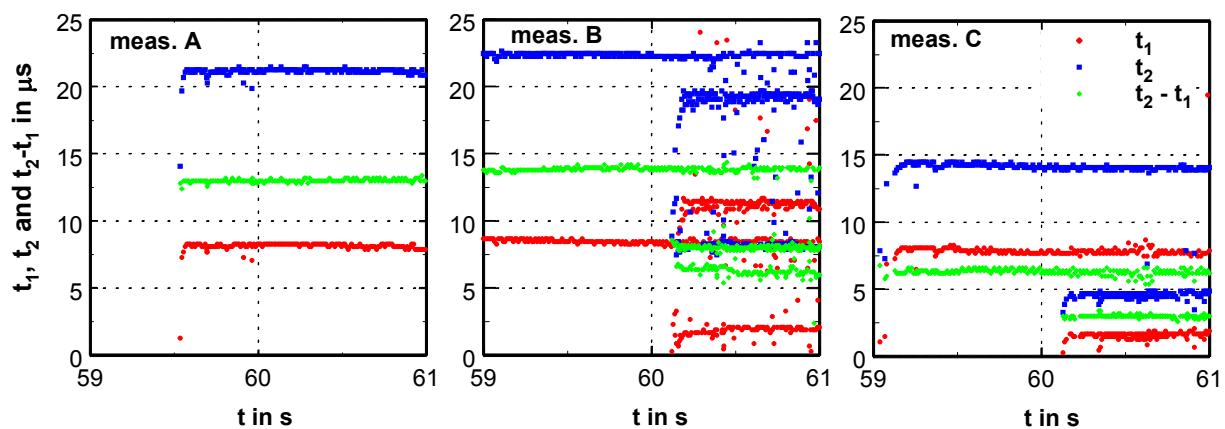
Fig. 4.20: Parameters t_1, t_2 and $t_2 - t_1$ over time for the selected time $59\ s < t < 61\ s$

for the three measurements

Other parameters as e.g. the zero crossings t_3 and t_4 after the peaks can also be efficiently used to characterize the shape of the impulse signals. Depending on the kind of the connection to the high voltage supply, the discharges produced by the defects shift especially the zero crossings t_3 after the first peak towards longer times. Thus a plot of these times can also be used to characterize the shapes of the curves and thus to identify the defects.
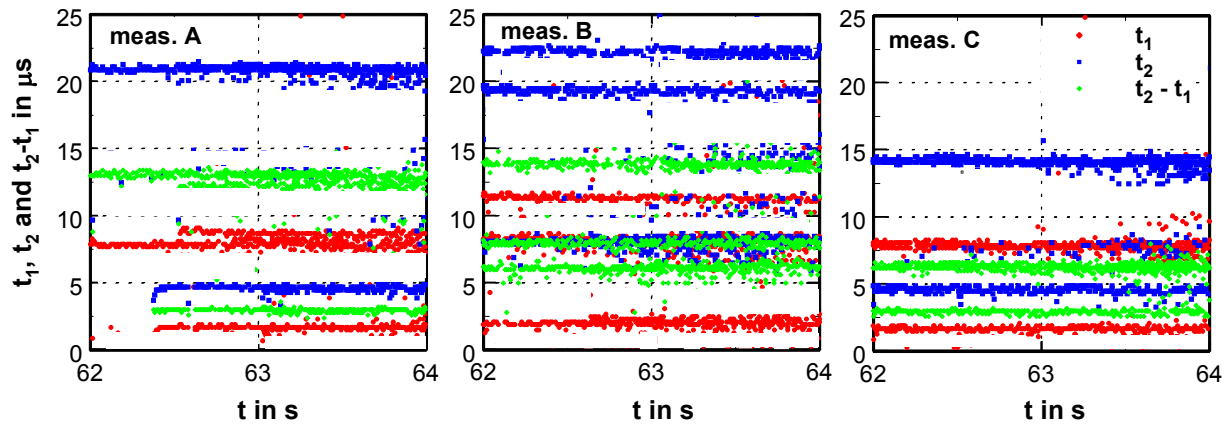
Fig. 4.21: Parameters t_1, t_2 and $t_2 - t_1$ over time for the selected time **62 s < t < 64 s** for the three measurements

4.6 Summary

For better insight into the partial discharge processes not only the PD magnitude and its polarity should be taken into account but also additional information that can be drawn from the actual pulse shape of the single discharge pulse. Hence the PD pulse shape is characterised by the first two peaks I_1 and I_2 of the oscillating PD signal, the times t_1 and t_2 at which the peaks occur and the times t_3 and t_4 of the following zero crossings and time t_5 of the beginning of the curve. The results of the more detailed analysis of the pulse shapes can be concluded as follows:

- The oscillating PD signals generated in geometrically extended test objects as well as on the small laboratory test objects revealed that there are differences in accordance to the type of the PD-active defect. These differences were used to identify and then to separate the discharge signals from different sources or spots for separate analysis. With this procedure different sources or even different stages of the degradation processes were identified and characterized to monitor the different stages of ageing.

- Pulse Shape Analysis is used also to eliminate noise from the PD signals. The different parameters of the pulse shape such as the time t_1 of the first peak, the time difference $t_1 - t_2$ between the first two peaks and/or the ratio I_2 / I_1 of the magnitudes of these peaks were used successfully to separate noise from real partial discharge signals.

- Anomalous discharges (discharge with the second relative peak of the PD signal higher than the first peak of the PD signal) may occur even without the electro-technical phenomenon of the travelling wave due to the quick alterations of the local space charge distribution.

- In electrical trees in polyethylene consecutive discharges may occur with time intervals of typically some **10 μs**. In the negative half waves of the applied voltage, 'multiple' discharges could occur with a mean time difference of about **27 μs**.

- The experimental results on the stator windings of a small motor have shown in how far the different pulse shapes of the output signal of the band pass filter can be used to identify different defects located in different regions of the winding.

- The evaluation of discharge signals from a stator reveals that the shape of the oscillating signal is characteristic for the position of a defect within the winding. The parameters t_1, t_2 and $t_2 - t_1$ are used efficiently to separate signals from different sources. In the experiments in which the voltage was applied to only one end of the winding and the opposite is left on free potential. The phase angle distributions of the discharges had been identical in all cases, but the shapes of the oscillating signals showed the existence of two PD-active defects with different behaviour depending on the applied voltage. According to different parameters of the pulse shape these defects are clearly separated.

It is clearly shown in this investigation that the use of Pulse Shape Analysis of partial discharge data sets is very helpful for a detailed interpretation.

5   Space Charges and their Influence on Partial Discharge Processes

In this chapter it will be shown from measurements of different electric apparatus, in how far the partial discharge phenomena are influenced by charges accumulated as the consequence of prior discharges. This influence of space charges will be then discussed on the basis of a model of an improved PD equivalent circuit.

5.0   Introduction

A partial discharge in a solid dielectric or a commercial insulation consisting of different insulating materials often generates **local charge accumulations** that change the local electric field in the surrounding of the defect. Hence the conditions for the ignition of the following discharge are changed. Consequently in many cases a **correlation between consecutive partial discharges** exists that can be used for a better understanding of the local degradation processes.

The **Pulse Sequence Analysis** has shown that space charges generated by previous partial discharges determine the further sequence of discharges and the method has proven to be very efficient in characterizing the defect type. Especially the **time differences Δt_n** and the **voltage changes ΔU_n between consecutive discharges** have shown to be very meaningful parameters.

5.1   Space charges in solid dielectrics

As a consequence of the **Poisson equation**, space charges modify the local field distribution. If in a partial discharge process charge carriers are injected into and/or moved within a dielectric, depending on the actual properties of this dielectric a local accumulation of charge carriers around the discharge active defect may occur. In this case – characteristic for solid and liquid dielectrics – the partial discharge phenomena are influenced. Partial discharges in gaseous insulations do not produce space charges that influence the ignition, because the drift velocity of the charge carriers is so high that no relevant space charges stay in the surrounding of the defect. If a defect is surrounded by a solid or liquid dielectric in most cases the influence of space charges will be predominant, because the charges injected from a defect are trapped close by and modify the local electric field.

As mentioned already partial discharges always occur, if in a limited region in an electric apparatus the local electric field exceeds the electric strength of the material in this specific area. In composite insulations these regions often contain separate gas phases, and a local breakdown occurs because the electric strength of gases is usually smaller than that of liquid or solid materials. The local breakdown generates a small **avalanche of high energetic charge carriers** that may lead to a **local degradation** of the material (e.g. via bond scission) and at the boundaries of the gas phase an **accumulation of charge carriers**. The build-up of space charges and

surface charges at dielectric interfaces causes a superimposed local space charge field at the site. In this case the resulting local field is no longer determined by the externally applied voltage only but also by the space charge field from previous discharge pulses. Consequently, the phase angle of the external voltage where the following discharge occurs is no meaningful parameter, because the phase of occurrence does not imply significant information on the magnitude of the actual local electric field.

The standard methods for analyzing partial discharges usually examine only the whole data sets accumulated in dependence of the actual phase angles of the applied voltage and do not take into account any correlations between consecutive pulses. However each partial discharge modifies the distribution of space or surface charges and hence changes the local electric field and consequently modifies the condition for the ignition of the next discharge [Ben04a]. The use of the Pulse Sequence Analysis i.e. the analysis of the **sequence of the discharges** permits a better insight into the space charge and degradation phenomena [Hoo94, Hoo95].

In many cases the analysis of sequences of discharges shows a **systematic shift of the phase angles of occurrence.** This phenomenon occurs with small specimens in the lab (e.g. a needle in polyethylene) as well as with commercial apparatuses (stators of small motors, HV transformers or AlN cooling devices). As a result of the different mobility of different charges (electrons or ions) often a non-symmetric behaviour with regard to the applied voltage exists. In some cases the accumulated charge changes periodically and thus also the characteristic sequences of PD events.

It is well known that partial discharge processes change with time [Ben04]. Due to space charges in solid dielectrics a continuous shift of the phase angles of occurrence and often a more or less periodic behaviour due to a repetitive build-up of space charges (with a reset inbetween) may occur. Also without an irreversible change of the defect, space charges may lead to a different phenomenological appearance of partial discharge sequences over time [Pat02, Pat03]. Hence in many cases it is more meaningful to **evaluate the sequence** of a small number of consecutive discharges instead of the evaluation of a huge number of discharge pulses accumulated without taking care of the sequence [Pat01]. From a data set of discharges e.g. the sequence of the actual voltages U_n at which discharges occur over the time t_n, or the sequence of the voltage differences $\Delta U_n = U_{n+1} - U_n$, or the time intervals $\Delta t_n = t_{n+1} - t_n$ between consecutive discharges may be extracted and used for the analysis. These or other sequences often reveal a characteristic behaviour with a systematic structure. In the following, sequence correlated data from different specimens will be discussed in detail.

5.1.1   Electrical treeing

The phenomenon of a systematic shift in the phase angles at which partial discharges occur was first found in electrical treeing in polyethylene [Hoo95a]. In this case the external voltage levels at which (within a half cycle of the applied voltage) discharges occurred changed step

by step. The accumulated phase angle distribution of the discharges showed a broad scatter, while the voltage changes ΔU concentrated around three or four characteristic values. The phase angles of occurrence shifted, thus indicating a random like behaviour, but the voltage differences between consecutive discharges were nearly constant.

For demonstration **Fig. 5.1** shows some results from electrical treeing of the epoxy resin in a needle-plane electrode arrangement. Also in this case, the phase angles as well as the voltages show a broad scatter, while the voltage changes concentrate around four distinct values. The time differences Δt between consecutive discharges show some scatter, but they indicate that there is only one PD-active defect. When examining the direct sequence of voltage values at which the discharge occur, a conspicuous behaviour in a few cycles of applied voltage can be observed. Especially if the test voltage is increased slowly, at first partial discharges usually occur only at one spot in the specimen and mostly only one discharge per half cycle occurs. In this case a clearly structured correlation between consecutive discharges can be found.
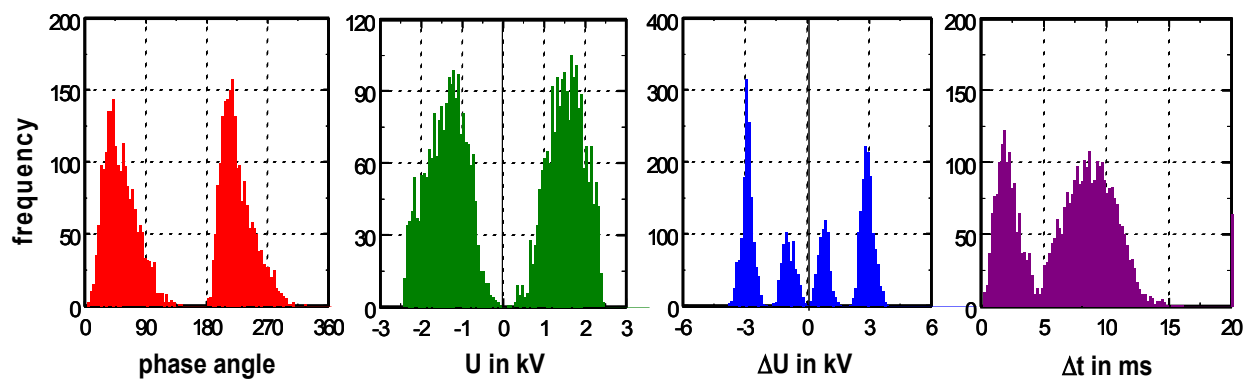
Fig. 5.1: Phase angles of occurrence ϕ, external voltages **U**, time differences Δt between consecutive discharges and voltage changes ΔU between consecutive discharges during electrical treeing in epoxy resin

Fig. 5.2 shows a series of discharges from a measurement of a needle in polyethylene. The voltages at which the discharges occur show a behaviour which is especially characteristic of the early stage of tree growth, during which the solid-state phenomena within the polymer around the needle tip play the decisive role. At voltages just above the partial discharge inception voltage, there is only one discharge event within a half cycle of the voltage. After a few cycles of applied voltage a reset occurs and – with or without a discharge free time interval in-between – the shift starts again. The voltage differences ΔU between consecutive discharges are nearly constant. The time differences Δt show a sort of oscillation and are alternatively (in most cases) either bigger or smaller than **10 ms** whereby two consecutive time differences often add up to **20 ms**. After discharges following positive voltage changes ΔU usually time dif-

ferences of more than **10 ms** occur, discharges after negative voltage changes are usually followed by time differences of less than **10 ms**.
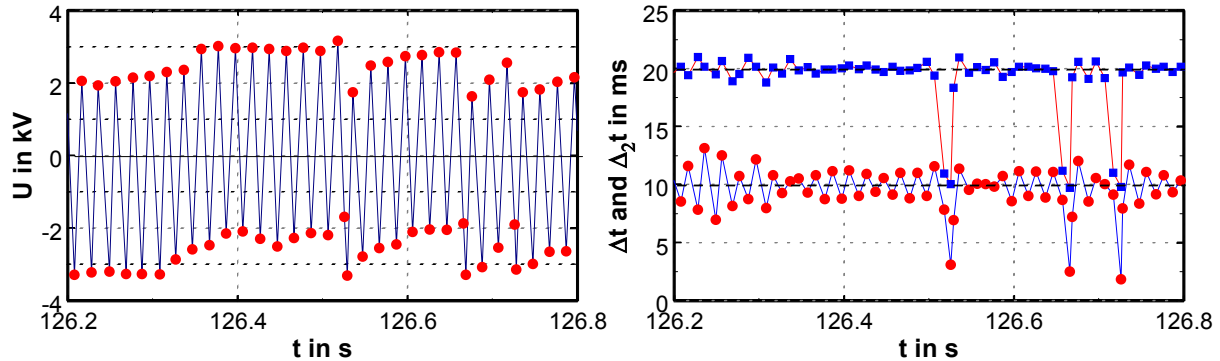
Fig. 5.2: Voltages **U** at which discharges occur, time differences Δ**t** (•) between consecutive discharges and time differences Δ$_2$**t** (■) between next but one discharges for a needle in polyethylene

5.1.2   Partial discharges in a high voltage test transformer

Measurements performed on a commercial high voltage test transformer show a similar phenomenon, with an even more systematic behaviour [Pat06a]. As an example **Fig. 5.3** shows some results performed with a HV test transformer for the voltage level of **100 kV** (TEO 100/10) at constant voltage load. The phase angle histograms show mainly two groups of partial discharges, a relatively sharp one in the inclining part of the positive half waves and another comparatively broad one in which the discharges occur during almost the entire rise time up to the negative peak voltages.
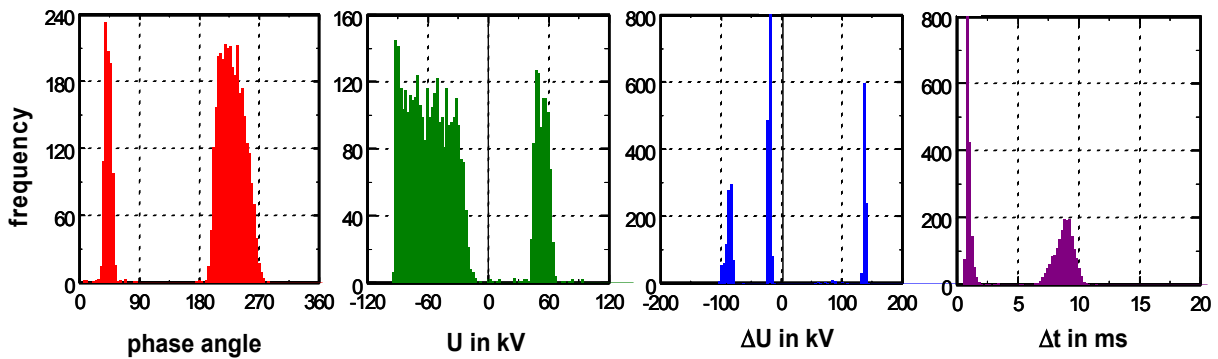
Fig. 5.3: Phase angles of occurrence ϕ, external voltages **U**, voltage changes Δ**U** and time differences Δ**t** between consecutive discharges for a measurement of a **100 kV** test transformer

There are much more discharges in the negative half waves, and most discharges occur after small negative change **ΔU**. The frequency distribution of the voltages at which the discharges occur is nearly constant and shows only a small increase towards the peak voltage. If the frequency distribution of the voltage changes **ΔU** between consecutive discharges is taken, a different distribution with three very sharp peaks is found. For the time differences between consecutive discharges **Δt** a triangular distribution with a peak at about **9 ms** and a very narrow and high peak at about **1 ms** occur.
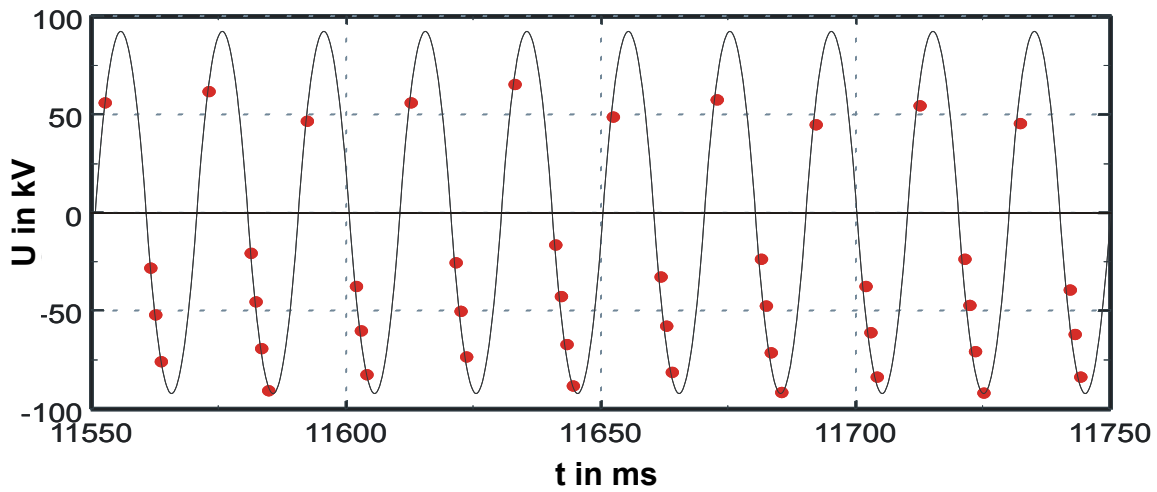
Fig. 5.4: Sequence of partial discharges in the paper-oil insulation
of a **100 kV** test transformer

Fig. 5.4 shows a sequence of the partial discharges for 10 consecutive cycles. There is only one discharge in each positive half cycle, but 3 or 4 events in the negative ones. While the voltages at which the discharges occur change from cycle to cycle, the voltage changes between consecutive discharges are very definite.

The reason for this non-symmetric behaviour with regard to the polarity of the applied AC voltage is the fact that the pulse heights are different for both polarities. Discharge pulses in the negative half cycles are comparatively small and hence produce only a small opposing voltage that is overcome after a corresponding increase of the applied AC voltage of about **-25 kV** and a consecutive partial discharge occurs within the same negative half cycle. The pulse heights in the positive half cycles are much higher, hence the corresponding opposing voltage is higher and consequently the next pulse occurs only when the polarity of the voltage has changed i.e. in the following negative half cycle. This behaviour leads to multiple discharges in the negative half cycles (separated by about **1 ms**), while in the positive ones there is only

one event per cycle. Detailed analyses show, that the time constant for the decay of the accumulated charges is much larger than the cycle of the test voltage and Δ**U** is very reproducible. The defect in the specimen discussed in Fig. 5.3 is a gas filled gap in the paper-oil insulation. The non symmetric behaviour indicates that the boundaries of the gas inclusion are different i.e. the defect is probably situated at one of the electrodes. The sequence of the voltage levels at which discharges occur (shown in Fig. 5.4 in detail for ten consecutive cycles of the AC test voltage) supports this explanation.

Another interesting behaviour is shown in the two following sets of measurements on the same HV transformer. The first measurement was performed at **70 kV$_{rms}$** and the second at **100 kV$_{rms}$**. **Fig. 5.5** shows the voltages **U$_n$** at which discharges occur and the corresponding time differences Δ**t$_n$** between consecutive discharges, split up according to the polarity of the corresponding voltage changes Δ**U$_n$**, for a measurement with a voltage load of about **70 kV$_{rms}$**. The actual voltage plot shows that there is -normally with two events per cycle a monotonous shift of the voltage levels that ends with a reset and starts again from the initial values. While at the beginning of the sequence the positive voltage changes are slightly higher than the negative ones, which lead to the shift to more positive voltage values at which the discharges occur, this change seems to reach a state of saturation before the reset occurs.

The Δ**t$_n$** diagram reveals that the time differences from the negative pulses to the positive ones increase from under **10 ms** to **13 ms**, while the ones in the opposite polarity decrease from slightly above **10 ms** to about **7 ms**. Interestingly, two consecutive time differences Δ**t$_n$** in most cases add up to **20 ms**, which is the cycle length of the test voltage. In case of a reset there is always a discharge-free cycle that leads to a discharge free time interval of about **23 ms** before the next sequence starts.
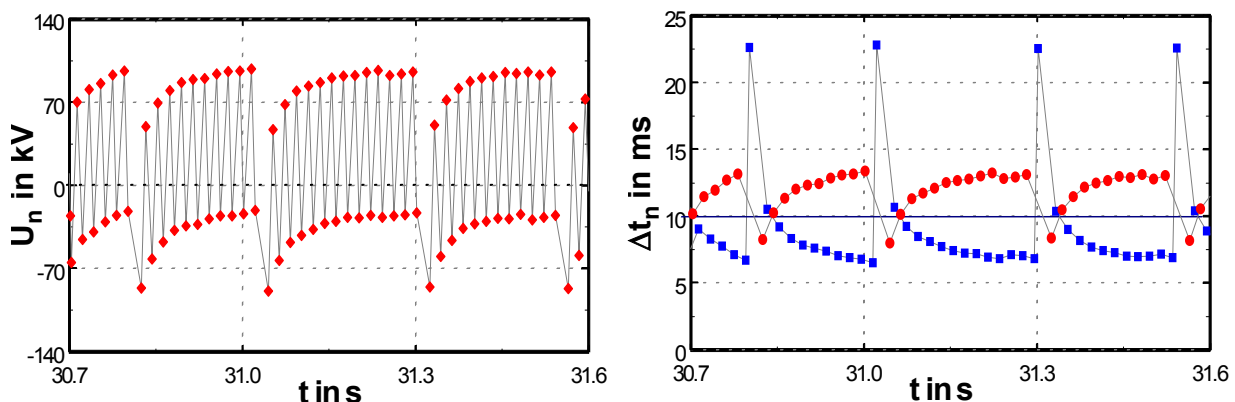
Fig. 5.5: Voltages **U$_n$** at which discharges occur and sequences of time differences Δ**t$_n$**
between consecutive discharges (for positive (●) and negative (■) voltage
changes Δ**U$_n$**) for a HV test transformer

Fig. 5.6 shows the same parameters as above for a measurement performed with a higher test voltage. The behaviour in this case is also periodic but in some aspects quite different from the one described above. The most significant differences are the almost linear change of the voltage levels at which the discharges occur and a second discharge in the same negative half cycle instead of a discharge-free cycle when a reset takes place. This second discharge in the negative half cycle occurs about **4 ms** after the first one and is also the first discharge of the new sequence. The voltage changes ΔU_n are almost constant, but slightly higher for positive going transitions than for negative ones. As there is, in this case, a strong correlation between the voltage changes ΔU_{n-1} and the amplitudes I_n of the impulses, the positive impulses are about 10 - 20% higher than the negative ones. The time intervals between resets are much longer than in the first example.
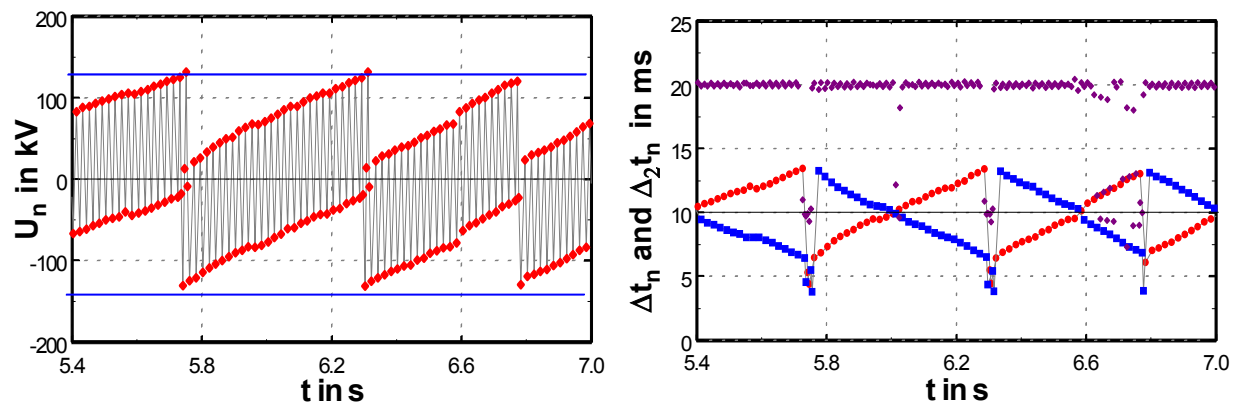
Fig. 5.6: Voltages U_n at which discharges occur, time differences Δt_n between consecutive discharges (for positive (●) and negative (■) voltage changes ΔU_n) and time differences $\Delta_2 t_n$ (♦) between next but one discharges for a HV test transformer; the blue lines indicate the peak voltages of the applied voltage

An explanation for these phenomena is that after a discharge a unipolar local space or surface charge exists whose magnitude and polarity (in most cases) changes with the next discharge. This charge accumulation generates an additional local DC field. The resulting local field is the superposition of a component generated by the externally applied voltage and this local DC field. Consequently a negative DC component causes the discharges in the negative half waves to appear at lower values of the external test voltage, while discharges in the positive half waves occur at higher values of the external voltage. As the voltage changes ΔU_n between a positive and the following negative discharge and, along with this, the amplitudes of the negative impulses are generally smaller than that of the positive ones, the amount of negative charges generated by negative discharges is not sufficient to compensate the increase of the

positive charges due to the positive discharges. So the positive charge accumulation decreases with each cycle of the test voltage which leads to an increasing negative field offset.
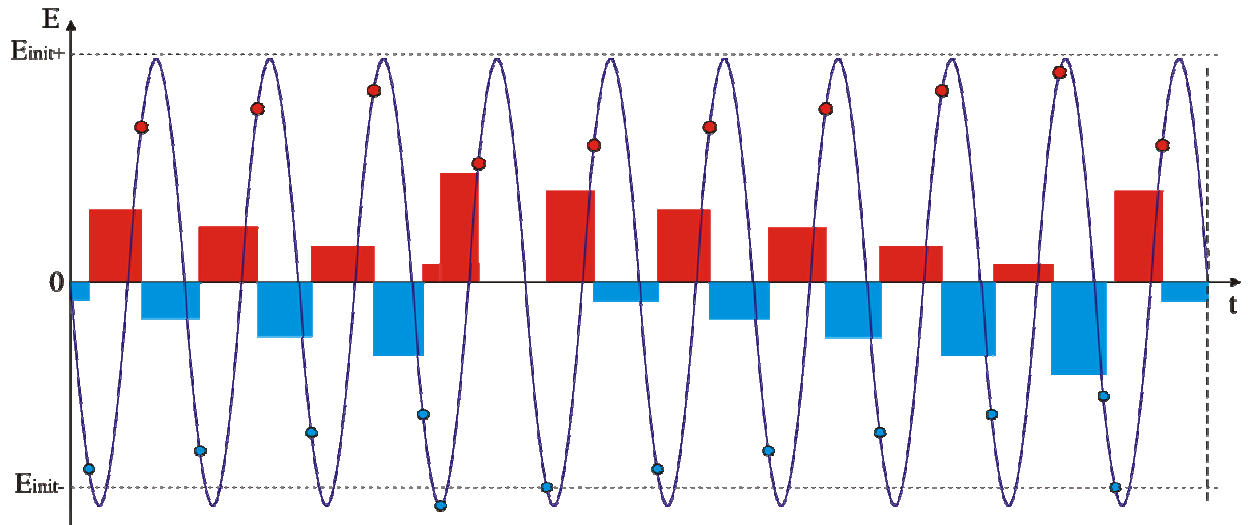
Fig. 5.7: Simplified model for a PD sequence with influence of accumulated charges (corresponding to Fig. 5.6)

Fig. 5.7 shows a simplified model calculation for a PD sequence with the influence of accumulated charges. The parameters shown are the sinusoidal field component produced by the externally applied voltage and the local DC field offset generated by the accumulated charges. In most cases every discharge changes the polarity of the DC offset. As the model is intended to show the basic principle of the phenomenon, the field thresholds for ignition and the initial values of the DC field are chosen arbitrarily, but it is obvious that the model shows a similar behaviour as shown in Fig. 5.6. The negative field offset increases step by step with each cycle, while the positive offset field decreases step by step, until the positive offset field after a negative discharge is so small, that a second discharge in the negative half wave can occur. Due to the amount of charges shifted by these two consecutive negative discharges, the positive field offset is sufficiently large to allow a partial discharge already in the inclining part of the positive half cycle, and a new sequence starts.

The behaviour shown in Fig. 5.5 cannot be explained by these simplifying assumptions. It is likely that in this case the decrease of the accumulated charge in the time interval before the following discharge plays an important role. This means that the time constant of the decrease of the charge accumulation – and consequently the decrease of the DC offset field with time – is in the same range as the cycle time of the externally applied voltage, at least for one polarity. As the DC field component produced by the external voltage influences the decrease of the

charge accumulation, the behaviour becomes very complex. The measured data show that the effects generated by the charge accumulation may lead to a change in the apparent behaviour of the partial discharge process, even if there is only one PD source active and the basic behaviour remains the same.

5.1.3   Surface discharges on an inorganic surface

Even on the inorganic insulating materials the systematic shift in the phase angles at which partial discharges occur can be found. **Figs. 5.8** show some results obtained an AlN cooling device for semiconductor press-packs with different voltages (another method to get a better understanding of the discharge process).

In repetitive measurements one of the cooling devices was stressed with **2.19** and **2.38 kV$_{rms}$** between circular shaped high voltage electrodes. In both cases 2000 discharges are taken as data basis. The corresponding discharge rates are **1.84** per cycle and **3.48** per cycle for the two voltages, but this does not explain the differences shown in Fig. 5.8.

As shown in Fig. 5.8, the frequency distributions of the phase angles are significantly different when the measurement is done with slightly different voltages – with **2.19** and **2.38 kV$_{rms}$** respectively –. The standard evaluation e.g. on the basis of the skewness of the distribution of the phase angles would indicate two characteristically different defects in both cases.
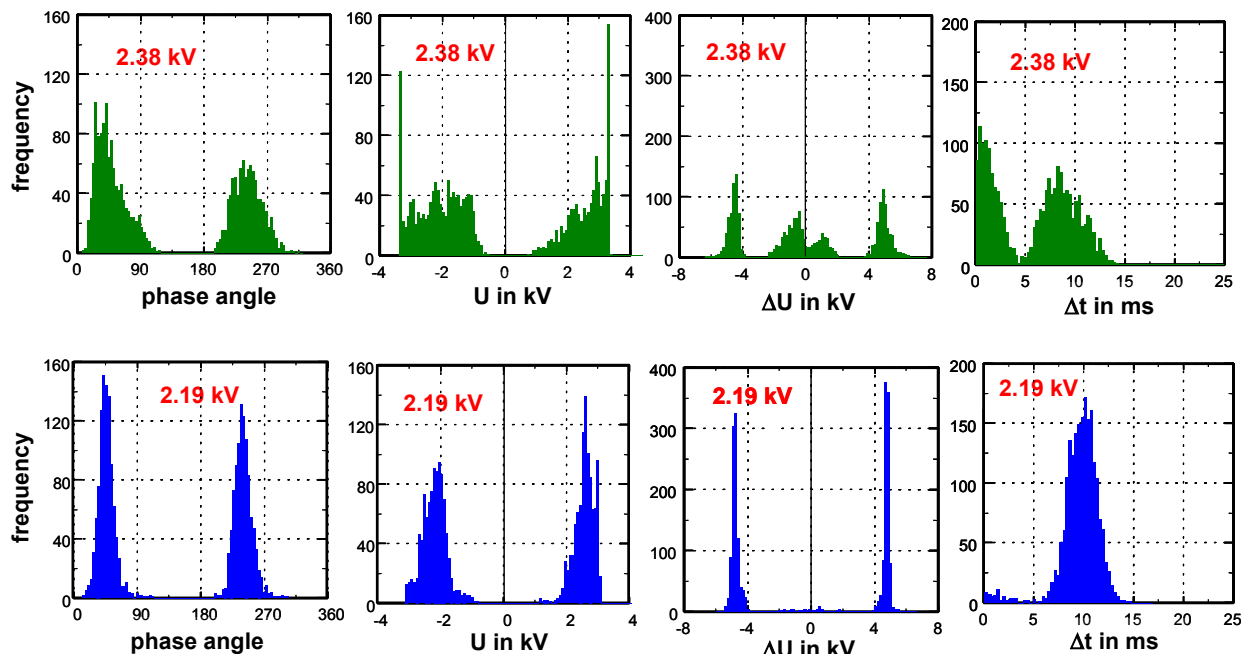
Fig. 5.8: Phase angles of occurrence ϕ, external voltages **U**, voltage changes Δ**U** and time differences Δ**t** between consecutive partial discharges in a AlN cooling device

The frequency distributions of the actual voltages **U** at which discharges occur also show significant differences. While for the lower voltage most discharges occur below the peak voltage, at the higher voltage well defined groups of discharges occur at the peak voltages. In addition, the distribution shows a marked polarity dependence.

The evaluation of the voltage differences ΔU between consecutive discharges indicates that in contrast to the apparent scatter in the phase angles of occurrence, for the lower voltage level the discharges occur after very definite voltage changes. For the measurement with the higher voltage additional discharges occur after smaller voltage changes.

The evaluation of the time differences Δt between consecutive discharges indicates that with the lower measuring voltage most discharges occur with time differences around **10 ms**. With the higher measuring voltage the peak value of the corresponding distribution is shifted to about **8 ms** with nearly as many discharges with time differences below **5 ms,** whereby these differences are distributed at random. The scatter of the time differences around **10 ms** is apparently due to changes in the local surface or space charge field generated by the discharges.

For further demonstration **Fig. 5.9** shows the frequency distributions of the time differences Δt and $\Delta_2 t$ for the whole data set. For the measurement with **2.19 kV** the scatter of the $\Delta_2 t$ values is astonishingly small compared to that of the Δt values. The reason for this is the step by step build-up of the unipolar surface charge.

For the measurement with **2.38 kV** there is a broad scatter of the Δt values, but also a comparatively small scatter of the $\Delta_2 t$ values around **20 ms**, i.e. some of the discharges show the same sequences as with the lower measuring voltage, while in most cycles more than two discharges occur.

For the higher measuring voltage the distribution around **10 ms** l ooks similar for Δt and $\Delta_2 t$ (except for a small shift that leads to a nearly symmetric distribution of the $\Delta_2 t$ values around **10 ms**), while the exponential distribution found for the small values of Δt changed into a
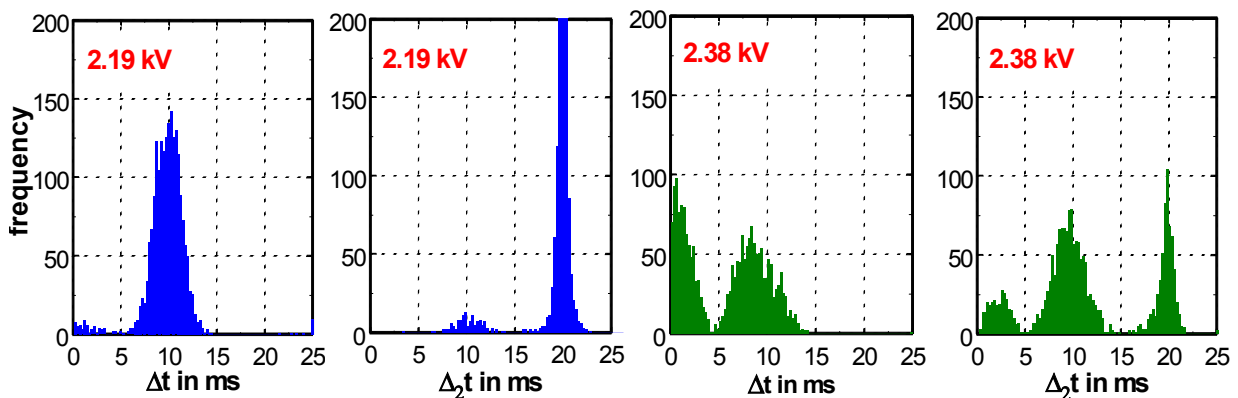
Fig. 5.9: Frequency distributions of the time differences Δt and time differences $\Delta_2 t$ between next but one discharge signals for measurements of a specimen with two different voltages

peaked one around **2 ms** for the $\Delta_2 t$ values. This is an indication for two or more small Δt values in sequence.

In this case there is only one type of PD-active defect that produces **surface discharges**. At the lower measuring voltage there is only one active spot and only two discharges per cycle occur, while with the higher measuring voltage at least one other spot is active and produces additional partial discharge signals.

From this we can conclude that with the higher measuring voltage there are either frequently discharges at one spot with two discharges per cycle, or discharges at two (or more) simultaneously active defects. But also with a constant measuring voltage time different types of discharges may occur and thus also the different fractions of different types can be used for the diagnosis or as an indication of ageing processes if measurements are performed at different times.

Even with surface discharges on inorganic insulating materials the influence of surface charges can be found (e.g. with an AlN cooling device) [Pat03b].

If now only a short sequence of discharges is looked at in detail, a characteristic behaviour with a systematic structure can be found. At voltages just above the partial discharge inception voltage, partial discharges of a single defect often occur at a rate of **2 per cycle**. The mean time differences between these consecutive discharges are **10 ms** with more or less scatter of the single values. The discharges do not necessarily occur at the peak voltages but in most cases during the voltage increase.

The charge moved during the discharge in the defect region levels off the local electric field and hence – although the external voltage continues to increase – the next discharge occurs in the following half cycle with opposite polarity. In this polarity the field releasing space charge during the preceding half cycle leads to an increase of the local electric field and hence the discharge occurs at a lower voltage level. The monotonous change of the voltage at which the discharges occur is an indication for a non-symmetric behaviour.
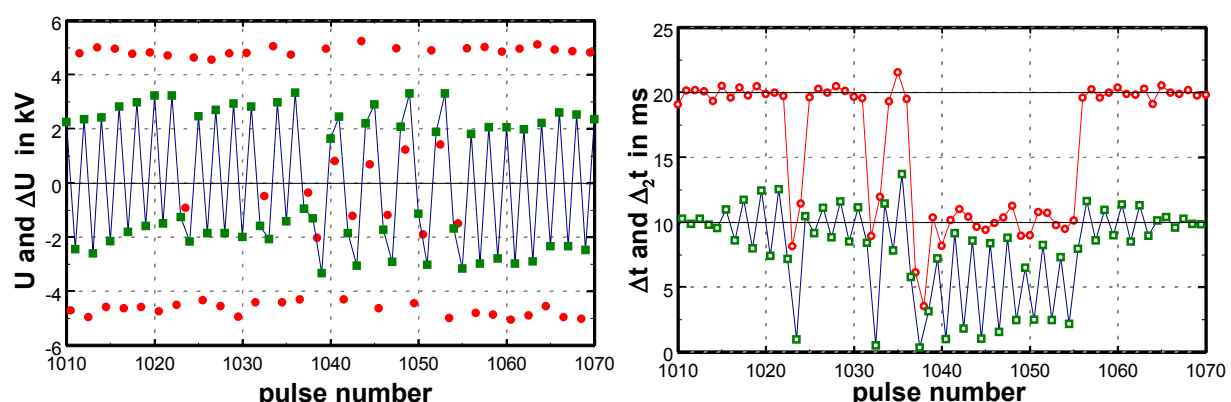
Fig. 5.10: Sequence of voltages **U** (■), voltage differences ΔU (●), time differences Δt (□) between consecutive and time differences $\Delta_2 t$ (○) between next but one discharges

Fig. 5.10 (left graph) shows a series of discharges from the measurement with **2.19 kV**. For the first discharges, the voltages **U** at which the discharges occur increase in the positive half cycles, whereas in the negative half cycles the discharges occur at step by step lower absolute values of the external voltage curve. After about 25 discharges for some cycles of the applied voltage two discharges per half cycle occur, followed again by a series with only one discharge per half cycle. Except for the region with the two discharges per cycle, the voltage differences **ΔU** between consecutive discharges are nearly constant.

The right graph of Fig. 5.10 shows time differences found in the same data set. Although in the first group there are exactly two discharges per cycle and one would expect about **10 ms** time difference – maybe with some statistical scatter – there is a characteristic sequence of consecutive time differences **Δt**. After a few discharges with time differences of **10 ms**, alternatively shorter and longer time differences with increasing split-up occur. A more detailed analysis reveals that the time differences **Δt > 10 ms** always occur after a discharge in the negative half wave (see **Fig. 5.12**).
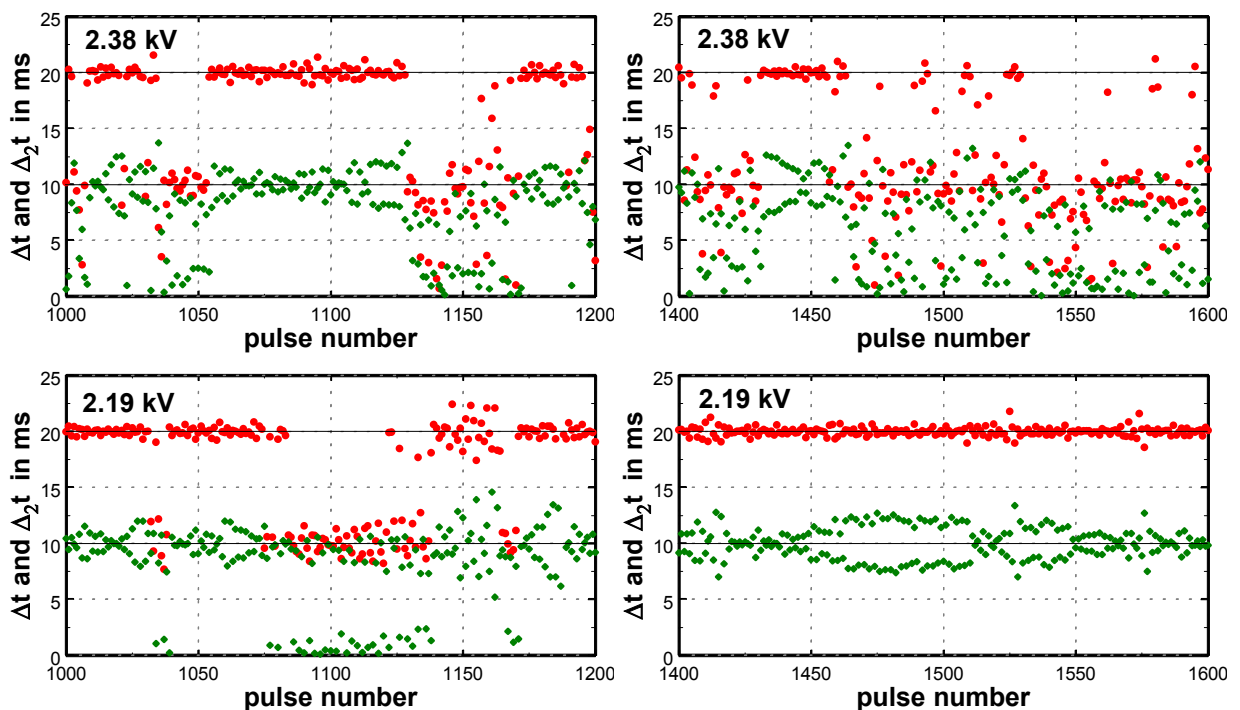
Fig. 5.11: Sequence of time differences **Δt** (♦) between consecutive and time differences **Δ₂t** (•) between next but one discharge events for different applied voltages

The continuous shift to higher positive voltages (shown in Fig. 5.10) can be interpreted by a continuous build-up of positive space charges 'opposite' to the discharge triggering spot at high potential or of negative space charges if the discharge triggering spot is at ground potential in the measuring circuit. After about 10 discharges a reset occurs followed by a similar sequence as before. This reset happens via a second discharge in the negative half cycle and

apparently leads to the disappearance of the space or surface charge. After that a sequence of two discharges per half cycle, occurs followed again by a sequence with only one discharge per half cycle. Fig. 5.10 also contains the corresponding time differences Δ_2t between next but one discharges. Interestingly in the series with two discharges per cycle every two time differences Δt add to nearly exactly **20 ms**.

The change in the parameters Δt and Δ_2t during longer sequences of discharges is shown in **Fig. 5.11** for two measurements performed with different measuring voltages [Pat02b]. With the lower measuring voltage two types of discharge sequences exist: A very frequent one with $\Delta_2t = $ **20 ms** and less frequently a second one with $\Delta_2t \approx$ **10 ms**. The Δt sequences occasionally show a systematic split-up as discussed in connection with Fig. 5.10b. With the higher measuring voltage $\Delta_2t = $ **20 ms** is less frequent and in addition to $\Delta_2t \approx$ **10 ms** some sequences with $\Delta_2t <$ **10 ms** occur. The height of the measuring voltage apparently influences the type of the partial discharge or at least the fragmentation into different types.

5.1.4   Polarity dependence

Surface discharges on ceramic insulating materials seem to show a more or less symmetric behaviour with one discharge in every half cycle. Semiconductor cooling devices were stressed with two AC voltages. Fig. 5.9 has shown that for the lower voltage load the time differences between consecutive discharges are about **10 ms**. For the higher voltage load more than two discharges per cycle occur. In addition there are discharges after time differences of a few ms.

Looking at these data in more detail reveals that surface charges may be of importance also in this case. If the distribution of the time differences between consecutive discharges which shows a symmetric distribution with a peak at about **10 ms**, are split up into those discharges with a positive voltage change between the consecutive discharges and a corresponding set of data with a negative voltage change, two distributions occur. One shows a peak around less than **9 ms** and a second one a peak around **11 ms** (**Fig. 5.12**).

The explanation of this phenomenon comes from the fact that the local electric field is not symmetric as one could expect from the symmetric applied AC voltage. There is an additive positive electric field that is added to the initially symmetric AC field. Hence the discharges occur at apparently lower external positive fields than negative fields.

In contrast to the space or surface charge phenomena in paper-oil insulations discussed in the previous paragraph with surface charges on AlN the polarity of the surface charges does not change periodically with time. The amount of surface charges may increase or decrease with time, but – at least for the begining of the voltage load – the time differences for positive voltage changes are always smaller than **10 ms** and those for negative voltage changes are always bigger than **10 ms**. The interesting point is that with increasing time of voltage load the polarity dependence decreases. For the first two seconds with a low voltage the polarity of the sur-

face charge is constant. After about 2000 discharge pulses the influence of the surface charge seems to be weaker, there is no such pronounced effect on the time difference. For the experiment with the higher voltage the change in the process appears earlier.
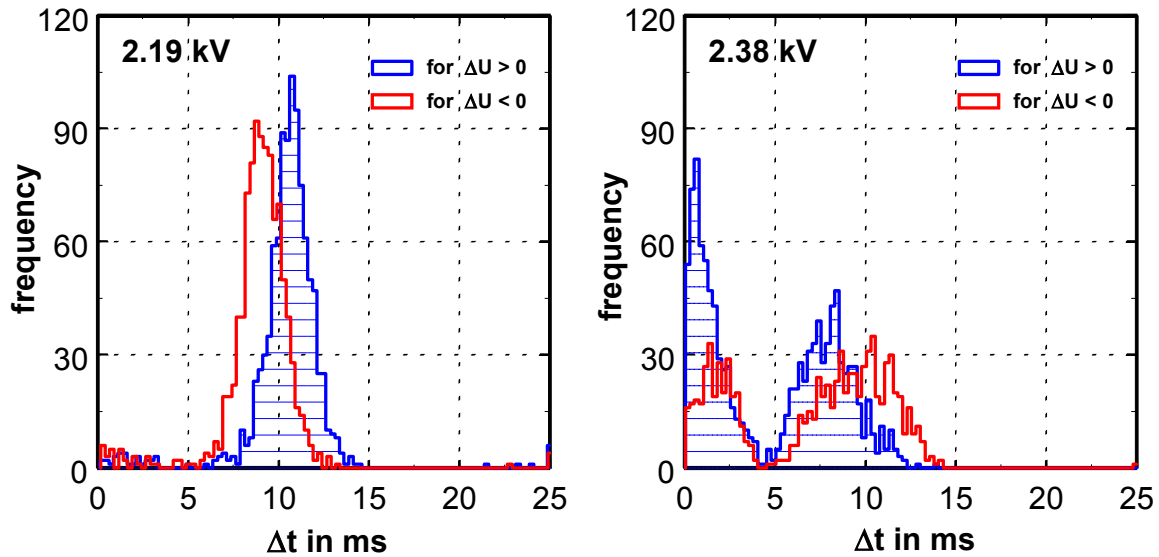
Fig. 5.12: Frequency distributions of the time differences **Δt** for measurements split up into those discharges with a positive and negative voltages change between the consecutive discharges

5.1.5   Partial discharges in the stator of a small motor

Other sets of experiments were performed with stators of small commercial motors with ramped voltage load. **Fig. 5.13** shows some of the results performed with a ramp rate of about **190 V$_{rms}$/min** and a sensitivity of about **2 pC**.
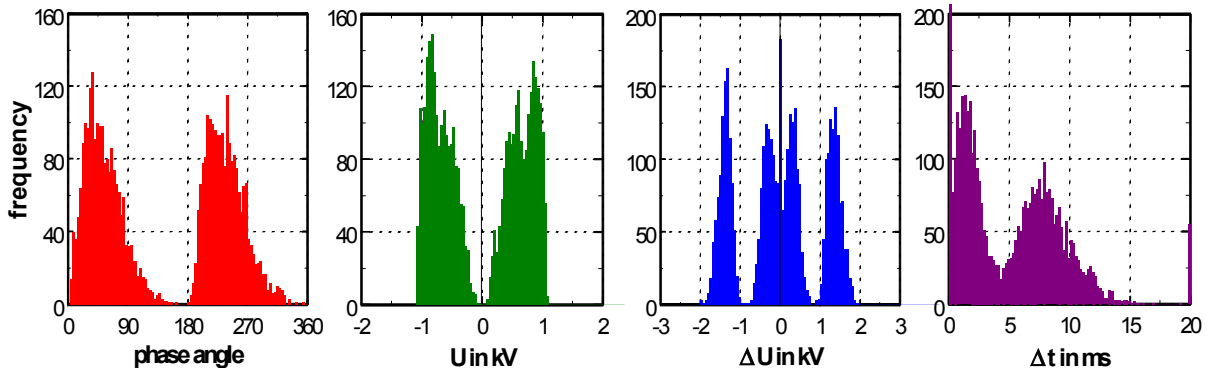
Fig. 5.13: Phase angles of occurrence ϕ, actual voltages **U**, voltage changes **ΔU** and time differences **Δt** between consecutive partial discharges in the stator of a small motor

In this case, the partial discharges cross the air gap between neighbouring insulated wires, and consequently no polarity dependence occurs. Especially the histogram of the time differences Δt indicates that there is more than one PD-active spot.

Fig. 5.14 shows an interesting behaviour. The results indicate the existence of constant surface or space charges for some hundreds of cycles, after which a change of the polarity of the charge accumulation occurs. Indeed, after positive discharges time differences Δt of more than **10 ms** occur, while the time differences after negative discharges are smaller than **10 ms**. As the test voltage increases, the behaviour suddenly changes (at about **t = 181 s**) and the Δt after positive discharges are now below **10 ms** and those after negative discharges vice versa. Nevertheless two consecutive time differences add up to **20 ms**. After this change an apparently constant positive field offset exists that leads to positive discharges near the positive crest voltage, while the negative discharges occur mostly already during the inclining part of the negative half waves. At about **183 s** additional discharges after very short time differences occur, an indication of an additional discharge process [Pat03a].
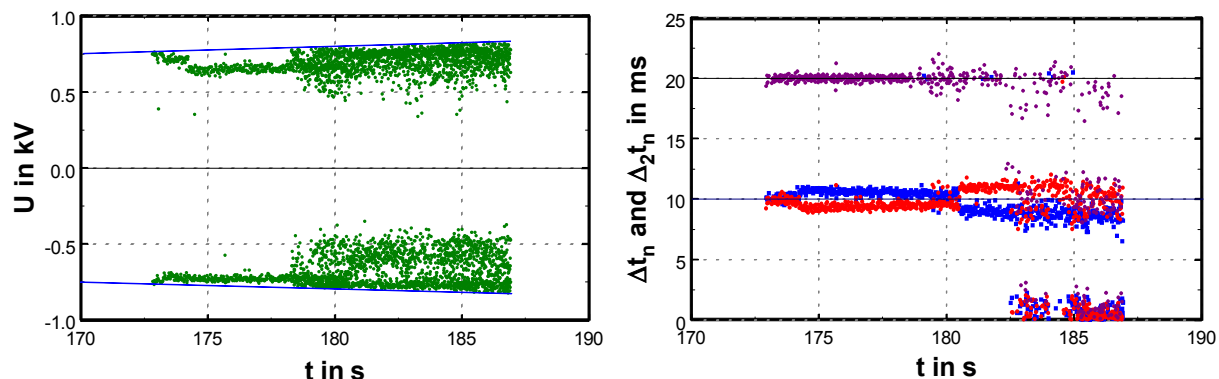
Fig. 5.14: Voltages **U** at which discharges occur, time differences Δt between consecutive discharges (for positive ($\bullet$) and negative ($\blacksquare$) voltage changes Δ**U**) and time differences $\Delta_2 t$ ($\blacklozenge$) between next but one discharge events over time for a small stator at ramped voltage load; the blue lines indicate the peak voltages of the applied voltage

The presented measurement results from different test objects show the importance of the influence of accumulated charges in the PD processes. It is also obvious that the detailed evaluation of a small subset of the data – especially if the sequence correlated information is used – reveals more information about the defect than the analysis of a larger data set, accumulated without sequence information.

In the following the influence of space charges will be discussed on the basis of the improved PD equivalent circuit.

5.2   Description of space charge effects with the improved PD equivalent circuit

Partial discharge processes in solid or liquid insulations consisting of different materials usually show a significant correlation between consecutive partial discharges [Hoo95, Pat95]. Every single discharge moves electric charges in the defect area that finally change the local electric field at the defect, and thus the conditions for the ignition of a consecutive discharge. The decisive point for the ignition of a discharge is then not the externally applied voltage **U** but the change of the local electric field since the preceding discharge. For DC voltages this has been discussed in [Fro95], for AC voltages especially the correlation between the externally applied voltage and the local electric field at the PD-active defect has to be discussed, and the result is, that the externally measured phase angle is not necessarily representative for the local electric conditions at the site of the defect. To take this into account in contrast to the commonly used equivalent circuit (Fig. 1.8), an equivalent circuit with an **additional RC-element in series with the spark gap** has to be used. **Fig. 5.15** shows such a circuit (after [Pat02]). According to this circuit a partial discharge occurs, as soon as $U_1 - U_4$ is higher than the ignition voltage U_F' of the spark gap **F**.
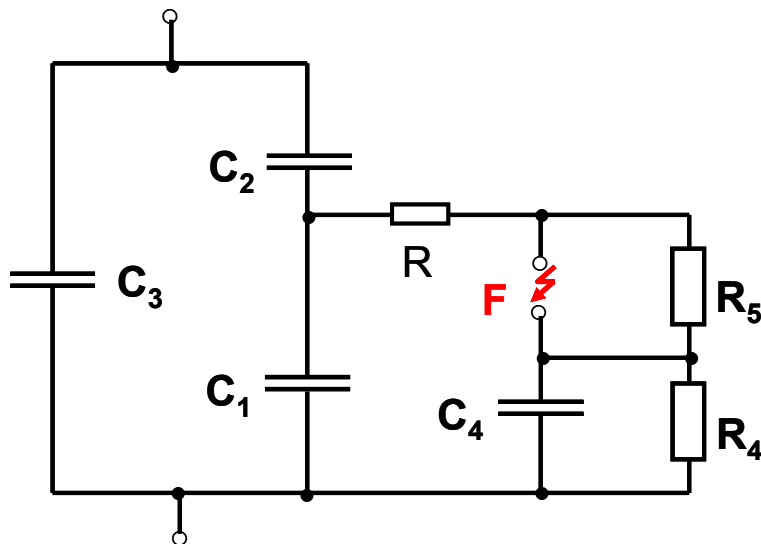
Fig. 5.15: Improved PD equivalent circuit to describe space charge effects

During the partial discharge process the capacitor C_1 charges the capacitor C_4 via the spark gap **F**, the voltages U_1 across C_1 and U_4 across C_4 are changed and the discharge stops as soon as $U_1 - U_4$ is smaller than the voltage drop that is necessary for the spark gap to be sufficiently conductive. If an AC voltage is applied, the next partial discharge occurs (within the same half wave) as soon as U_1 is increased sufficiently via the change of the externally applied

voltage, or after U_4 is sufficiently decreased via R_4, that $U_1 - U_4$ is again higher than the ignition voltage $U_F{'}$ of the spark gap. If this does not occur before the crest voltage, the polarity of the applied voltage will change and in this half wave U_4 will increase the voltage across the spark gap with respect to the voltage generated by the external AC voltage. Hence the next partial discharge will occur earlier, and U_4 will be changed again.

The step by step change of U_4 often produces an apparently random-like behaviour of the phase angles at which discharges occur, although the process itself is highly deterministic. It is obvious, that without taking the information contained in the sequence of the partial discharges, relevant information about the PD process is lost. In many cases a PD pulses has the same polarity as the externally applied voltage. In some defects PD may occur in which the polarity of a partial discharge pulse is opposite to the polarity of the applied voltage or even the preceding voltage change ΔU [Pat00]. The equivalent circuit contains the resistor R_5 that is responsible for a change of U_4 without PD.

It is then obvious that – if space charges are of importance – the commonly used phase resolved analysis of partial discharge data that takes all discharges as independent from each other will give only poor results because relevant information is not taken into account. The phase angle of the applied voltage U is not necessarily correlated to the phase angle of U_1 and not meaningful for the voltage U_F across the spark gap that determines the ignition of the next partial discharge.

5.3   Influence of space charges on the PD pulse heights

In the following the results of measurements of a HV transformer for the voltage level of 100 kV (already discussed in paragraph 5.1.2) will be discussed here on the basis of the improved PD equivalent circuit. In this experiment, PD occurred in the inclining parts of the applied AC voltage. Characteristic for the measurements was the phenomenon that the pulse heights were constant independent of the actual voltages at which the discharges occurred.

As shown in Fig. 5.5 – a plot of the sequence of the voltages at which the discharges occurred for a measurement with a voltage load of about **70 kV$_{rms}$** –, in some cases two negative discharges were in sequence but in most cases positive and negative discharges alternated. All discharges occurred in the inclining parts of the voltage half cycles but in different patterns for positive and negative voltage increases. As mentioned already, in many cases only one discharge per half cycle occurred. In most cases there was an alternating sequence of the polarity of the voltage changes, but every 6 or 7 cycles two negative ΔU appeared in sequence, interestingly very systematic after **23 ms**.

The measurement performed with a higher test voltage, Fig. 5.6 has shown also a periodic behaviour but some significant differences were found. The voltage levels at which the discharges occur shows a linear change and additional discharge take place in the same negative half cycle instead of a discharge-free cycle when a reset occurs.

Fig. 5.16 shows the plots of the discharge intensities over the actual value of the applied voltage at which the discharges occurred for the two measurements. The pulse magnitudes of the PD signals show a constant behaviour independently of the actual voltages at which the discharges occurred.
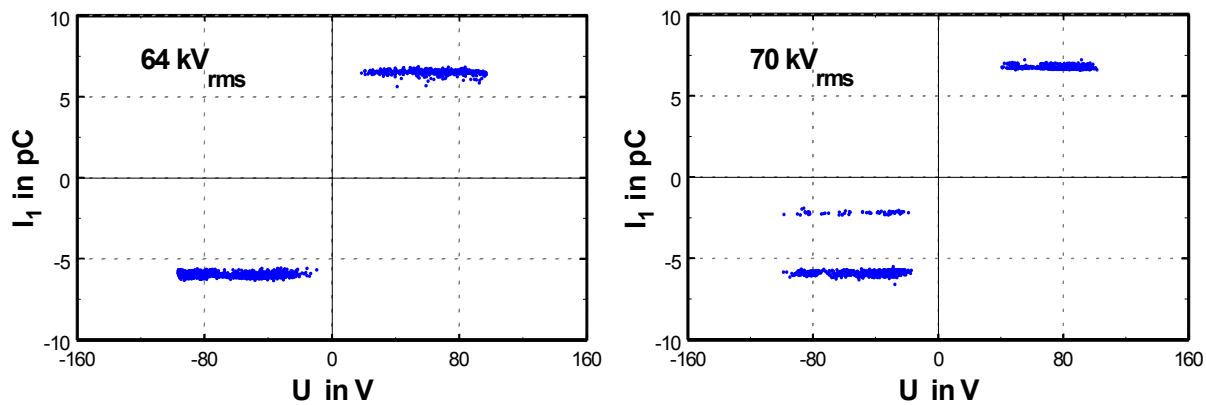
Fig. 5.16: Pulse heights of discharges I_1 in a HV transformer over the actual external voltage **U** at which discharges occurred

The analysis of the discharges during the first half second of the first measurement (immediately after the voltage application), that means for **25** consecutive cycles of the applied **50 Hz** AC voltage, showed that the pulse heights for positive pulses were about **7 pC** and the pulse heights for negative pulses were about **- 6 pC**. The sensitivity of the measurement was about **2.5 pC**.

For the measurement performed at higher test voltage the amplitude of the PD pulses seams to have the same behaviour as for the lower voltage.

With the use of the Pulse Sequence Analysis i.e. the analysis of the sequence of the discharges, the behaviour shown in Fig.5.5 and Fig. 5.6 can be explained. However the behaviour of the pulse height shown in Fig. 5.16 can be explained only on the basis of the **improved PD equivalent circuit**.

A partial discharge always occurs if in the equivalent circuit (see Fig. 5.15), the voltage U_F across the spark gap **F** exceeds the ignition voltage U_F' of this spark gap. In this case charge carriers from capacitance C_1 flow into the capacitance C_4 until both have the same voltage. At this moment the voltage across the spark gap becomes zero and no further current is flowing. A current limiting resistor is not shown in this circuit although there is a limitation of the current amplitude. This resistor does not influence the basic phenomena, so it is not shown here.

If U_F' with $U_F = U_1 - U_4$ is the voltage at which the spark gap is triggered, then the voltage U_1 across C_1 is reduced during the partial discharge process because charges flow through the spark gap into the capacitor C_4. This process continues until the `new´ voltage $U_1'$ across $C_1$ equals the `new´ voltage U_4' across C_4.

For this the charge Δq is moved from C_1 to C_4. Obviously this charge or the corresponding current cannot be measured. With:

$$U_1 - \Delta U_1 = U_4 + \Delta U_4 \tag{5.1}$$

or

$$U_1 - \frac{\Delta Q}{C_1} = U_4 + \frac{\Delta Q}{C_4} \tag{5.2}$$

follows

$$\Delta U_1 = U_1 - U_4 - \frac{C_1}{C_4} \Delta U_1 \tag{5.3}$$

and finally

$$\Delta U_1 = \frac{C_4}{C_1 + C_4}(U_1 - U_4) \tag{5.4}$$

for the decrease ΔU_1 of the voltage U_1. The charge q needed for a compensation of this voltage decrease ΔU_1 in the path C_1 in series with C_2 is given by:

$$q = \frac{C_1 C_2}{C_1 + C_2} \frac{C_4}{C_1 + C_4}(U_1 - U_4) \tag{5.6}$$

This charge is supported from a sufficiently large coupling capacitor C_c that is commonly connected in parallel to the specimen. This "apparent charge" q that is needed to compensate ΔU_1 in the path C_1 in series with C_2 can be measured in the loop formed by the specimen and the coupling capacitor by means of a coupling quadripole in this loop.

With $U_1 - U_4 = U_F$, for a constant ignition voltage U_F' of the spark gap, independent of the actual voltage U that is externally applied at the moment of the partial discharge, an apparent charge $q = $ **const.** is found (see Fig. 5.16).

Fig. 5.16 indicates that there may exist two different places for discharges in the specimen. Interestingly the pulse heights are higher for positive pulses than for negative pulses in the case of the low applied voltage measurement and vice-versa in the measurement done at higher applied voltage.

For a equivalent circuit shown in Fig. 5.15 no such non symmetric effect should appear, especially as long as the capacitance of C_4 and the resistor R_4 are independent on the polarity of the applied voltage. On the other hand the spark gap and especially the ignition voltage is not necessarily symmetric for both polarities. If gas discharges play a role, a non symmetric behaviour should be expected.

The physical reality of the PD active defect in the HV transformer probably consists of a small flat void between two strips of paper. If the voltage across the gap is sufficiently high a local breakdown occurs that deposits charges on the inner surfaces.

In dependence on the applied voltage and the actual condition of the defect a different PD behaviour may occur. The situation that the pulse height does not depend on the actual voltage at which they occur, can be explained by the assumption of a flat cavity in which surface discharges generated by the discharge change the local electric field. The situation that two different discharge intensities are possible, can be explained by the assumption that there may be two different places in the flat cavity at which discharges may occur, whereby a discharge at one side prevents the second discharge from firing.

A fixed correlation between U_1 and U exists only if there is no capacitor C_4, or $C_4 \approx \infty$. Without the capacitance C_4, i.e. $U_4 \approx 0$ holds and a dependence $q \sim U_1$ is found:

$$q \approx \frac{C_1 C_2}{C_1 + C_2} U_1 \tag{5.7}$$

In this case discharges occur in the inclining part of the half waves and because $q \sim U_1$ is valid. Different defects may show $q \sim U$ with different proportionality factors.

If space or surface charges are generated in the discharge process an additional electric field exists in the area in which the partial discharge takes place that influences the conditions for the ignition of the following discharges. Hence in general terms the phase angle does not say anything about the voltage U_1.

Nevertheless if $R_4 C_4$ is sufficiently high (compared to the cycle time) a fixed correlation between ΔU_1 and ΔU exists. Hence a plot of ΔU values contains much information about the discharge process.

As a consequence of the series circuit of C_2 and C_1 any change of ΔU leads to a change of ΔU_1 and $\Delta U = U_F'$ is the condition for a breakdown of the spark gap **F** and thus a partial discharge.

$$\Delta U_1 = \frac{C_2}{C_1 + C_2} \Delta U \tag{5.8}$$

In many cases a dependence between the pulse heights and the actual voltages at which discharges occur is found. In these cases no influence of space charges exists. **Fig. 5.17** show typical examples of PD measurements of **transformer oils** in a needle plane arrangement with a gap distance of about **15 mm**. Discharges occurred only in the positive half waves and show an increase with the actual voltage level at which the PD occur. There is no influence of space charges; the **discharges occur at random** [Pat06].

If in a partial discharge measurement the voltage is ramped up with time, the first discharges are small in intensity and they increase with increasing applied voltage. In dependence on the applied voltage, the actual condition of the oil and the amount of dissolved impurities, different amounts of gaseous components are created by PD, and a void filled with gas may be formed, in which gas discharges may occur. The change of the pulse shape of the PD signal can be used to monitor the oil quality [Pat07].
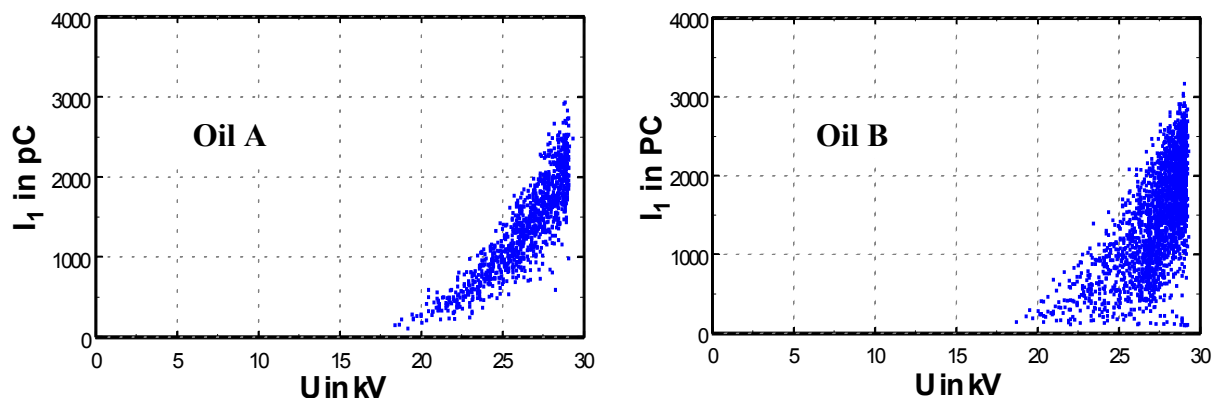
Fig. 5.17: Pulse heights of discharges I_1 over the actual external voltage **U** at which discharges occurred for two different oils

Some specimens show different defects with different correlations between the actual voltages at which the discharges occur and the pulse heights. As an example **Fig. 5.18** shows measurements on different **model stator bars** of high voltage machines in which different I_n-U_n-correlations exist.
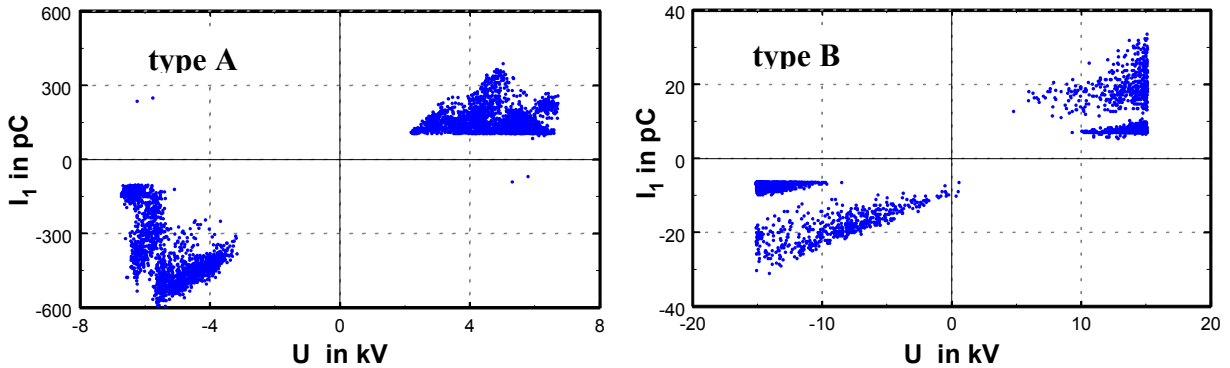
Fig. 5.18: Pulse heights I_1 of discharges in model stator bars over the actual voltages **U** at which discharges occurred

In the case in which space charges play no role, the capacitance C_1 discharges totally during the partial discharge process and the voltage U_1 is zero after the partial discharge. Hence the charge that has to be supplied by the coupling capacitor is proportional to C_1.

C_1 and $\Delta q = \dfrac{C_2}{C_1 + C_2} U_1$ holds. In these cases only discharges in the inclining part of the half cycles occur.

In general $\Delta U \sim \Delta U_1$ is valid, irrespective of any existing space charges. But a proportionality between **q** and ΔU_1 exists only in specific cases, usually if the capacitance C_1 is only insignificantly discharged by the partial discharge. In this case the ratio between U_1 and **U** is kept nearly constant. Physically this can be explained in a way that the spark gap discharges only a small part of C_1. The signals should be very small in these cases.
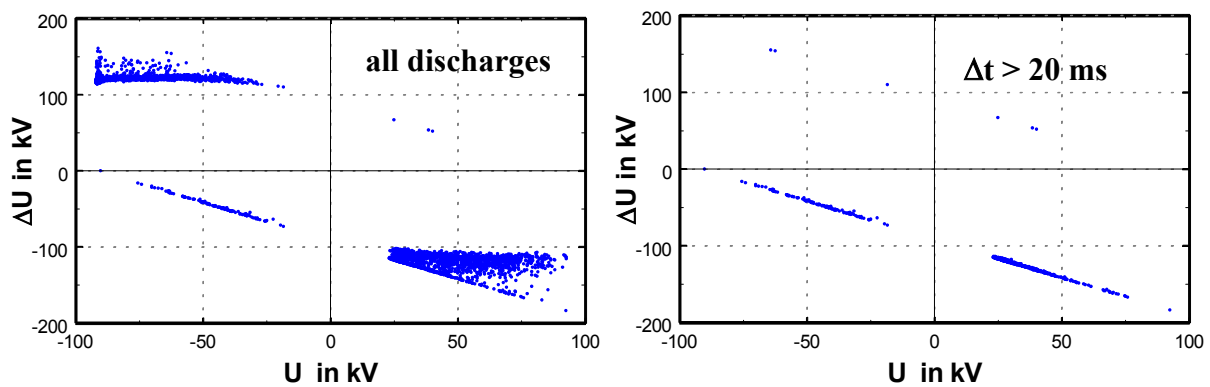
Fig. 5.19: Voltage changes in a HV transformer over actual voltages at which discharges occurred for all discharges (left) and discharges after $\Delta t > 20$ ms

For demonstration, **Fig. 5.19** shows ΔU_n-U_n-correlations for a measurement performed on a HV transformer at an applied voltage of **62 kV$_{rms}$**. Despite the fact that the pulse heights are constant independent of the actual voltages at which the discharges occurred, the voltage changes between consecutive discharges show a different behaviour. In the left diagram the whole data set is represented while in the right diagram only the selected data with a discharge-free time of more than **20 ms** after PD in negative half cycles and more than **30 ms** of the PD in positive half waves are represented. As shown in Fig. 5.15 the pulse heights do not depend on the actual voltage **U** or the preceding voltage change ΔU.

5.4 Partial discharges during electrical treeing in polyethylene

Electrical treeing in polymers has been examined since more than 40 years. Nevertheless the **Pulse Sequence Analysis** can show some details of this process that had not been found and discussed before. In the following some results of the experiments with needles embedded in polyethylene will be reported.

5.4.1 Electrical tree initiation

In one set of experiments with a needle in PE the AC voltage was slowly increased with a ramp rate of **15 V$_{rms}$/s**. For a curvature of the needle of about **5 µm** and a gap of **2 mm** the discharges started at about **12.8 kV$_{rms}$**. **Fig. 5.20** shows the actual voltages **U** at which discharges occurred and the corresponding voltage changes ΔU between consecutive discharges over the region of an applied AC voltage between **12.8** and **12.9 kV$_{rms}$**. The discharges occur in both polarities of the applied voltage, but most discharges occur in the negative half cycles with an increased probability at higher negative voltages.
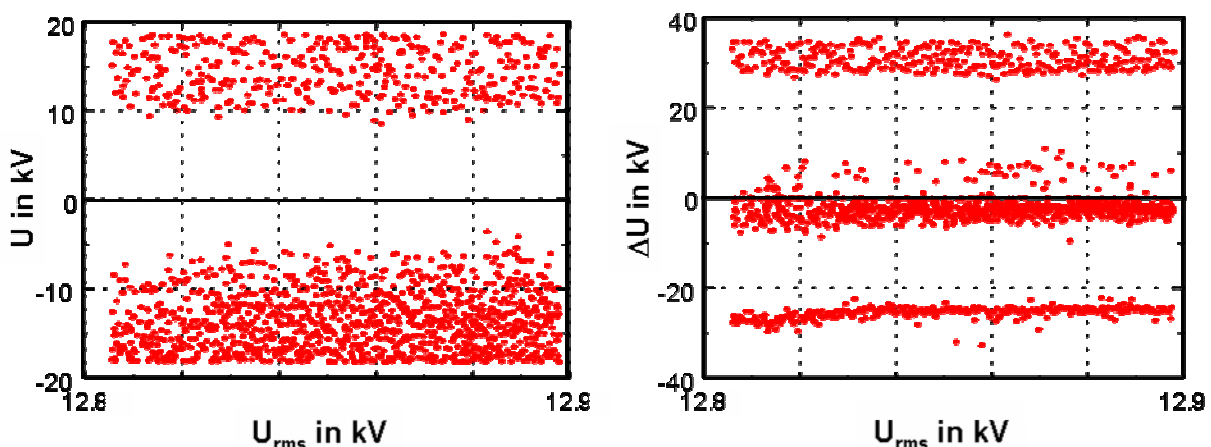
Fig. 5.20: Actual voltages **U** at which PD occurred and the voltage differences ΔU between consecutive discharges during electrical treeing over the externally applied AC voltage **U$_{rms}$**

Interestingly in contrast to the broad scatter in the left diagram and the apparently stochastic occurrence of the voltages **U** at which discharges occur, the voltage changes **ΔU** concentrate around three values and seem to obey a specific system. Positive **ΔU** values are higher than negative ones that show less scatter. In addition also many small negative **ΔU** values occur.

Fig. 5.21 shows in the left diagram the correlations between the actual voltages **U** at which the discharges occurred and the following voltage changes **ΔU** before the next discharge occurred and in the right diagram the correlations between the actual voltages **U** at which the discharges occurred and the time intervals **Δt** before the next discharge occurred. The lines in the left diagram mark the highest possible voltage changes **ΔU** after a PD at the voltage **U** with (**U** + **ΔU** ≤ **2√2 U$_{rms}$**).

Also in these plots characteristic differences between discharges in the positive and negative half cycles show up, are visible. The constant negative **ΔU** values shown in the left diagram lead to smaller **Δt** values after discharges at higher voltages in the preceding positive half cycles. Again the polarity dependent behaviour can be found.
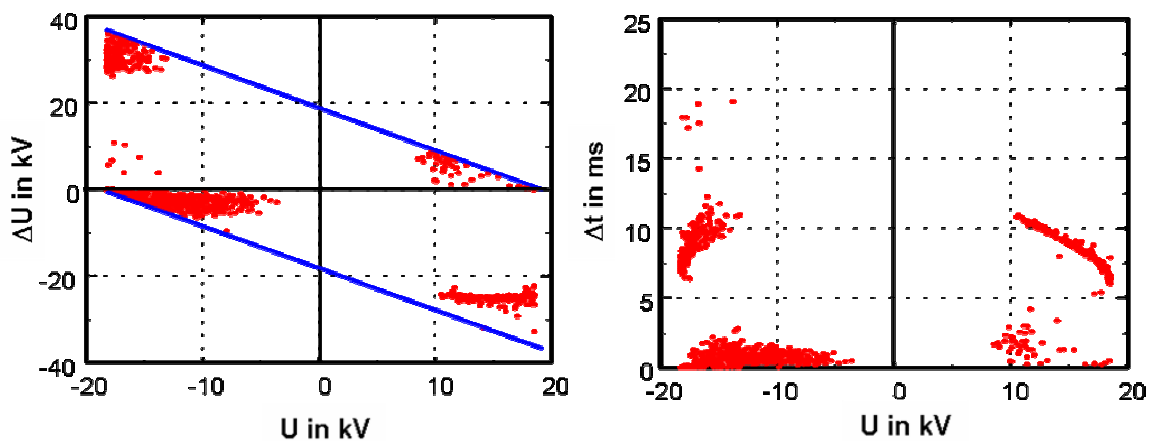
Fig. 5.21: Voltage changes **ΔU** before the occurrence of the next PD and the time intervals **Δt** before the occurrence of the next PD over the actual voltages of a PD

It is remarkable that after discharges in the upper part of positive half cycles in most cases nearly constant negative voltage changes **ΔU ≈ -24 kV** occur, irrespective of the voltage heights **U** at which the preceding discharges occurred. After discharges in the negative half cycles, either small negative **ΔU > -7 kV** or comparative large positive **ΔU > 26 kV** occurred. This polarity dependent behaviour seems to be a consequence of **unipolar space or surface charges** generated in the partial discharge process and the different behaviour of the two types of charge carriers, namely electrons and positive ions or positions in the polymer chains, where an electron had been stripped off. The important point of this finding is, that not the externally

applied voltage **U**, but the change of the local electric field since the preceding discharge – characterized by the external voltage change Δ**U** – is decisive for the ignition of the following discharge.

For discharges in the negative half cycles electrons are injected from the needle tip that move towards the flat electrode thus reducing the opposing negative field very quickly. Thus consecutive negative discharges can occur in the same negative half cycle. Only discharges at very high negative voltages are followed by a discharge in the following positive half cycle.

Discharges in the positive half cycles of the applied voltage accelerate electrons towards the needle, thus leaving behind positively charged molecules. While the electrons enter the metallic needle, the positive charges stay immobile and generate a local electric field that modifies the electric field generated by the externally applied voltage. The field of the charged molecules does not change in the time scale of a few ten ms.

This phenomenon is taken care of by the elements **C₄** and **R₄** in series with the spark gap **F** in the improved equivalent circuit shown in Fig. 5.15. In contrast to the classical equivalent circuit from Gemant and Philippoff a capacitor **C₄** in series with the spark gap exists that is charged by the capacitor **C₁** during the partial discharge process. A consecutive discharge occurs only if the voltage **U**$_F$ = **U₁** - **U₄** reaches the ignition voltage **U**$_F$**'** of the spark gap. This may happen by a change of U₁ by the external voltage or by a change of **U₄** (via a discharging process over **R₄**) or by both. In the situation shown in **Fig. 5.21** (Δ**U**-**U**-correlation), after a positive discharge the voltage **U₄** does not change with time, thus the consecutive discharge occurs only after a change Δ**U₁** of the voltage **U₁** in accordance to a change Δ**U** of the externally applied voltage. Numerically Δ**U₁** = Δ**U** **C₂** / (**C₁** + **C₂**) holds. Hence for a constant ignition voltage **U**$_F$**'** a constant Δ**U** occurs. For the explanation of the phenomena shown in Fig. 5.20 it might be necessary to use two different capacitors **C₄** for positive and negative discharges.

5.4.2   Electrical tree growth

The effect of electrical ageing on the PD characteristics of an electrical tree in polyethylene was also investigated. It is known that the partial discharge process may depend on the voltage applied and thus just one experiment at one applied voltage does not give us all the information that can be gained. Ramping the voltage comparatively quickly allows the examination of the growth rate or the PD processes at different voltage loads. In each run the voltage was ramped up comparatively quickly with a ramp rate of about **700 V**$_{rms}$**/s** until 4096 PD pulses had occurred. The higher ramp rate has the advantage that electrical treeing can be analyzed at different voltage loads while the situation of the tree is nearly unchanged. The experiment was repeated many times and thus the growth process could be analyzed in different stages of tree growth at different voltage loads.

To generate the ageing, a sinusoidal AC voltage of **6 kV$_{rms}$** was applied to the polyethylene sample for up to about **640 hours** and the PD characteristics were observed from time to time with a ramped voltage of **700 V$_{rms}$ /s**. The very high ramp rate allows us to obtain the PD characteristics in different stages of the tree growth at different applied voltages in one measurement run.
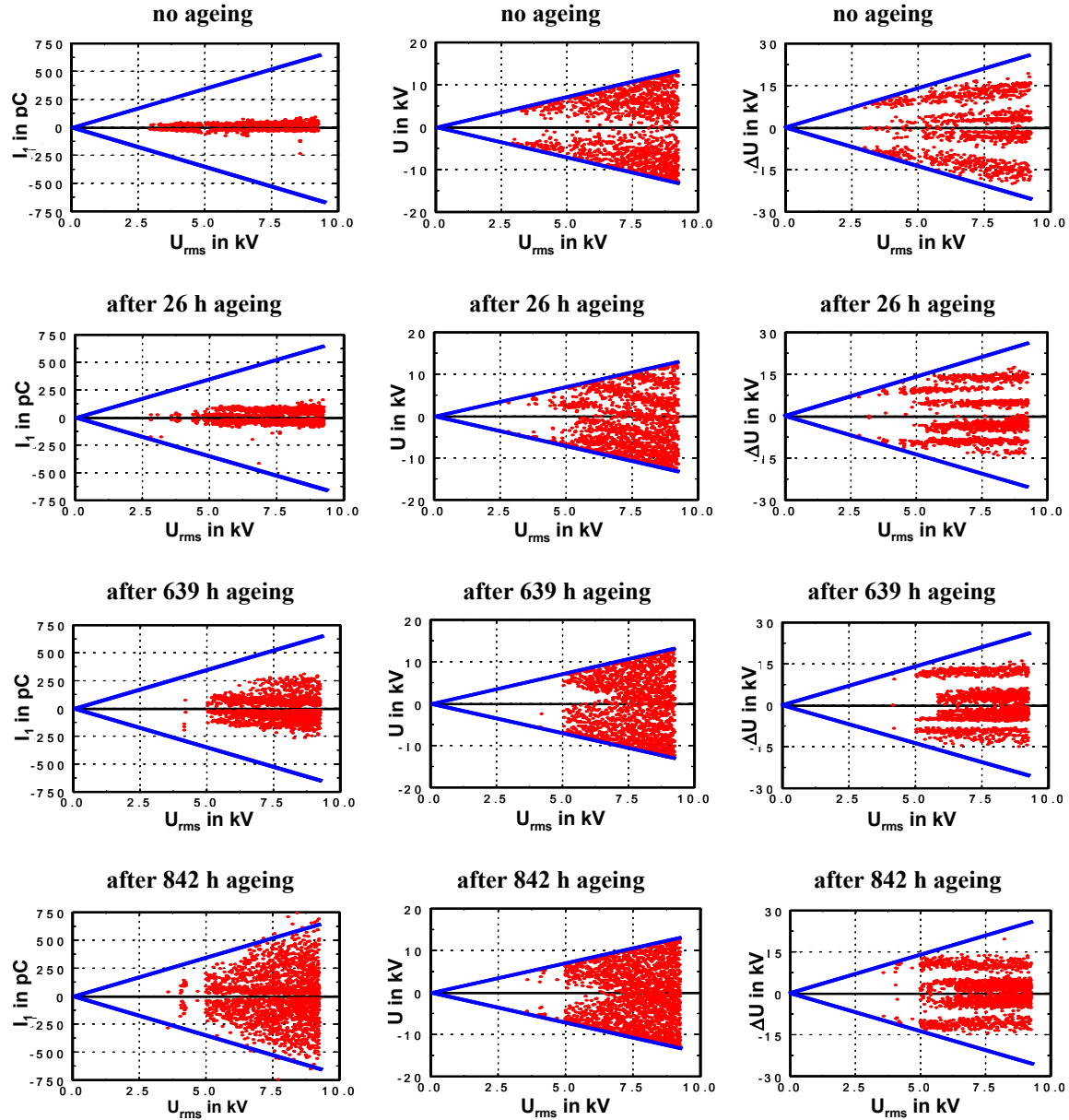
Fig. 5.22: Discharge magnitudes **I$_1$**, actual voltages **U** and voltage differences Δ**U** over the externally applied AC voltage **U$_{rms}$** for different stages of electrical treeing in PE

Fig. 5.22 shows the discharge magnitudes **I$_1$**, the actual voltages **U** at which the discharges occur and the voltage differences Δ**U** between consecutive discharges over the applied voltage for different stages of electrical treeing in PE. The lines in the graphs indicate the highest pos-

sible values of the represented parameters in dependence on the applied voltage. As illustrated in these different representations, the effect of tree growth produces a significant change in the PD characteristics.

5.5 Polarity dependence of the build-up of space charges

In another sets of experiments partial discharges characteristics of polyethylene material in a needle-plane electrode arrangement were examined with different AC voltages, sinusoidal voltages and rectified half-waves of both polarities. With the help of the improved equivalent circuit the results will be discussed in terms of the local space charge generated by every partial discharge [Pat07a]. As known one interesting point in the needle-plane electrode arrangement is that the generation of local space charges occur in extremely non homogeneous fields and that modify the local electric field prior to the ignition of a discharge (e.g. via R_5 in Fig. 5.15). This may even lead to a situation that the polarity of a discharge pulse is opposite to the voltage change ΔU of the externally applied voltage since the preceding discharge [Pat99a, Pat01]. In general the changed electric field (characterized by $U_1 - U_4$ in Fig. 5.15) is responsible for the occurrence of the next partial discharge.

To examine the influence of these space charges, electrical treeing was examined with AC voltages, as well as with rectified half- waves of both polarities. Due to the coupling capacitor of **250 pF** and a discharging resistor of **10 MΩ** the time constant for the final decrease of the rectified half-waves was about **2.5 ms**. The sensitivity was set to about **6 pC**. The sample was loaded with a ramped **50 Hz** AC voltage (or rectified positive or negative half-waves) with a very quick ramp rate of **700 V_{rms}/s** until **4096** PD pulses had occurred. Hence each experiment included different values of the externally applied voltage.

5.5.1 Sinusoidal AC voltage

Fig. 5.23 shows the voltages **U** at which the discharges occurred and the voltage differences ΔU_n between consecutive discharges over the externally applied voltage for the AC voltage load. The lines indicate the highest possible values of **U** and ΔU respectively.

Partial discharges started at an applied voltage of about **5.5 kV_{rms}** and at about **10.7 kV_{rms}** 4096 partial discharges had occurred. Initially only two discharges per cycle occurred at the peak voltages. With increasing voltage the number of discharges increased up to more than 10 discharges per cycle. Interestingly the higher the applied voltage was, the lower the voltages (within the cycles) at which the partial discharges started. With regard to the polarity of the applied voltage no systematic differences seem to exist.
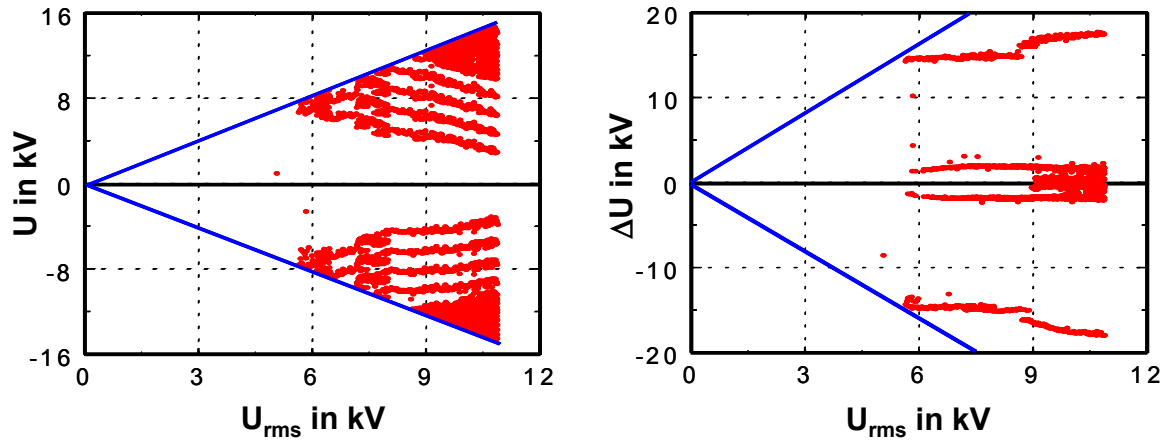
Fig. 5.23: Actual voltages **U** at which discharges occurred and voltage differences Δ**U** between consecutive discharges over the externally applied AC voltage **U$_{rms}$**

As shown the voltage differences Δ**U** between consecutive discharges concentrate at character-istic values around of some values. Not depending on the value of the externally applied AC voltage, most voltage differences have values of about plus or minus **2 kV**, or plus or minus **15 kV**. For voltages above **9 kV$_{rms}$** additional small Δ**U** values around zero occur and the maximum values of Δ**U** increase slightly. However, the values remain clearly below the theoretical limit of $2\sqrt{2}$ **U$_{rms}$**. The behaviour shown in Fig. 5.23 is typical for a step by step **build-up of space charges** and can be explained by a step by step change of the voltage **U$_4$** in the improved equivalent circuit described Fig. 5.15.
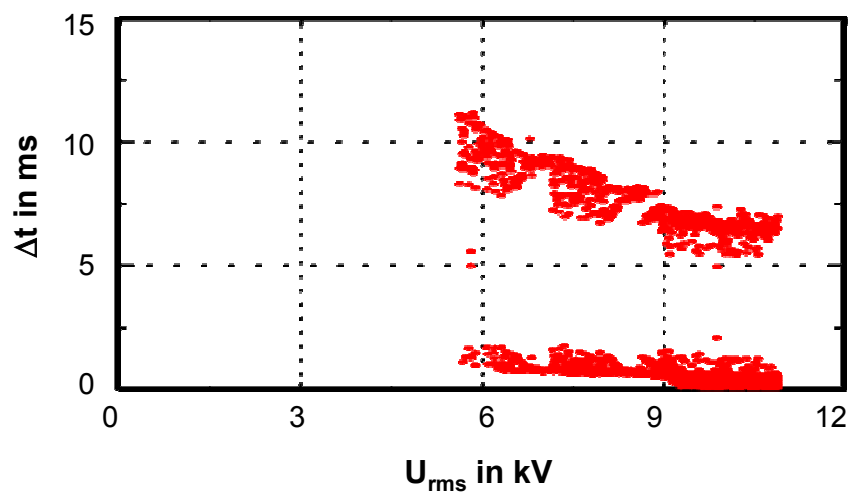
Fig. 5.24: Time intervals Δ**t** between consecutive discharges over the externally applied AC voltage **U$_{rms}$**

Fig. 5.24 shows the corresponding time intervals **Δt** between consecutive discharges over the externally applied voltage. After a characteristic start with **2 discharges per cycle** and corresponding values of **Δt** around **10 ms**, additional discharges occur after time differences of a few ms i.e. after the small values of **ΔU** in Fig. 5.23 (consecutive discharges within the same positive or negative half wave).

5.5.2   Rectified sinusoidal half-waves

The application of rectified positive or negative half-waves of an AC voltage leads to different growth rates of electrical trees in polyethylene [Pat79]. The result shows that the voltage load with rectified half-waves of an AC voltage revealed a different behaviour for positive and negative polarity. This is due to the different build-up of **space charges** in the region close to the needle tip. Space charges around the needle tip play a significant role because they change the local electric field and thus the conditions for the ignition of the next discharge.
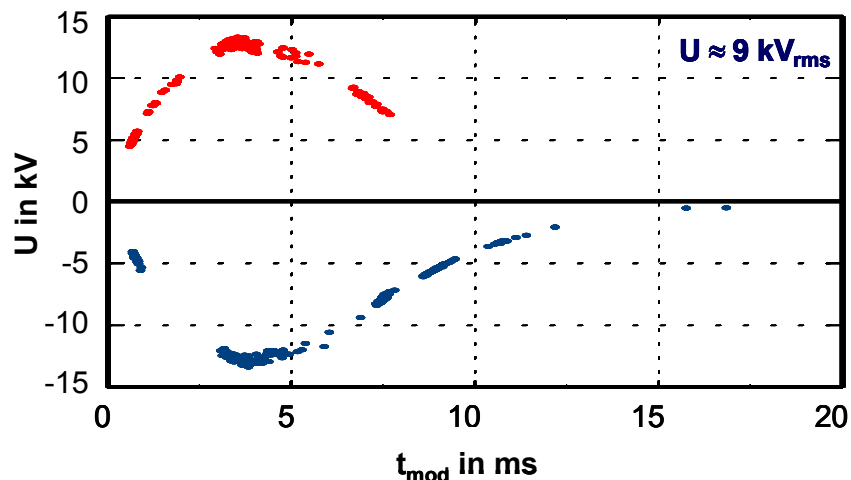
Fig. 5.25: Phase of PD occurrence for rectified half-waves for an applied voltage of about **9 kV$_{rms}$** (for positive and negative half-waves)

Fig. 5.25 shows the phase of PD occurrence for rectified positive and negative half-waves. Partial discharges occurred not only in the inclining parts of the externally applied voltage but also in the declining parts, whereby the behaviour was significantly different in positive and negative half-waves.

Fig. 5.26 shows the voltages at which the discharges occurred over the externally applied voltage for rectified positive and negative half-waves. The straight lines indicate the peak values of the applied voltage. For positive rectified half-waves, not depending on the height of the applied voltage, most discharges occurred at about **5 kV** or – especially at higher applied volt-

ages – at the peak voltages. In some cases discharges occurred at voltages between **5 kV** and the peaks of the rectified positive half-waves. For negative rectified half-waves, as a result of **space charges**, a fixed correlation seems to exist between the voltages at which the discharges occur.

For positive rectified half-waves space charges seem to be of less importance. Most PD occur when the applied voltage exceeds about **5 kV** in the inclining part of the rectified half-waves. A second discharge may occur near the peak voltage for rectified AC voltages of more than about **9 kV$_{rms}$**.
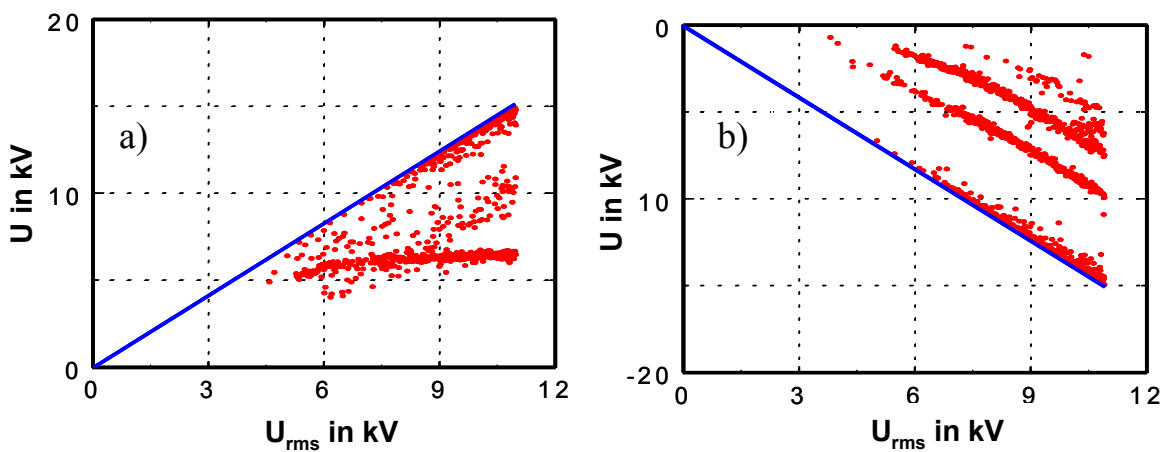
Fig. 5.26: Actual voltages **U** at which discharges occurred over the externally applied AC voltage **U$_{rms}$ a)** for rectified positive and **b)** for rectified negative half-waves

Fig. 5.27 shows the voltage differences Δ**U** between consecutive discharges over the externally applied voltage for rectified positive and for rectified negative half-waves. For positive voltage loads the external voltage determines the PD behaviour, while for negative voltage loads **electrons** that are injected by the needle electrode build-up **space charges** that influence the local electric field and thus determine the PD processes. This leads to some extent to a decoupling of the local electric field (responsible for the ignition of the next PD) from the externally applied voltage.

Fig. 5.28 shows the corresponding time intervals Δ**t** between consecutive discharges over the externally applied voltage for rectified positive and for rectified negative half-waves. Interestingly, for rectified positive half-waves nearly constant time differences Δ**t** seem to exist between consecutive discharges, while for rectified negative half-waves – as a consequence of the nearly constant values of Δ**U** – in dependence on the magnitude of the applied voltage shorter or longer time intervals occur.
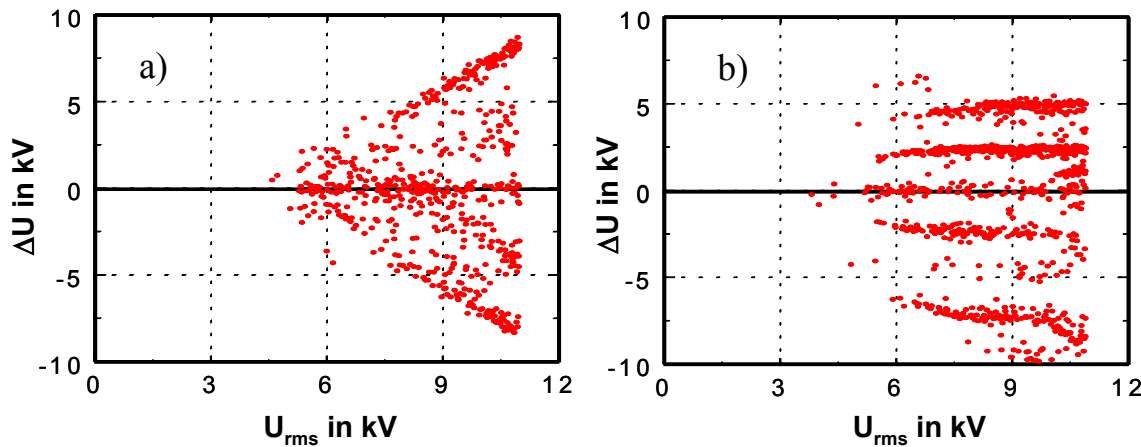
Fig. 5.27: Voltage differences ΔU between consecutive discharges over the externally applied AC voltage U_{rms} **a)** for rectified positive and **b)** for rectified negative half-waves
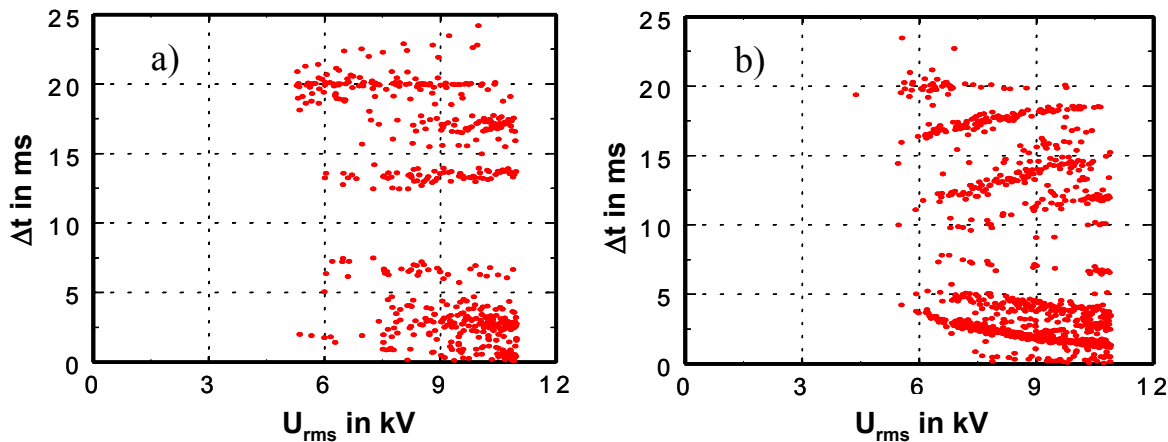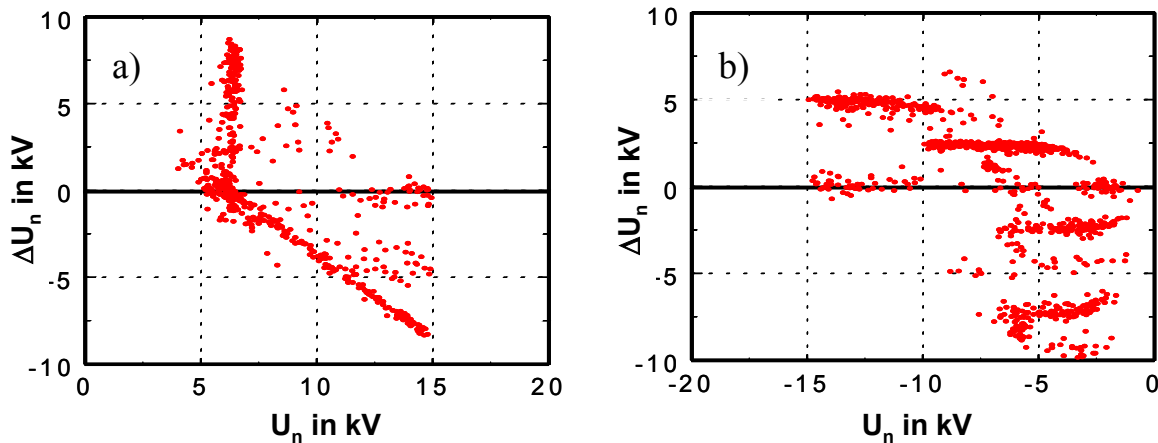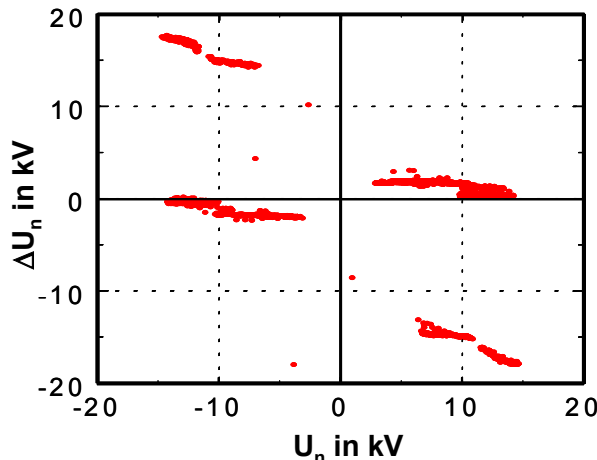
Fig. 5.28: Time intervals Δt between consecutive discharges over the externally applied AC voltage U_{rms} **a)** for rectified positive and **b)** for rectified negative half-waves

Fig. 5.29 shows the correlations between the actual voltages U_n at which discharges occurred and the voltage changes ΔU_n before the next discharge. For rectified positive half-waves no space charge influence seems to exist, while for rectified negative half-waves the nearly constant ΔU_n values indicate a strong influence of space charges. Fig. 5.29 is equivalent to Fig. 5.26 and shows the correlation ΔU_n and U_n for all pulses.

Fig. 5.30 shows the voltages differences ΔU_n between consecutive discharges after a PD over the actual voltages U_n at which the PD occurred for the AC voltage load. In this case the influence of space charges seems to be less pronounced.

Figs. 5.29: Voltage differences ΔU_n between consecutive discharges after a PD over
the actual voltages U_n at which the PD occurred
a) for rectified positive and **b)** for rectified negative half-waves

Figs. 5.30: Voltage differences ΔU_n between consecutive discharges after a PD over
the actual voltages U_n at which the PD occurred for the AC voltage load

5.6.3   Discussion on the basis of the improved PD equivalent circuit

Basically, the different voltages at which discharges occur can be explained using the im-
proved equivalent circuit for partial discharges (Fig. 5.15). Not depending on the actual shape
of the wave form of the applied voltage partial discharges lead to the occurrence of a voltage
across the capacitor C_4 and the next discharge only starts if the voltage difference with $U_1 - U_4$
reaches the ignition voltage U_F' of the spark gap F.
An interesting result of the experiments with a needle-plane electrode arrangement in polyeth-
ylene with rectified half waves is that a discharge of a positively charged capacitor C_1 leads to

different space charge phenomena compared to a negatively charged capacitor. The build-up of space charges and/or their decay with time is highly polarity-dependent. Hence a different behaviour with different polarities of the applied voltages occurs.

Another interesting point is the **polarity of the partial discharge signals** compared to the polarity of the voltage. In the inclining parts of the rectified positive half-waves the impulse polarities are positive, in the declining parts they are negative. The opposite holds for the application of the rectified negative half waves.

For an AC voltage load and/or a rectified negative half-wave load due to **electron injection** a voltage U_4 is generated that does not significantly change with time, thus a consecutive discharge occurs only after a change ΔU_1 of the voltage U_1 in accordance to a change ΔU of the externally applied voltage U. Numerically $\Delta U_1 = \Delta U \, C_2 / (C_1 + C_2)$ holds. Hence for a constant ignition voltage U_F' a constant value of ΔU occurs. For a rectified positive half-wave load the influence of a PD seems to be different, at least no constant voltage U_4 seems to exist.

5.7 Summary

PD measurements on the laboratory specimens as well as on different electric apparatus revealed in how far the partial discharge phenomena are influenced by **charges accumulated as a consequence of prior discharges**. The detailed evaluation of the sequence correlated information of a small subset of the data revealed more information about the defect than the analysis of a larger data set accumulated in dependence of the actual phase angles of the applied voltage without taking into account any correlations between consecutive pulses.

- Due to space charges in solid dielectrics a continuous shift of the phase angles of occurrence and often a more or less periodic behaviour due to a repetitive build-up of space charges (with a reset in-between) may occur.
- As a result of the different movement of charges of different polarities and the existence of different trapping centers a polarity dependent behaviour exists.
- To examine the phenomenon in more detail, the PD activity of different types of electric equipment was measured with constant and ramped voltage load. The results revealed that different defects behave differently.
- The sequence of the actual voltages U_n at which discharges occur over time t_n, or the sequence of the voltage differences $\Delta U_n = U_{n+1} - U_n$, or the time intervals $\Delta t_n = t_{n+1} - t_n$ between consecutive discharges were extracted and used for the analysis.
- The analysis of **PD sequences** – and not solely data sets accumulated on the basis of the phase angles of occurrence only – revealed the influence of surface and space charges generated by the individual partial discharges.

- When examining the direct sequence of voltage values at which the discharges occur, a conspicuous behaviour can be observed. Especially if the test voltage is increased slowly, at first partial discharges occur at one spot in the specimen only with mostly only one discharge per half cycle. In this case a clearly structured **correlation between consecutive discharges** can be found.

- In a measurement of a needle in polyethylene, at voltages just above the partial discharge inception voltage only one discharge event within a half cycle of the voltage occurs and the phase angles of occurrence shift step by step. After a few cycles of the applied voltage a reset occurs and – with or without a discharge free time interval inbetween – the shift starts again. The voltage differences **ΔU** between consecutive discharges are nearly constant and the time differences **Δt** show a sort of oscillation and are alternatively (in most cases) either bigger or smaller than **10 ms** whereby two consecutive time differences add up to **20 ms**.

- Measurements on a HV test transformer with a constant voltage load show a similar phenomenon with an even more systematic behaviour. The actual voltages at which the discharges occur show that there is a monotonous shift of the voltage levels that ends with a reset and starts again from the initial values. The Δt diagram reveals that the time differences from the negative pulses to the positive ones increase from under **10 ms** to **13 ms**, while the ones in the opposite polarity decrease from slightly above **10 ms** to about **7 ms**. Two consecutive time differences Δt_n and Δt_{n+1} add up to **20 ms**. A simplified model for a PD sequence with influence of accumulated charges was proposed to explain this phenomenon. This model is based on the superposition of a DC component on the externally applied AC voltage.

- Even with surface discharges on inorganic insulating materials the influence of surface charges can be found. A continuous shift to higher positive voltages seems to show a more or less symmetric behaviour. This can be interpreted by a continuous build-up of positive space charges 'opposite' to the discharge triggering spot at high potential or of negative space charges.

- In the measurements of stators of small commercial motors with ramped voltage load, the results indicate the existence of **constant surface or space charges** for some hundreds of cycles, after which a change of the polarity of the charge accumulation may occur.

The correlation between the externally applied voltage and the local electric field at the PD-active defect has been discussed on the basis of an improved PD equivalent circuit, and the result is:

- The externally measured phase angle is not necessarily representative for the local electric conditions at the site of the defect.

- In dependence on the applied voltage and the actual conditions of the defect a different PD behaviour may occur.

- A formula of the apparent charge **q** on the basis of the improved PD equivalent circuit was established.

- On the basis of this formula the influence of space charge can be determined.

- The situation that the pulse height **I₁** does not depend on the actual voltage **U** at which a PD occurs was discussed. This behaviour is interpreted as due to the influence of space charges. The PD-active defect in the HV transformer consists of a small flat, gas filled void.

- Some measurements on the different test objects in which a proportionality between **I₁** and **U** had been found were discussed. In this case the influence of space charges seems not to exist.

PD characteristics of electrical treeing in needle-plane arrangement in polyethylene (needle on HV) have been investigated. The voltage was increased linearly with time with a slow rate to examine the electrical tree initiation and with a comparatively quick voltage ramp rate to examine the electrical tree growth and the electrical ageing. The influence of the polarity of the sinusoidal voltage cycle on the build-up of space charges was also examined. The results can be concluded as follows:

- In general, at tree initiation discharges occurred more frequently in the negative half cycles of the applied voltage.

- Partial discharges in the positive half waves were mostly bigger and frequently followed by a discharge in the consecutive negative half cycle, after a constant negative voltage change **ΔU**.

- The change of the local electric field since the preceding discharge – characterized by the external voltage change **ΔU** and not the externally applied voltage **U** – is decisive for the ignition of the following discharge.

- In electrical trees in polyethylene, consecutive discharges may occur with time intervals of typically some **10 µs**. This time seems to be necessary to reduce the gas pressure in the channels to allow a next discharge at the same voltage level of the AC voltage.

- In the negative half cycles of the applied voltage, 'multiple' discharges could occur with the mean time difference of about **27 µs**. There seems to be no ´stable` space charge that reduces the local electric field.

- Repetitive measurements of the PD activity of electrical trees during their growth within more than 30 days showed significant changes of the characteristic parameters.

- PSA characteristic patterns can be used to observe PD behaviour during ageing processes.

- The analysis of the electrical treeing phenomenon in polyethylene in a needle-plane electrode arrangement with sinusoidal AC voltage and rectified half-waves of both polarities showed that space charges play an important role in the PD process.

- Due to a different build-up of **space charges** in the region close to the needle tip positive and negative rectified half waves lead to different PD phenomena.

- Partial discharges occurred not only in the inclining parts of the externally applied half-waves but also in the declining parts, whereby the behaviour in positive and negative half-waves was significantly different.

- With positive half-waves after a PD at peak voltage in most cases the next PD occurs in the inclining part of the following positive half-wave.

- With negative half-waves after a PD at peak voltage the following two (or three) discharges occur in the declining part of the half-wave before jumping to the inclining part of the following negative half-wave.

- In other cases the build-up of space charges as a consequence of a PD in the inclining part of a negative rectified half-wave is so large that the following PD occurs not at the peak voltage, but in the declining part of the half-wave.

- For rectified positive half-waves no space charge influence seems to exist, while for rectified negative half-waves a strong influence of space charges exist.

6   Partial Discharges in the Insulation System of Rotating Machines

Partial discharge measurements and analyses are often used as a non-destructive diagnostic tool to monitor degradation phenomena in the insulation system of electrical power equipment. Local defects caused by electrical, thermal or mechanical stress generate characteristic sequences of partial discharges that contain information about the critical regions in which partial discharges occur. The **Pulse Sequence Analysis** combined with **Pulse Shape Analysis** have proven to be an efficient method to analyse and to characterize PD-active defects [Pat02a]. This chapter reports on the investigation of partial discharge measurements and analysis of samples of stator windings of small AC motors and samples of stator bars of a high voltage rotating machine.

6.0   Introduction

The insulation system of electrical power equipment, especially electric machines is subjected to combined thermal, mechanical, electrical and environmental stresses during operation which may alter the dielectric properties [Cyg90]. The condition of the electrical insulation systems of high voltage equipment will strongly influence the economical and technical lifetime as well as the reliability of the supply of the generated or distributed electrical power.

Partial discharge activities are both the main deterioration factor and the most prominent indicator for the assessment of insulation deterioration. In many cases the insulation system of high voltage equipment is resistant against PD. Partial discharges of some **nC**, caused for example by small voids inside of the insulation system are tolerable in oil-filled or especially in mass-impregnated power cables and in large machine insulation. But large PD pulses caused by large single defects or defects produced by changes due to multiple stress ageing can degrade the insulation system.

Stator windings of high voltage rotating machines are of a very complex design and the assessment of their actual insulation conditions is not easy [Bou04]. For a more detailed insight into the physics of the local degradation processes and their relevance for the ageing process of this equipment, investigations are carried out on the both kinds of stators: stator windings of a small motor for domestic application (stator of refrigerator) and model stator bars of a high voltage rotating machine.

6.1   PD measurements on the stator windings of a small AC motor

The windings of small AC motors normally consist of isolated, varnished wires randomly wound, without special further isolation treatments. The investigation of the actual state of insulation deterioration and therefore the comprehension of the physical processes of ageing

which lead to the total degradation of the insulation system of the windings is a demanding task.

6.1.1   Start of PD process

The detailed analysis of short sequences of partial discharges in the stator windings of a small motor with the applied voltage increased linearly with time shows that in the beginning of the PD process i.e. at PD inception voltage and for the following cycles of the applied AC voltage a characteristic change in the PD process occur. The PD causes the build-up of space charges or surface charges at the dielectric interface between the windings. These charges which can be constant for some cycles or change in a characteristic pattern lead to the change of the local electrical field that influences the ignition of the following discharge [Ben04].

Typical changes in the PD phenomena are clearly found in the pulse heights and in the time intervals between discharges. At the beginning of the discharge process the magnitudes of the PD at first increase and then become more or less constant. A discharge free time with a restart can occur i.e. the process that leads to the pulse increase may occur a few times with or without pause in-between (see **6.1.2**) or another discharge site with different discharge amplitudes can occur (see Fig. 6.1a). At low test voltages only two discharges per cycle of the applied voltage occur.
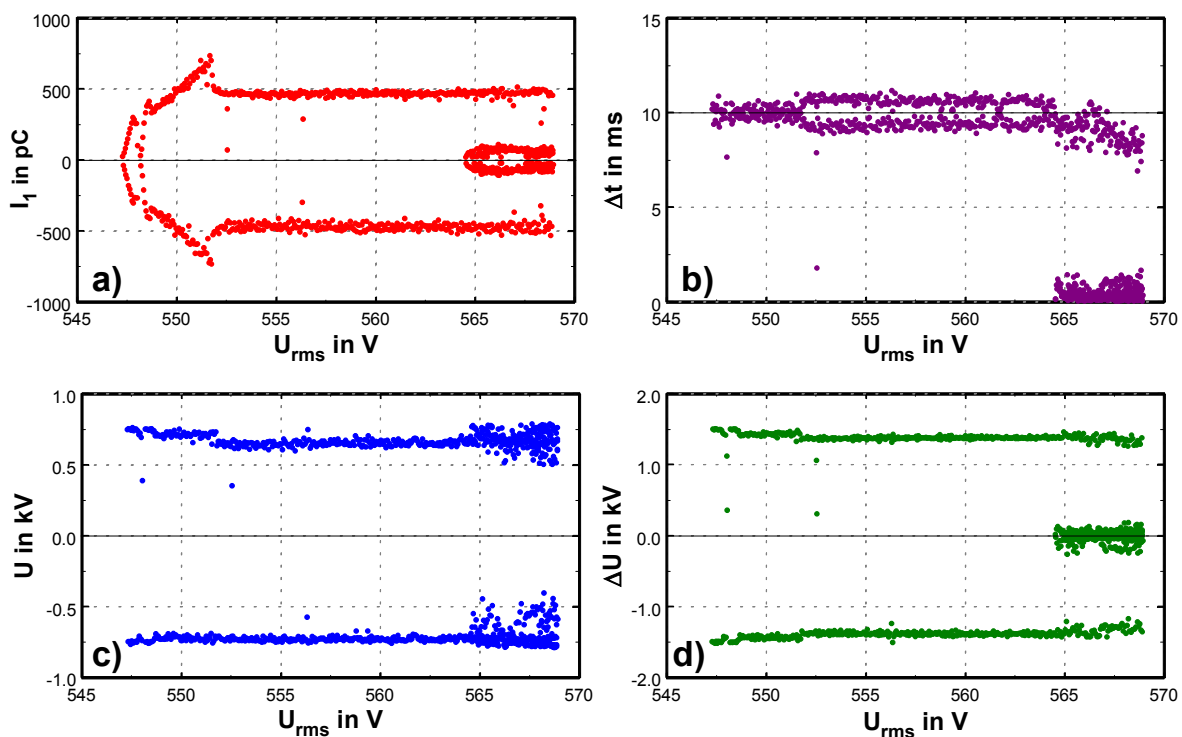

Fig. 6.1: Pulse heights I_1, time intervals Δt between consecutive discharges, actual voltages U at which discharges occur and voltage changes ΔU between consecutive discharges over applied voltage U_{rms}

In these cases a clearly structured correlation between consecutive discharges can be found (see **Fig. 6.1b** for **552 < U$_{rms}$ < 565 V**). At higher voltages often more than one PD per half cycle occurs. In these cases different defects may be simultaneously active and the interpretation of pulse sequences is not easy without additional analyses with the Pulse Shape Analysis (see § **6.1.4)**.

As an example **Fig. 6.1** shows results of a PD measurement on the stator winding with a ramped applied voltage of about **190 V/min** and a sensitivity of about **± 20 pC**. The electrical characteristics of the stator winding and its electrical connection to the high voltage supply are described in chapter 2.
Fig. 6.1a shows the pulse heights **I$_1$** over the applied voltage **U$_{rms}$** for the first **1000** PD. The amplitudes of the PD pulses in both polarities increase quickly during the first **20** PD. Then a reset occurs, i.e. discharges occur again with small amplitudes and increase quickly. The increase of the pulse heights become smaller and stops after **140** pulses (at about **552 V**). The correspondent mean time intervals between consecutive discharges (**Fig. 6.1b)** in this region are about **10 ms** with some scatter.

For higher voltages the PD behaviour changes and time differences **Δt** of either **9** or **11 ms** (approximately) occur. The amplitudes of the PD pulses become constant (Fig. 6.1a**)** and a non-symmetric behaviour occurs in the actual voltages **U** at which the discharges occur (**Fig. 6.1c)**. The discharges in the positive half cycles do not occur at the peak of the external voltage but in the inclining part of the external voltage curve. This leads to the fact that the time intervals **Δt** between consecutive discharges are no longer centred around **10 ms** but those after positive discharges are around **11 ms** and those after negative discharges are around **9 ms**, (Fig. 6.1b**)** whereby two consecutive time differences **Δt** always add up to **20 ms** (see Fig. 5.14).

The explanation is given by the build-up of charges on the surface of the insulation of the wires as a consequence of the occurrence of PD. The presence of these charges (electrons or negative or positive ions) on the interfaces between the winding insulations leads to an increase of the local electrical field in the positive half waves of the applied voltage. As a consequence PD occur in positive half cycles before the peak voltage is reached.

Interestingly the voltage differences **ΔU** between consecutive discharges show no polarity dependence but the absolute values seem to be smaller than at lower voltages (**Fig. 6.1d)**.
At about **564 V** another characteristic change occurs as a consequence of a second defect which starts to produce partial discharges with small magnitudes and time differences **Δt** less than **1 ms**. Frequently PD from two defects can be separated by using the Pulse Shape Analysis (see paragraph **6.1.4)**.

6.1.2 Influence of the ramp rate of the test voltage

In electrical power equipment where typically several discharge processes may simultaneously occur, the separation of discharge sources is a demanding task. This problem, however, cannot be efficiently solved by testing the apparatus at a fixed voltage level. Since different discharge sites usually have different PD inception voltages, a more suitable test procedure is the use of a slow increase of the test voltage. In this case it is possible to detect the inception of each discharge site and to identify the types of these sources by separating the single site patterns from the multi-site pattern.

To study the influence of the ramp rate of the test voltage, PD measurements with two differently ramped AC voltages have been performed. The test voltage was linearly ramped at first with a fast ramp rate of about **190 V/min** and then with a slow ramp rate of about **50 V/min** respectively. The PD sensitivity was adjusted to about **± 20 pC**.

Fig. 6.2a and **Fig. 6.2b** illustrate the pulse heights I_1 over the applied voltage U_{rms} for the two selected ramp rates. The inception voltage does not depend on the ramp rate of the applied voltage since in both cases the inception voltage appears approximately at the same voltage value (about **621 V_{rms}**).

For the comparatively quick rate (**190 V/min**), initially the pulse heights I_1 increase continually with increasing applied voltage and then become more or less constant at about **625 V_{rms}**. At about **637 V_{rms}** and after a brief increase in the PD amplitude, an abrupt change in the pulse height behaviour occurs and only small amplitudes are found. With the lower voltage increase, the time intervals **Δt** between consecutive discharges are about **8** or **12** to **13 ms**. The time differences **Δ$_2$t** between next but one discharges are close to **20 ms** (**Fig. 6.2c**). For higher voltages where more than one PD defect is active, the time differences **Δt** are around **10 ms** and in addition values below **3 ms** occur. Thus two consecutive time differences **Δ$_2$t** between next but one discharges do not add to **20 ms**.

The analysis of the actual voltages (**Fig. 6.2e**) shows at first the already discussed symmetric behaviour, then the symmetry disappears and in both polarities the discharges occur at the peak and in the inclining part of the external voltage curve.

The behaviour of the pulse heights I_1 at the slow ramp rate of the test voltage is interesting. The typical change in the amplitudes with the fast voltage ramp occurs a few times with characteristic resets in-between. After a first increase of the amplitudes of the PD pulses a discharges free time occurs and the PD activity starts again with increasing amplitudes. At about **638 V** a similar change as found with the slow ramp rate occurs. From this voltage on, the time difference **Δt** between discharges do not concentrate in two groups around **8 ms** and **12 ms** but in one group around less than **10 ms** (**Fig. 6.2d**). In addition discharges with the time intervals **Δt** less than **2 ms** occur and the pulse heights shift to smaller values. The analysis of the actual voltages U at which the discharges occur (**Fig. 6.2e** and **Fig. 6.2f**) shows clearly the transition.
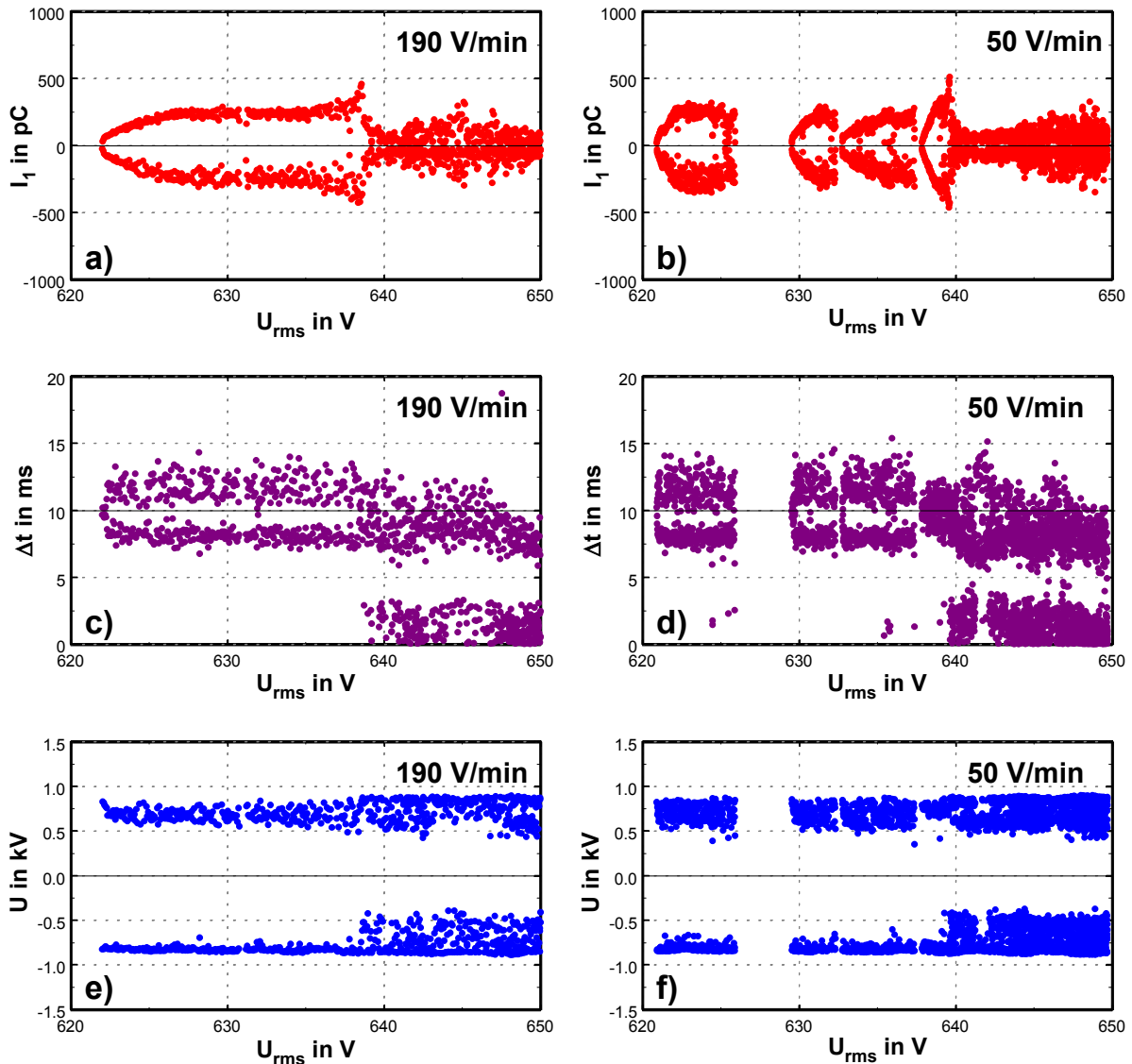
Fig. 6.2: Pulse heights I_1, time intervals Δt between consecutive discharges and actual voltages **U** over applied voltage U_{rms} for the two selected voltage ramps

6.1.3 Polarity of the applied test voltage

Obviously only the discharges that occur in the negative polarity of the test voltage lead to the occurrence of space charges which affect the ignition of the next discharge. This can be related to the kind of the electric connections of the stator to the high voltage. Indeed, for the analysis of the stator windings of a motor, the voltage is usually applied to both ends of one of the phase windings while the others and the iron core are grounded. In the previous measurement the main winding is connected to ground potential and the auxiliary winding is connected to high voltage in order to avoid the deformation of the PD signals due to the large capacitance of the main winding. To investigate the influence of the polarity of the applied test voltage a PD

measurement was realized on the stator with the main winding on the high voltage and the auxiliary winding on the ground.

Fig. 6.3 shows the frequency distributions of the actual voltages **U** at which the discharges occur for the two kinds of electric connections. The result shows that the non-symmetry of the actual voltage depends from the polarity of the electric connection of the test object. In the first measurement discharges occur at the peak of the negative half cycle and before the peak of the positive half wave (**Fig. 6.3a**). The second measurement shows the opposite case (**Fig. 6.3b**).
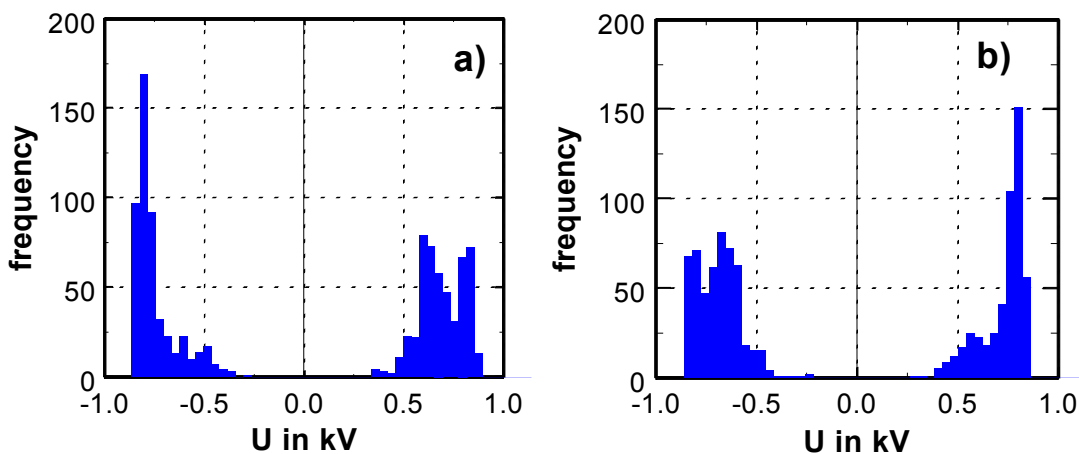
Fig. 6.3: Frequency distributions of the actual voltages **U** at which the discharges occur
a) auxiliary winding on high voltage and **b)** main winding on high voltage

6.1.4   Multiple discharge sites

If different defects are simultaneously active (especially at higher test voltages) the analysis of the data becomes more complicated and the interpretation of the pulse sequences is not so easy. In this case the deterministic sequences of the defects mix and hence some of the correlations between consecutive discharge signals disappear.

For demonstration **Fig. 6.4** shows the pulse heights I_1, the time intervals Δt between consecutive discharges, the actual voltages **U** and the voltage differences ΔU between consecutive discharges over the applied voltage U_{rms} obtained in a PD measurement on another stator of a small motor.

Partial discharges start to occur at about **554 V** with two discharges per cycle. With the increase of the applied voltage a second defect starts (at about **563 V)** to produce small discharges. The analysis of the pulse heights (**Fig. 6.4a**) can help initially to identify the additional defect and also sometimes to separate these different defects by the selection of characteristic values (in this case for example here I_1 < **50 pC** for U_{rms} > **563 V**) of the PD magnitude. At higher applied voltages the defects mix together and the selection will be difficult.

The analysis of the time differences Δt between consecutive discharges (**Fig. 6.4b**) also give some information whether there is only one active discharge site or two or more that are independent from each other. For two or more independent discharge sites of the same type, the time interval between discharges have small values of a few ms (here below **2 ms**).

The existence of two non-correlated discharge-active defects leads also to a characteristic change of the voltages **U** and the voltages changes ΔU diagrams. The **U** diagram (**Fig. 6.4c**) shows that the discharges in the beginning only occur at the crest voltages, after then additional discharges occur in the inclining part before the crest voltage. This can also clearly be seen in the ΔU diagram (**Fig. 6.4d**). At the lower measuring voltages, the curve of the voltage changes ΔU shows only two values in both polarities. With the increase of the measurement voltage additional discharges also occur in the inclining part of the applied voltage which has as a consequence additional small values of ΔU near zero.
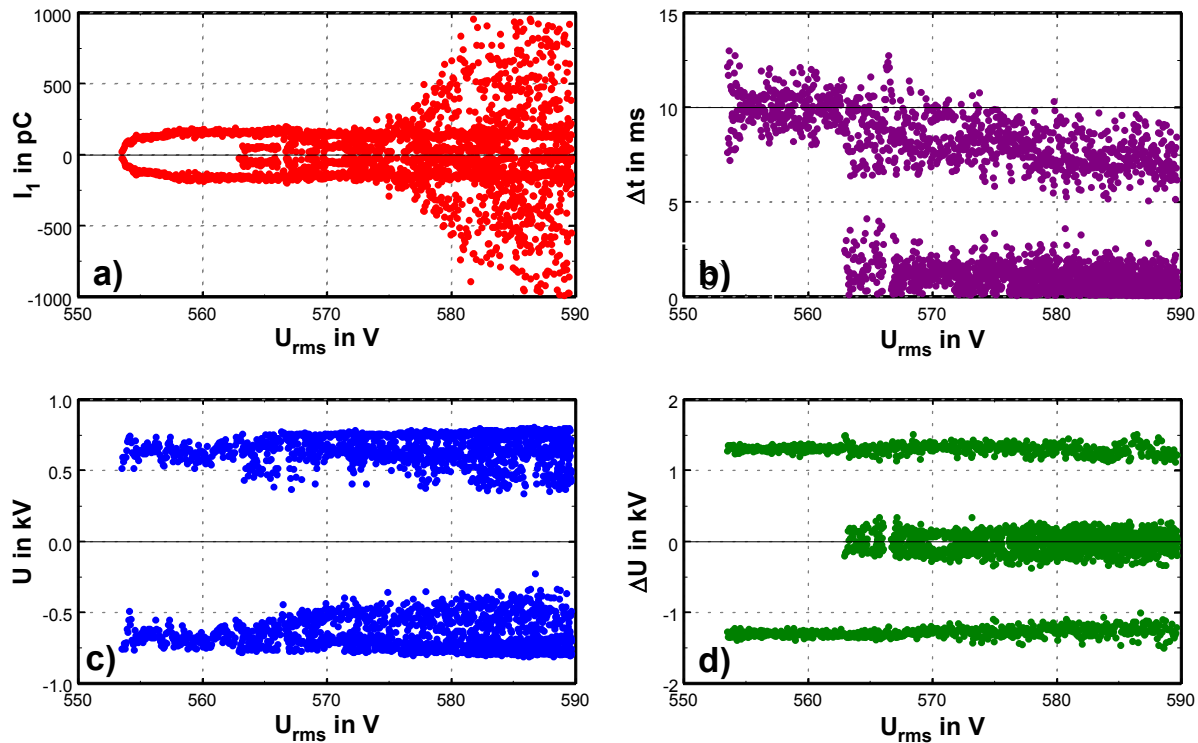
Fig. 6.4: Pulse heights I_1, time intervals between discharges Δt, actual voltages **U** and voltage differences ΔU between discharges over the applied voltage U_{rms}

In many cases, the Pulse Sequence Analysis can be helpful to identify and to characterize the defects, but if different defects are simultaneously active the analysis becomes more difficult. One of the key steps in the analysis of these complex partial discharge data sets is the separation of signals from different sources which allows the separation of the measured data sets into different subsets that are characteristic for specific defects and can be separately analyzed.

As already discussed in chapter 4, Pulse Shape Analysis is the very effective tool to separate different defects. For this purpose, different parameters derived from the actual shape of the signal (i.e. the height and/or the position of the highest positive and negative peak) can be used for separation of the PD signals and thus the PD pulses from different sources can be analyzed separately.

Fig. 6.5 shows as an example the use of the parameters t_1 and $t_2 - t_1$ to analyze the measurement data set discussed in Fig. 6.4. By choosing the time intervals of the two first peaks of the PD signals $t_2 - t_1 < 3.5\ \mu s$ only the defect that generates discharges with constant PD pulse amplitudes I_1 will be selected. In the other case, choosing the time intervals $t_2 - t_1 > 3.5\ \mu s$ combined with the time of the first peak $t_1 > 1.7\ \mu s$ only the defect that generates discharges with variable PD pulse amplitudes will be selected. Thus both defects will be separated in two different data sets and can be analysed separately.
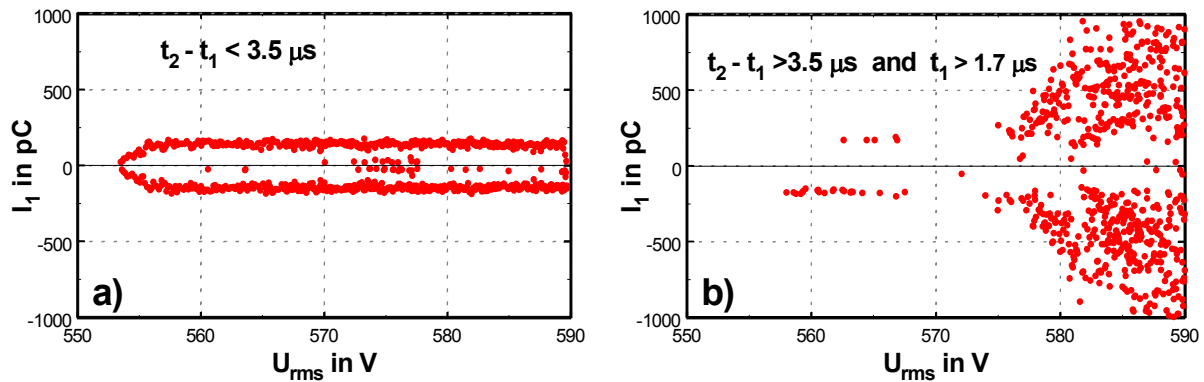
Fig. 6.5: Pulse height I_1 over applied voltage U_{rms} for the selected parameters t_1 and $t_2 - t_1$
a) $t_2 - t_1 < 3.5\ \mu s$ and b) $t_2 - t_1 > 3.5\ \mu s$ and $t_1 > 1.7\ \mu s$

6.1.5   Effect of temperature and influence of thermal ageing on stator windings

The properties of many insulating materials of electric machines are temperature-dependent [Mug90]. In general, the rate of the deterioration, i.e. ageing, increases with temperature [Lor02]. In most cases the off-line PD testing does not take into account the real operating conditions of the electric machine. During operation the stators are often used at higher temperatures, which accelerate the ageing of the dielectric materials. The temperature has an important impact on the life of the insulator, thus a winding insulation system must be evaluated for its capability under realistic thermal conditions. The multiple stresses ageing i.e. the combination of electrical, mechanical and thermal ageing can quickly degrade the insulation system. Local defects caused by these multiple stresses generate characteristic sequences of partial discharges that contain information about critical regions in which partial discharges occur.

In order to investigate both the temperature effect and the thermal ageing on the partial discharge behaviour, PD measurements were performed on the stator winding at different temperatures according to the procedure showing in **Fig. 6.6**. After a first measurement at room temperature (**20 °C**), the stator was aged for one day at a temperature of **100 °C**.

After this period, the heating was stopped and in the cooling phase two further measurements were carried out. One measurement was done at a temperature of **60 °C** and the other measurement at a temperature of **23 °C**.
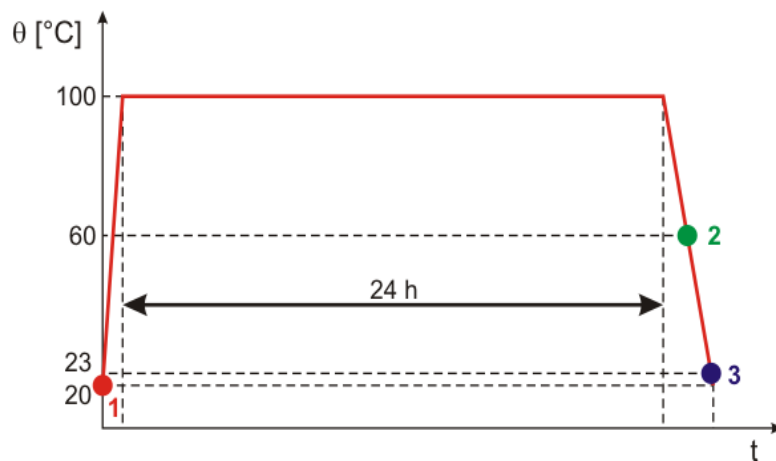
Fig. 6.6: Schematic representation of the experimental procedure

The analysis of the cumulative numbers of PD over the applied voltage **U_{rms}** for the three measurements shows the effect of temperature on the partial discharge behaviour. **Fig. 6.7** illustrates clearly a dependence of the PD inception voltage on the temperature. The result shows that the partial discharges appear at lower voltages for higher temperature. The PD inception voltage decreases from **580 V** to about **520 V** when the temperature is increased from room temperature to **60 °C**.
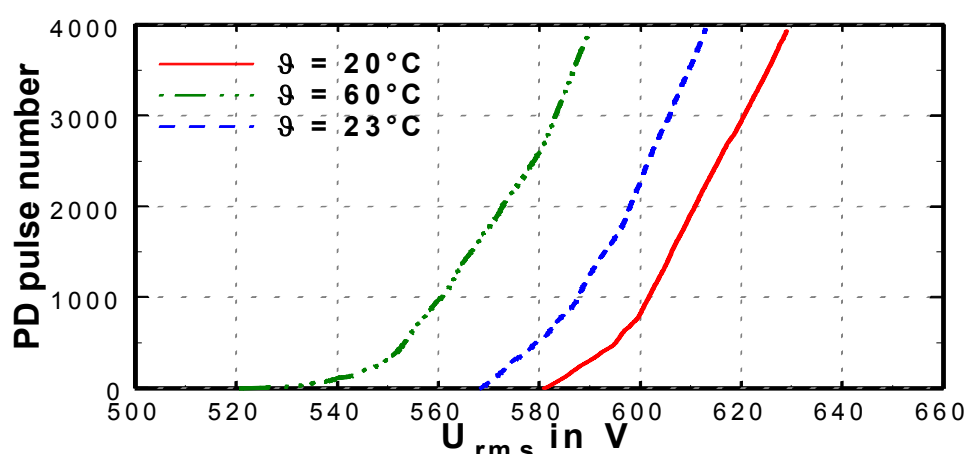
Fig. 6.7: PD pulse number over applied voltage **U_{rms}** for the three temperatures

To examine the effect of temperature on the pulse heights, correlation diagrams between the discharge amplitudes and the actual voltages are shown in **Fig. 6.8**. The representations of the PD pulse heights I_1 over the actual voltages **U** at which the discharges occur for the measurements done at **20 °C**, at **60 °C** and at **23 °C** show a different behaviour. The comparison between the first measurement (**20 °C**) and the second measurement (**60 °C**) shows that the amplitude of the PD pulses increases from **250 pC** to more than **500 pC**. This increase in the PD pulse heights is not due to the effect of the measuring temperature since the third measurement done at **23 °C** shows also values at about **500 pC**. The increase of the pulse heights can be explained as an effect of the thermal ageing after one day at **100 °C**.
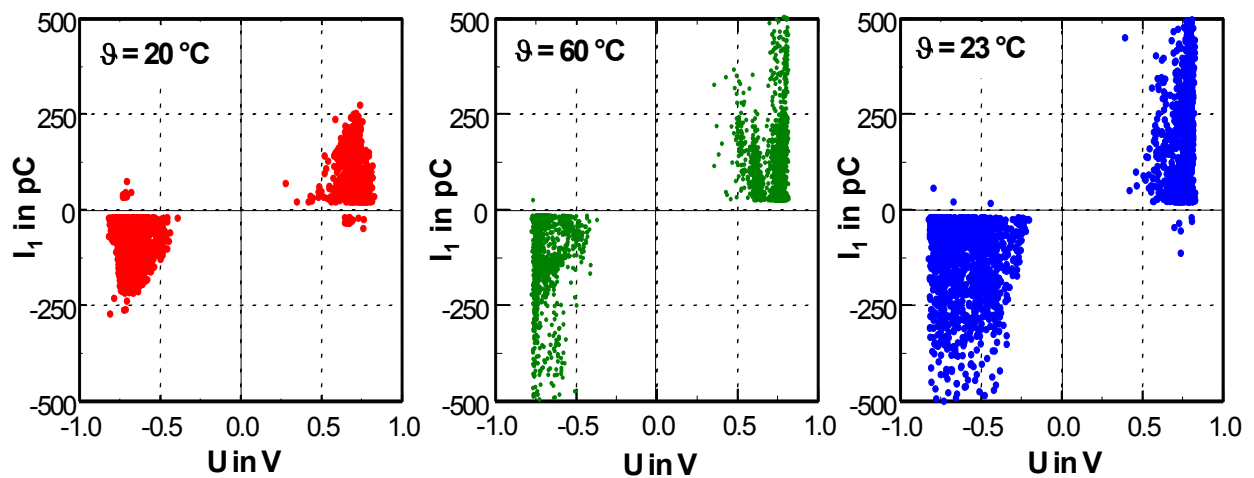

Fig. 6.8: PD pulse heights I_1 over actual voltages **U** at which the discharges occur for the three measurements

Another interesting finding is shown in Fig. 6.8 for the measurement done at **60 °C**. Partial discharges with different PD pulse heights occur at different voltage levels. In addition to the discharges with small PD pulse amplitudes that occur at lower voltage levels, a second type of discharges with higher amplitudes and higher voltage levels occurs. In most cases this behaviour is related to the existence of more than one type of PD-active defect. The presence of an additional PD-active defect only in the second measurement is due to an effect of the temperature i.e. due to thermal expansion. The use of Pulse Shape Analysis is a powerful tool to clarify this assumption.

It is well-known from earlier investigations that the shape of the oscillating signal is characteristic for the position of a defect within the winding and the different parameters derived from the oscillating signal can be used as a good criterion to identify and to separate signals from different sources. **Fig. 6.9** shows examples of typical discharge signals found in the three sets of measurements. Interestingly the deformation observed in the shape of the PD signals for the measurement at high temperature (**60 °C**). The pulse shape of a partial discharge signal is

modified on its way from the location of the defect and superposed to an additional oscillating signal. The different Pulse Shape Analysis parameters can be then helpful for separating these different PD signals.

One parameter that can be used to characterize the differences between these PD signals are the time differences $t_2 - t_1$ of the first two peaks of the PD signals. **Fig. 6.10** shows the frequency distribution of the time intervals $t_2 - t_1$ for the three measurements. Here, the measurement at higher temperature (**60 °C**) shows clearly that obviously two PD-active defects exist. For the measurements done at room temperature and at **23 °C** only PD pulses with time intervals $t_2 - t_1 > 3.8\ \mu s$ occur while for the measurement at **60 °C** also PD pulses with time intervals $t_2 - t_1 < 3.8\ \mu s$ occur. These differences can be used to separate discharge signals from different sources and to split up the measurement data sets into different sets to accomplish further analysis.
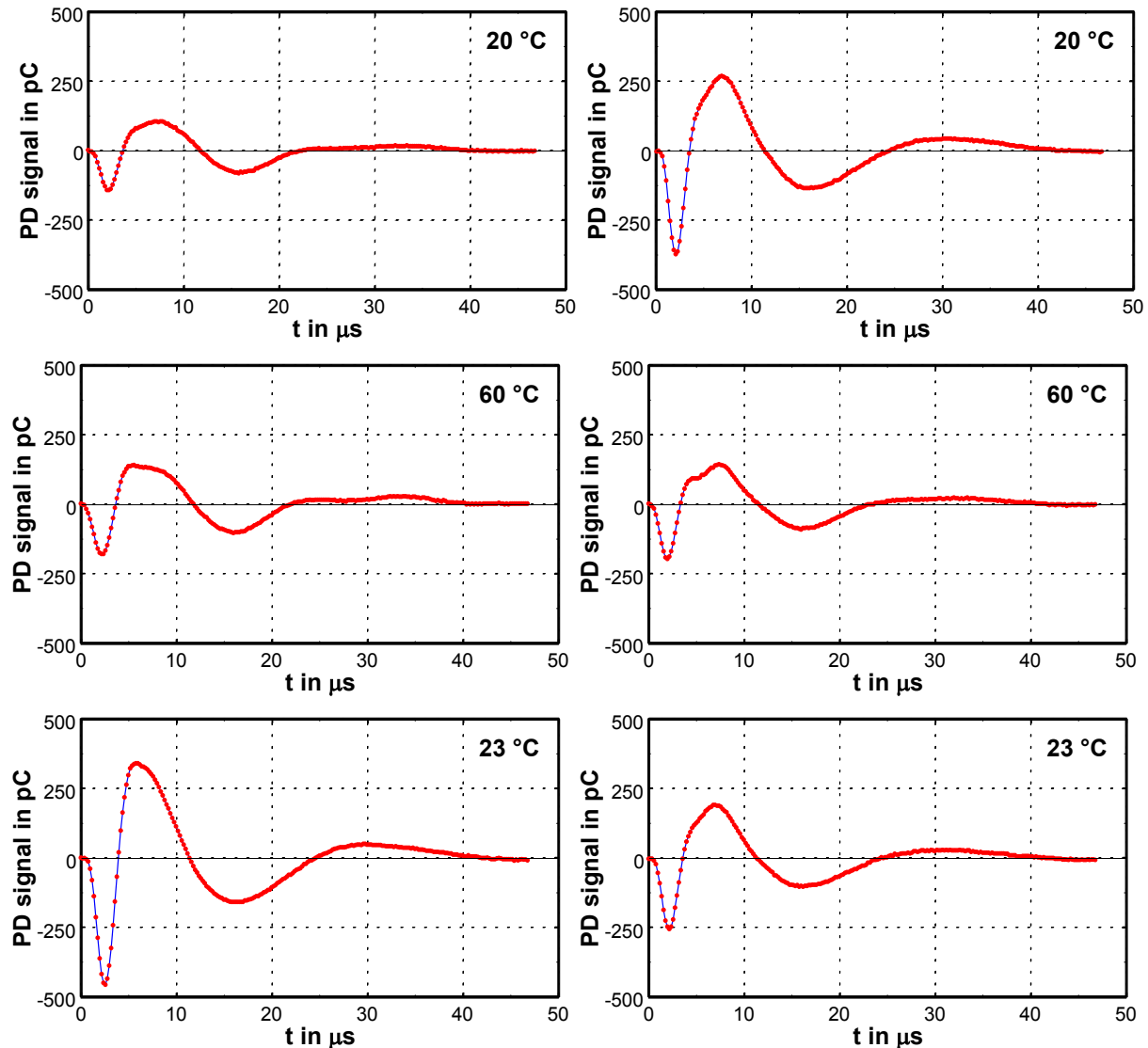
Fig. 6.9: Examples of typical discharge signals found in the three measurements

Fig. 6.11 displays the cumulative numbers of consecutive PD over the applied voltage U_{rms} for the two selected domains of the time intervals $t_2 - t_1$ in the three measurements. It shows clearly that the types of the PD signals with the time intervals $t_2 - t_1 < 3.8$ μs occurred only at higher temperature. In this case only the PD defect produced at higher temperature is active. The analysis of the sequences of partial discharges of the selected data set can reveal more detailed information that can be used to characterize the defect.

Fig. 6.12 shows the time intervals between discharges, the actual voltages at which discharges occur and the voltage differences between discharges over the applied voltage for the measurement done at **60 °C**. The graphs show the results obtained for all discharges and for the discharges selected according to the time intervals $t_2 - t_1$. The analysis of the time intervals Δt
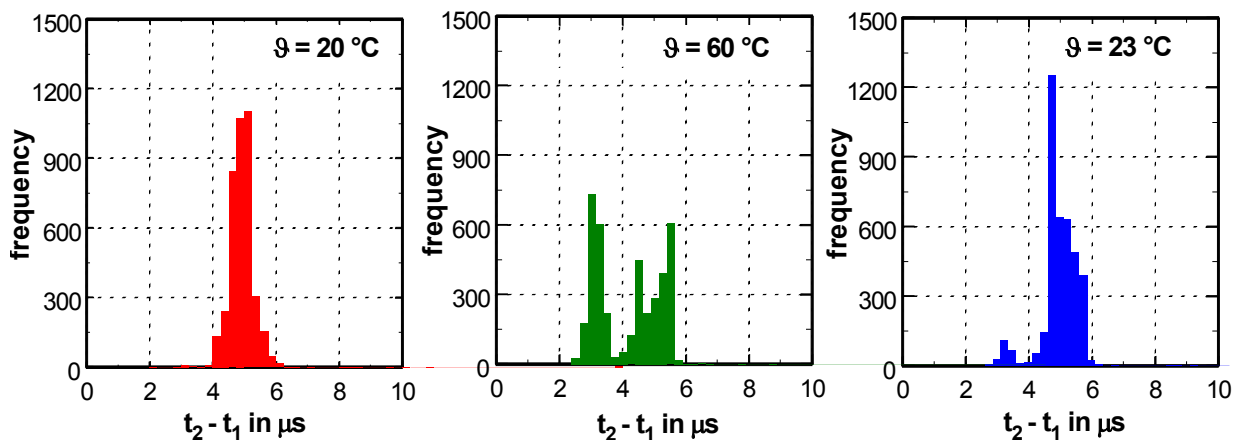
Fig. 6.10: Frequency distribution of the time intervals $t_2 - t_1$ between the first two peaks of the PD signals for the three measurements
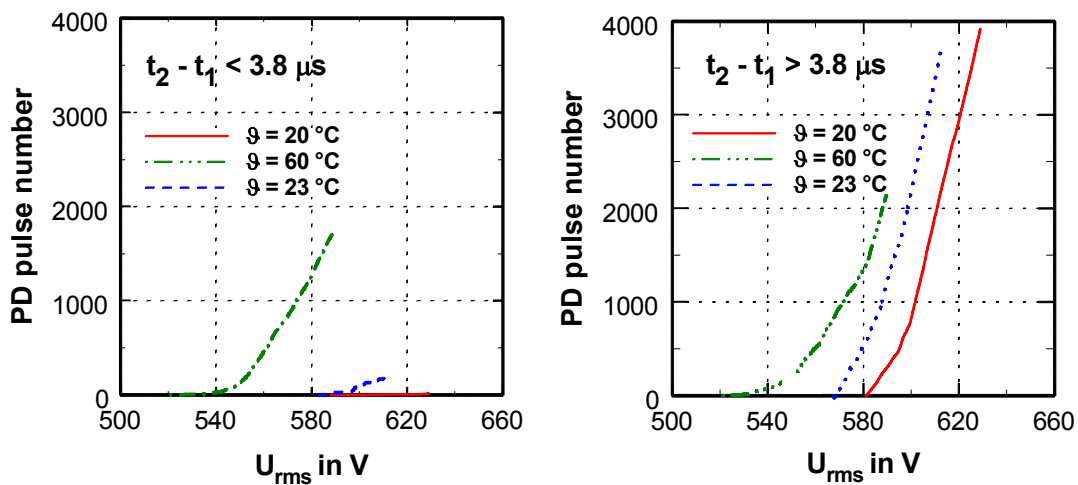
Fig. 6.11: PD pulse number over applied voltage U_{rms} for the selected domains of the time intervals $t_2 - t_1$ in the three measurements

between consecutive discharges shows that the selected group with the time intervals $t_2 - t_1 <$ 3.8 µs has substantially more defined values than the group with the time intervals $t_2 - t_1 >$ 3.8 µs.
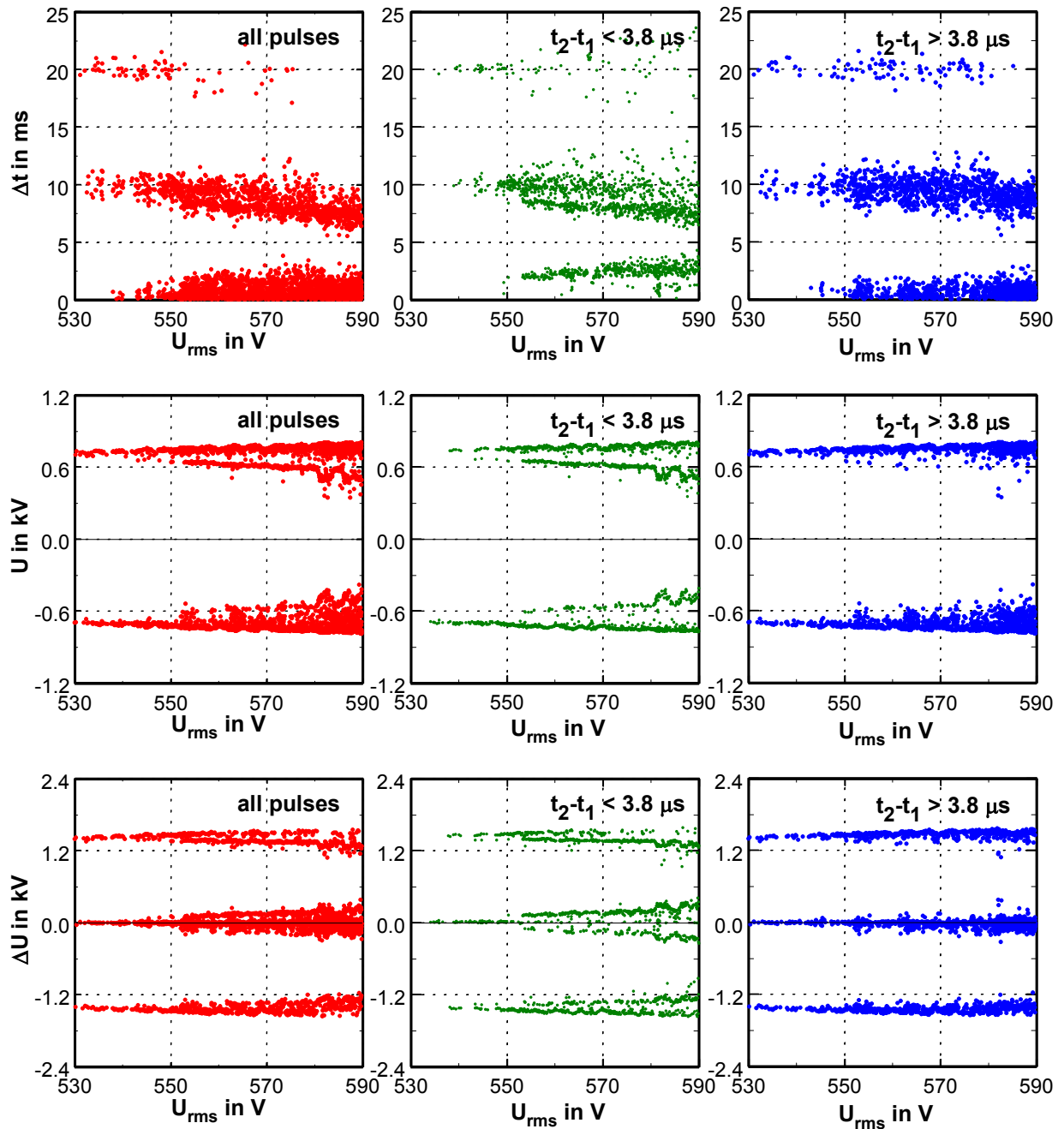
Fig. 6.12: Time intervals between consecutive discharges Δt, actual voltages **U** at which discharges occur and voltage differences ΔU between discharges over applied voltage U_{rms} for all discharges and for the discharges selected according to the parameter $t_2 - t_1$ (measurement at **60 °C**)

As shown in Fig. 6.2 the **'high temperature pulses'** with the time intervals $t_2 - t_1 < 3.8$ μs start first (for the lower measurement voltage) with time differences of about **10 ms**. For slightly higher voltages additional pulses occur with intervals of about **2** and **8 ms**. With the continuous increase of the voltage these additional discharges shift systematically to **3** and **7 ms** respectively and the number of discharges with time intervals of about **10 ms** is consequently reduced.

This behaviour points on the fact that at first only one discharge occurs at the peak of each half cycle. With increased test voltage an additional discharge occurs after about **8 ms** i.e. at about **2 ms** before the peak and shifts with the continuing increase of the test voltage to the small actual voltage values. The reason for this behaviour is an increase of the surface charges at the site of defect.

The difference in the PD behaviour for the two kinds of defects is also recognizable in the diagrams of the actual voltage **U** at which the discharges occur and the voltage differences Δ**U** between discharges.

To examine the effect of the surface and/or space charges on the PD behaviour especially at high temperatures, the frequency distributions of the time intervals of the first **500** pulses for the three measurements are represented in **Fig. 6.13**. The detailed analysis of the time intervals between discharges shows that in the case of two discharges per cycle the time intervals are not always **10 ms** but alternate between less and more than **10 ms**.
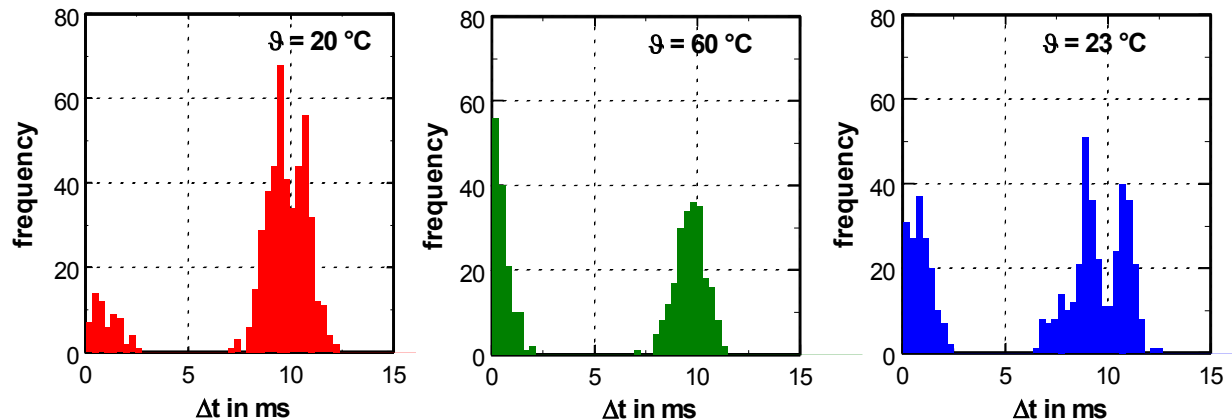
**Fig. 6.13:** Frequency distributions of the time intervals Δ**t** of consecutive discharges for the first **500** pulses in the three measurements

For both measurements done at room temperature, the histograms of the time intervals show two peaks, below and above **10 ms**. The reason for this behaviour is the **unipolar surface charge** at the solid boundary surfaces that leads – although the local ignition field strength

might be the same in both polarities – to the occurrence of an non-symmetry of the external voltage levels of the PD events. For the measurement done at **60 °C** the non-symmetry does not occur and the time intervals **Δt** scatters statistically around **10 ms** i.e. the polarity effect obviously does exist at higher temperatures. Obviously the charge carriers are more easily movable at higher temperature on the varnished surface, so that in the following half cycle no charge exists for the change of the field and thus the local field strength is symmetrical.

The behaviour of the interfaces boundary 'varnished surface/air' depends obviously strongly on the ambient temperature. Discharges with defined sites occur at higher temperature but not at lower temperature. The reason is probably the change of the surface conductivity of the varnish, which leads to different voltage distributions along the surface and thus to different local field strengths. With the increase of the temperature the dielectric strength of the air-filled gap between the windings is exceeded, which allows the occurrence of partial discharges.

6.2   PD measurements on stator bars of high voltage rotating machines

High voltage stator windings often produce partial discharges as a symptom of many conditions, including loose windings, overheated insulations and contaminated winding isolations. The partial discharges in the insulation system of rotating machines can occur as surface discharges, end winding discharges, slot discharges, internal discharges, discharges between bars of different phases, interfaces copper conductors and inter-turn discharges [Fra06, Vog03, Far03]. The most dangerous PD type are slot discharges in combination with mechanical and/or thermal ageing which cause an erosion of the insulation system and may result in a breakdown of the insulation system.

Only three of the above cited types of defects – slot discharges, end winding discharges and internal discharges – will be investigated here. The slot discharges are simulated by a surface defect produced by an artificial damage of the semi-conductive coating; the end winding discharges are studied with and without anti corona insulating tape; for internal discharges the influence of thermal ageing was analyzed [Ber03]. The influence of different temperature conditions on partial discharge activities of stator bars will also be discussed.

6.2.1   Surface defects (electrical slot discharges)

As described in chapter 2, a semi-conductive coating is placed on the surface of stator bars to prevent partial discharges in unavoidable gaps between insulation and stator iron. The slot discharges occur between the magnetic core and the bar of the stator winding when the bar's semi-conductive coating partially looses contact with the slot wall or if the semi-conductor does not have a sufficiently high conductivity. The deterioration of the semi-conductive coat-

ing involves the apparition of partial discharges between the bar and the core which attack the ground-wall insulation and may lead to damage of the machine.

To simulate these slot discharges, a surface defect was made at the middle of the semi-conductive coating area of a model of stator bar of a high voltage rotating machine. To produce this artificial defect, the external conductive shielding of the main insulation was removed in an area of **7x7 mm^2** as shown in **Fig. 6.14**.
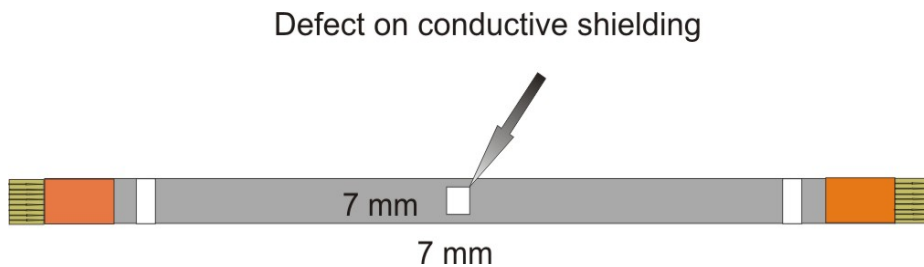
Fig. 6.14: Schematic representation of a model of stator bar with defective coating

The investigation of the influence of a defective insulation coating of a stator bar was performed with PD measurements on a model of stator bar without and with this artificial defect **(meas.1)**. In order to simulate the grounded slot a grounded copper wire **(meas.2)** or a grounded sharp needle **(meas.3)** were placed close to the defect.
The stator bar used in this experiment is described in detail in chapter 2. The applied voltage was ramped (with a ramp rate of about **2.5 kV$_{rms}$/min)** from zero until 4096 PD pulses were recorded. The sensitivity of the PD was adjusted to about **100 pC**.

The first step in the study of the influence of an artificial slot defect on the PD process is the analysis of the cumulative numbers of consecutive discharges. In **Fig. 6.15** the PD pulse numbers are represented in dependence on the applied voltage **U$_{rms}$** for the three measurements of the stator bar. The first measurement (**meas.1**) was done with the stator bar with the artificial defect. The second measurement (**meas.2**) was done with the stator bar with the artificial defect and a grounded copper wire placed remote to the surface at about **1.5 mm** from the failure**.** The third measurement (**meas.3**) corresponds to the stator bar with the artificial defect and a grounded sharp needle placed at **1 mm** from the defect.

Without the artificial defect no PD occurred below **6 kV$_{rms}$**. With the presence of the defects the obtained results show that the behaviour of partial discharges changes. The PD inception

voltages are lower. For the measurement of the stator bar with defective coating only, the PD inception voltage is about **4.5 kV$_{rms}$** (**meas. 1**) and decreases to about **4 kV$_{rms}$** with the presence of the grounded wire (**meas.2**). The PD inception voltage decreases to **3.5 kV$_{rms}$** if the defect is more important (needle closer to the removed external shielding, **meas.3**).
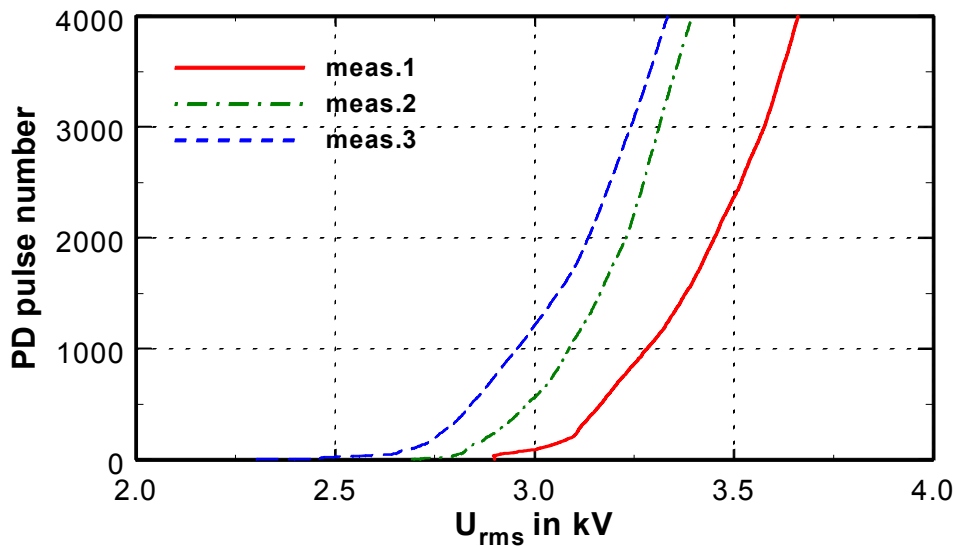
Fig. 6.15: PD pulse number over the applied voltage **U$_{rms}$** for a model of a stator bar
(**meas. 1**) artificial defect only
(**meas. 2**) artificial defect and grounded copper wire placed at **1.5 mm** distance to the defect
(**meas. 3**) artificial defect and grounded sharp needle placed at **1 mm** distance to the defect

6.2.1.1   Influence of the artificial defect on PD rate

Obviously in dependence on the magnitude of the applied voltage and on the different levels of artificial defects different partial discharge processes prevail.

Fig. 6.16 shows the actual voltages **U** at which the discharges occur and the voltage differences **ΔU** between consecutive discharges for different applied voltages for the three measurements. The influence of the defect type on the PD rate is shown in the graphs of **meas.2** and **meas.3**.
There is a specific PD activity in the negative half waves of the applied voltage (**meas.3**). Above **4 kV$_{rms}$** the maximum voltage changes do not depend on the applied voltage but are nearly constant (about + or **- 11 kV**)**,** a behaviour that tends to occur also in **meas.2**, but definitively not in **meas.1**. The reasons are surfaces charges on the non shielded insulation generated by discharges in the air gap.
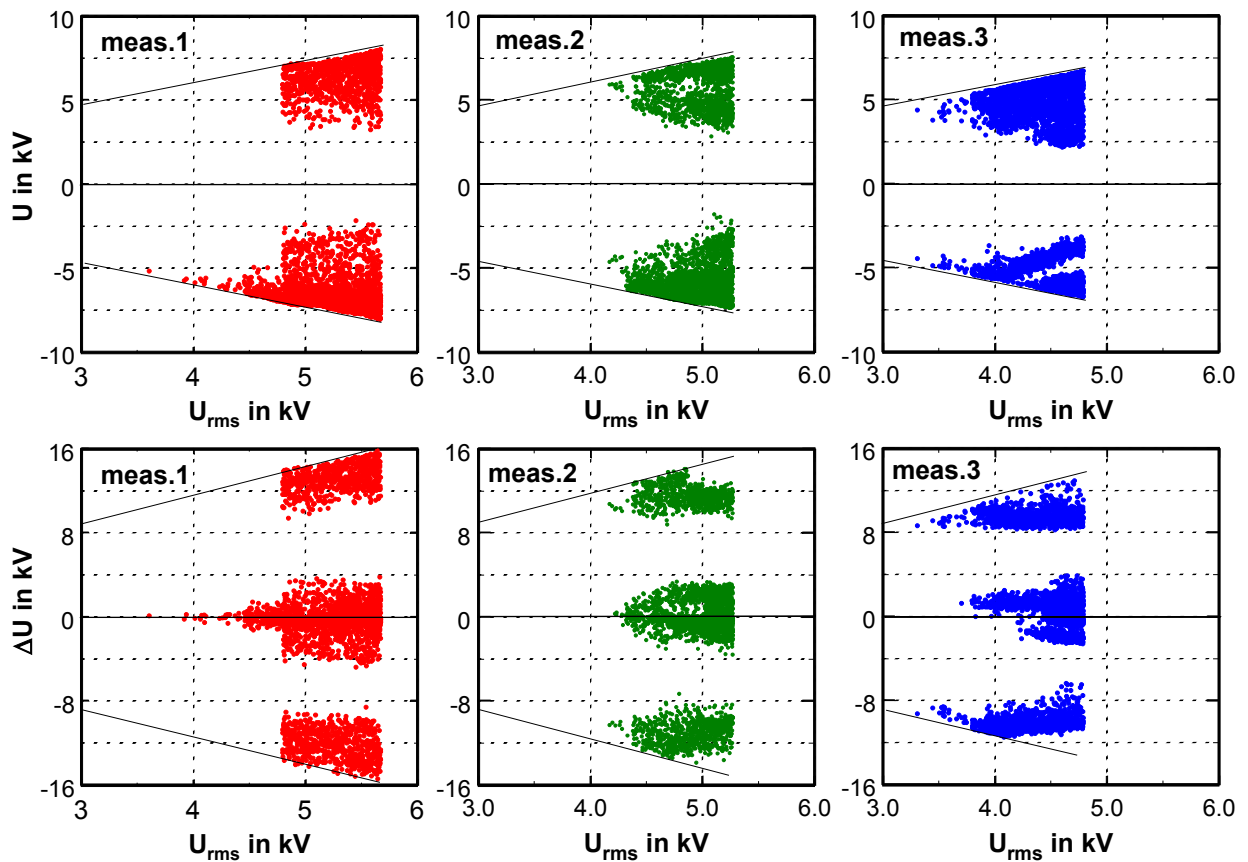
Fig. 6.16: Actual voltages **U** and voltage changes **ΔU** between consecutive discharges over
the applied voltages for a stator bar with different artificial defects

(**meas. 1**) artificial defect only

(**meas. 2**) artificial defect and grounded copper wire placed at **1.5 mm** distance to the defect

(**meas. 3**) artificial defect and grounded sharp needle placed at **1 mm** distance to the defect

6.2.1.2   Standard Analysis (phase resolved evaluations)

As well-known most standard evaluations just use the frequency distributions of the phase an-
gles of occurrence of the discharges, in part correlated with the corresponding pulse heights. In
general the frequency distributions of the phase angles at which the discharges occur are often
very broad and indicate many stochastic processes. The actual shapes of the distribution are
often used to characterise defect types [Gul91].

The corresponding phases of occurrences histograms for the three measurements are repre-
sented in **Fig. 6.17**. The plots show characteristic differences. In case of the stator with defec-
tive shielding (meas.1) the graph shows non-symmetric triangular distributions with a broad
statistic scatter. About **75%** of the discharges occurred in the negative half cycles of the ap-
plied AC voltage, nearly exclusively in the inclining parts of the half cycles. The ϕ-

distributions change in dependence on the presence of the additional defects. Meas.2 and meas.3 show more discharges in the positive half waves. The shape of the distributions with phase angles between **200-280°** became broader and for meas.3 a separate peak at about **220°** occurred. This peak corresponds to discharges at a voltage of about **-4 kV** shown in Fig. 6.16.
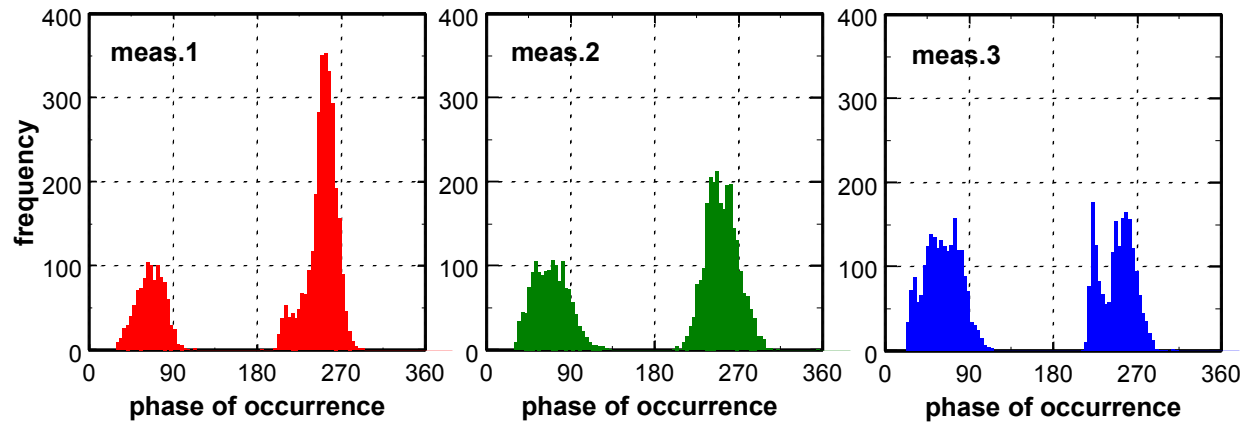
Fig. 6.17: Phase of occurrence histograms ϕ for a model of stator bar
> (**meas. 1**) artificial defect only
> (**meas. 2**) artificial defect and grounded copper wire placed at **1.5 mm** distance to the defect
> (**meas. 3**) artificial defect and grounded sharp needle placed at **1 mm** distance to the defect

6.2.1.3   Evaluations of sequential parameters

The analysis of the sequence of discharges in different high voltage apparatuses revealed that in many cases a systematic shift of the phase angles of PD occurrence with a periodicity of a few cycles of the applied voltage occurs (see chapter 5). This phenomenon is a consequence of the build-up or modification of local space charges by every partial discharge pulse. These space charges generate an additional local electric field that superimposes on the field generated by the externally applied voltage. Under these conditions the phase angle of the applied voltage cannot be taken as a representative parameter for the local electric field that determines the partial discharge process. Partial discharge analyses involving sequence related parameters such as ΔU, Δt or the ratio $\Delta U/\Delta t$ propose more reliable results [Pat02, Pat03].

6.2.1.3.1   Voltage changes ΔU related evaluations

As shown in Fig 6.16 and in contrast to the aforementioned parameter phase angle ϕ, the parameter voltage differences ΔU between consecutive discharges is much more sensitive to changes in the discharge process. In many cases this parameter allows the separation between correlated and non-correlated discharges [Ber02a], an important information for the decision, whether there is one or more defects in the test object.

Fig. 6.18 shows the frequency distributions of the voltage changes **ΔU** between consecutive discharges for the above three measurements of the stator bar. The **ΔU** histograms for the first two measurements of the stator bar with the artificial defects show a large number of non-correlated PD pulses with the distribution maximum around **0 kV**. There are much less PD pulses with **ΔU ≈ 0** in the third measurement. The two broad distributions concentrated around **+ or - 12 kV** shown in the graph (**meas.1**) shift to lower voltages in the two following measurements (**meas.2**, **meas.3**). Compared to Fig 6.17 there is much less scatter in the **ΔU** histograms than in **U** histograms.
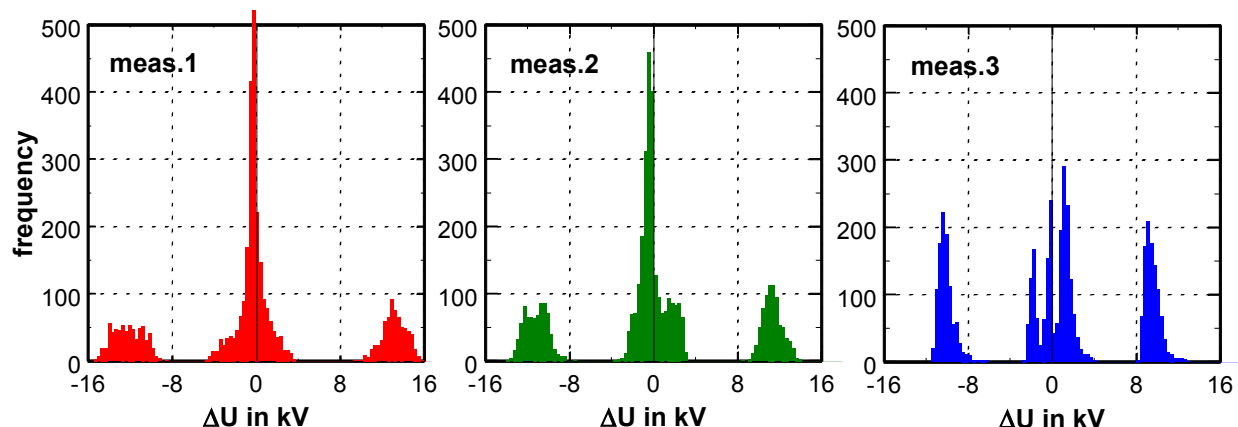
Fig. 6.18: Histograms of voltage changes **ΔU** between consecutive discharges for a model of stator bar

(**meas. 1**) artificial defect only
(**meas. 2**) artificial defect and grounded copper wire placed at **1.5 mm** distance to the defect
(**meas. 3**) artificial defect and grounded sharp needle placed at **1 mm** distance to the defect

6.2.1.3.2   Time intervals Δt related evaluations

Due to the phenomenon of correlated or non-correlated discharge sequences the evaluation of the time differences **Δt** between consecutive discharges may be a very helpful analysis too because with one discharge site in a solid dielectric, discharges occur only after distinct voltage changes and hence after distinct time differences. Discharge events from an independent second discharge site occur 'at random' with regard to the discharge site mentioned first [Pat03].

The corresponding histograms of the time intervals **Δt** of the three measurements are represented in **Fig. 6.19**. While for the measurement without additional defects some PD events can occur with **Δt > 20 ms,** for the measurements with the additional defects the PD events tend to occur with **Δt < 10 ms**. The frequency distributions of the histograms change with the types of defects and show an increase of the number of correlated pulses. The distribution of PD with time differences below **3 ms** indicates that there may exist more than one defect that is active.

Apparently two (or more) defects of the same type and hence with a similar behaviour seem to contribute in **meas.1**. Surface discharges may occur simultaneously from different spots around the removed shielding.
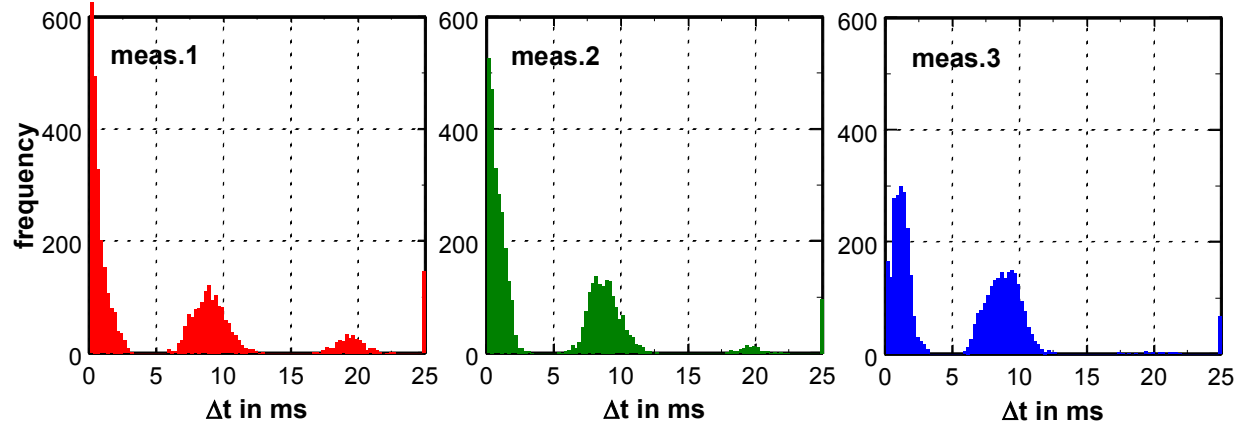
Fig. 6.19: Histograms of time intervals Δt of consecutive discharges for a model of stator bar
        (**meas. 1**) artificial defect only
        (**meas. 2**) artificial defect and grounded copper wire placed at **1.5 mm** distance to the defect
        (**meas. 3**) artificial defect and grounded sharp needle placed at **1 mm** distance to the defect

The frequency distributions of the time intervals $\Delta_2 t$ between next but one discharges indicate two or more non-correlated discharges per half cycle for **meas.1** (**Fig. 6.20**). For **meas.3** the main activity is related to one defect that definitively produces two discharges per half cycle. This defect is the needle close to the removed shielding.
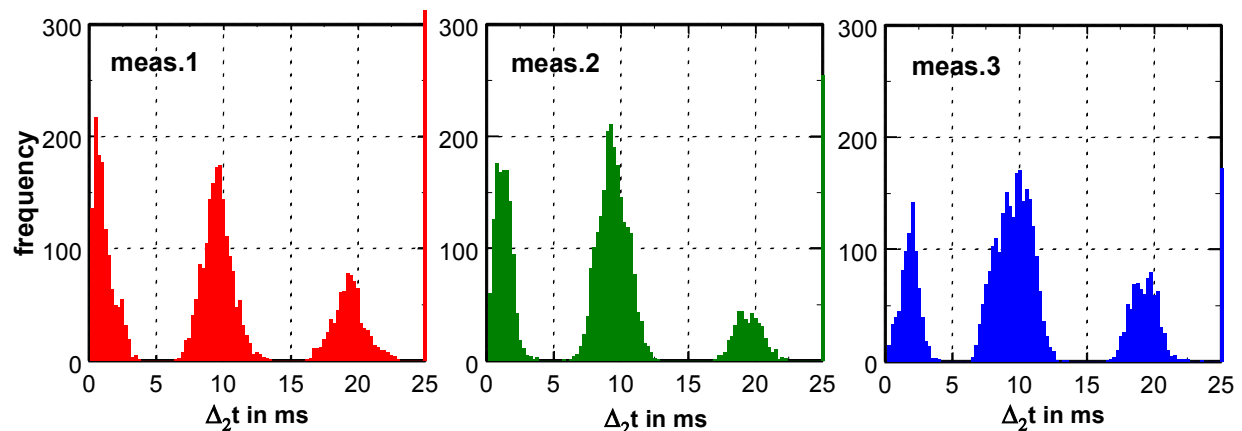

Fig. 6.20: Histograms of time intervals $\Delta_2 t$ between next but one consecutive discharges for a model of stator bar
        (**meas. 1**) artificial defect only
        (**meas. 2**) artificial defect and grounded copper wire placed at **1.5 mm** distance to the defect
        (**meas. 3**) artificial defect and grounded sharp needle placed at **1 mm** distance to the defect

6.2.1.3.3   Combined parameter ΔU/Δt evaluations

In many cases the use of more than one basic parameter is advisable for PD analyses. Especially the mean differential ratios **ΔU/Δt** – plotted over the voltage **U** at which the fist of two consecutive discharges occurred – revealed to be a meaningful parameter. For frequent discharge events with small time differences compared to the cycle length of the applied voltage the data points lie on an elliptic curve. Discharges with time differences of several milliseconds produce a characteristic pattern [Ber03].
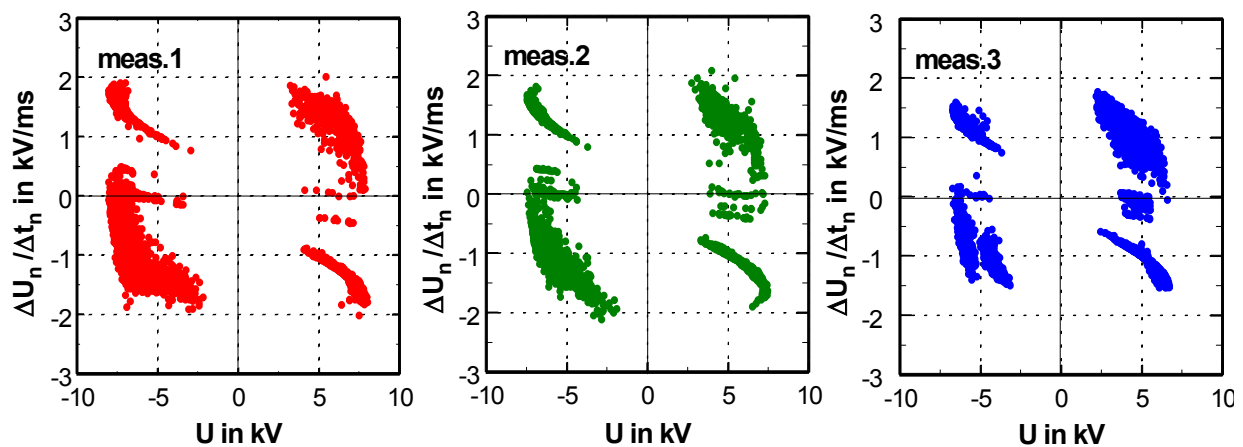
Fig. 6.21: Mean differential ratios **ΔU/Δt** between discharges over actual voltages **U** for a model of stator bar

(**meas. 1**) artificial defect only

(**meas. 2**) artificial defect and grounded copper wire placed at **1.5 mm** distance to the defect

(**meas. 3**) artificial defect and grounded sharp needle placed at **1 mm** distance to the defect

Fig. 6.21 shows the **ΔU/Δt** over **U** diagrams for the aforementioned three measurements of the stator bar. For all three cases, PD pluses occur in the inclining part of the external voltage curve with short time differences in between generated in **ΔU/Δt** diagrams an pattern with two characteristically shaped areas in the second and fourth quadrant. Those regions are typical for corona or surface discharges [Ber02]. The significant change after the introduction of the several artificial defects in the stator bar can be seen in the third quadrant. Two distinct areas of PD event appear instead of the broad area in **meas.1** and **meas.2**.

6.2.1.4   Influence of the defect on the PD pulse amplitude

The influence of the defect on the PD pulse amplitude is displayed in **Fig. 6.22**. The graphs illustrate the PD amplitude I_1 over the actual voltages **U** at which the discharges occur for the three measurements. The result shows that the discharges with defect produce a characteristic

pattern. The initial maximum values of the amplitudes of PD pulses (Fig. 6.21, meas.1) are up to **± 800 pC**. With the presence of additional defects the beginning of partial discharge seems to occur not only at lower effective voltages as described in Fig. 6.15 but also at lower actual voltages with small values of the PD amplitudes of about **± 500 pC**. This surface defect can be characterized with PD pulses that occur at lower voltage with small PD amplitudes.
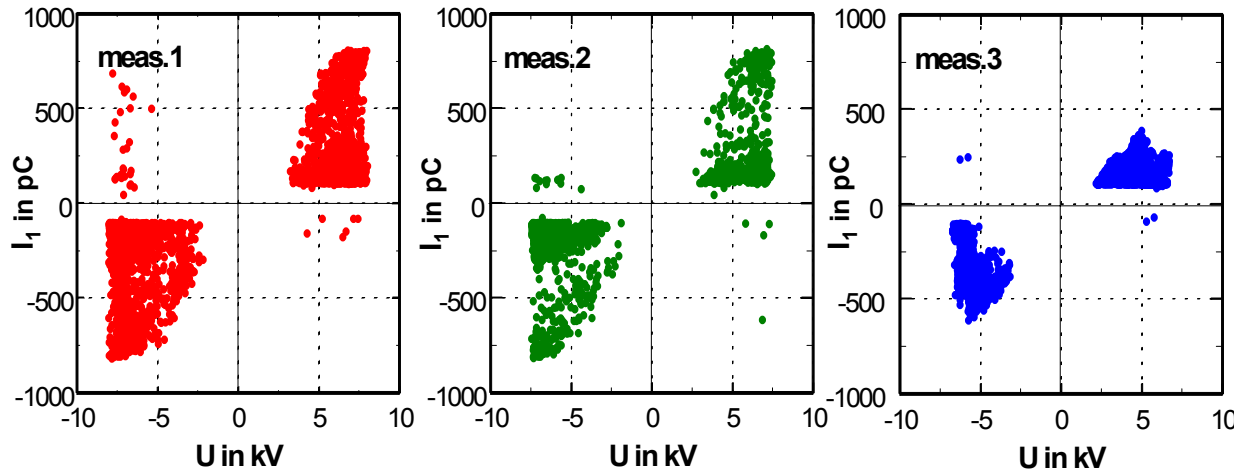
Fig. 6.22: PD pulse heights I_1 over actual voltages **U** for a model of stator bar

        (**meas. 1**) artificial defect only

        (**meas. 2**) artificial defect and grounded copper wire placed at **1.5 mm** distance to the defect

        (**meas. 3**) artificial defect and grounded sharp needle placed at **1 mm** distance to the defect

6.2.2   Influence of the anti-corona insulating tape (coil-end corona shield)

Partial discharges in the end-winding area may also occur at several locations with high electric field. Usually these discharges occur at interfaces between different components of the stator winding overhang part. If the end-corona protection becomes ineffective because of poorly designed interfaces, contamination, porosity, thermal or other effects, the reliable electrical field grading is no longer ensured. The partial discharges will then gradually erode the material and after a certain time lead to flashover across the end-corona protection.

As described before, the end of the stator bars are wound with semi-conductive anti-corona insulating tape, which operates as a coil-end corona shield.

To study the effect of the anti corona insulating tape, the area of the semi-conductive coating was covered with a conductive foil. PD measurements were performed on stator bar with and without corona protection shield.

Fig. 6.23 shows the plots of the mean differential ratios **ΔU/Δt** over the instantaneous voltage **U** at which the preceding discharge had occurred for a stator bar with and without the coil-end

corona shield. The beneficial influence of the corona shield is obvious. **Fig. 6.24** shows the histograms of time intervals Δ**t** between consecutive discharges for both measurements. Note that for the measurement without corona protection shield many PD events occur with time intervals smaller than **1 ms**.

The anti-corona shield is characterized with non-correlated time difference (Δ**t < 1ms**) and scatter distributions of the combined parameter Δ**U/**Δ**t**.
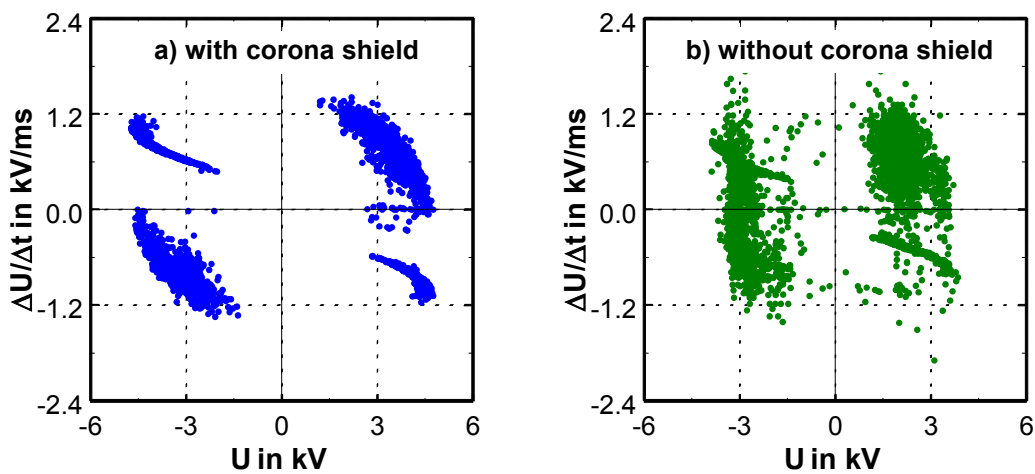
Fig. 6.23: Mean differential ratios Δ**U/**Δ**t** between discharges over the actual voltage **U** for the stator bars
**a)** with corona shield and **b)** without corona shield
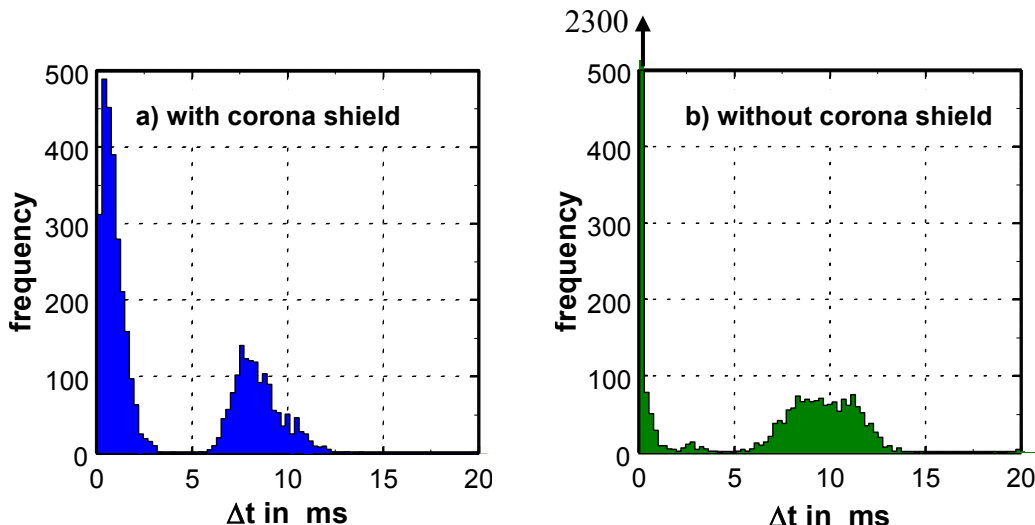
Fig. 6.24: Frequency distributions of time intervals Δ**t** of consecutive discharges for a model of a stator bar
a) with corona shield and **b)** without corona shield

6.2.3   Influence of the thermal stress

Stator windings are of complex design with numerous electrical, mechanical and thermal constraints. They must operate not only under high electrical fields but also under high temperature conditions. Large motors are exposed to frequent start/stop operations and pumped-storage generators or hydro-generators frequently have load changes. All of those operations cause rapid heating and cooling, i.e. thermal cycling effects on the stator insulation. In the long term, all these multiple stresses lead to the ageing of the insulation and cause a gradual insulation deterioration and ultimate failure. The influences of the operating temperature and the thermal ageing on the PD behaviour were investigated.

6.2.3.1   Temperature effect

The durability of insulating materials in electrical equipment depends on different factors, namely on chemical, mechanical and electrical parameters as well as on thermal stresses. The latter is particularly of great importance in the winding insulation system, since the stress caused by the operating temperature induces gradual insulation deterioration. The high temperature may also cause a chemical reaction (oxidation) when operated above a threshold temperature. An oxidation process can make the insulation brittle and/or cause delamination in form-wound ground-wall insulations. The delamination leads to the separation of the ground-wall tape layers due to the loss of bonding strength and/or impregnating compound.
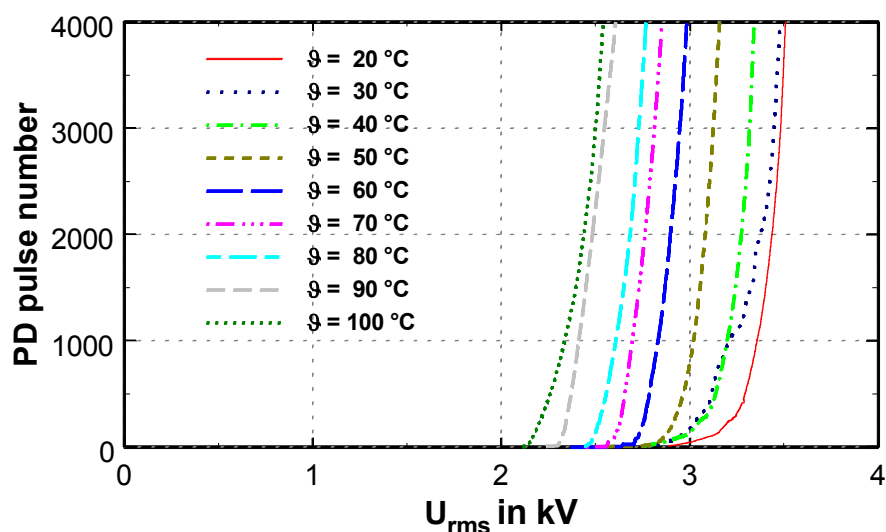

Fig. 6.25: Cumulative numbers of consecutive PD over the externally applied voltage
U_{rms} of the stator bar for temperatures between **20 °C** and **100 °C**

Although the electrical machines in operation are submitted to different thermal conditions, the off-line PD diagnostic is often done only at ambient temperature. In order to study the partial discharge behaviour of high voltage equipment under realistic thermal conditions, experimental investigations have been performed on a model stator bar of a high voltage machine at different temperatures.

The model stator bar was heated before the PD measurement procedure using a transformer regulated box-type-furnace. In order to avoid any noise the heater was switched off during the PD measurement. The temperature was measured before and after each measurement to take into account the variation of temperature. The test voltage was raised with a ramp rate of **460 V/min**, the sensitivity was adjusted to about **± 8 pC** and the temperature was varied between **20 °C** and **100 °C**.

Fig. 6.25 illustrates the cumulative numbers of consecutive PD over the applied voltage for measurements in the temperature range between **20 °C** and **100 °C**. The results show that in general for higher temperatures the curves are shifted to lower voltages.

The quantitative influence of the temperature on the partial discharge behaviour of stator bars is displayed in **Fig. 6.26**. The histograms of the effective voltages at which the discharges start to occur, shows a characteristic behaviour in the temperature range between **20 °C** and **100 °C**. For the low temperatures i.e. below **50 °C** the PD inception voltages of about **2.7 kV$_{rms}$** hardly changes. With the further increase of the temperature, the PD inception voltages decrease continually to about **2.1 kV$_{rms}$** at the temperature of **100 °C**.
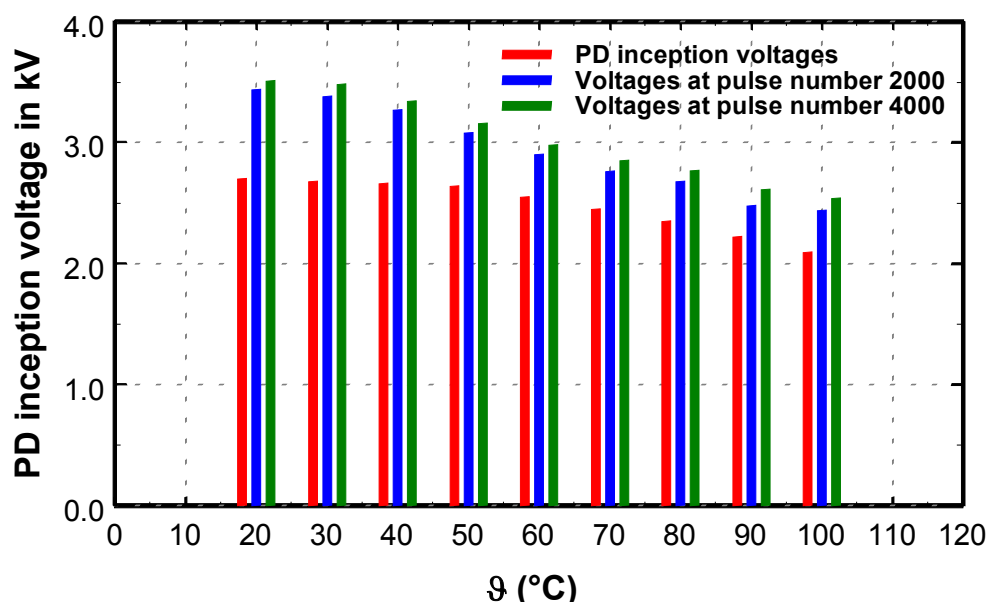

Fig. 6.26: Histograms of the PD inception voltages and the voltages at pulse numbers 2000 and 4000 for measurements of a stator bar at temperatures between **20 °C** and **100 °C**

The voltages at which 2000 and 4000 discharges had occurred in each run are lower for higher temperatures. For temperatures **20 °C** and **100 °C** 4000 discharges have occurred with **3.5 kV$_{rms}$** and **2.5 kV$_{rms}$** respectively. At the end of each run the pulse rates are similar at all temperatures.

The change of the PD inception voltage with temperature can be explained by an increase of the field strength in the gas filled void inside the dielectric. With the increase of the temperature the relative dielectric constant of the insulating material is increased, while that of air is constant. According to the Paschen law and ideal gas law, gas discharges may occur in the void and with the increase of the temperature the partial pressure gradient between the gas filled void and the surrounding insulating increased also so that a diffusion of the gas molecules (in the direction of smaller partial pressure) can take place. Thus a decrease of the relative gas density in the cavity will occur. Since the ignition dielectric strength of the cavity gas is dependent on relative density, a reduction of the inception voltage occurs with increasing temperature.
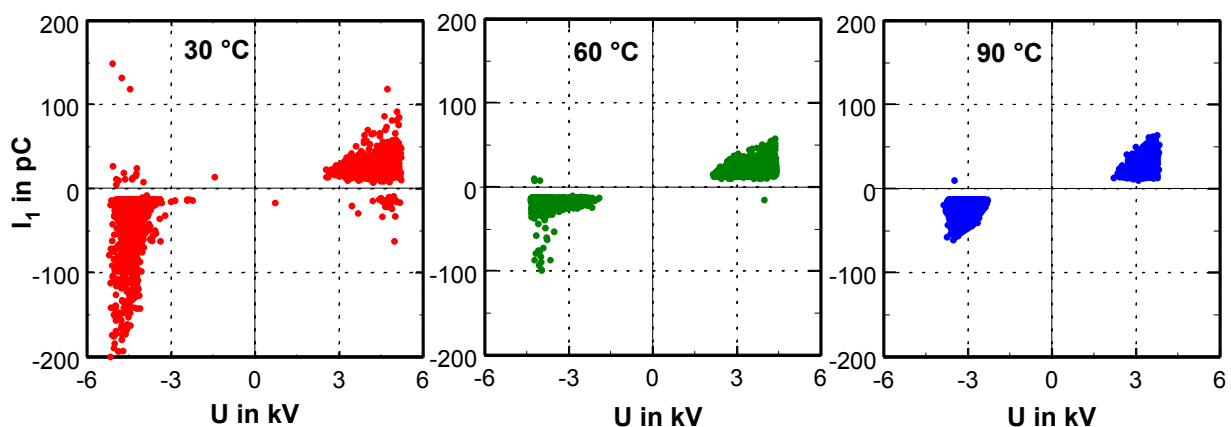
Fig. 6.27: PD pulse heights **I$_1$** over actual voltages **U** for three selected temperatures of the measurements of a model stator bar

The influence of the temperature on the PD pulse amplitude is displayed in **Fig. 6.27**. The graphs illustrate the PD amplitude **I$_1$** over the actual voltage **U** at which the discharges occur for three selected temperatures **30 °C**, **60 °C** and **90 °C**. This representation also shows that the discharges occur at lower voltages when the temperature increases. At first sight the magnitude of the PD pulses seems to decrease with increasing temperature. However, the PD in the three measurements occur at different voltage levels. If only the common voltage range of the three measurements is take in consideration, i.e. between **3.2** and **3.4 kV**, the PD amplitude increases from below **20 pC** at **30 °C** to more then **50 pC** at **90 °C**. The increase of the temperature leads to the occurrence of partial discharges at lower voltages and with higher amplitudes.

Fig. 6.28 shows the plots of the mean differential ratios $\Delta U/\Delta t$ over the actual voltages **U** at which the preceding discharge had occurred for the three selected temperatures **30 °C**, **60 °C** and **90 °C**. The PD behaviour changes with temperature.
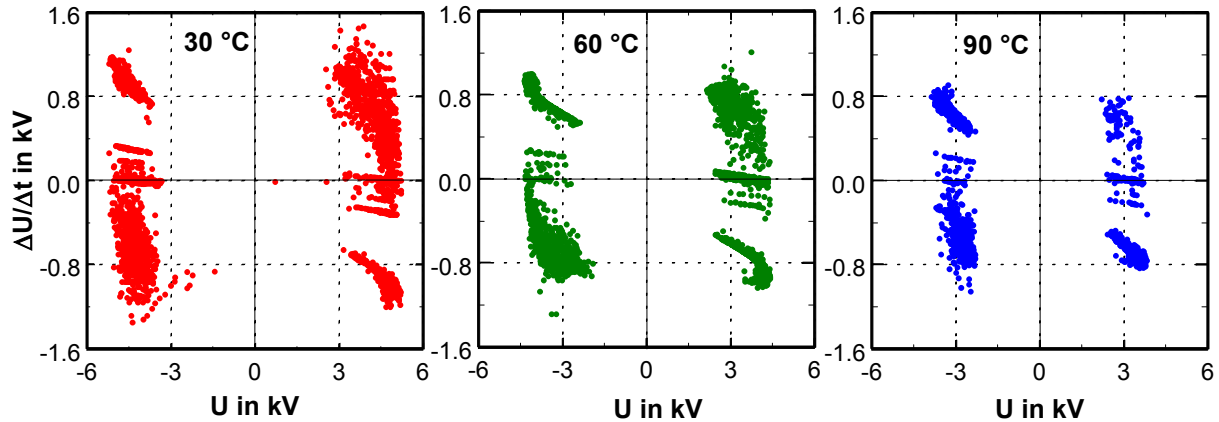
Fig. 6.28: Mean differential ratios $\Delta U/\Delta t$ between discharges over actual voltages **U** for three selected temperatures of the measurements of a model stator bar

The behaviour of the PD at different temperatures is also shown in the Δt and $\Delta_2 t$ histograms for the three measurements. The corresponding histograms of the time intervals of the three measurements are represented in **Fig. 6.29**.

For the measurement at low temperature the PD events with time intervals $\Delta t < 5$ **ms** tend to occur with an exponential distribution, while for the measurements at high temperature the
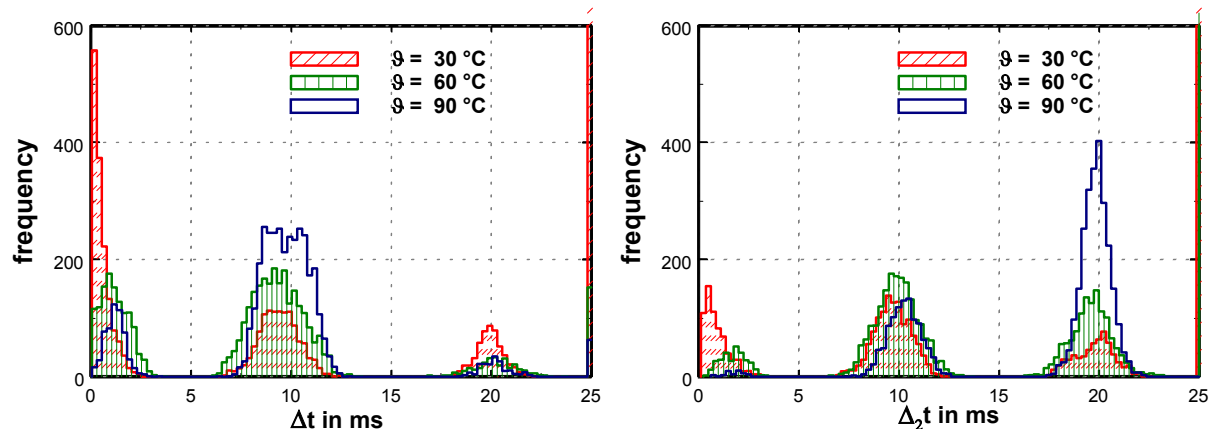
Fig. 6.29: Histograms of time intervals Δt of consecutive discharges and time intervals $\Delta_2 t$ between next but one discharges of the model stator bar for three selected temperatures

PD events tend to occur only with defined time intervals around $\Delta t \approx 2$ **ms**. A tendency for a polarity effect around $\Delta t \approx 10$ **ms** for higher temperature can be also seen.

6.2.3.2   Thermal ageing effect

Thermal ageing causes mainly delamination of the insulation. Chemical changes such as molecular decomposition and oxidation may occur during the thermal ageing and lead to a decrease of the adhesive strength of epoxy resin. As a result, delamination at the interface between mica and epoxy resin appears. The thermo-mechanical force accompanied with thermal ageing may result in the formation of delamination at the conductor. Thermal ageing may also cause brittleness of the epoxy resin isolation, and as a result, cracks will appear under mechanical stress.

To investigate the influence of thermal ageing on the partial discharge activity of stator bars, PD measurements were performed at ambient temperature on the non-aged and on the thermally aged specimen. The stator bar was stressed up to **500** hours at a temperature of **120 °C**. The test voltage was raised with a ramp rate of **525 V/min** and the sensitivity was adjusted to about ± **8 pC**. **Fig. 6.30** and **Fig. 6.31** show the pulse heights I_1 and the mean differential ratios $\Delta U/\Delta t$ respectively over the actual voltages **U** for the model stator bar before ageing and after **200 h** and **500 h** of thermal ageing.

The result shows that the PD behaviour of the model stator bar after a thermal ageing is similar to that one obtained in the case of the stator winding of small motors. The thermal ageing defect leads to the occurrence of partial discharges at lower voltages and with higher amplitudes
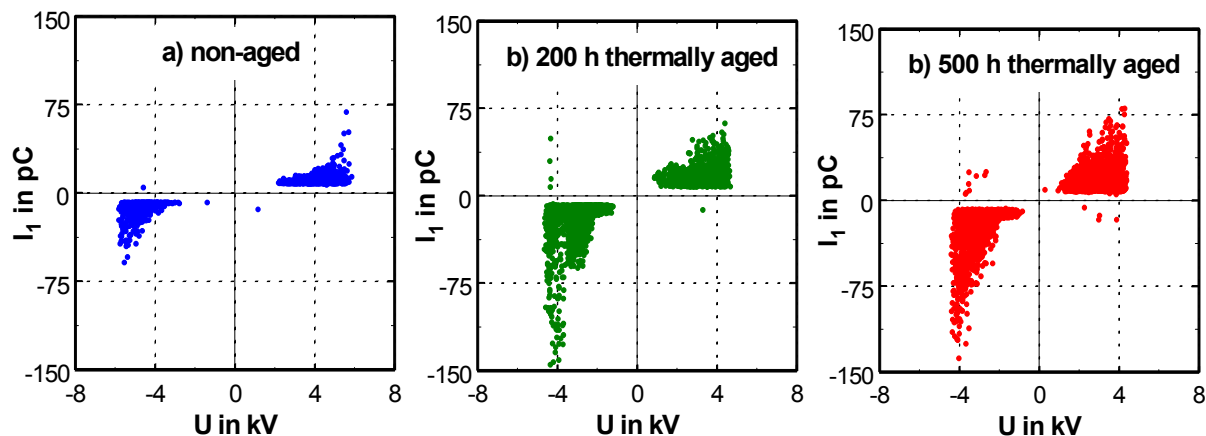
Fig. 6.30: Pulse heights I_1 over actual voltages **U** for a model stator bar aged at **120 °C**
a) non-aged, **b) 200 h** thermally aged and **c) 500 h** thermally aged

The comparison between the measurements before and after ageing shows that the amplitude of the PD pulses increases from below **± 60 pC** to more than **± 150 pC** and the actual voltages at which the discharges occur decrease from **6 kV** to **4.2 kV**. A characteristic change can also be seen in the **ΔU/Δt** diagrams.
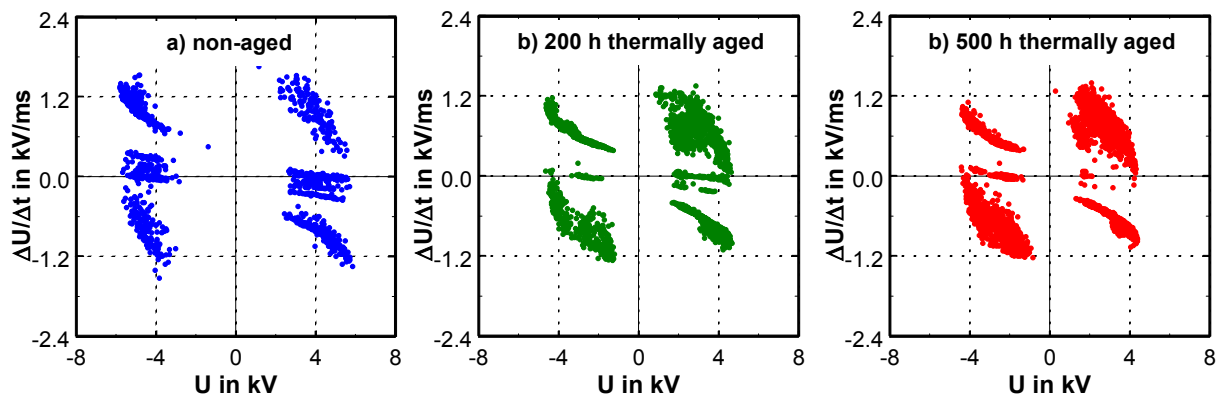
Fig. 6.31: Mean differential ratios **ΔU/Δt** between discharges over the actual voltages **U** for stator bar aged at **120 °C**
a) non-aged, **b) 200 h** thermally aged and **c) 500 h** thermally aged

6.3   Summary

The Pulse Sequence Analysis combined with the Pulse Shape Analysis are used here as tools of diagnosis and analysis of insulation systems of electric machines. Partial discharge measurements and analyses of samples of stator windings of small AC motors were evaluated. The results can be concluded as:

- The first discharges just after PD inception are characteristically different from discharges some 10 or 100 cycles later.
- This change in the PD behaviour is caused by the build-up of space charges or surface charges at the dielectric interfaces between the windings and/or between windings and core.
- The PD behaviour may change or not, with or without discharge free time in-between.
- The typical changes in PD behaviour are clearly found in the pulse heights and in the time intervals between consecutive discharges.
- The benefit of measurements with a ramped voltage instead of a constant test voltage and the influence of the ramp rate were shown.

- PD measurements with differently ramped AC voltages showed that the PD inception voltage is not depending on the rise velocity of the applied voltage. Changes in PD behaviour seem to occur after a certain number of discharges.
- The build-up of space charges is polarity dependent. A reversal of the connections to the AC voltage supply reverses the polarity of the PD phenomena.
- The existence of multiple discharge sites (especially at higher measuring voltages) can be identified and characterized with the Pulse Sequence Analysis. The separation of these non-correlated discharges can be realized with the help of the Pulse Shape Analysis.
- The effect of the temperature and the influence of the thermal ageing on the stator windings were investigated. The result shows that the PD inception voltage depends on the temperature and that the thermal ageing leads to the increase of the pulse heights. At higher measuring temperature the existence of more than one type of PD-active defects is found. The different Pulse Shape Analysis parameters allow the separation of these different PD signals. The behaviour of the boundary 'varnished surface/air' obviously depends strongly on the ambient temperature. The reason is probably a change of the surface conductivity of the varnish, which leads to different voltage distributions on the surface and thus to different local field strengths.

Investigations on a model of stator bars of a high voltage rotating machine were also carried out. Three types of defects – slot discharges, end winding discharges and internal discharges – as well as the influence of different temperatures on the partial discharge activity were studied.

- The PD inception voltage appears earlier with the presence of the surface defects and it appears earlier if the defects are more serious.
- The PD rate is influenced by the presence of surface defects.
- A characteristic change in the **ΔU**-diagram and **Δt**-diagram occurs with the presence of a surface defect.
- Surface defects produce a characteristic pattern in the **I-U**-correlation.
- The advantage of the anti corona insulating tape protection was shown.
- PD inception voltage decreases with the increase of the temperature.
- The PD pulse heights increase with the increase of the temperature.
- The thermal ageing effect leads to the occurrence of partial discharges at lower voltages and with higher amplitudes.

7   General Conclusions

Partial discharge phenomena in power apparatus play an important role in ageing and degrada-
tion processes that can significantly reduce the technical life of electric equipment and thus can
influence the reliability of the power supply. The analysis of partial discharges is a common
diagnostic tool used to monitor and to examine the long term degradation of electrical equip-
ment. However in most cases only the frequency distribution of the **phase angles** at which the
discharges occur and the distribution of the **pulse heights** are used as parameters. These analy-
ses are an integral description of the specific data set but do not tell too much about the local
physical processes and in most cases are not suitable to interpret the local electric conditions at
the defects. The **Pulse Sequence Analysis** and the **Pulse Shape Analysis** can be used for a
better understanding of the local degradation processes by separating data from different
defects and analyzing local changes by utilizing **sequence correlated data**.

The work reported in this thesis concerns the use of the Pulse Sequence Analysis and the Pulse
Shape Analysis as diagnostic tools to investigate the degradation phenomena in the insulating
systems of electric equipment. The results can be concluded with the following points:

An adequate **software** has been developed to analyze the enormous amounts of complex data
sets generated by PD measurements. With the help of this software tool different possibilities
for the analysis and treatment of the partial discharge data sets using the Pulse Sequence
Analysis were performed. The comparison of different parameters used for the interpretation
of partial discharge measurements shows that **sequence correlated parameters** contain much
more relevant information than the standard parameters extracted from standard data sets
that ignore the **influence of a discharge event on the ignition of the next discharge** (as done
e.g. with accumulated sets of phase angles of occurrence, the so-called phase resolved evalua-
tion).

The **pulse shape of the PD signal** was used as relevant parameter to **characterize different
types** of the PD-active defects. Different parameters extracted from the oscillating PD signals
were used to identify and to separate the discharge signals from different sources. With this
procedure different sources or even different stages of the degradation process were identified
and characterized to monitor the different stages of ageing. These parameters were also used to
discriminate noise signals from real partial discharge signals.

PD measurements on laboratory specimens as well as on different electric apparatus revealed
in how far the partial discharge phenomena are influenced by **charges** accumulated locally as
the consequence of prior discharges. The detailed evaluation of a small subset of the data – the
sequence correlated information – revealed more information about the defect than the analysis

of a larger data set accumulated in dependence of the actual phase angles of the applied voltage without taking into account any correlations between consecutive pulses.

The build-up of space charges as a consequence of partial discharges has been discussed on the basis of an **improved PD equivalent circuit**. The interpretation of results obtained in PD measurements on a HV transformer and in electrical treeing in polyethylene was given on the basis of this equivalent circuit.

The **Pulse Sequence Analysis** combined with the **Pulse Shape Analysis** have been applied for the investigation and the analysis of partial discharges on the insulation system of electric machines. Different types of defects on the stator windings of small motors and stator bars of high voltage machines were characterized. Thermal ageing and the influence of the temperature on the partial discharge behaviour have also been investigated.

References

[Ari07]   Arief, Y.Z.; Patsch, R.; Benzerouk, D.; Menzel, J.: Partial Discharge Characteristics in Polyethylene using Pulse Shape and Pulse Sequence Analysis. **IPEC'07**, Singapore, (2007), 399-404

[Asc00]   Aschenbrenner, D.; Lapp, A.; Kranz, H. G.; Bomeburg, D.; Peier, D.: Application of an automated PD Faillure identification system for EMC-assessment strategies of multiples PD defects at HV-insulators. **DMMA'00**, Edinburgh, UK, (2000)

[Bar68]   Bartnikas, R.: Note on discharge in helium under ac conditions. **J. Appl. Phys. D**, **1**, (1968), 659-661

[Bar02]   Bartnikas, R.: Partial Discharges, Their Mechanism, Detection and Measurement. IEEE Trans. on **DEI**, **2**, (2002), 763-808

[Ben04]   Benzerouk, D.; Patsch, R: Zum Auftreten von Oberflächenladungen bei Teilentladungen in Statorwicklungen. **ETG'04**, Köln, Germany, (2004), 405-9

[Ben04a]   Benzerouk, D.; Patsch, R.; Menzel, J.: Partial Discharge Analysis - a Comparison of Different Parameters used, **APTADM'04**, Wroclaw, Poland, (2004), 46-50

[Ben07]   Benzerouk, D.; Menzel, J.; Patsch, R: The role of Accumulated Charges in Partial Discharge Processes. **ICSD'07** Winchester, UK, (2007), 552-5

[Ber01]   Berton, F.; Patsch, R.: The Role of Space Charge in PD-Processes. **APTADM'01**, Worclaw, Poland, (2001), 139-42

[Ber01a]   Berton, F.; Patsch, R.: Teilentladungsdiagnose – welche Vorteile bringt die Puls-Sequenz-Analyse. **IWK'01**, Ilmenau, Germany, (2001), 241-2

[Ber02]   Berton, F.; Patsch, R.: The Use of Time Intervals between Consecutive Discharges to Characterize PD-Sources. **ISEI'02**, Boston, USA, (2002), 527-30

[Ber02a]   Berton, F.: Development and Application of a DSP-Controlled Partial Discharge Measuring System for PD Diagnostics of Insulation Systems (in German). PhD Thesis, University of Siegen, Germany, (2002), **ISBN** 3-8322-1104-7

[Ber03]   Berton, F.; Patsch, R.; Benzerouk, D.: Digital-Signal-Prozessor basierte TE-Diagnose an Modellen von Statorstäben eines Hochspannungsmotors mit der Anwendung der PSA, **IWK'03**, Ilmenau, Germany, (2003), 457-8

[Bog90]   Boggs, S. A.: Partial Discharge: Overview and Signal Generation. IEEE **El. In. Mag.**, **6**, (1990), 33-9

[Bou04]   Boulter, E. A.; Stone, G. C.: Historical Development of Rotor and Stator Winding Insulation Materials and Systems. Electrical Insulation for Rotating Machines_Design, Evaluation, Ageing Testing and Repair, published by IEEE and John Wiely, (2004)

[Bru91]   Brunt, van R.J.: Stochastic Properties of Partial-Discharge Phenomena. IEEE **EI-26**, (1991), 902-48

[Cav05]   Cavallini, A.; Montanari, G.C.; Puletti, F.: A Fuzzy Logic Algorithm to Detect Electrical Trees in Polymeric Insulation Systems. IEEE Trans. **DEI-12**, (2005), 1134-44

[Cha88]   Chalmers, B. J.: Electric Motor Handbook. Butterworths, London, (1988), **ISBN** 0-408-00707-9

[Cha96]   Champion, J.V.; Dodd, D.J.: Systematic and reproducible partial discharge patterns during electrical tree growth in an epoxy resin. **J. Appl. Phys.**, **29**, (1996), 862–8

[Cha02]   Chang, C.; Su, Q.: Memory propagation of negative point-to-plane corona under AC voltage. IEE **Proc. Sci. Meas. Technol.**, **149**, (2002), 117-26

[Cro59]   Croitoru, Z.: Space Charges in Dielectrics. **Prog. Diel. 6, (**1959), 105–46

[Cyg90]   Cygan, P.; Laghari, J. R.: A Review of Electrical and Thermal Multistress Aging Models. **SEI'90**, Toronto, Canada, (1990), 15-20

[Dan93]   Danikas, M. G.: The definitions Used for Partial Discharge Phenomena. IEEE Trans. on **EI-28**, (1993), 1075-81

[Dan00]   Danfoss compressor GmbH, Flensburg, (2000)

[Dev84]   Devins, J. C.: The physics of partial discharge in solid dielectrics. IEEE Trans. on **EI-19**, (1984), 475-94

[Dis92]   Dissado, L.A.; Fothergill, G.C.: Electrical degradation and breakdown in polymers. Peter Peregrinus Ltd., London, (1992), UK, **ISBN** 0 86341 196 7

[Dis97]   Dissado, L.A.; Dodd, S.J.; Champion, J.V.; Williams, P.I.; Alison, J.M.: Propagation of electrical tree structures in solid polymeric insulation. IEEE Trans. on **DEI-4**, (1997), 259–79

[ElM82]   El Moslemany, M. A.: Some observations on tree patterns in PMMA under alternating voltages. IEEE Trans. on **EI-17,** (1982), 76–80

[Eng98]   Engel K.: Bewertung von Teilentladungen in spaltförmigen Isolierstoffdefekten. PhD Thesis, University of Dortmund, Germany, (1998)

[Far06]   Farahani, M. S.: Zustandsbertung eines Isoliersystems für rotierende Hospannungsmaschinen mit elektischen und dielektrischen Messverfahren. PhD Thesis, University of Hannover, Germany, (2006)

[Far03]   Farahani, M. S.; Borsi, H.; Gockenbach, E.; Kaufhold, M.: Partial discharge patterrn recognition as as diagnostic tool for stator bar defects. **ISH'03**, Netherlands, (2003), 318

[Fro47]   Froehlich, H.: On the theory of dielectric breakdown in solids. **Proc. R. Soc. A**, **188, (**1947), 521–32

[Fro95]   Fromm, U.: Partial Discharge and Breakdown Testing at High DC Voltage. PhD-Thesis, TU Delft, Netherlands, (1995)

[Fru90]   Fruth, B.; Fuhr, J.: Partial discharge pattern recognition – a tool for diagnosis and monitoring of aging. **CIGRE'90**, Paris, France, paper 15/33-12, (1990)

[Fuh05]   Fuhr, J.: Procedure for Identification and localization of Dangerous PD Sources in Power Transformers. IEEE Trans. on **DEI-12**, (2005), 1005-14

[Gae05]   Gäfvert, U.: Influence of Geometric Structure and Material Properties on Dielectric Frequency Response of Composite Oil Cellulose Insulation. **ISEIM'05,** Kitakyushu, Japan (2005), 73-6

[Gem32]   Gemant, A.; Philippoff, W.: Die Funkenstrecke mit Vorkondensator. **Z. tech. Phys.**, **13**, (1932)

[Gul91]   Gulski, E.: Computer-aided recognition of partial discharges using statistical tools. PhD. Thesis, Delf University Press, Netherlands, (1991)

[Gul95]   Gulski, E.: Digital analysis of partial discharges. IEEE Trans. on **DEI-2**, (1995), 828-37

[Gul95a] Gulski, E.: Diagnosis of HV Components by Digital PD Analyzer. IEEE Trans. on **DEI-2**, (1995), 630-40

[Hae86]   Haefely Test Systems: Partial Discharge Detector Type 561. Bedienungsanleitung D 8176.3, (1986)

[Hij06]   Hijazi, S.: Entwicklung einer Software zur Puls-Sequenz-Analyse (PSA). Studienarbeit, FB12-WED, Universität Siegen, Germany, (2006)

[Hip37]   Hippel, von A.: Electric breakdown of solid and liquid insulators. **J. Appl. Phys. 8,** **(**1937), 815–32

[Hoo94]   Hoof, M.; Patsch, R.: Analyzing Partial Discharge Pulse Sequences - A New Approach to Investigate Degradation Phenomena. **ISEI'94**, Pittsburgh, USA, (1994), 314-7

[Hoo95]   Hoof, M.; Patsch, R.: Pulse-Sequence-Analysis: A New Method to Investigate the Physics of PD-Induced Ageing. IEE Proc. **Sci. Meas. Technol.**, **142**, (1995), 590-601

[Hoo95a] Hoof, M.; Patsch, R.: TE-Impulsfolgen-Analyse, eine neue Methode zur Untersuchung dielektrischer Schädigungsmechanismen. **ETG'95**, Esslingen, Germany, (1995), 117-22

[Hoo97]   Hoof, M.; Patsch, R.: A physical Model, Describing the Nature of Partial Discharge Pulse sequences. **ICPADM'97**, Seoul, South Korea, (1997), 283-6

[Hoo97a] Hoof, M.: Impulsfolgen-Analyse: Ein neues Verfahren der Teilentladungsdiagnostik. PhD Thesis, University of Siegen, Germany, (1997)

[IEC00]   IEC60270. High-voltage test techniques-Partial discharge measurements. IEC, Geneva, Switzerland, (2000)

[Jam97]   James, R. E. et al.: Effect of Moisture and Temperature of PDs in Oil-Impregnated Insulation. **AUPEC'97**, Sydney, Australia, (1997), 607-14

[Jon95]   Jones, W. K. et al.: McM C/Mixed Technologies and Thick Film Sensors. Kluwer Academic Publishers, (1995), **ISBN-10** 0792334604

[Kan00] Kaneiwa, H.; Suzuoki, Y.; Mizutani, T.: Partial discharge characteristics and tree inception in artificial simulated tree channels. IEEE Trans. on **DEI-7**, (2000), 843–8

[Kle78] Klein, N.: Electrical breakdown mechanisms in thin insulators. **Thin Solid Films 50, (**1978), 223–32

[Kön69] König, D.: Impulslose Teilentladungen in Hohlräumen von Epoxydharzformstoff-Isolierungen. ETZ-Archiv **90**, (1969), 156-8

[Kön93] König, D.; Narayana, Y. R.: Partial Discharge in Electrical Power Apparatus. vde-verlag, Berlin, Germany, (1993), **ISBN** 3-8007-1760-3

[Kra06] Krause, W.: Zeitaufgelöste Teilentladungsimpuls-Klassifikation mit Neuronaler Online-Identifikation und –Unterdrückung stochastischer Störer. PhD Thesis, University of Wuppertal, Germany, (2006)

[Kra93] Kranz, H.: Diagnosis of partial discharge Signals using Neural Networks and Minimum Distance classification. IEEE **Trans. on EI- 28**, (1993), 1016

[Kre93] Kreuger, F. H.; Gulski, E.; A. Krivda: Classification of Partial Discharges. IEEE Trans. on **EI**, **28**, (1993), 917-31

[Kri97] Krivda, A.; Halén, S.: Recognition of PD patterns in generators. **ICPADM'97**, Seoul, South Korea, (1997), 206-11

[Kru00] Krueger G.: Go to Java 2; Addison Wesley Verlag, Germany, (2000)

[Kuf84] Kuffel, E.; Zaengl, W. S.: High Voltage Engineering Fundamentals. A. Wheaton &Co. Ltd., Exeter, (1984), **ISBN** 0-08-024213-8

[Kum02] Kumar, s.s.: Development of Novel Techniques for Partial Discharge Measurement, Analysis and Representation. PhD Thesis, University of Bangalore, Indian, (2002)

[Lau81] Laurent C.; Mayoux, C.; Sergent, A.: Electrical breakdown due to discharges in different types of insulation. IEEE Trans. on **EI-16**, (1981), 52–8

[Lau03] Laurent, C.; Teyssedre L.: Hot electron and partial-discharge induced ageing of polymers. **Nucl. Instr.** and **Meth. in Phys. Res.** B 208, (2003), 442-7

[Lem06] Lemke, E. et. al.: Practical Experiences in on-site PD Diagnosis Tests of HV Power Cable Accessories in Service. Conference Record of the IEEE **ISEI**, (2006), 498-501

[Lor02] Lorenzo del Casale M Di; Schifani, R.: Direct Interaction between Partial discharge and temperature on epoxies: phenomenological life models. **J. Phys. D:** Appl. Phys., **35**, (2002), 33-9

[Löf76] Löffelmacher, G.: Über die physikalisch-chemischen Vorgänge bei der Ausbildung von Entladungskanälen in Polyäthylen und Epoxidharz im inhomogenen Wechselfeld. PhD Thesis, Technical University Hannover, Germany (1976)

[Luc79] Luczynski, B.: Partial discharges in artificial gas-filled cavities in solid high-voltage insulation. PhD Thesis, Technical University of Denmark, (1979)

[Lun00]   Lundgaard, L. E.: Partial Discharges in Transformer Insulation.**CIGRE'00**, Paris, France, (2000), paper 15-302

[Mas51]   Mason, J. H.: The deterioration and breakdown of dielectrics resulting from internal discharges. Proc IEEE, **Part 1**, **98**, (1951), 44-59

[McM64]   McMahon E. J.; Perkins J R.: Evaluation of polyolefin high voltage insulating compounds; dendrite (tree) formation under highly divergent fields. IEEE Trans. on **PAS 83, (**1964), 1253–60

[Mor91]   Morshuis, P. H. F.; Kreuger, F.H.: The evaluation of the discharge mechanism in a dielectric bounded cavity due to surface effects. **ICPADM'91**, Tokyo, Japan, (1991), 672-5

[Mor92]   Morshuis, P.H.F.: Time-Resolved discharge Measurements. **ISCD'92**, Sestri Levante, Italy (1992), 209-14

[Mor93]   Morshuis, P.H.F.: Partial discharge mechanisms, mechanisms leading to breakdown, analyzed by fast electrical and optical measurements. PhD Thesis, Delft University, Netherlands, (1993)

[Mue03]   Mueller, K.: Entwicklung und Anwendung eines Messystems zur Erfassung von Teilentladungen bei Frequenzumrichtern betriebenen elektrischen Maschinen. PhD Thesis, University of Duisburg-Essen, Germany, (2003)

[Mug90]   Cachay-Muguerza, O. E.: Das Teilentladungs-Verhalten von Gießharzimprägnierten Transformatorspulen. PhD Thesis, University of Hannover, Germany, (1990)

[Mwb85]   Hochspannungs-Erzeugung und Messungen. MWB Messwandler-Bau AG (1985)

[Nie95]   Niemeyer, L: A generalized Approach to Partial Discharge Modelling. IEEE Trans. on **DEI-2**, (1995), 510-28

[Nie84]   Niemeyer, L.; Pietronero L.; Wiesmann H. J.: Fractal dimension of dielectric breakdown. **Phys. Rev. Lett. 52, (**1984), 1033–6

[Pat75]   Patsch, R.: Breakdown of Polymers: Tree Initiation and Growth. **CEIDP'75**, Gaitherburg, USA, (1975), 323-34

[Pat79]   Patsch, R.: On the Growth-Rate of Trees in Polymers. **ISH'79**, Milano, Italy, (1979), paper 21.14

[Pat92]   Patsch, R.: Electrical and Water Treeing. A Chairman's View. IEEE Trans. on **EI-27**, (1992), 532-42

[Pat94]   Patsch, R.; Hoof, M: The influence of space charges and gas pressure during tree initiation and growth. **ICPADM'94**, Brisbane, Australia, (1994), 397-400

[Pat98]   Patsch, R.; Hoof, M: Physical Modeling of Partial Discharge Patterns. **ICSD'98**, Västeras, Sweden, (1998), 119-22

[Pat99]   Patsch, R.; Berton, F.: Zur Charakterisierung und Lokalisierung von Fehlstellen in Isoliersystemen mit der PSA. **ETG'99**, Bad Nauheim, Germany, (1999), 191-6

[Pat99a]   Patsch, R.; Berton, F.: Pulse-Sequence-Analysis - Chances to Characterize Defects. **CEIDP'99**, Austin, Texas, USA, (1999), 243-8

[Pat01]   Patsch, R.; Berton, F.: The Role of Space Charges in PD-Processes. **ISEIM'01**, Himeji, Japan, (2001), 21-24

[Pat02]   Patsch, R.; Berton, F.: Pulse Sequence Analysis - a Diagnostic Tool based on the Physics behind Partial Discharges. **J. Phys. D**: **Appl. Phys. 35**, (2002), 25-32

[Pat02a]   Patsch, R.; Berton, F., Benzerouk, D: PD-Source Identification and Characterization on the Basis of Pulse Shape Analysis. **CEIDP'02** , Cancun, Mexico, (2002), 728-31

[Pat02b]   Patsch, R.; Berton, F.: The Use of Time intervals between Consecutive Discharges to Characterize PD-Sources. **ISEI'02**, Boston, USA, (2002), 527-30

[Pat03]   Patsch, R.; Benzerouk, D.; Berton, F.: Time Differences Between Partial Discharge Events – What Do They Tell Us?. **NORD-IS'03**, Tampere, Finland, (2003), 135-42

[Pat03a]   Patsch, R.; Benzerouk, D.: Analysis of Partial Discharges in Stator Windings. **CEIDP'03**, Albuquerque, New Mexico, USA, (2003), 641-4

[Pat03b]   Patsch, R.; Berton, F.; Benzerouk, D.: Partial Discharge Analysis- The Benefit of the Evaluation of the Time Difference. **ACEID'03**, Chongqing, China, (2003), 363-5

[Pat04]   Patsch, R.; Benzerouk, D.: Characterization of Partial Discharge Processes- What Parameters work best?. **ICSD'04**, Toulouse, France, (2004), 636-9

[Pat06]   Patsch, R.; Menzel, J.; Benzerouk, D: The Use of the Pulse Sequence Analysis to Monitor the Condition of Oil. **CEIDP'06**, Kansas City, USA, (2006), 660-3

[Pat06a]   Patsch, R.; Menzel, J.; Benzerouk, D: The analysis of PD-Sequences from Different Defects. **ICPADM'06**, Bali, Indonesia, (2006), 31-5

[Pat07]   Patsch, R.; Menzel, J.; Benzerouk, D.: Partial Discharge Analysis to Monitor the Condition of Oils. **EIC'07**, Nashville, USA, (2007), 166-9

[Pat07a]   Patsch, R.; Arief, Y. Z.; Benzerouk, D.; Menzel, J.: Space Charges in Polymers and their Influence on Electrical Treeing. **CEIDP'07**, Vancouver, Canada, (2007), 208-12

[Pei95]   Peier, D.; Engel, K.: Rechnergestützte Auswertung von TE-Meßergebnissen - Neuronale Netze und Multivariate Statistik. **ETG'95**, Esslingen, Germany, (1995) 69-78

[Pem00]   Pemm, A. J. M.: Detection of Partial Discharges in Stator Windings of Turbine Generators. PhD Thesis, University of Eindhoven, Netherlands, (2000)

[Pra73]   Praehauser, Th.: Measurement of partial discharges in high voltage appartus with the balanced circuit. Haefly Publication, Translated from Bulletin ASE, Bd. 64, 19, (1973), 1183-9

[Rae64]   Raether H.: Electron Avalanches and Breakdown in Gases. Butterworths, London, UK, (1964)

[Rue99]   Ruemenapp, T.; Peier, D.: Dielectric breakdown in aluminium nitride. **ISH'99,** London, UK, (1999), 373-6

[Sah99]   Saha, T. K. et al.: Investigating the Effect of Thermal Degradation on the Properties of Power Transformer Insulation. **IEEE** Transaction on Power Delivery, 14, (1999), 1359-67

[Sei49]   Seitz, F.: On the theory of electron multiplication in crystals. **Phys. Rev. 76, (**1949), 1376–93

[Sta55]   Stark K. H.; Garton, C. G.: Electric strength of irradiated polythene. **Nature 176, (**1955), 1225–6

[Sto02]   Stone, G., C. et al.: Electrical Insulation for Rotating Machines. IEEE Press, Piscataway, USA, **ISBN** 0-471-44506-1

[Suw96]   Suwarno, Suzuoki, Y., Komori, F., Mizutani, T.: Partial discharges due to electrical treeing in polymers: phase resolved and time-sequence observation and analysis. **J. Appl. Phys.**, **29**, (1996), 2922–31

[Tan86]   Tanaka, T.: Internal partial discharge and material degradation. IEEE Trans. on **EI-21**, (1986), 899-905

[Tem00]   Temmen, K.: Evaluation of surface changes in flat cavities due to ageing by means of phase-angle resolved partial discharge measurement. **J. Phys. D.** Appl. Phys., **33**, (2000), 603-08

[Tow01]   Townsend, J. S.: **Phil. Mag. 1**, 198 (1901)

[Vee05]   Veen, J.: On line Signal Analysis of Partial Discharges in Medium-Voltage Power Cables. PhD Thesis, University of Eindhoven, Netherlands, (2005)

[Vog03]   Vogelsang, R.; Brütsch, R.; Fröhlich: Effect of electrical tree on breakdown in mica insulation. **ISH'03**, Netherlands, (2003), 375

[Vog06]   Vogelsang, R. et al: Electrical Breakdown in High-Voltage Winding insulations of Different Manufacturing Qualities. IEEE **El. Ins. Mag, 22**, 3, (2006), 5-12

[War00]   Warren, V.; Hamilton, J.: Partial Discharge as a Quality Assurance Test for Motor Stator windings. EPRI Motor Insulation Conference, Norfolk, USA, (2000)

[Wei06]   Weiers, T. et al.: Partial discharges in VPI winding insulations in dependence on the impregnating resin. **ICPADM'06**, Bali, Indonesia, (2006), 183-6